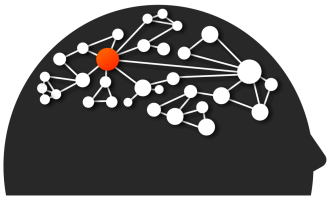

the connected brain

martijn van den heuvel

the connected brain

Our brain is a ***network***. It consists of many different regions that each have their own speciality, but which are always communicating to each other, forming one integrative network. Neuroscience has learned us a lot about the function of each specific brain region, but how functional communication ***between*** brain regions is organized remains largely unexplored.

Examining the brain as a dense network of interconnected brain regions, we show that communication within the brain is not just a random mess, but that it is organized according to one of the most ***efficient*** topologies that nature has to offer, combining a high level of efficient ***local*** information processing with a relative ease to travel globally within the entire network for maximum efficient ***global*** information integration.

The concept of a ***brain network*** does not differ that much from other networks that we know from everyday life, like for example the internet, road and flight grids. Flight grids are organized in small local airports, combined with larger hub-airports that host intercontinental flights. As such, when traveling from Amsterdam to New York, it is much more efficient to have a direct flight, rather than to fly from Amsterdam to London first, then from London to Washington, and finally from Washington to New York.

Our brain is organized in a very similar way. In this thesis we look at the brain, not as a set of independent regions, but as an integrative network. We explore its overall network topology, examine how efficiently it is organized both locally and globally. We explore the idea that regions are not just randomly linked to all other brain regions, but that they tend to form strongly intraconnected ***clusters***, called ***resting-state networks***. But how is functional communication between these anatomical separated brain regions possible? Mapping the ***structural information highways*** of the brain, we examine whether resting-state ***functional networks*** overlap with white matter structural connections in the brain, ***linking*** functional connectivity to structural connectivity. Furthermore, measuring the functional travel distance of different brain networks, we show that the most ***efficient networks*** belong to the most intelligent people, exploring the concept that ***intellectual performance*** might be related to how efficiently our brain can integrate information across different systems. Our findings suggest that our level of intellectual performance (and maybe other skills as well) might not be exclusively pinpointed to the properties of just one region, but rather that it might be a property of an entire network.

Our brain is a network. *Let's go* ***connect*** *some dots....*

the connected brain

het verbonden brein
(met een samenvatting in het Nederlands)

proefschrift

ter verkrijging van de graad van doctor aan de Universiteit Utrecht op gezag van de rector magnificus, prof. dr. J.C. Stoof, ingevolge het besluit van het college voor promoties in het openbaar te verdedigen op donderdag 3 september 2009 des ochtends te 10.30 uur

door

martijn pieter van den heuvel

geboren op 24 juli 1980
te Gouda

promotoren: Prof. dr. H.E. Hulshoff Pol
Prof. dr. R.S. Kahn

the connected brain

The studies described in this thesis were performed at the Rudolf Magnus Institute of Neuroscience, Department of Psychiatry, University Medical Center Utrecht, The Netherlands.

Research in this thesis was supported in part by a grant form the Netherlands Organization for Scientific Research (NWO): ZON-MW-VIDI Program (H.E.H., 917.46.370) and in part by a High Potential grant of the University Utrecht (O&O/06.21180).

Van den Heuvel, **Martijn** Pieter
the connected brain

ISBN: 978-90-39351239

table of contents

chapter 1

introduction

the connected brain

Our brain is a complex network. It is a network in which information is continuously processed and transported between structurally and functionally linked regions. Although each region of the brain network has a specific function, all regions have to continuously share information with each other. This integration of information is a never ending process that goes on even when we are 'at rest' and enables us to respond quickly and flexibly to the complex situations that we encounter in daily life. Every second our brain processes billions of bits of information, containing both new and stored information. It has to process incoming information and compare and integrate this with information we have learned and stored in the past. For this, our brain has specialized regions that are responsible for the processing of incoming information, specialized regions that control the muscles of our body and specialized regions that are responsible for the storage and retrieval of information. When we have to perform a difficult task, for example driving a car, all regions of the brain have to work together and share their specific information, forming one functionally interconnected network. Among an extensive amount of ongoing processes, the brain has to process all incoming visual information from the eyes, integrate this information with stored knowledge about cars, roads and behavior of other drivers, provide feedback to regions that process the visual information to focus on specific road-signs, design a plan which roads to use to drive from city A to city B, link all this information with our intention to go visit a friend and control our limbs to control the car. But how is our functional brain organized in order to integrate all these different types of information?

aim of this thesis

From neuroimaging studies, we have learned an incredible amount of information about the specific functions of each brain region. However, in contrast, how functional communication *between* brain regions is organized remains largely unresolved. How is our functional brain network organized to form a consistent integrative network? Which regions are most strongly connected? How *efficiently* are brain regions connected to each other? How does this functional communication relate to the structural connections of the brain? This thesis is aimed to develop and explore the use of novel graph analysis techniques in probing the topology of the complex functional brain network. The main goals are to develop and explore the use of new resting-state fMRI and graph-analysis techniques and to provide new insights about *how* and how *efficiently* the functional connections of our brain are organized, how these functional connections are related to the *structural* properties of the brain and to explore how the organization of the brain network is related to *cognitive behavior*. In short, we try to learn more about the organization of the functional brain as a *network*.

measuring brain activity: conventional fMRI

With the help of advanced neuroimaging techniques, like functional Magnetic Resonance Imaging (fMRI), neuroscientists are able to examine the specific function of a brain region by measuring its level of neuronal activity during the performance of a cognitive task. As such, fMRI studies can learn us an incredible amount of information about the brain, especially about mapping the specific functions of the different brain regions. For example, with the help of fMRI we are able to visualize which regions become active when we look at an image, which regions become active when we move our fingers and which regions are needed to correctly solve a difficult equation.

Conventional task-dependent fMRI studies are designed to measure which regions become active when a specific task is performed. This is typically achieved by contrasting the level of activation that is recorded during the performance of the task with the level of activation that is recorded during a period when no task is performed. figure 1.1 explains the basics of a conventional task-related fMRI experiment. In a typical fMRI experiment a subject is instructed to perform a specific task inside the Magnetic Resonance scanner, for example moving his or her fingers when asked, while his/her brain activity is measured. In half of the time the subject is instructed to perform the task and in half of the time the subject is instructed to be at rest. Throughout the experiment, the Blood Oxygenation

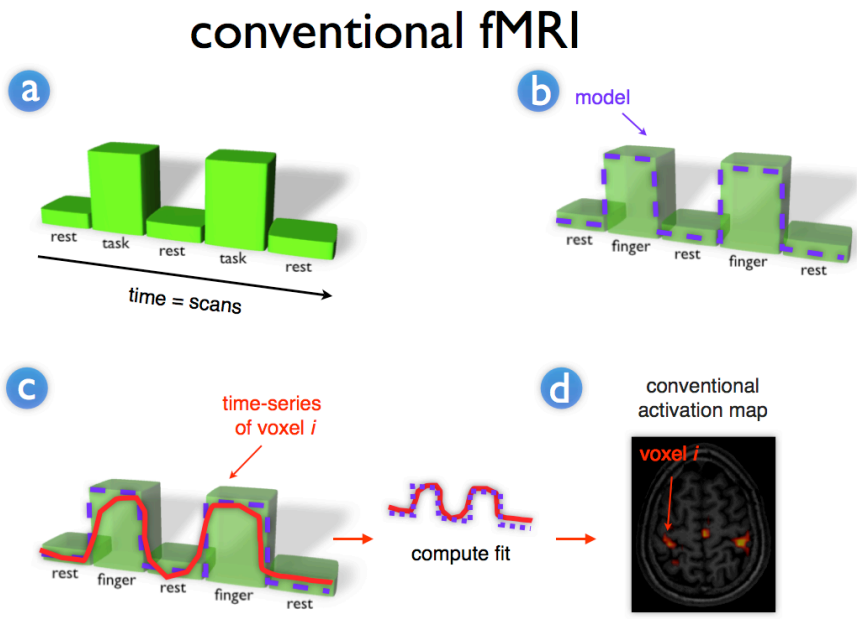

figure 1.1 conventional fMRI analysis ***panel a*** During a typical (block-design) fMRI experiment a subject is asked to perform a specific task for a period of time (usual around 30 seconds, called *task* condition), alternated with periods of rest (*rest* condition). During the performance of the task the Blood Oxygenation Level Dependent fMRI signals are measured, believed to indirectly represent the level of neuronal activity of a particular brain region. In our example, the subject was instructed to perform a 'finger tapping task', with the instructions to tap his/her fingers when asked. ***panel b*** The performed task defines a model, indicating which scans were made during the task condition and which scans were made during the rest condition. ***panel c*** Within the analysis of the fMRI dataset, the time-series of each independent voxel is tested against the defined model (representing when the subject performed the task), computing the fit between the 'model' and the 'recorded' BOLD time-series. ***panel d*** Computing this fit for every voxel of the brain, results in a activation map, defining which voxels were significantly more activated during the performance of the finger tapping task than during the rest condition, showing which brain regions were activated in performing the task. In our example, this analysis revealed the involvement of left and right motor cortex in moving the right and left fingers.

Level Dependent (BOLD) fMRI signal of all gray matter regions is continuously measured, as an indirect measure of the level of neuronal activity of these regions. After the scanning experiment, for each individual brain region it is tested separately how well the region's recorded BOLD

box 1. cities, highways, traffic and the brain

Why is it important to examine our brain as a network? Well, because the human brain is not a set of independent regions, but a complex system in which information is continuously processed and transported between regions with coherent dynamics. In that sense, our brain is a network of functionally linked regions. Let's explain the importance of this with the help of an analogy between our brain and the road map of a country. Similar to our brain, a country does not solely consist of a number of independent cities, but all cities are interconnected by structural highways, which are vital for the economy of a country. Figure 1.2a presents a satellite image of Holland, a small country in Europe. Figure 1.2b shows the same image, but now some of the main cities of Holland are drawn

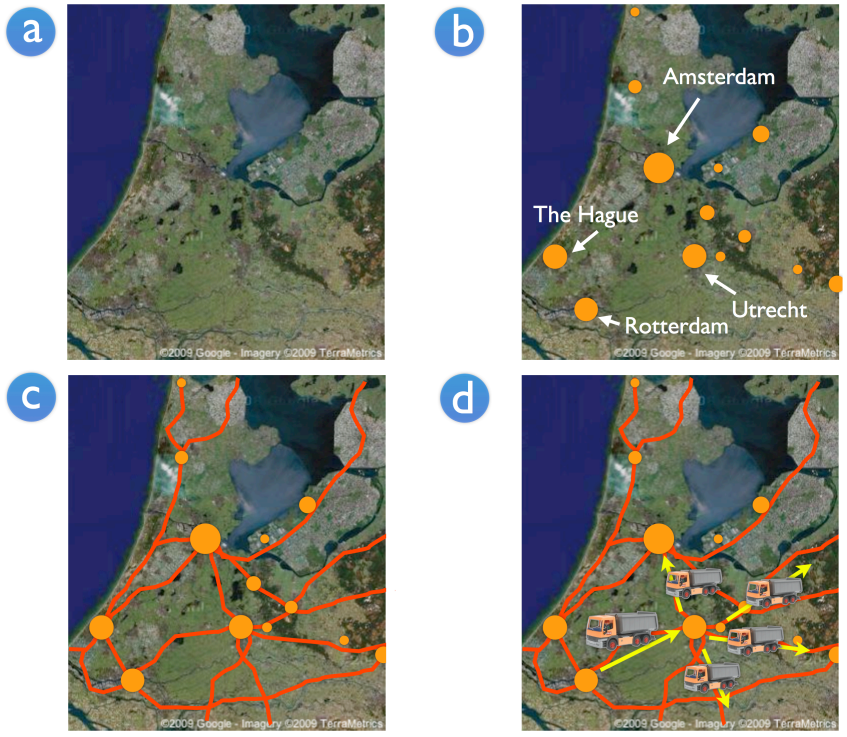

figure 1.2 the Holland network Panel a shows a satellite image of Holland (satellite image taken from Google Maps). **Panel b** shows some of the major cities of Holland. In **panel c** a number of important highways are shown, clearly showing that Holland is a network of structurally interconnected cities. The existence of these structural connections enable constant transport of people and products between cities, indicating a high level of functional communication between the different cities (**panel d**).

box 1.1 (continuing)

into the image, including Amsterdam (the capital city) and Utrecht (where the University of Utrecht and the University Medical Center Utrecht are located). These cities are like the different regions of our brain, each with their own identity and their own function. It is clear that the cities of Holland are not independent from each other. If we draw in a number of important highways, we can see that Holland is a network in which all cities are directly and indirectly linked to each other (figure 1.2c). Structural highways enable a high level of functional communication between the different cities (figure 1.2d). Continuously, people travel between the different cities and products are shipped from one place to another. These processes go on 24 hours a day and form the core of our economy.

By examining Holland as a dynamic network, we can learn important properties about it's organization. Within the Holland network the highways reflect the existence of structural connections that enable functional communication between the different cities. Using this framework, we can examine which cities are the most strongly functionally connected, how functional communication is organized locally between nearby cities, how functional communication is linked to the quality of structural connections and how the overall organization of the road network is related to the economy of Holland. For example, in our Holland network, some cities are much more locally connected to each other than to the rest of the network and form a sub-group within the full network, indicating a high level of local clustering and modularity of the overall road network. Furthermore, the structural quality of the highways is likely to form an important role in the total level of functional communication between cities. Improving a highway from four to five lanes is likely to also improve the level of transport between two cities. This suggests that the quality of structural connections between regions in a network is related to the level of functional communication between these regions. In addition, it is easy to understand that a short average communication distance between the cities of Holland is linked to the level of how efficient people can travel between cities and in turn this is likely to have an effect on the quality of the economy of Holland. In short, defining Holland as a network enables us to probe its overall organization and examine important aspects of Holland, that we were not able to measure if we just only examined the cities of Holland.

the brain network and its organization

Our brain network is not that different from this Holland network. It consists of a large number of different brain regions, that each have their own function and task, but, just like the Holland network, information is continuously transported between the different regions of our brain, forming one integrative network of functionally linked regions. By examining our brain as a network, we can learn important things about the organization of our brain. Such an examination may learn us important things about how the functional connections of our brain are organized, how they are linked to the structural properties of our brain, and how their level of efficient wiring is linked to the overall level of ' brain economy'.

time-series responded to performing the task. This procedure identifies which regions were involved in the task and which were not. In a finger-tapping task this would reveal brain regions that are involved in controlling our fingers, overlapping regions of the motor cortex.

However, within a conventional fMRI experiment each brain region is tested separately. Therefore, conventional task-related fMRI experiments are not able to provide information about communication *between* the different regions of our brain. As such, task-related fMRI studies are limited in examining the brain as the integrative network that it is.

examining the brain's connectivity architecture

Why is it so important to examine the functional connectivity architecture of the human brain? Well, although a lot is known about the specific function of each individual brain region, it remains largely unresolved how functional communication between these regions is organized. Examining the functional connections of the brain network can reveal new insights about core aspects of the human brain, which remain invisible by just looking at the regions alone. Box 1 and figure 1.2 illustrate the essence of the notion that representing a dynamic system as a network can reveal important aspects about that system, using an analogy of the roadmap of Holland, a small country in Europe. When we look at the road map of Holland, we clearly see that Holland is not a collection of independent cities, but a network of cities that are interconnected by structural highways that enable functional communication between these cities (figure 1.2). Representing Holland as a complex network can reveal important information about core aspects of this country, like which cities are most strongly connected, how functional communication between cities is related to the structural infrastructure and how the level of efficient transport of products is related to the state of Holland's economy. In a similar way, examining the brain as a complex integrative network may provide new important information about how the human brain is organized. As our brain is an integrative complex dynamic system of functionally linked regions, looking at it as a complex network can provide new insights about core aspects of how functional communication within the human brain is organized.

functional connectivity

resting-state fMRI

How do we define a functional connection within the brain network? As we have seen, conventional fMRI analysis techniques provide important information about the *total amount* of brain activity of independent brain regions, but not about functional connectivity *between* regions. *Functional connectivity* between two cortical regions is defined as the temporal dependence between their level of neuronal activity (Aertsen et al., 1989; Friston et al., 1993) and can be investigated by measuring the level of coherent behavior between resting-state fMRI BOLD time-series (Biswal et al., 1995; Lowe et al., 1996; Cordes et al., 2000). During a typical resting-state experiment, subjects are instructed to relax and to think of nothing in particular, while their spontaneous brain activity is measured throughout the duration of the experiment. Around 15 years after the first task fMRI experiments, Biswal and colleagues were the first to show that during rest, the left and right hemispheric regions of the primary motor network show a high level of coherence between their fMRI BOLD signals, suggesting a high level of ongoing functional connectivity between the regions of the motor network during rest (Biswal et al., 1995; Biswal et al., 1997). Figure 1.3 describes the pioneering experiment of Biswal et al. and explains the basic principles of resting-state analysis. Multiple resting-state studies have replicated the findings of Biswal, demonstrating the existence of resting-state functional connectivity between the regions of the motor network, but also between regions of other known functional networks, including the primary visual network, auditory network and even high order cognitive networks (Lowe et al., 1996; Xiong et al., 1999; Cordes et al., 2000; Lowe et al., 2000; Greicius et al., 2003; Beckmann et al., 2005; Damoiseaux et al., 2006; De Luca et al., 2006; Fox and Raichle, 2007). These studies suggest that brain regions are not idle during rest, but rather show a vast amount of spontaneous neuronal activity that is highly synchronized between regions that form a functional network. In contrast to conventional fMRI studies that are focused on mapping out the function of a specific brain region, resting-state fMRI studies are designed to map the functional connections of the brain by measuring the level of functional connectivity *between* regions as reflected by the level of coherence between resting-state time-series of brain regions during rest.

origin of spontaneous fMRI signals

Of special interest are the low frequency oscillations (~0.01 - 0.1Hz) of resting-state BOLD fMRI time-series (Biswal et al., 1995; Lowe et al., 1996;

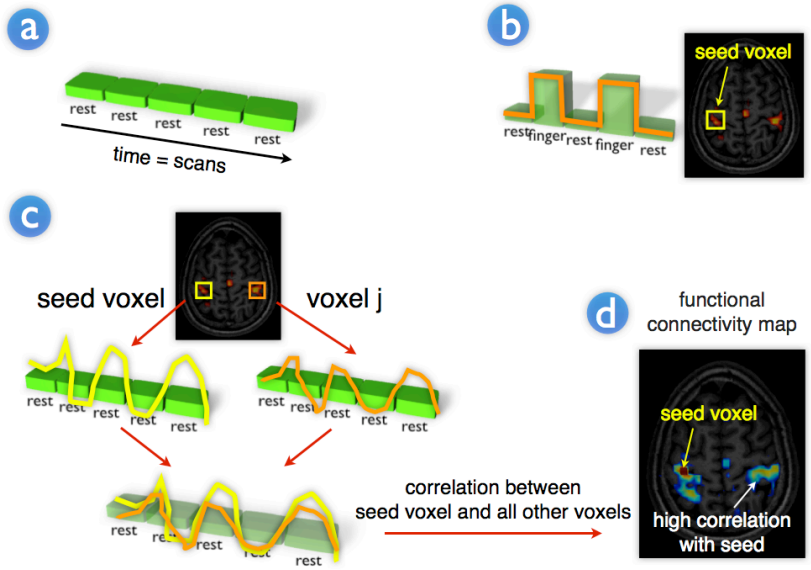

figure 1.3 resting-state fMRI analysis In contrast to conventional task-dependent fMRI studies, resting-state fMRI studies are designed to examine the interaction between (spontaneous) activation patterns of brain regions. Within a typical resting-state experiment, the level of spontaneous neuronal activity of brain regions is measured. Subjects are placed into the scanner and asked to close their eyes and to think of nothing in particular, without falling asleep. Similar to conventional fMRI, the BOLD fMRI signal is measured throughout the experiment, but now the subjects do not have to perform a task (only rest condition) (***panel a***). Typically, to examine the functional connections of a specific brain region, conventional task-dependent fMRI is used to select a specific brain region. If we are for example interested in examining the functional connections of the motor network, one can use a conventional activation map of a finger tapping experiment to select a so-called seed region as a group of voxels that showed a high activation in the tapping task. As this voxel showed a high activation during the finger tapping task, these voxels to represent regions of the motor network (***panel b***). To examine the level of functional connectivity between the selected seed region (voxel *i*) and a second brain region (for example a region in the contralateral motor cortex), the resting-state time-series of the seed voxel is correlated with the resting-state time-series of a second voxel (voxel *j*, ***panel c***). Furthermore, to map out all functional connections of the selected seed region, the time-series of the seed voxel *i* can be correlated with the time-series of all other voxels in the brain, resulting in a functional connectivity map, reflecting all voxels that show a high level of functional connectivity with the selected seed voxel (***panel d***).

Cordes et al., 2000). Where these oscillations originate from is not yet fully understood. In the past 5 years, there has been an ongoing discussion on whether these correlations originate from synchronization in the underlying spontaneous neuronal activation patterns of these regions, measured through a hemodynamic response function (Gusnard et al., 2001; Greicius et al., 2003; Buckner and Vincent, 2007) and to what extend these resting-state BOLD signals result from physiological processes, like respiratory and cardiac oscillations (Wise et al., 2004; Birn et al., 2006; Shmueli et al., 2007; Birn et al., 2008; Chang et al., 2009). The view of a neuronal basis of resting-state fMRI BOLD signals is supported by the observation that most of these correlations have been observed between cortical regions that share a common function, for example regions of the motor, visual and auditory network (Biswal et al., 1995; Lowe et al., 2000; Damoiseaux et al., 2006; De Luca et al., 2006). This suggests that brain regions that often have to work together form a functional sub-network, with a high level of ongoing spontaneous neuronal activity during rest that is highly synchronized between the anatomically separated regions that form the network. Further support for a neuronal basis of resting-state fMRI signals comes from studies who report that the observed spontaneous BOLD signals of cortical regions, as measured using resting-state fMRI, are mainly dominated by lower frequencies (< 0.1 Hz) with only a minimal contribution of higher cardiac and respiratory oscillations (> 0.3 Hz) (Cordes et al., 2000; Cordes et al., 2001). Furthermore, recent studies have linked spontaneous BOLD fluctuations directly to concurrent fluctuations in neuronal spiking (Shmuel et al., 2002; Nir et al., 2008; Shmuel and Leopold, 2008), providing strong support of a direct association between resting-state time-lag BOLD signals and spontaneous neuronal activity. Taken together, it is now widely believed that resting-state BOLD fluctuations of cortical and sub-cortical regions originate, at least in part, from spontaneous neuronal activity and that the observed temporal coherence between the fMRI time-series of anatomically separated regions is reflecting synchronization between the underlying neuronal activation patterns of these regions and a high level of ongoing functional connectivity during rest. This makes resting-state fMRI oscillations a robust measure to examine functional connections between brain regions on a whole brain scale.

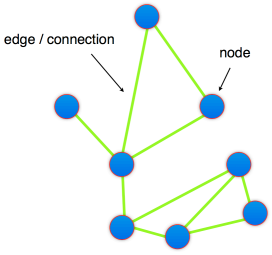

figure 1.4a

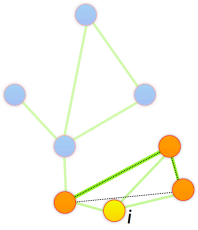

figure 1.4b

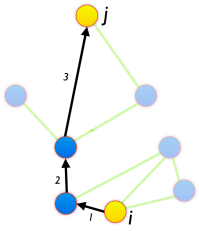

figure 1.4c

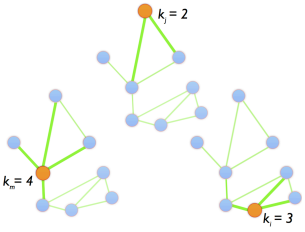

figure 1.4d

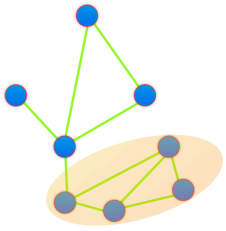

figure 1.4e

the functionally connected brain network

graph theory

The last few years the neuroscience community has become more and more interested in examining resting-sate fMRI patterns as a measure of functional connectivity between *specific* brain regions, and a number of studies have

figure 1.4a a graph A network can be represented as graph *G=(V,E)*, with *V* the collection of nodes and *E* the collection of edges, also called connections, defining which nodes are connected.

figure 1.4b clustering-coefficient The clustering-coefficient of node i provides information about the level of local connectedness in the graph and is given by the ratio of the number of connections between the direct neighbors of node i and the maximum number of possible connections between the neighbors of node i. The clustering-coefficient provides information about the level of local connectedness of the graph.

figure 1.4c characteristic path length The characteristic path length of node i provides information about how close node i is connected to all other nodes in the network and is given by the average distance d(i,j) between node i and all other nodes j in the network. Distance d (i,j) can be defined as the number of connections that have to be crossed to travel from node i to node j in the graph. Path length L provides important information about the level of global communication efficiency of a network.

figure 1.4d node degree The degree of node i is defined as the number of connections of node i. The degree distribution of a graph is given by the distribution of the number of connections over all nodes of the graph. The degree probability distribution P(k) describes the probability that a node is connected to k other nodes in the network.

figure 1.4e modularity The modularity of a group of nodes defines how well a group of nodes in the network forms a relative isolated community within the full network.

examined functional connectivity of, for example, primary motor and visual systems and even more high order systems. However, less is known about the *overall* connectivity architecture of the brain network. To probe the overall complex structure of functional brain networks we need a well-defined theoretical framework. *Graph theory* has been extensively used to examine the properties of networks like the internet, aircraft flight patterns

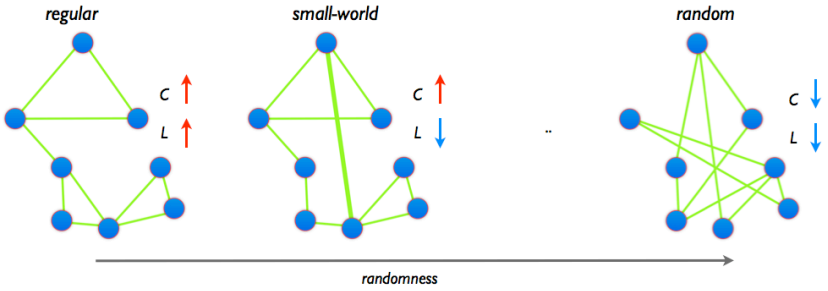

figure 1.5a small-world networks Regular networks have local character, indicated by a high clustering-coefficient and a high path length L. In contrast, random networks have a high global character, showing a low level of clustering (low C) and a short node-to-node distance (short L). Watts and Strogatz (1998) showed that if the connections of a regular network are reconnected randomly with a probability p, that for a small p a network has an intermediate character, showing both a high level of local clustering C, but still with a short path length L. These networks have a so-called small-world organization. Small-world networks are characterized by a high level of both local and global efficiency and a high level of robustness.

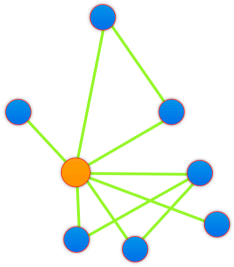

figure 1.5b scale-free networks Scale-free networks have a degree distribution that follows a power-law function $P(k) \sim k^{-\gamma}$. Within a scale-free network, on average a node has a relative low number of nodes, but with the existence of a small number of highly connected hub-nodes that have many more connections that the average node (see orange node). This in contrast to random networks, in which all nodes have on average the same number of connections.

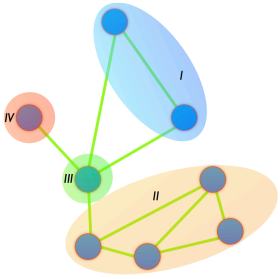

figure 1.5c modular networks Modular networks show the formation of strongly local interconnected sub-networks within the full network. A group of nodes that is mostly connected to each other and to a lesser extent to the rest of the nodes of the network forms a sub-network or module within the full network.

and complex biological systems. Using graph theory, a complex network can be expressed as a graph $G = (V,E)$, with V the collection of nodes and E the collection of connections or edges between the nodes. With the help of graph theory one can collect information about key characteristics about the organization of a network, for example the level of local and global connectivity organization of the network, how connected each node is, and whether sub-networks are formed within the full network.

graph characteristics

Figure 1.4 describes the idea of a graph and some key graph properties, including the clustering-coefficient, characteristic path length, node degree and degree distribution and modularity. The clustering-coefficient of a graph provides information about the level of local neighborhood clustering within a graph, expressing how close the neighbors of node are connected themselves. This indicates the level of local connectedness of a graph (figure 1.4-b). The characteristic path length of a graph describes how close on average a node of the network is connected to every other node in the network, providing information about the level of global connectivity of the network (figure 1.4-c). Furthermore, the degree of a node describes the number of connections a node has (figure 1.4-d). In turn, the degree distribution P(k) of a graph describes the probability that a node has k connections. In addition, the modularity (figure 1.4-e) of a graph describes to which extent groups of nodes in the graph are more connected to each other than that they are connected to the rest of the network, indicating the possible formation of sub-networks within the full network. Taken together, graph theory provides us with a rich framework in which we can express and examine the topology of complex networks.

network organization: small-world, scale-free and modular networks

The level of local and global connectedness and the degree distribution provide information about the overall organization of a network (figure 1.5-a-c). *Regular* networks (figure 1.5-a left) have a local character, characterized by a high level of local clustering and a long global travel distance, as reflected by a high clustering-coefficient and a high path length. In contrast, *random* networks (figure 1.5-a right) have a global character, showing a low level of clustering and a short path length. Small-world networks have an intermediate organization (figure 1.5-a middle), characterized by a high level of local clustering, but still with a relative short average travel distance due to a small number of long-distance connections that ensure a high level of global communication efficiency in the network (figure 1.5-a)(Watts and

Strogatz, 1998). Furthermore, a scale-free network has a degree distribution $P(k)$ that follows a power-law function $P(k) \sim k^{-\gamma}$, indicating that on average the nodes in the network have a small number of connections, but with the existence of a few hub-nodes that are much more connected than the average node in the network, ensuring a high level of overall global connectivity (figure 1.5-b)(Barabasi and Albert, 1999; Barabasi and Bonabeau, 2003; Grigorov, 2005). In contrast, random networks have a more Poisson shaped degree distribution, indicating that on average all nodes have around the same number of connections. A third category are *modular* networks, which are networks that show the formation of sub-networks within the full network (figure 1.5-c). A group of nodes that is mostly connected to each other and to a lesser extent to the rest of the nodes of the network forms a module within the full network. Modular networks are characterized by the formation of strongly intraconnected node-communities (Sporns et al, 2007).

defining the functional brain network using graph theory

Using graph theory the functional brain network can be expressed by *nodes* reflecting the different regions of the brain and *connections* between those brain regions reflecting functional connections between regions (Sporns et al., 2004; Salvador et al., 2005b; Achard et al., 2006; Stam and Reijneveld, 2007). Representing our brain as a functionally linked network based on resting-state fMRI data can be done in a few easy steps. First, to set up the connectivity graph, we have to define our set of nodes (figure 1.6-1). Up to now, most resting-state fMRI studies have used an anatomical template approach, dividing the brain network into a small number of predefined nodes (~90 regions) that each overlap a large cortical region (for example Brodmann areas). Such a regional simplification has the advantage to keep the number of nodes to a minimum. However, using a template approach limits the examination to inter-regional connectivity (Salvador et al., 2005b; Achard et al., 2006; Achard and Bullmore, 2007; Liu et al., 2008). In this thesis, we propose a voxel-wise approach, using the true resolution of the resting-state fMRI acquisition. In this approach, the functional brain network is defined as a network of around 9000 to 10000 cortical and sub-cortical voxels, a voxel being a small brain region of around 4 cubic millimeters, rather than of ~90 regions each overlapping large cortical areas. A voxel-wise approach allows for the model-free examination of both *inter-regional* as well as *intra-regional* connectivity, providing a fine grained representation of the brain network.

Next, besides the nodes, we need to define the connections between the nodes of the brain network (figure 1.6-2). As we have seen, the level of

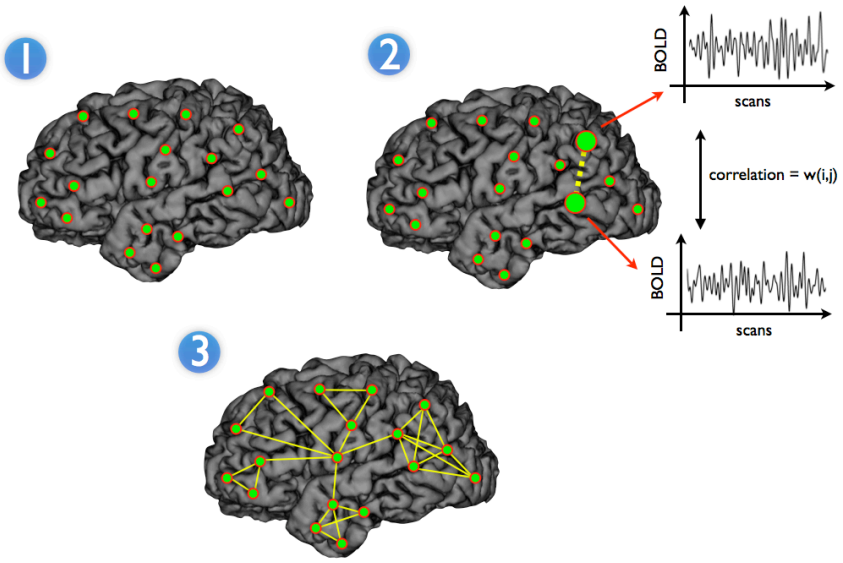

figure 1.6 modeling the functional brain network The functional connected brain can be modeled as network, consisting of nodes, defined as brain regions, and edges (or connections) between those regions that are functionally linked. First, the collection of brain regions has to be defined. This can be done by using a predefined template (using a parcellation of the cortex into a relative small number of regions, for example the Brodmann Areas). Otherwise, the collection of regions can be taken as the total of collection of grey matter voxels, providing a more spatially detailed brain network (***step 1***). Second, the level of functional connectivity between the nodes in the network can be computed as the zero-lag correlation between their resting-state time-series, which is believed to reflect the level of synchronization between spontaneous neuronal activity. This correlation is computed for each possible pair of nodes (i.e. between all possible regions or voxel pairs) (***step 2***). The existence of a connection between two points can be defined as whether their level of functional connectivity exceeds a certain threshold. As a result, this results in the modeling of our brain as a functional network, with connections between functionally linked brain regions and the absence of a connection between regions that are not functionally linked (***step 3***).

functional connectivity between two voxels can be expressed by the temporal dependence between their resting-state fMRI signals, believed to reflect the level of synchronization between the underlying neuronal activity patterns of these regions (Biswal et al., 1995; Shmuel et al., 2002; Nir et al., 2008; Shmuel and Leopold, 2008; Lowe et al., 2000; Damoiseaux et al., 2006;

De Luca et al., 2006). The existence of a functional connection between two cortical voxels *i* and *j* can be defined as whether their level of pair-wise functional connectivity exceeds a certain threshold *T* (figure 1.6-3). All correlations above this threshold are interpreted as the existence of a functional connection between these regions, which is represented as a connection between the nodes *i* and *j* of the brain network. Computing the level of temporal coherence between all cortical and sub-cortical voxels provides a functionally interconnected brain network (figure 1.6-3) (Achard, 2006; Salvador et al., 2005a; Achard and Bullmore, 2007; Liu et al., 2008). As such, we can express the functional brain as a dynamic network, allowing us to examine its complex functional organization using graph theory.

examining the brain network

topology of the functional brain network, a combined small-world and scale-free organization?

Now that we have defined a way to model the functional brain network we are able to explore its complex network topology. Examining the organization of a network can provide important information about how the different regions of our brain are linked together and how efficiently they can integrate information as the organization of a network is known to be directly linked to its level of robustness, capability to integrate information and communication efficiency (Latora and Marchiori, 2001; Mathias and Gopal, 2001; Buzsaki and Draguhn, 2004; Grigorov, 2005; Chen et al., 2006; Achard and Bullmore, 2007; Bullmore and Sporns, 2009). In the past decade, a small number of pioneering studies have suggested a *small-world* organization of functional brain networks (Sporns et al., 2000; Sporns and Zwi, 2004; Stam, 2004; Eguiluz et al., 2005; Salvador et al., 2005a; Achard et al., 2006; Micheloyannis et al., 2006; Sporns, 2006; Rubinov et al., 2007; Sporns et al., 2007; Stam et al., 2007; Liu et al., 2008; Smit et al., 2008). As mentioned, a small-world organization is characterized by a high level of neighborhood clustering, together with the existence of a small number of crucial more global oriented connections that ensure a high level of global communication efficiency across the entire network. Typically, small-world networks show a *clustering-coefficient* that is much higher and a *characteristic path length* that is around the same order as a comparable random network of similar size (Watts and Strogatz, 1998). In addition, a *scale-free* organized network is characterized by a degree distribution that follows a power-law function, indicating that on average the nodes of the network have only a few connections, but with the existence of a few nodes in the network that

have many more connections than the other nodes, ensuring a high level of overall global connectivity (Barabasi and Albert, 1999; Barabasi and Bonabeau, 2003; Grigorov, 2005). Together, a *small-world* and *scale-free* organization ensures an extremely robust network architecture in which information can be transferred and integrated with a high level of both local and global communication efficiency (Latora and Marchiori, 2001; Mathias and Gopal, 2001; Sporns et al., 2004). This makes them an attractive model for the functionally connected human brain (Salvador et al., 2005a; Achard et al., 2006; Stam and Reijneveld, 2007; Sporns et al., 2004; Sporns and Zwi, 2004; Stam and Reijneveld, 2007). However, as mentioned, these pioneering studies have mainly focused on the examination of inter-regional connectivity. Representing the brain as a network of large brain regions does not incorporate intra-regional connections and functional connections between sub-parts of brain regions. Therefore, examining the functional brain network on a voxel level could provide a more detailed insight about how functional communication within the brain is organized and provide a much better model to explore the functional brain network. Especially, such an examination could provide new information about a possible combined small-world and scale-free organization of the brain network and provide a better link to cognitive behavior.

topology of the functional brain network, a modular organization? formation of functionally linked resting-state networks

The high clustering-coefficient of the brain network shows a high level of local connectedness within the brain network. Although not a necessary consequence of a high clustering-coefficient, a high level of local connectedness may suggest the possible formation of strongly locally clustered sub-networks within the full network. This hypothesizes a possible *modular* organization of the functional brain network. Indeed, a limited number of resting-state fMRI studies have shown the formation of strongly functionally connected groups of anatomically separated brain regions that show a high level of functional connectivity during rest. These strongly intraconnected sub-networks are often referred to as *resting-state networks* (Xiong et al., 1999; Kiviniemi et al., 2003; Beckmann et al., 2005; Damoiseaux et al., 2006; De Luca et al., 2006). A number of model-free methods have been applied to individual PET and resting-state fMRI data (Friston et al., 1993; Worsley et al., 2005; Calhoun et al., 2001; Beckmann et al., 2005; Thirion et al., 2006). However, group analysis of resting-state data is still a complex task and often involves manual intervention in selecting the number of meaningful group networks. In **chapter 3** we aim to examine the formation

of functional sub-networks within the full brain network as an indication of a possible modular organization of the functional brain network by reporting on a novel model-free group graph clustering approach based on graph theory.

Interestingly, the reported resting-state networks show large overlap with networks that have a known functional role, like the primary motor, visual and auditory networks, but also cognitive networks, for example networks of regions involved in attention processing (Xiong et al., 1999; Salvador et al., 2005b; Beckmann et al., 2005; Damoiseaux et al., 2006; De Luca et al., 2006). One of the most consistently found resting-state networks is the *primary motor network*. It is well known that the primary motor cortex is not a homogeneous brain region, but rather consists of many sub-regions that each have their own function, like controlling our feet, our fingers and other body parts (Penfield and Boldrey, 1937; Rasmussen, 1977). Until now group resting-state studies have reported all motor regions to form a single resting-state network and little is known about the specific organization of the functional connections between sub-regions of the primary motor network. As the primary motor cortex consists of several sub-regions that each have their own function, we hypothesize the possible subdivision of the primary motor network in functional sub-networks, overlapping left and right hemispheric primary motor regions that have a shared motor function. In **chapter 4** we will focus on the organization of the functional connections between the specialized regions of the primary motor network.

structural core of functional resting-state brain networks

But how is all this ongoing resting-state functional communication between these functionally linked but anatomically separated brain regions possible? Up to around 8 to 10 large resting-state networks have been consistently found across group resting-state studies, including the *primary motor* and *visual* networks, a *network* of insular and anterior cingulate cortex, lateralized *parietal-frontal attentional networks* and the so-called *default mode network* (**chapter 3**; Beckmann et al., 2005; Damoiseaux et al., 2006; De Luca et al., 2006). Interestingly, these resting-state networks all consist of anatomically separated brain regions. If the observed coherence between the resting-state fMRI BOLD signals of these regions truly reflect ongoing neuronal communication, one would expect the existence of structural communication channels between these regions to facilitate this interregional communication. Within our brain, the functional units, called *neurons*, are linked together by *axons*, which allow a neuron to send information from one neuron to another neuron. Brain regions consist of millions of neurons and anatomically separated brain regions are connected to each other by

large bundles of millions of axons, called *white matter tracts,* that directly structurally interconnect the spatially separated groups of neurons together. As such, white-matter tracts form the structural information highways of our brain. Considering resting-state functional connectivity, one would expect the existence of a structural network of white-matter pathways to support the ongoing spontaneous neuronal communication between resting-state network regions during rest. However, until now little is known about the structural core of resting-state networks. Are these functionally linked networks truly 'hard-wired' into our brain? In **chapter 5** we will focus on the existence of structural white matter pathways between functionally linked regions and examine the existence of a structural core of resting-state networks.

Among the reported resting-state networks, the *default mode network* is of special interest, as it is suggested to play an important role in human cognition (Greicius et al., 2003). The default mode network functionally connects the medial frontal cortex (MFC), precuneus/posterior cingulate cortex (PCC) and regions overlapping the inferior parietal lobule (Gusnard et al., 2001; Raichle et al., 2001; Greicius et al., 2003). Interestingly, the regions of the *default mode network* have been reported to show an elevated level of neuronal activity during rest, suggesting to reflect a *default state* of brain activity (Raichle et al., 2001). Furthermore, these increased levels of neuronal activity show a high level coherence between the regions of the default mode network, suggesting a high level of spontaneous functional connectivity between these regions (Greicius et al., 2003). Activity and synchronization of the default mode network has been linked to core process of human cognition, like the integration of cognitive and emotional processing (Greicius et al., 2003), monitoring the world around us (Gusnard et al., 2001) and mind-wandering (Mason et al., 2007).

To further probe the structural and functional properties of the default mode network, it would be of high importance to examine the relationship between the organization of the interconnecting structural pathways and the level of functional communication between the default mode network regions. The white-matter *cingulum* tract has been suggested to play an important role in structurally interconnecting the active regions of the *default mode network* (Greicius et al., 2008)(**chapter 5**), but it remains unknown how these structural connections affect the level of default mode functional connectivity. However, these two forms of connectivity are likely linked. Like the modernization of a structural highway makes more and faster transport possible between the cities it connects, the level of microstructural organization of the cingulum is likely to be linked with the level of functional connectivity between the regions of the default mode

network. Extending a highway from 4 to 5 lanes allows the amount of traffic between cities to grow, increasing the level of functional communication between cities. Interestingly, within the brain network similar associations between the properties of structural and functional connections have been reported. The microstructural organization of interconnecting tracts between the primary visual regions have been found to be associated with their level of activation in a visual task (Toosy et al., 2004) and interhemispheric synchronization has been linked to organization of interconnecting corpus callosum tracts in the developing brain (Fornari et al., 2007). In this context, it would be reasonable to speculate about a direct relationship between the microstructural organization of the white matter cingulum tract and the level of resting-state functional connectivity between the regions of the default mode network. Such an association might provide more insight in the structural core of the functional default mode network and the relationship between structural connectivity and resting-state functional connectivity in general. In **chapter 6**, we will focus on the association between the microstructural organization of the cingulum tract and the level of default mode functional connectivity.

do more efficiently wired brain networks have a higher level of 'brain economy'?

The overall structure of the brain network is known to be organized according to a *small-world* organization, indicating a highly robust and efficient organization of the functional connections of our brain (Stam, 2004; Achard et al., 2006)(**chapter 2**). As we have seen, *small-world modular* networks are specifically characterized by a high level of local connectedness and the formation of specialized functional sub-networks that are linked together by a small number of long-distance connections that ensure a high level of global communication efficiency across the full network (Sporns et al., 2004; Sporns and Zwi, 2004). Interestingly, the short characteristic path length of a small-world network ensures that the average travel distance between any two nodes in the network is still short, indicating a high level of *global* communication efficiency within the overall network.

Probably one of the most clear examples of the high level of global efficiency of small-world networks is given by the organization of social networks. We are all familiar with the notion that social networks have a high global character. How many times have you bumped into someone on your holiday that lived next door to somebody that knew the housekeeper of some famous person? Most often we are amazed when such an event happens and say "what a small world!". Together with the high level of clustering, the short node-to-node distance of social networks forms the basis of this phenomena. Small-world social networks tend to follow the rule

of 'six degrees of separation', referring to the notion 'that if a person is one step away from every person they know and two steps away from every person that is known by the persons they know, than every body in the world is no more than six steps away from every other person in the world' (Wikipedia). The small-world organization of social networks marks that they are highly efficiently organized, as all people on earth are only a few steps away from each other. Interestingly, recent studies have indicated that the functional connections of our brain are organized in a similar small-world fashion, supporting the idea that all brain regions, although each having their specialized function and role in the network, are only a few functional connectivity steps away from each other.

But how efficient is our brain network? *Small-world* and *scale-free* organization are known for their high level of efficient global communication with a minimum of congestion problems (Latora and Marchiori, 2001; Mathias and Gopal, 2001; Grigorov, 2005; Achard and Bullmore, 2007). Within this context, it is easy to imagine that the *more* efficient a network is organized, the *higher* its level of efficient output. Within a more efficient organized road network the shipping of products between cities would be faster and therefore more productive. But what about the functional brain network? Its efficient small-world topology raises the question about how the level of efficient wiring of the functional connections of the brain network is related to our level of intellectual performance. Neuroimaging studies have linked intelligence to the developmental course of specific high order brain regions (Shaw et al., 2006), total brain volume (Posthuma et al., 2002), focal brain structure (Thompson et al., 2001; Haier et al., 2004; Hulshoff Pol et al., 2006; Choi et al., 2008) and the functional dynamics of specific high cognitive brain regions (Duncan et al., 2000; Gray et al., 2003; Choi et al., 2008; Song et al., 2008). However, it remains unresolved how the level of efficient organization of the brain network is related to intellectual performance. In **chapter 7** of this thesis, using resting-state fMRI recordings and graph theory, we aim to examine whether, and if so how, the level of overall communication efficiency within the brain network is linked to intelligence.

outline of this thesis

The outline of this thesis is as follows. In **chapter 2**, we propose a voxel-wise representation of the functional brain network during resting-state to probe the overall network organization of the brain network in a much higher spatial detail than done before. In **chapter 3**, we examine the possible formation of clustered sub-networks within the full network, referred to as

resting-state networks, as an indication of a possible *modular* organization of the brain network at rest. We propose a new voxel-wise clustering method, called *normalized cut group clustering* to select resting-state networks from resting-state fMRI recordings on a group level. This graph clustering approach is designed to cluster voxels into group resting-state networks that consistently show a high level of resting-state functional connectivity across a group of subjects. Furthermore, in **chapter 4** we zoom in on the *primary motor network*, examining the possible formation of somatotopic organized functional sub-networks within the resting-state primary motor network.

In **chapter 5** and **6** we aim to examine the structural basis of functionally linked resting-state networks by combining resting-state fMRI recordings with Diffusion Tensor Imaging. In **chapter 5** we probe the structural core of resting-state networks. By examining whether the functionally linked regions of resting-state networks are structurally interconnected by anatomical white-matter tracts we aim to demonstrate the existence of a structural core of functional resting-state networks. In **chapter 6** in a combined resting-state fMRI/DTI study we zoom in on the structural and functional connections of the *default-mode network*. In this chapter, we examine a hypothesized association between the microstructural organization of the structural cingulum tract and the level of default mode functional connectivity.

In **chapter 7** we will examine the association between the level of efficient functional wiring of brain networks and human intelligence. The architecture of a network is known to be highly related to the level of efficient communication between the nodes of the network and in **chapter 7** we aim to examine whether and if so how the efficient small-world organization of the functional brain network is related to human intellectual performance.

What can these studies tell us about the functional organization of the healthy human brain? In **chapter 8** we will summarize the findings of our studies and discuss the interaction between the different studies in a broader perspective and propose suggestions for future research.

references

Achard S, Bullmore E (2007) Efficiency and cost of economical brain functional networks. PLoS Comput Biol 3:e17.

Achard S, Salvador R, Whitcher B, Suckling J, Bullmore E (2006) A resilient, low-frequency, small-world human brain functional network with highly connected association cortical hubs. J Neurosci 26:63-72.

Aertsen AM, Gerstein GL, Habib MK, Palm G (1989) Dynamics of neuronal firing correlation: modulation of "effective connectivity". J Neurophysiol 61:900-917.

Barabasi AL, Albert R (1999) Emergence of scaling in random networks. Science 286:509-512.

Barabasi AL, Bonabeau E (2003) Scale-free networks. Sci Am 288:60-69.

Beckmann CF, DeLuca M, Devlin JT, Smith SM (2005) Investigations into resting-state connectivity using independent component analysis. Philos Trans R Soc Lond B Biol Sci 360:1001-1013.

Birn RM, Diamond JB, Smith MA, Bandettini PA (2006) Separating respiratory-variation-related fluctuations from neuronal-activity-related fluctuations in fMRI. Neuroimage 31:1536-1548.

Birn RM, Smith MA, Jones TB, Bandettini PA (2008) The respiration response function: the temporal dynamics of fMRI signal fluctuations related to changes in respiration. Neuroimage 40:644-654.

Biswal B, Yetkin FZ, Haughton VM, Hyde JS (1995) Functional connectivity in the motor cortex of resting human brain using echo-planar MRI. Magn Reson Med 34:537-541.

Biswal BB, Van Kylen J, Hyde JS (1997) Simultaneous assessment of flow and BOLD signals in resting-state functional connectivity maps. NMR Biomed 10:165-170.

Buckner RL, Vincent JL (2007) Unrest at rest: Default activity and spontaneous network correlations. Neuroimage 37:1091-1096.

Bullmore E, Sporns O (2009) Complex brain networks: graph theoretical analysis of structural and functional systems. Nat Rev Neurosci 10:186-198.

Buzsaki G, Draguhn A (2004) Neuronal oscillations in cortical networks. Science 304:1926-1929.

Calhoun VD, Adali T, Pearlson GD, Pekar JJ (2001) A method for making group inferences from functional MRI data using independent component analysis. Hum Brain Mapp 14:140-151.

Chang C, Cunningham JP, Glover GH (2009) Influence of heart rate on the BOLD signal: the cardiac response function. Neuroimage 44:857-869.

Chen BL, Hall DH, Chklovskii DB (2006) Wiring optimization can relate neuronal structure and function. Proc Natl Acad Sci U S A 103:4723-4728.

Choi YY, Shamosh NA, Cho SH, DeYoung CG, Lee MJ, Lee JM, Kim SI, Cho ZH, Kim K, Gray JR, Lee KH (2008) Multiple bases of human intelligence revealed by cortical thickness and neural activation. J Neurosci 28:10323-10329.

Cordes D, Haughton VM, Arfanakis K, Wendt GJ, Turski PA, Moritz CH, Quigley MA, Meyerand ME (2000) Mapping functionally related regions of brain with functional connectivity MR imaging. AJNR Am J Neuroradiol 21:1636-1644.

Cordes D, Haughton VM, Arfanakis K, Carew JD, Turski PA, Moritz CH, Quigley MA, Meyerand ME (2001) Frequencies contributing to functional connectivity in the cerebral cortex in "resting-state" data. AJNR Am J Neuroradiol 22:1326-1333.

Damoiseaux JS, Rombouts SA, Barkhof F, Scheltens P, Stam CJ, Smith SM, Beckmann CF (2006) Consistent resting-state networks across healthy subjects. Proc Natl Acad Sci U S A 103:13848-13853.

De Luca M, Beckmann CF, De Stefano N, Matthews PM, Smith SM (2006) fMRI resting state networks define distinct modes of long-distance interactions in the human brain. Neuroimage 29:1359-1367.

Duncan J, Seitz RJ, Kolodny J, Bor D, Herzog H, Ahmed A, Newell FN, Emslie H (2000) A neural basis for general intelligence. Science 289:457-460.

Eguiluz VM, Chialvo DR, Cecchi GA, Baliki M, Apkarian AV (2005) Scale-free brain functional networks. Phys Rev Lett 94:018102.

Fornari E, Knyazeva MG, Meuli R, Maeder P (2007) Myelination shapes functional activity in the developing brain. Neuroimage 38:511-518.

Fox MD, Raichle ME (2007) Spontaneous fluctuations in brain activity observed with functional magnetic resonance imaging. Nat Rev Neurosci 8:700-711.

Friston KJ, Frith CD, Liddle PF, Frackowiak RS (1993) Functional connectivity: the principal-component analysis of large (PET) data sets. J Cereb Blood Flow Metab 13:5-14.

Gray JR, Chabris CF, Braver TS (2003) Neural mechanisms of general fluid intelligence. Nat Neurosci 6:316-322.

Greicius MD, Krasnow B, Reiss AL, Menon V (2003) Functional connectivity in the resting brain: a network analysis of the default mode hypothesis. Proc Natl Acad Sci U S A 100:253-258.

Greicius MD, Supekar K, Menon V, Dougherty RF (2008) Resting-State Functional Connectivity Reflects Structural Connectivity in the Default Mode Network. Cereb Cortex.

Grigorov MG (2005) Global properties of biological networks. Drug Discov Today 10:365-372.

Gusnard DA, Raichle ME, Raichle ME (2001) Searching for a baseline: functional imaging and the resting human brain. Nat Rev Neurosci 2:685-694.

Haier RJ, Jung RE, Yeo RA, Head K, Alkire MT (2004) Structural brain variation and general intelligence. Neuroimage 23:425-433.

Hulshoff Pol HE, Schnack HG, Posthuma D, Mandl RC, Baare WF, van Oel C, van Haren NE, Collins DL, Evans AC, Amunts K, Burgel U, Zilles K, de Geus E, Boomsma DI, Kahn RS (2006) Genetic contributions to human brain morphology and intelligence. J Neurosci 26:10235-10242.

Kiviniemi V, Kantola JH, Jauhiainen J, Hyvarinen A, Tervonen O (2003) Independent component analysis of nondeterministic fMRI signal sources. Neuroimage 19:253-260.

Latora V, Marchiori M (2001) Efficient behavior of small-world networks. Phys Rev Lett 87:198701.

Liu Y, Liang M, Zhou Y, He Y, Hao Y, Song M, Yu C, Liu H, Liu Z, Jiang T (2008) Disrupted small-world networks in schizophrenia. Brain 131:945.

Lowe MJ, Mock BJ, Sorenson JA (1996) Resting State fMRI Signal Correlations in Multi-slice EPI. Neuroimage 3.

Lowe MJ, Dzemidzic M, Lurito JT, Mathews VP, Phillips MD (2000) Correlations in low-frequency BOLD fluctuations reflect cortico-cortical connections. Neuroimage 12:582-587.

Mason MF, Norton MI, Van Horn JD, Wegner DM, Grafton ST, Macrae CN (2007) Wandering minds: the default network and stimulus-independent thought. Science 315:393-395.

Mathias N, Gopal V (2001) Small worlds: how and why. Phys Rev E Stat Nonlin Soft Matter Phys 63:021117.

Micheloyannis S, Pachou E, Stam CJ, Breakspear M, Bitsios P, Vourkas M, Erimaki S, Zervakis M (2006) Small-world networks and disturbed functional connectivity in schizophrenia. Schizophr Res 87:60-66.

Nir Y, Mukamel R, Dinstein I, Privman E, Harel M, Fisch L, Gelbard-Sagiv H, Kipervasser S, Andelman F, Neufeld MY, Kramer U, Arieli A, Fried I, Malach R (2008) Interhemispheric correlations of slow spontaneous neuronal fluctuations revealed in human sensory cortex. Nat Neurosci 11:8.

Penfield W, Boldrey E (1937) Somatic motor and sensory representation in the cerebral cortex of man as studied by electrical stimulation. Brain 60:54.

Posthuma D, De Geus EJ, Baare WF, Hulshoff Pol HE, Kahn RS, Boomsma DI (2002) The association between brain volume and intelligence is of genetic origin. Nat Neurosci 5:83-84.

Raichle ME, MacLeod AM, Snyder AZ, Powers WJ, Gusnard DA, Shulman GL (2001) A default mode of brain function. Proc Natl Acad Sci U S A 98:676-682.

Rasmussen TB (1977) Wilder Penfield: his legacy to neurology. Surgical treatment of epilepsy. Can Med Assoc J 116:1369-1370.

Rubinov M, Knock SA, Stam CJ, Micheloyannis S, Harris AW, Williams LM, Breakspear M (2007) Small-world properties of nonlinear brain activity in schizophrenia. Hum Brain Mapp.

Salvador R, Suckling J, Schwarzbauer C, Bullmore E (2005a) Undirected graphs of frequency-dependent functional connectivity in whole brain networks. Philos Trans R Soc Lond B Biol Sci 360:937-946.

Salvador R, Suckling J, Coleman MR, Pickard JD, Menon D, Bullmore E (2005b) Neurophysiological architecture of functional magnetic resonance images of human brain. Cereb Cortex 15:1332-1342.

Shaw P, Greenstein D, Lerch J, Clasen L, Lenroot R, Gogtay N, Evans A, Rapoport J, Giedd J (2006) Intellectual ability and cortical development in children and adolescents. Nature 440:676-679.

Shmuel A, Leopold DA (2008) Neuronal correlates of spontaneous fluctuations in fMRI signals in monkey visual cortex: Implications for functional connectivity at rest. Hum Brain Mapp.

Shmuel A, Yacoub E, Pfeuffer J, Van de Moortele PF, Adriany G, Hu X, Ugurbil K (2002) Sustained negative BOLD, blood flow and oxygen consumption response and its coupling to the positive response in the human brain. Neuron 36:1195-1210.

Shmueli K, van Gelderen P, de Zwart JA, Horovitz SG, Fukunaga M, Jansma JM, Duyn JH (2007) Low-frequency fluctuations in the cardiac rate as a source of variance in the resting-state fMRI BOLD signal. Neuroimage 38:306-320.

Smit DJ, Stam CJ, Posthuma D, Boomsma DI, de Geus EJ (2008) Heritability of "small-world" networks in the brain: a graph theoretical analysis of resting-state EEG functional connectivity. Hum Brain Mapp 29:1368-1378.

Song M, Zhou Y, Li J, Liu Y, Tian L, Yu C, Jiang T (2008) Brain spontaneous functional connectivity and intelligence. Neuroimage 41:1168-1176.

Sporns O (2006) Small-world connectivity, motif composition, and complexity of fractal neuronal connections. Biosystems 85:55-64.

Sporns O, Zwi JD (2004) The small world of the cerebral cortex. Neuroinformatics 2:145-162.

Sporns O, Tononi G, Edelman GM (2000) Connectivity and complexity: the relationship between neuroanatomy and brain dynamics. Neural Netw 13:909-922.

Sporns O, Honey CJ, Kotter R (2007) Identification and classification of hubs in brain networks. PLoS ONE 2:e1049.

Sporns O, Chialvo DR, Kaiser M, Hilgetag CC (2004) Organization, development and function of complex brain networks. Trends Cogn Sci 8:418-425.

Stam CJ (2004) Functional connectivity patterns of human magnetoencephalographic recordings: a 'small-world' network? Neurosci Lett 355:25-28.

Stam CJ, Reijneveld JC (2007) Graph theoretical analysis of complex networks in the brain. Nonlinear Biomed Phys 1:3.

Stam CJ, Jones BF, Nolte G, Breakspear M, Scheltens P (2007) Small-world networks and functional connectivity in Alzheimer's disease. Cereb Cortex 17:92-99.

Thirion B, Dodel S, Poline JB (2006) Detection of signal synchronizations in resting-state fMRI datasets. Neuroimage 29:321-327.

Thompson PM, Cannon TD, Narr KL, van Erp T, Poutanen VP, Huttunen M, Lonnqvist J, Standertskjold-Nordenstam CG, Kaprio J, Khaledy M, Dail R, Zoumalan CI, Toga AW (2001) Genetic influences on brain structure. Nat Neurosci 4:1253-1258.

Toosy AT, Ciccarelli O, Parker GJ, Wheeler-Kingshott CA, Miller DH, Thompson AJ (2004) Characterizing function-structure relationships in the human visual system with functional MRI and diffusion tensor imaging. Neuroimage 21:1452-1463.

Watts DJ, Strogatz SH (1998) Collective dynamics of 'small-world' networks. Nature 393:440-442.

Wise RG, Ide K, Poulin MJ, Tracey I (2004) Resting fluctuations in arterial carbon dioxide induce significant low frequency variations in BOLD signal. Neuroimage 21:1652-1664.

Worsley KJ, Chen JI, Lerch J, Evans AC (2005) Comparing functional connectivity via thresholding correlations and singular value decomposition. Philos Trans R Soc Lond B Biol Sci 360:913-920.

Xiong J, Parsons LM, Gao JH, Fox PT (1999) Interregional connectivity to primary motor cortex revealed using MRI resting state images. Hum Brain Mapp 8:151-156.

chapter 2

small-world and scale-free organization of voxel based resting-state functional connectivity in the human brain

martijn van den heuvel, cornelis stam, maria boersma, hilleke hulshoff pol

neuroimage 2008 43 (3)

The brain is a complex dynamic system of functionally connected regions. Graph theory has been successfully used to describe the organization of such dynamic systems. Recent resting-state fMRI studies have suggested that inter-regional functional connectivity shows a small-world modular topology, indicating an organization of the brain in highly clustered sub-networks, combined with a high level of global connectivity. In addition, a few studies have investigated a possible scale-free topology of the human brain, but the results of these studies have been inconclusive. These studies have mainly focused on inter-regional connectivity, representing the brain as a network of brain regions, requiring an arbitrary definition of such regions. However, using a voxel-wise approach allows for the model-free examination of both inter-regional as well as intra-regional connectivity and might reveal new information on network organization. Especially, a voxel-based study could give information about a possible scale-free organization of functional connectivity in the human brain. Resting-state 3 Tesla fMRI recordings of 28 healthy subjects were acquired and individual connectivity graphs were formed out of all cortical and sub-cortical voxels with connections reflecting inter-voxel functional connectivity. Graph characteristics from these connectivity networks were computed. The clustering-coefficient of these networks turned out to be much higher than the clustering-coefficient of comparable random graphs, together with a short average path length, indicating a small-world organization. Furthermore, the connectivity distribution of the number of inter-voxel connections followed a power-law scaling with an exponent close to 2, suggesting a scale-free network topology. Our findings suggest a combined

small-world and scale-free organization of the functionally connected human brain. The results are interpreted as evidence for a highly efficient organization of the functionally connected brain, in which voxels are mostly connected with their direct neighbors forming clustered sub-networks, which are held together by a small number of highly connected hub-voxels that ensure a high level of overall connectivity.

introduction

The brain is a complex dynamic system in which information is continuously processed and transferred to other interconnected regions with correlated functional dynamics (Sporns et al., 2000; Sporns et al., 2004). The temporal dependence of neuronal activity between different brain regions is known as functional connectivity (Aertsen et al., 1989; Friston et al., 1993) and is widely investigated by measuring the coherence of resting-state BOLD fMRI time-series. Of special interest are the low frequency oscillations (~0.01 - 0.1Hz) of BOLD fMRI time-series recorded during rest, as they have been observed to show correlated patterns between anatomically separated brain regions (Biswal et al., 1995; Cordes et al., 2000; Lowe et al., 2000). There is an ongoing debate on whether these resting-state BOLD signals predominantly result from physiological processes, like respiratory and cardiac oscillations (Wise et al., 2004; Birn et al., 2006) or whether these correlations originate from synchronization in the underlying neuronal activation patterns of these regions observed through a hemodynamic response function (Gusnard et al., 2001; Greicius et al., 2003; Buckner and Vincent, 2007). The latter view is supported by the observation that most of these correlations occur between cortical regions that are known to participate in the same functional network, for example regions of the motor, visual and auditory network (Biswal et al., 1997; Cordes et al., 2000; Greicius et al., 2003; Fox and Raichle, 2007). In addition, within cortical regions, these observed spontaneous BOLD patterns are mainly dominated by lower frequencies (< 0.1 Hz), with a minimal contribution of higher cardiac and respiratory oscillations (Cordes et al., 2000; Cordes et al., 2001). Furthermore, recently spontaneous BOLD fluctuations have been found to correlate with concurrent fluctuations in neuronal spiking, suggesting a direct link between resting-state time-lag BOLD signals and intrinsic neuronal activity (Shmuel and Leopold, 2008). In this context, it is believed that the resting-state BOLD fluctuations of cortical and sub-cortical regions, at least in part, originate from intrinsic neuronal activity (Biswal et al., 1995; Gusnard et al., 2001; Greicius et al., 2008); (Shmuel and Leopold, 2008) and that the observed temporal coherence between anatomically separated regions is reflecting

synchronization between the underlying neuronal activation patterns of these regions. Regions that show such a synchronized behavior are suggested to form functional resting-state brain networks (Biswal et al., 1995; Biswal et al., 1997; Xiong et al., 1999; Cordes et al., 2001; Gusnard et al., 2001; Greicius et al., 2003; Kiviniemi et al., 2003; Sun et al., 2004; Beckmann et al., 2005; Fox et al., 2005; Horwitz et al., 2005; Salvador et al., 2005a ; Damoiseaux et al., 2006; Thirion et al., 2006; Van den Heuvel et al., 2008).

To further probe the complex structure of functional brain networks a well-defined theoretical framework is needed. Biological systems can be represented as complex networks and examined by using 'graph theory'. A graph $G = (V,E)$ is a mathematical description of a network, consisting of a collection of elements (nodes) V and connections (edges) E interconnecting the nodes of the graph. Within this approach, the functionally connected brain can be represented as a network of regions with connections describing inter-regional functional connectivity (Sporns et al., 2000; Stam et al., 2003; Salvador et al., 2005a). Examining the connectivity architecture of the human brain may provide important information about its organization and function (Sporns et al., 2004), as the organization of a network is directly linked to its level of robustness, capability to integrate information and communication efficiency (Latora and Marchiori, 2001; Mathias and Gopal, 2001; Buzsaki and Draguhn, 2004; Grigorov, 2005). Two classes of networks are of special interest. *Small-world* networks are characterized by a high level of clustering and a short average node-to-node distance (Watts and Strogatz, 1998). In addition, *scale-free* networks are characterized by an average low number of connections per node, but with the existence of a small number of highly connected nodes that ensure a high level of global connectivity (Barabasi and Albert, 1999; Barabasi and Bonabeau, 2003). Small-world and scale-free organized networks are known to show a robust network architecture in which information can be transferred and integrated with a high level of efficiency (Latora and Marchiori, 2001; Mathias and Gopal, 2001; Sporns et al., 2004), forming an attractive model for the functionally connected human brain (Sporns and Zwi, 2004; Achard et al., 2006; Liu et al., 2008).

The most important properties that describe the topology of complex networks and characterize whether networks are small-world and/or scale-free organized are the distribution of the number of connections, the level of clustering and the average path length between the nodes of the network (Grigorov, 2005). The connectivity distribution $P(k)$ provides information about the connectivity organization of a network and is defined as the probability that a node is connected to k other nodes in the network. Furthermore, the clustering-coefficient C of a graph describes the

connectedness of the direct neighbors of the nodes and gives information on the level of local neighborhood clustering in the graph. The characteristic path length *L* is defined as the average shortest path between each two nodes in the graph and gives information on the global level of connectedness of a network. Together, *P(k)*, *C* and *L* provide important information about the connectivity topology of a network. *Scale-free* networks are characterized by a connectivity distribution that follows a power-law scaling $P(k) \sim k^{-\gamma}$, indicating that most of the nodes have only a limited number of connections, but that a small number of so-called hub-nodes have a large number of connections and are holding the network together (Barabasi and Albert, 1999 ; Grigorov, 2005). This in contrast to *random* connected networks, in which on average all nodes have the same number of connections (Barabasi and Albert, 1999 ; Grigorov, 2005). Furthermore, random connected networks have a low clustering-coefficient, suggesting a low formation of connected sub-graphs and a short average path length *L,* indicating that two nodes are never really far apart. *Small-world* organized networks show highly connected sub-networks, resulting in a high clustering-coefficient *C,* but still with a high level of global connectivity, as indicated by a typical short average path length *L* (Watts and Strogatz, 1998; Sporns et al., 2004). In general, small-world networks are characterized by a much higher clustering-coefficient than that of random organized networks, but still with an average path length that is of the same length of that of a random network (Watts and Strogatz, 1998). More formally, a small-world network is characterized by a ratio *gamma* γ between the clustering-coefficient *Cnet* and the clustering-coefficient *Crandom* of a random graph of >1 and a ratio *lambda* λ between the path length *Lnet* and the path length *Lrandom* of a random graph of ≈1. The small-world-ness of a graph can be expressed in a single parameter *sigma*, defined as the ratio between *gamma* and *lambda*. Sigma is typically >1 for networks with a small-world organization (Humphries et al., 2006).

A small number of studies have successfully investigated the small-world organization of resting-state functional connectivity using EEG, MEG and resting-state fMRI recordings, in both animal (Sporns and Zwi, 2004) and human studies (Breakspear et al., 2003; Stam, 2004; Eguiluz et al., 2005; Salvador et al., 2005b; Achard et al., 2006; Micheloyannis et al., 2006 ; Achard and Bullmore, 2007; Liu et al., 2008). Furthermore, functional networks have been suggested to overlap with underlying structural networks (Honey et al., 2007), suggesting that a small-world topology might be a general organization principle of the human brain. However, fMRI imaging studies have been less conclusive about a possible scale-free topology of the human

brain. Eguiluz et al. (Eguiluz et al., 2005) have reported a scale-free organization of the functionally connected brain on a voxel scale during the performance of a number of simple motor and auditory tasks, but a recent paper of Achard et al. (Achard et al., 2006) demonstrated a small-world organization of inter-regional connectivity, but not a scale-free architecture. However, most resting-state fMRI studies have focussed on inter-regional connectivity, examining the functional brain as a network of a fixed number of around 90 regions (Salvador et al., 2005b; Achard et al., 2006; Achard and Bullmore, 2007; Liu et al., 2008), reducing the data from a voxel resolution to a regional resolution. These studies have not taken into account intra-regional connectivity and functional interactions between sub-parts of brain regions. Examining the organization of the functionally connected resting brain on a voxel scale could provide additional information on the characteristics of the functionally connected brain. Especially, a voxel-wise approach could give more insight in a possible scale-free organization of the human brain.

In this study, the organization of the functionally connected human brain during a resting state was examined on a voxel scale. This resulted in a fine-grained representation of the functionally connected human brain in around 10000 voxels, rather than in the often used template driven parcellated representation of around 90 regions (Salvador et al., 2005b; Achard et al., 2006; Achard and Bullmore, 2007; Liu et al., 2008). Resting-state BOLD fMRI was acquired in 28 healthy subjects on a 3 Tesla MR scanner. For each individual dataset, a functional connectivity graph was formed out of all cortical and sub-cortical voxels, with the pair-wise correlation between the resting-state fMRI time-series as weighted connections between all voxels. From these individual connectivity networks a number of graph characteristics were computed, including the clustering-coefficient C and characteristic path length L and compared to the topology of random graphs with a similar connectivity degree and distribution (Watts and Strogatz, 1998). The small-world index was calculated as a marker of small-world organization (Humphries et al., 2006). Furthermore, the connectivity degree distribution $P(k)$ was examined as an indication of a possible scale-free organization of the functionally connected brain (Barabasi and Albert, 1999; Grigorov, 2005).

materials and methods

subjects

Data was acquired on a 3 Tesla Philips Achieva Medical scanner (Philips Medical Systems, Best, The Netherlands) at the University Medical Center Utrecht, The Netherlands. 28 healthy subjects with no psychiatric history (age mean/std : 25.1/7.1 ; gender: 14 male, 14 female) participated in this study after providing written informed consent as approved by the medial ethics committee for research in humans (METC) of the University Medical Center Utrecht, The Netherlands. During the resting-state fMRI, the scanner room was darkened and subjects were instructed to relax with their eyes closed and think of nothing in particular without falling asleep. Directly after the resting-state experiment the subjects were asked if they had not fallen asleep during the scanning session. Subjects who reported to have fallen asleep or reported to be close to falling asleep were excluded and a new subject was included as a replacement, resulting in the described group of 28 subjects.

acquisition

Resting-state Blood Oxygenation Level Dependent (BOLD) signals were recorded during a period of 8 minutes using a fast fMRI sequence (3D PRESTO (Golay et al., 2000; Neggers et al., 2008), acquisition parameters: TR/TE 22ms/32ms using shifted echo, flipangle of 9 degrees; SENSE p/s reduction 2/2; a dynamic scantime of 0.5 sec, 1000 timeframes, total duration 8 minutes; FOV 256x256 mm, isotropic voxelsize 4mm, 32 slices were acquired covering the whole brain). The high temporal acquisition was used to minimize possible back-folding effects (i.e. aliasing) of respiratory and cardiac oscillations (~0.3 Hz and ~0.9-1.0 Hz, respectively) into the lower resting-state frequencies of interest (0.01 - 0.1 Hz). Directly after the functional time-series an additional PRESTO scan with a better anatomical contrast was acquired due to an increased flipangle of 25 degrees for co-registration purposes. In addition, a T1 weighted image was acquired for anatomical reference (3D FFE, acquisition parameters: TR/TE 10ms/4.6ms, SENSE p/s reduction 1.7/1.4; FOV 256x256 mm, voxelsize 0.75x0.75x0.8mm, 200 slices).

preprocessing

All fMRI preprocessing steps were done with the SPM2 software package (http://www.fil.ion.ucl.ac.uk). First, the fMRI time-series were realigned to the last functional scan to correct for possible head-motion during the rest experiment. Registration to the last functional scan was used to maximize

the spatial overlap of the fMRI time-series with the high contrast functional scan. The realigned time-series were then coregistered to the high contrast functional scan, using the last functional scan as a source and the high contrast functional scan as a target. The T1 image was coregistered to the high contrast functional scan, to provide spatial alignment between the functional time-series and the anatomical image. Next, the T1 image and the fMRI time-series were normalized to standard space, using the MNI 305 T1 brain (Collins et al., 1994) as a template and the T1 image as a source. The T1 and fMRI time-series were normalized to correct for anatomical variation between the subjects, as possible differences in anatomical structure (e.g. the total number of (sub)-cortical voxels) could affect the graph analysis. It should be noted that the spatial normalization of fMRI time-series involves the interpolation of fMRI voxels and this could introduce (local) artificial correlations between voxels that are related to spatial smoothing and not to functional connectivity. To minimize further interpolation, no spatial filtering was applied to the fMRI time-series.

After registration, the functional time-series were bandpass filtered with a finite impulse response (FIR) bandpass filter to select the low resting-state frequencies of interest (0.01 - 0.1 Hz). The relatively high sampling-rate of the used resting-state fMRI PRESTO sequence enabled the proper sampling of cardiac and respiratory signals. Band-pass filtering minimized the influence of low frequency MR scanner noise (e.g. slow scanner drifts, typical < 0.01 Hz) and high frequency oscillations of cardiac or respiratory signals up to 1 Hz (> 0.1 - 1 Hz)(Cordes et al., 2001). Due to the nature of the PRESTO signal, PRESTO fMRI images have a low anatomical contrast between white matter and grey matter (Ramsey et al., 1998; Neggers et al., 2008). Therefore, cortical and subcortical voxels were selected based on a cortical segmentation of the T1 image. Cortical segmentation of the T1 was performed with the widely used and freely available Freesurfer software package (http://surfer.nmr.mgh.harvard.edu/). The segmentation maps were resliced to the 4x4x4 mm resolution of the resting-state fMRI times-series. For each individual dataset, the cortical segmentation was visually checked by overlapping the individual cortical segmentation map on the individual T1 image to verify a proper grey matter classification. No large misclassifications of white matter or cerebral spinal fluid (CSF) voxels as gray matter voxels were found in any of the individual T1 images. Supplementary figure 2.1 shows the cortical segmentation map of one of the subjects overlaid on the individual T1 image (supplementary figure 2.1a) and a 4x4x4 resliced version overlapped on one of the PRESTO fMRI images of this subject (supplementary figure 2.1b). Finally, the resliced segmentation maps were normalized to standard space, using the normalization

parameters of the T1 image, to overlap the filtered normalized fMRI time-series.

After preprocessing, the resting-state functional time-series were analyzed using a graph-theoretical approach. For each individual functional dataset, a graph *Gnet* was constructed out of all cortical and subcortical voxels and graph characteristics of *Gnet* were calculated (see below). In summary, from *Gnet* the clustering-coefficient *Cnet,* the characteristic path length *Lnet* and the distribution degree *P(k)* was calculated. *Cnet* and *Lnet* were compared to the clustering-coefficient and path length (i.e. *Crandom* and *Lrandom)* of a number of random graphs with a number of nodes *k* and a degree distribution *P(k)* similar to that of *Gnet.* Furthermore, the ratios *gamma* and *lambda* were computed as well as the small-world index (Humphries et al., 2006) as an indication of a possible small-world organization. The connectivity distribution of *Gnet* was computed as the occurrence probability *P(k)* of nodes of degree *k* in *Gnet* and fitted a power-law function as an indication of a possible scale-free organization of the functionally connected brain at a voxel scale.

graph analysis

graph formation

For each individual functional dataset, a connectivity graph *Gnet = (V,E)* was formed, with V the collection of N grey matter voxels and E the collection of connections (edges) between the functionally connected voxels. N varied around 10000 across the groups of subjects. figure 2.1 illustrates the various steps of the applied graph analysis. The first step (figure 2.1, panel a) consisted of the computation of the zero-lag temporal correlations between the filtered resting-state time-series of all voxel-pairs, believed to reflect the level of inter-voxel functional connectivity. These inter-voxel correlations were represented as a correlation matrix *M* with cell *M(i,j)* holding the zero-lag temporal correlation between the fMRI time-series of voxel i and voxel j (figure 2.1, panel b). Next, *M* was thresholded by a threshold *T*, setting all cells of M to 1 that exceeded the threshold and all cells to 0 that did not exceed this threshold, resulting in a binary valued matrix B (figure 2.1, panel c). This procedure resulted in the conversion of *M* in an unweighted graph *Gnet* (figure 2.1, panel d). In this, *Gnet = (V,E)* represented a network of all sub-cortical and cortical voxels of the brain with connections E between all functionally connected voxels.

T varied between 0 and 0.75 (with steps of 0.05). With increasing *T* more and more edges were removed from *Gnet* making the graph more and

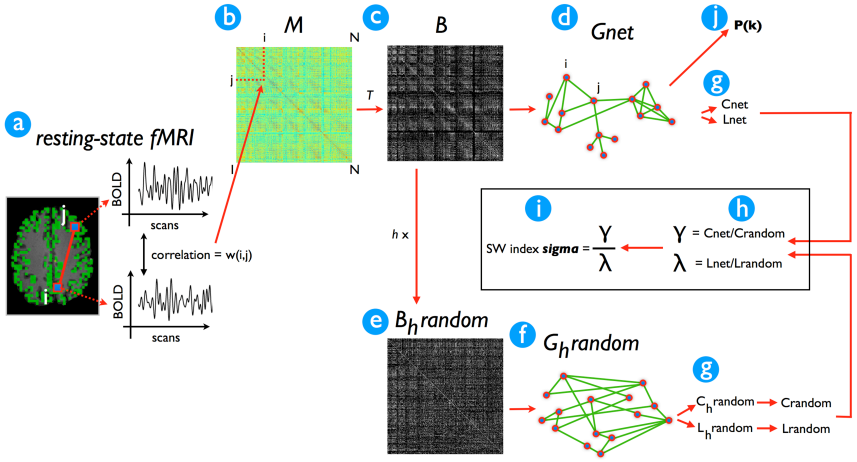

figure 2.1 schematic illustration of the graph analysis The first step (***panel a***) consisted of calculating the temporal zero-lag correlations between the filtered fMRI BOLD time-series of all voxels, which was believed to reflect inter-voxel functional connectivity. The computed correlations were represented as a correlation matrix *M*, with cell *M(i,j)* holding the level of functional connectivity between voxel *i* and voxel *j* (***panel b***). *M* was thresholded with a threshold T (***panel c***), resulting in a binary connectivity matrix B, representing an unweighted graph *Gnet* (***panel d***). *T* varied between 0 and 0.75 (with steps of 0.05) and a range of fixed k between 4000 and 10. For each fixed k, *M* was thresholded with a computed *T* that corresponded exactly to a connectivity degree of *k* for that particular individual dataset. Next, *B* was randomized (***panel e***) to create a random graph *Grandom*, with a similar connectivity distribution *P(k)* as *Gnet*, but with a random organization of connections. *h* random graphs were formed per *Gnet*. From *Grandom* and *Gnet* the graph characteristics *Cnet*, *Lnet*, *Crandom*, *Lrandom* were computed (***panel g***). *Crandom* and *Lrandom* were created by averaging the clustering-coefficient and path length of the *h* random graphs. Next, γ and λ were computed, defined as *Cnet*/*Crandom* and *Lnet*/*Lrandom* (***panel h***), as well as the small-world index sigma as the ratio between γ and λ (SW index, ***panel i***) expressing the small-world-ness of *Gnet*. In addition, the connectivity distribution *P(k)* of *Gnet* was computed (***panel j***). Finally, the individual computed graph characteristics were averaged over the group of subjects and the group averaged connectivity distribution *P(k)* was fitted a power-law function to examine a possible scale-free organization of the functionally connected human brain.

more sparse. Increasing T would eventually lead to disconnecting voxels from the total graph (i.e. removing all the edges from a voxel). The maximum T was empirically set to 0.75 to minimize the number of disconnected voxels to a maximum of 5% of the total amount of voxels in Gnet over the group of subjects. In addition, for each threshold T, the size of

the largest connected component was computed to verify whether setting threshold *T* would lead to the formation of one large connected component, rather than the formation of multiple relatively large but mutually disconnected components. For thresholds $T \leqq 0.65$ the largest connected cluster included more than 90% and for $T \leqq 0.75$ the largest connected cluster included more than 80% of all nodes in *Gnet* over the group of subjects, indicating that thresholding with threshold *T* indeed resulted in the formation of one large connected component with only a relative small number of disconnected voxels for all used thresholds of *T* (data show in supplementary figure 2a). For each individual dataset, thresholding connectivity matrix *M* with increasing *T* resulted in 16 binary thresholded connectivity matrices (i.e. *B*) representations of *Gnet*, thresholded with increasing *T*. In addition, to account for possible varying effects of T on the individual connectivity graphs, the connectivity matrices were also thresholded as a function of the average connection degree k of *Gnet*. *k* was varied for 16 different settings between 4000 and 10 and for each k the *Gnet* was thresholded with the individual T that exactly corresponded to the selected k. This resulted in an additional 16 unweighted graphs *Gnet* for each individual dataset. For $4000 \leqq k \leqq 50$ the largest connected group of nodes consisted of more than 90% of the total group of nodes (supplementary figure 2b). For the lowest number of $k = 20$ and 10, the largest connected group of nodes consisted of 83% and 72% of all nodes in *Gnet* (supplementary figure 2b).

network characteristics

Next, the organizational characteristics of *Gnet* were calculated, including the *clustering-coefficient Cnet*, *characteristic path length Lnet* and the *connectivity distribution P(k)*.

The clustering-coefficient C_i of node *i* expresses the level of connectedness of the direct neighbors of node *i* and gives information on whether they form a connected subgroup in the total network. The clustering-coefficient C_i of voxel *i* is defined as the ratio of the number of edges between the neighbors of voxel *i* and the total number of possible edges between its neighbors. *Cnet* is defined as the average clustering-coefficients of all voxels in the graph (Watts and Strogatz, 1998; Sporns et al., 2004) :

$$Cnet = \frac{1}{N}\sum_{i \in G} C_i \tag{2.1}$$

with

$$C_i = \frac{\#\, edges\ in G_i}{\frac{1}{2}k_i(k_i - 1)} \tag{2.2}$$

and G_i the sub-graph of neighbors of voxel *i* and k_i the number of edges of voxel *i*.

The characteristic path length *Lnet* of a graph is defined as the average minimal distance between any two voxels in the graph and expresses how well the graph is connected globally. Taken distance *d(i,j)* the minimum distance between voxel *i* and *j* as the minimal number of edges that have to be crossed to travel from voxel *i* to voxel *j*, *Lnet* is defined as the average distance over all voxel-pairs. Formally,

$$Lnet = \frac{1}{N(N-1)}\sum_{i \neq j, i, j \in G} d(i, j) \tag{2.3}$$

for all *i* and *j* in *Gnet* with N the number of voxels in *Gnet*.

With increasing *T* more and more paths are removed from *Gnet* and this could result in disconnecting voxel *i* from the graph, giving an infinite distance *d(i,j)* between voxel *i* and all other voxels in *Gnet*. Therefore, disconnected voxels could have an effect on the computation of *Lnet* and *Cnet*. In this study, this effect was believed to be minimal, as the maximum *T* was selected to result in a maximum of only ≈ 500 (5% of the size of *Gnet*, 2% up to $T = 0.7$) disconnected voxels. To verify this believed minor effect, two solutions for handling with disconnected voxels were explored for the computation of *Lnet*. First, all disconnected voxels were removed from the graph, which would probably lead to a small underestimation of *Lnet*, as the maximum distances *d(i,j)* are removed. Second, all disconnected voxels were given a distance of the maximum distance in *Gnet* + 1, which would result in a small overestimation of *Lnet*. As expected, due to the fact that at maximum only a small number of the voxels in *Gnet* were disconnected, the two different solutions did not change the nature of the *Lnet* results, indicating that the disconnected voxels had only a minimal effect on the computation of *Lnet*. For the computation of *Cnet* two solutions were explored. First,

disconnected voxels were removed from the computation of *Cnet*, which would lead to an overestimation of *Cnet* as low connected nodes are ignored. Second, the disconnected voxels were given the absolute minimum of clustering-coefficient, i.e. a C_i of 0, which would lead to a small underestimation of *Cnet*. Similar to the computation of *Lnet*, these two methods of handling with disconnected voxels did not change the nature of the results of *Cnet*. This was believed to result from the fact that only a limited number of voxels in *Gnet* could be disconnected.

Cnet and *Lnet* express key characteristics of a graph, indicating whether the nodes of the graph are connected in a random or small-world order (Watts and Strogatz, 1998). Random networks are characterized by a low clustering-coefficient *Crandom*, indicating a limited formation of clustered sub-networks. Random networks have a more global connected character, indicated by a typical short path length *Lrandom*. In contrast, small-world networks show a high level of local ordering, indicating the formation of sub-graphs, but still with an average short path length of around the same length as the path length of random organized networks, ensuring an optimal level of global connectivity (Latora and Marchiori, 2001). Networks are called small-world if *Cnet* >> *Crandom* and *Lnet* ≈ *Lrandom*, with *Crandom* defined as the clustering-coefficient of a random network *Grandom* of similar size of *Gnet* (Sporns et al., 2004; Sporns, 2006) and with a similar average connection degree *k* and connectivity distribution *P(k)* to that of *Gnet* (Sporns and Zwi, 2004; Stam and Reijneveld, 2007). Similar, *Lrandom* is defined as the characteristic path length of *Grandom* (Watts and Strogatz, 1998). Small-world networks typically show a ratio *gamma* γ between *Cnet* and *Crandom* of >1, and a ratio *lambda* λ between *Lnet* and *Lrandom* of ≈1. γ and λ are formally given by:

$$\lambda = \frac{L_p^{net}}{L_p^{random}} \tag{2.4}$$

$$\gamma = \frac{C_p^{net}}{C_p^{random}} \tag{2.5}$$

The small-worldness of a graph can be expressed in the small-world index *sigma*, defined as the ratio between γ and λ (Humphries et al., 2006). *Sigma*

is typically >1 for networks with a small-world organization (Humphries et al., 2006).

The connectivity distribution *P(k)* of *Gnet* gives the probability that voxel *i* is connected to *k* other voxels in the graph and gives insight in the overall connectivity distribution of the graph. Scale-free networks were originally defined as networks that show a degree distribution that follows a power law of the form $P(k) \sim k^{-y}$ with an exponent *y* of 3 (Barabasi and Albert, 1999 ; Grigorov, 2005), but recent studies have also concluded scale-free properties for networks of exponents $2 < y < 3$ (Goh et al., 2001; Goh et al., 2002; Grigorov, 2005) and real-world biological networks have been classified with exponents around 2 (Goh et al., 2001). Most importantly, a scale-free architecture is characterized by a power-law scaled connectivity distribution, in contrast to random networks that show a Poisson shaped connectivity distribution (Barabasi and Bonabeau, 2003).

computed network characteristics

For each of the individual functional connectivity graphs *Gnet* the graph characteristics *Cnet* and *Lnet* were computed for varying *T* ranging from 0 to 0.75, with steps of 0.05 (figure 2.1, panel g). For each thresholded *Gnet*, *h* random graphs $G_h random$ were formed with similar *k* and *P(k)* as *Gnet* (figure 2.1, panel e). Sporns and Zwi (Sporns and Zwi, 2004) have suggested that statistical comparisons should be performed between networks of similar degree distributions. Theoretical random networks have a Poisson shaped degree distribution and this might differ from the degree distribution of *Gnet*. Therefore, for the creation of each random graph $G_h random$, *Gnet* was used as the original starting point and then for each node *i* the paths of node *i* were randomly distributed to random selected nodes in the graph, keeping the total number of connections of node *i* fixed (figure 2.1, panel e). This procedure was repeated for all nodes in *Gnet* until the connection topology of the original matrix (i.e. *Gnet*) was randomized, resulting in a random graph $G_h random$ with a degree distribution similar to that of *Gnet* (figure 2.1, panel f).

For each of the resulting random graphs $G_h random$ the graph characteristics $C_h random$ and $L_h random$ were computed (figure 2.1, panel g). From these *h* random graphs for each *Gnet, Crandom* and *Lrandom* were computed as:

$$Crandom = \frac{1}{h} \sum C_h random \qquad (2.6)$$

$$Lrandom = \frac{1}{h}\sum L_h random \qquad (2.7)$$

Next, γ, λ and the small-world index *sigma* were calculated for varying *T* (figure 2.1, panel h and i). *h* was set to 20 for $0.40 \leqq T \leqq 0.75$, to 10 for $0.2 \leqq T < 0.40$ and to 5 for $T < 0.2$ for computational reasons. In total, this resulted in 235 different thresholded graphs (i.e. *Gnet* and $G_h random$) of size N per individual dataset.

For each individual dataset, the frequency of occurrence of a voxel in *Gnet* having *k* connections was computed (figure 2.1, panel j). This resulted in an individual connectivity degree distribution *P(k)* for each of the varying correlation thresholds *T*.

In addition, to account for the varying effects of *T* on the individual connectivity graphs, *Cnet*, *Lnet*, *Crandom*, *Lrandom*, γ, λ, *sigma* and *P(k)* were also computed for a number of fixed *k*. Keeping *T* fixed could have varying effects on the connectivity graphs over the group of subjects, as the individual datasets are likely to vary in overall connectivity. Therefore, an additional analysis was performed, in which the average connectivity degree *k* was kept fixed over the individual datasets. For each fixed *k*, *M* was thresholded with a computed *T* that corresponded exactly to a connectivity degree of *k* for that particular dataset and *Cnet*, *Lnet*, *Crandom*, *Lrandom*, γ, λ, *sigma* and *P(k)* were computed. *k* varied for 16 settings, being 4000, 2000, 1500, 1000 - 100 (with steps of 100), 50, 20 and 10. The number of random graphs *h* per fixed *k* for the computation of *Crandom* and *Lrandom* was set to 10 for $20 \leqq k \leqq 700$, to 10 for $700 < k \leqq 1000$ and to 5 for $k \geqq 1500$ for computational reasons. This resulted in 260 different graphs (including both *Gnet* and $G_h random$) of size N per individual dataset.

For each individual dataset, this procedure resulted in a set of graph characteristics of the individual connectivity networks *Gnet*, including the clustering-coefficient *Cnet* and *Crandom*, path-length *Lnet* and *Lrandom*, γ, λ, and the small-world index *sigma* (figure 2.1). These resulting graph characteristics were averaged over the group of 28 subjects. In addition, the individual connectivity distributions were averaged over the group of subjects and fitted a power-law distribution

$$P(k) = ck^{-y} \qquad (2.8)$$

, as an indication of a possible scale-free organization of the functionally connected human brain.

connectivity map

A scale-free network is characterized by the existence of a small number of nodes that have many more connections than the other nodes of the network. The nodes that have such a high connectivity degree are referred to as hub-nodes and are suggested to play an important role in the overall network organization (Barabasi and Albert, 1999; Grigorov, 2005). An *exploratory* analysis was performed to examine the spatial location of these hub-regions in the brain. A group connectivity map (*group kmap*) was computed that reflected the topology of functional connectivity in the brain. First, individual connectivity maps *kmaps* were formed by flagging all sub-cortical and cortical voxel with their connectivity degree. In this exploratory analysis, the voxel-wise connectivity degrees were calculated for a T of 0.4. Second, the individual *kmaps* were smoothed with a 8 mm FWHM smoothing kernel (i.e. 2 fMRI voxels) to improve cross-subject overlap, but please note that smoothing may lead to an underestimation of the number of connections in thinner cortical regions. The individual *kmaps* were then scaled between 0 and 1, by dividing the connectivity degree values by the maximum value of the individual *kmap* to normalize the connectivity values over the group of subjects. Finally, a group *kmap* was formed by averaging the scaled individual *kmaps*. Voxels that showed a connectivity degree that was much higher than the average degree were marked as potential hub-voxels. An exploratory threshold was defined as the top 2.5% of the voxels that showed the highest connectivity degrees. This threshold was defined by sorting all group-wise connectivity degree values and selecting the first of the top 2.5% highest values. The voxels that showed a connectivity degree above this 2.5% threshold were marked as potential hub-regions.

results

clustering-coefficient and path length

The results for the group averaged clustering-coefficient *Cnet* and *Crandom* and their dependence on T are shown in figure 2a. *Cnet* was found to be significant higher than *Crandom*, for all values of $T \geqq 0.10$ [$p < 0.01$, Bonferroni corrected], indicating a higher level of ordering in the resting-state functional graph in comparison to a random connected graph. *Crandom* was calculated as the average clustering-coefficient of a set of h random graphs ($h = 20$ or $h = 10/5$ for less sparse graphs, see method section) with a

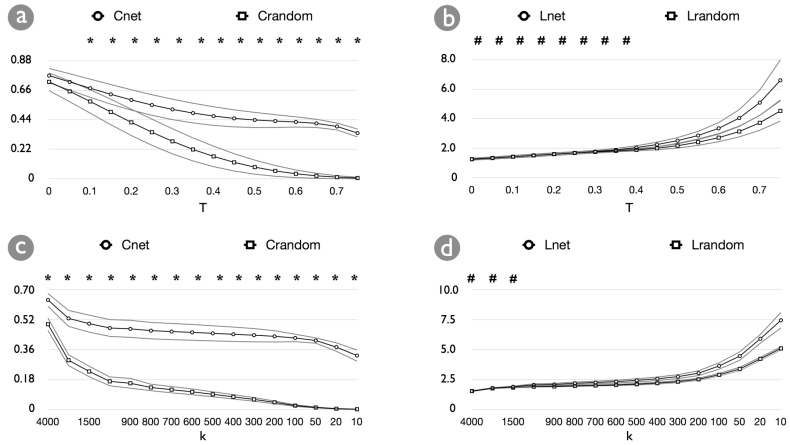

figure 2.2 group averaged clustering-coefficient and characteristic path length for varying *T* and varying k Figure 2.2a shows the group averaged clustering-coefficient *Cnet* of the graph representation *Gnet* of the functionally connected brain and its relation to the cut-off threshold *T*, as well as the clustering-coefficient *Crandom* of a random graph with similar connectivity degree k and distribution *P(k)* as *Gnet*. *Cnet* was found to be significant higher than *Crandom* for $T \geqq 0.10$ [$p < 0.01$, Bonferroni corrected, indicated by *]. Figure 2.2b shows the group averaged characteristic path length *Lnet* of *Gnet* as well as the characteristic path length *Lrandom* of a random graph with similar connectivity degree *k* and connectivity distribution *P(k)* and its dependence on *T*. *Lnet* was found not to be different from *Lrandom* for $T \leqq 0.35$ [$p < 0.01$, Bonferroni corrected, indicated by #]. Standard deviations are plotted in grey, expressing a low level of inter-subject variability over the group of subjects. No outliers were present in the group dataset. 2c and 2d show *Cnet*, *Crandom* and *Lnet*, *Lrandom* and their relation to the average connectivity degree k. *Cnet* was significant higher than *Crandom* for $k \leqq 4000$ [$p < 0.01$, Bonferroni corrected, indicated by *] and *Lnet* was found not to be different from *Lrandom* for $k \geqq 1500$ [$p < 0.01$, Bonferroni corrected, indicated by #]. Standard deviations of the group averaged clustering-coefficient and path length values are plotted in grey.

similar connectivity degree *k* and distribution *P(k)* as *Gnet*. As expected, *Cnet* decreased with increasing *T*, as more and more paths in graph *G* are removed. For the computation of *Cnet* and *Crandom* disconnected voxels were removed from the graph (see method section). The results for the group averaged characteristic path length *Lnet* and *Lrandom* and their relation to *T* are shown in figure 2b. The path length *Lnet* of the functional connected graph was found not to be significant different from the average

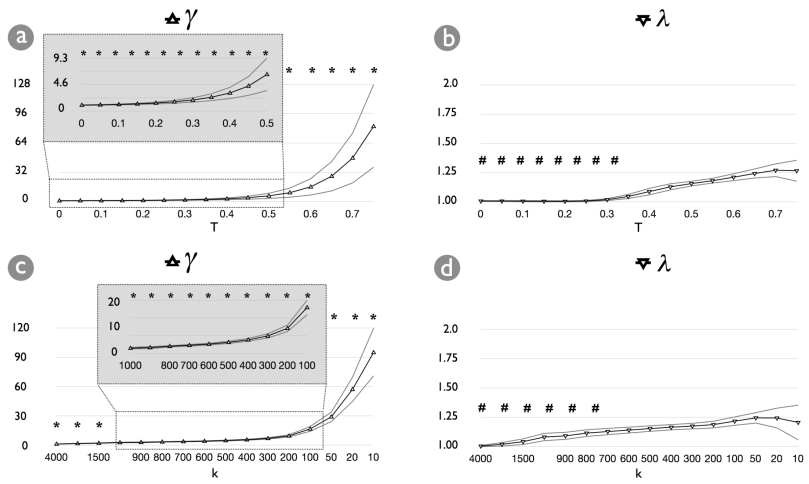

figure 2.3 γ **and** λ Figure 2.3a and 3b shows γ, defined as $Cnet/Crandom$ and λ defined as $Lnet/Lrandom$ and their dependence on the threshold *T*. γ was found to be significant >1 for all values of *T* [p < 0.01, Bonferroni corrected, indicated by *]. λ was found not to be different from 1 for *T* <0.4 [p < 0.01, Bonferroni corrected, indicated by *]. Figure 2.3c and 3d shows γ and λ and their dependence on k. γ was significant >1 for $k \leqq 4000$ [p < 0.01, Bonferroni corrected, indicated by *] and λ was found not to be different from 1 for $k \geqq 800$ [p < 0.01, Bonferroni corrected, indicated by #]. Error bars show the standard deviations of the group averaged γ and and indicate a low level of inter-subject variability of γ and λ over the group of subjects.

path length of a random network with similar *k* and *P(k)* for $T \leqq 0.35$ [p < 0.01, Bonferroni corrected]. As shown in figure 2b, *Lnet* increased with increasing *T*. This was expected as with increasing *T* more and more paths are removed and an increasing number of paths have to be crossed to travel from voxel *i* to voxel *j*, resulting in an overall increasing path length. The results for *Cnet*, *Crandom*, *Lnet* and *Lrandom* and their relation to *k* are given in figure 2c and 2d. *Cnet* was found to be significant higher than *Crandom* for $k \leqq 2000$ [p < 0.01, Bonferroni corrected]. *Lnet* and *Lrandom* were found not to be different for $k \geqq 1500$ [p < 0.01, Bonferroni corrected]. Error bars in figure 2.2 show the standard deviations of the group averaged *Cnet*, *Crandom*, *Lnet*, and *Lrandom*. The low standard deviations indicated a low level of inter-subject variability. The group data did not show any outliers.

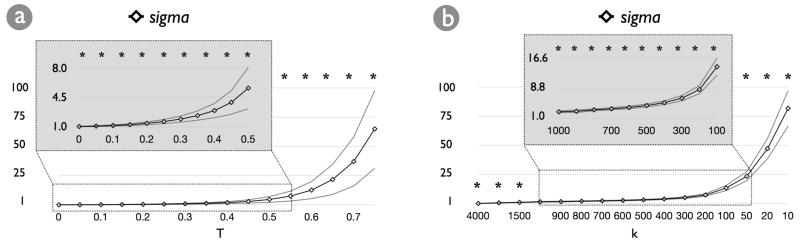

figure 2.4 small-world index sigma Figure 2.4a and 4b show the small-world index sigma (i.e. γ / λ) for varying *T* and varying *k*. Sigma was found to be significant >1 for all *T* (figure 2.4a) and for all $k \leqq 4000$ (figure 2.4b) [$p < 0.01$, Bonferroni corrected, indicated by *], suggesting a small-world organization of the functionally connected brain at a voxel scale. Standard deviations over the group of subjects are plotted in grey and suggest a low level of inter-subject variability.

γ *and* λ

Figure 2.3a and 3b show the group averaged γ and λ over the group of subjects for varying *T*. γ was significantly higher than 1 for all *T* [$p < 0.01$, Bonferroni corrected], λ was found not to be different from 1 for $T \leqq 0.40$ [$p < 0.01$, Bonferroni corrected]. Figure 2.3c and 3d show γ and λ and their dependence on *k*. γ was significantly higher than 1 for all *k* [$p < 0.01$, Bonferroni corrected] and λ was found not to be different from 1 for $k \geqq 800$ [$p < 0.01$, Bonferroni corrected]. Grey lines in figure 2.3 show the standard deviations over the group of subjects, indicating the level of inter-subject variability. No outliers were found.

small-world index sigma

The group averaged small-world index *sigma* for *T* varying between 0 and 0.75 and *k* varying between 4000 and 10 are given in figure 2.4a and 4b. *Sigma* was found to be significant higher than 1 for all $T \geqq 0.1$ and for all *k*, suggesting a small-world organization of *Gnet*. Standard deviation error-bars in figure 2.4 express the level of inter-subject variability. No outliers were found.

connectivity distribution

The group averaged connectivity distribution *P(k)* is shown in figure 2.5a for a threshold *T* of 0.65, 0.70 and 0.75. The group averaged *P(k)* suggested to follow a power-law scaling decaying as $P(k) \sim c\, k^{-y}$ with exponents close to 2 ($T = 0.65$, $y = 1.8$; $T = 0.70$, $y = 1.9$; $T = 0.75$, $y = 2.1$). Dotted-line in figure 2.5a illustrates a power-law distribution of $y = 2.0$. The average connectivity distribution *P(k)* for fixed *k* of 50, 20 and 10 are shown in figure 2.5b, together with a fitted power-law distribution of exponents of 2 (dotted-line) ($k = 50$, $y = 1.6$; $k = 20$, $y = 1.9$; $k = 10$, $y = 2.1$). No outliers were found in the group of subjects.

connectivity map

Figure 2.6 depicts the regions that showed the highest (scaled) connectivity degree values of the *group kmap* for a *T* of 0.4. The top 2.5% of the highest connectivity degree values reflected a threshold of 0.61, the maximum found group averaged (scaled) connectivity value was 0.82. Figure 2.6 depicts the regions that showed a connectivity degree above this 2.5% threshold, i.e. the voxels that showed the largest number of connections in *Gnet*. These regions included the right and left thalamus, bilateral superior temporal lobe (BA 22/40/42), bilateral anterior cingulate cortex (BA 24) and bilateral posterior cingulate cortex/(pre)cuneus (BA 30/31/18).

discussion

The main findings of this study are a possible *small-world* and *scale-free* organization of the functionally connected human brain on a voxel level. Resting-state fMRI of 28 healthy subjects was acquired on a 3 Tesla MR scanner. For each individual dataset, a network was constructed out of all cortical and sub-cortical voxels with connections between functionally connected voxels. From this connectivity network a number of graph organization characteristics were computed. The clustering-coefficient turned out to be much higher than that of a random connected network of the same size, but still with an average short path length (figure 2.2). This graph topology was reflected in a γ of >1 and a λ of ≈1 and a small-world index >1 (figures 3 and 4), suggesting a small-world organization (Watts and Strogatz, 1998; Humphries et al., 2006) of the functionally connected brain during a resting-state. Furthermore, the connectivity distribution *P(k)* suggested to follow a power-law distribution for a range of higher *T* and average connectivity degree *k*. These results suggest a possible scale-free

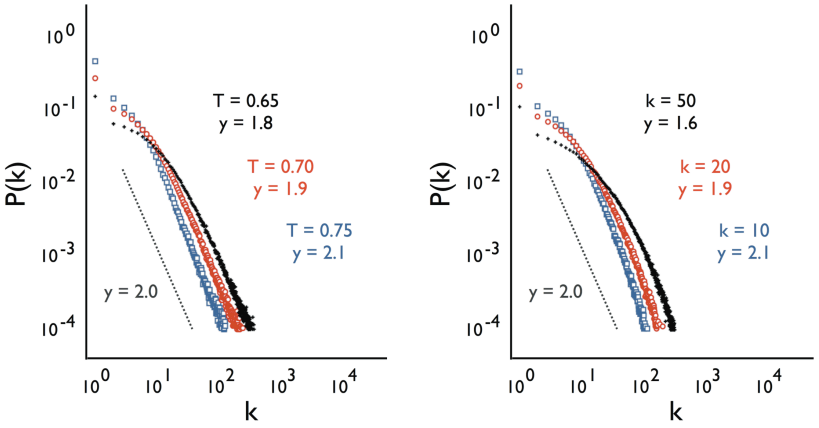

figure 2.5 connectivity distribution Figure 2.5a shows the connectivity distribution *P (k)* and fitted power-law functions for $T = 0.65$ (black cross), 0.7 (red circle) and 0.75 (blue square). Figure 2.5b shows the connectivity distribution *P(k)* and the fitted power-law functions for $k = 50$ (black cross), 20 (red circle) and 10 (blue square). The distributions followed a power-law function $P(k) \sim k^{-y}$, with exponents y close to 2, suggesting a possible scale-free organization of the functionally connected human brain at a voxel-scale. Note that figure has a different scaling from the version as published in Neuroimage.

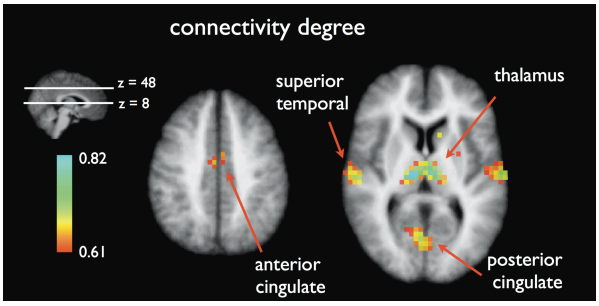

figure 2.6 potential hub-regions of the functional brain An additional analysis was performed to examine the topology of functional connectivity in the brain and to look for the location of potential hub-regions. Individual connectivity maps were smoothed (8mm FWHM, note that smoothing may lead to an underestimation of the connectivity degree of thin cortical regions) to improve cross-subject overlap and scaled between 0 and 1. Next, a group connectivity map was computed by averaging the scaled individual connectivity maps. The voxel-wise connectivity degree values were scaled between 0 and 1. A group connectivity maps was computed by averaging the individual scaled connectivity maps, reflecting the group averaged connectivity degree of all sub-cortical and cortical voxels. An

figure 2.6 (continuing)
exploratory threshold was set to the top 2.5% of the voxels that showed the highest scaled connectivity degree (i.e. the highest number of functional connections), reflecting a threshold of 0.61. The maximum value of the group connectivity map was found to be 0.82, indicating the maximum found connectivity degree. Figure shows the regions that showed a connectivity degree above the 2.5% threshold, indicating the regions with the highest connectivity degree of the functionally connected brain. These regions included the left and right thalamus, bilateral superior temporal lobe and anterior and posterior cingulate cortex/(pre)cuneus. The high connectivity degree of these voxels marks these regions as potential hub-regions.

topology of the functionally connected brain (figure 2.5) (Barabasi and Bonabeau, 2003). As far as we know, this is the first study that investigated a small-world and scale-free organization of functional connectivity in the human brain on a voxel scale during a resting-state.

Small-world networks are characterized by a high representation of strongly interconnected sub-networks, a property that follows directly from the high clustering-coefficient (Watts and Strogatz, 1998; Sporns and Zwi, 2004) and this suggests a high resilience to random loss of connections (Kaiser et al., 2007). The overall short characteristic path length demonstrates that nodes of the same sub-network and that of different sub-networks are generally connected by short paths (Watts and Strogatz, 1998), suggesting a high level of global communication efficiency (Latora and Marchiori, 2001). Furthermore, a possible a scale-free topology of the functionally connected brain suggests that the overall short path length is mediated by a small number of highly connected hub-regions. Scale-free networks show a surprising robustness to random failure of nodes, but are known to be vulnerable to target attack on the hubs (Albert et al., 2000; Callaway et al., 2000). A scale-free topology ensures an efficient and robust transport and flow processing in the network by avoiding congestion of information flow (Toroczkai and Bassler, 2004 ; Grigorov, 2005). The formation of scale-free networks has been suggested to follow a 'preferential attachment' principle, suggesting that new connections prefer to connect to nodes that already have a high number of connections (Albert and Barabasi, 2000). This effect is believed to be the result of a self-organized criticality principle (Levina et al., 2007). Taken together, a combined small-world and scale-free architecture may ensure an optimal form of network organization, forming a balance between maximum communication efficiency (Latora and Marchiori, 2001) and minimum wiring (Mathias and Gopal, 2001; Barabasi and Bonabeau, 2003).

These results raise the question about the functional implication of a possible small-world and scale-free organization of the human brain (Sporns et al., 2004). One interpretation of our results is that it might reflect an optimal minimized architecture (Mathias and Gopal, 2001) of the brain in which information is processed by highly interconnected networks of regions and efficiently transferred between networks for further processing (Salvador et al., 2005b; Achard and Bullmore, 2007; Liu et al., 2008). Indeed, recent group resting-state studies have suggested the consistent formation of a number of resting-state networks of regions that show a high level of resting-state functional connectivity (Beckmann et al., 2005; Damoiseaux et al., 2006; Van den Heuvel et al., 2008). Such an architecture of strongly connected networks is coherent with the observed high level of clustering. The overall short path length suggests an efficient communication transfer between regions that form such resting-state networks as well as a streamlined information transfer between regions of different networks. Furthermore, the observed power-law scaling of the connectivity distribution suggests a possible scale-free topology of the functional brain, which might indicate that most voxels are mostly connected to voxels within their specific sub-network and that inter-network communication is mediated by a small number, but highly connected hub-regions. An exploratory post-hoc analysis of the spatial topology of functional connectivity in the brain revealed a number of regions that showed a much higher connectivity degree than the rest of the nodes of the brain network (figure 2.6). These regions included the left and right thalamus and cortical regions overlapping the superior temporal lobe and anterior and posterior cingulate cortex and (pre)cuneus. The high connectivity degree marks these regions as potential hub-regions of the functional brain. These regions show large overlap with the hub-regions found by Archard et al. (Achard et al., 2006). Future studies are aimed to further investigate the key role of these hub-regions in the overall architecture of the functionally connected brain. Taken together, we believe that our results suggest a highly efficient organization of the functional brain, with an optimal balance between local and global connectivity (Watts and Strogatz, 1998), maximum communication efficiency (Latora and Marchiori, 2001 ; Achard and Bullmore, 2007) and minimum functional wiring between the regions of the brain (Mathias and Gopal, 2001).

In this study, a voxel-wise approach was used to investigate the organization of functional connectivity. Our results are coherent with the results of a number of recent studies reporting on a small-world organization of inter-regional functional connectivity in the human brain (Salvador et al., 2005b; Achard et al., 2006; Liu et al., 2006; Achard and

Bullmore, 2007; Liu et al., 2008). These studies have mainly focused on the organization of functional connectivity between brain regions, by using a predefined parcellation of the brain in around 90 regions. However, using a predefined regional template limits the examination to inter-regional connectivity and requires a model-based definition of such regions. In this study, both inter-regional as well as intra-regional connectivity was considered, forming a network out of voxels rather than 90 large regions. Using a voxel-based method, our results support previous regional-based findings and contribute to the idea of a small-world architecture of the human brain (Sporns and Zwi, 2004; Eguiluz et al., 2005; Salvador et al., 2005b ; Achard et al., 2006; Liu et al., 2006; He et al., 2007; Liu et al., 2008). In addition, our results also suggest a possible scale-free organization of the functional brain network. The results from two previous studies investigating such a scale-free topology of the brain have been inconclusive. A recent study of Achard et al. (Achard et al., 2006) investigating inter-regional resting-state functional connectivity reported a small-world, but not a scale-free organization of the human brain. In contrast, a study of Eguiluz et al. (Eguiluz et al., 2005) showed a combined small-world and scale-free topology. However, the results of that study were based on voxel-based task-induced fMRI measurements, rather than resting-state recordings. Task-induced fMRI recordings could have had an effect on the overall temporal activation patterns of the brain and as a result on the topology of functional connectivity. Therefore, in our study correlations between resting-state time-series were used as a more general measure of functional connectivity (Greicius et al., 2003; Salvador et al., 2005a; Achard et al., 2006). The observed power-law scaling with exponents close to 2 of the connectivity distribution for higher T in our study suggests a possible scale-free organization of the functionally connected brain. One explanation of the differentiating results of our study and the study of Achard et al. (Achard et al., 2006), concerning a possible scale-free organization, might lie in the included intra-regional connectivity in this study. Achard et al. focused on the organization of inter-regional functional connectivity between 90 brain regions, whereas in our study resting-state functional connectivity was investigated on a voxel scale, including both inter-regional as well as intra-regional connectivity. Interestingly, this differentiation in network topology of the brain might suggest a different organization of inter-regional connectivity and connectivity between smaller regions (i.e. voxels). One possible interpretation of our results might include that large brain regions are on average connected with around the same number of other brain regions, while sub-regions have on average a low number of connections,

but still stay globally connected through means of a small number of highly connected hub-regions.

The functional brain was represented as a network of small brain regions (i.e. voxels), without incorporating any information about the structural connections of the brain. An increasing body of evidence suggests a direct relation between these two forms of connectivity. For example, anatomical networks have been reported to show a similar small-world organization (Hagmann et al., 2007; He et al., 2007). In addition, networks of brain regions showing complex functional dynamics have been suggested to share common structural organization characteristics (Sporns et al., 2002; Sporns et al., 2000). Furthermore, regions of widespread functionally connected resting-state networks have been found to be connected by cortico-cortical anatomical tracts (Greicius et al., 2008; Lowe et al., 2008). Taken together, these results suggest a direct link between the functional and structural organization of the brain and a combined analysis could provide valuable information about the general architecture of the brain (Sporns et al., 2000; Sporns et al., 2004; Honey et al., 2007).

In this study we mainly focused on the overall connectivity architecture of the functionally connected human brain. However, the used voxel-wise approach allows for a much more specific examination of the functional brain network. It allows for the examination of functional connections on a high spatial resolution, for example the identification of inter-hemispheric and intra-hemispheric connections and a classification of their role in the network. Future studies are aimed to examine the specific role of different functional connections in the overall architecture of the brain network.

Analyzing the small-world properties of the functionally connected brain can be of importance in future clinical studies. Recent studies have suggested a disrupted small-world functional connectivity organization in schizophrenia in multiple EEG frequency bands (Micheloyannis et al., 2006; Rubinov et al., 2007). Furthermore, a recent resting-state fMRI study have reported disrupted small-world networks in schizophrenia (Liu et al., 2008). The use of a voxel-wise resting-state fMRI method could contribute to this field. It allows for the examination of disrupted functional connectivity in patients in high detail, providing information on which regions are affected. In general, examining the architecture of the brain on a voxel scale could provide a more detailed insight in the suggested disrupted functional organization in brain diseases, like schizophrenia (Liu et al., 2008) and Alzheimer's disease (Stam et al., 2007).

Some limitations to this study have to be considered in interpreting its results. First, the exact neuronal correlate of resting-state functional

connectivity is not fully understood. Although, it is believed that the coherency between the rest-recorded BOLD-sensitive fMRI time-series is related to a coherency in the underlying neuronal activation patterns of these regions (Biswal et al., 1997; Cordes et al., 2001; Greicius et al., 2003; Salvador et al., 2005b; Buckner and Vincent, 2007), it has also been suggested that physiological temporal patterns like respiratory and cardiac oscillations could confound the BOLD signal (Cordes et al., 2001; Wise et al., 2004). In this study, a high fMRI temporal acquisition was used to minimize the possible backfolding of cardiac and respiratory patterns into the lower frequencies of interest, enabling the proper filtering of these high frequency temporal patterns (Cordes et al., 2000; Cordes et al., 2001). However, cardiac related frequencies of >1 Hz could still be aliased into the lower frequencies of interest. In addition, there has been suggested that other non-neuronal related low frequency oscillations, like possible variations in heart rate or interactions between cardiac and respiratory signals can be present in the low resting-state frequencies of interest (~0.01 - 0.1 Hz) and could make the resting-state correlations less specific (Birn et al., 2006, 2008). Second, it should be noted that fMRI images show a certain level of intrinsic spatial smoothness and this could introduce artificial inter-voxel correlations that are not related to neuronal activity. Data interpolation as a result of the normalization of the fMRI time-series can further enhance this effect. Spatial smoothness could lead to an overestimation of the local inter-voxel correlations in *Gnet* and introduce a bias in the computation of the graph characteristics and have an effect on the scale-free aspects of the data. In this study, *Grandom* was formed by randomizing all connections of *Gnet* to maintain a similar connectivity distribution (Sporns and Zwi, 2004). However, when forming a comparable random graph *Grandom*, potential intrinsic spatial smoothness present in the fMRI recordings (and therefore present in *Gnet*) is destroyed. To examine the effect of spatial smoothness on the graph characteristics a post-hoc analysis was performed, in which the formation of *Grandom* was adjusted by redistributing only those connections of *Gnet* that connected voxels that were spatially separated by more than 10 mm (>2.5 voxels) (28 subjects, T varying between 0 and 0.7 with steps of 0.1, the number of random graphs h set to 1). As such, *Grandom* was formed in a much more conservative manner, maintaining *all* local connections that were present in *Gnet*, and thus ensuring a similar intrinsic smoothness profile as *Gnet*. Constructing *Grandom* in this alternative way did not change the nature of our results. As expected, the only difference found was that *Crandom* was slightly higher than the original *Crandom* (and only for high T). This difference was likely to result from the fact that *Grandom* was now more similar to *Gnet*. Taken together, these additional results suggest that the

intrinsic smoothness of fMRI data has only a minor influence on the computation of the graph characteristics and does not affect the main results of this study. In addition, to test the influence of the normalization step on the final results, a second post-hoc analysis was performed, in which *Gnet* was based on the native non-normalized individual time-series, rather than the normalized fMRI time-series. Analyzing the data in native space (i.e. non-normalized) did not change the nature of the results, which suggests that the normalization step had only a minor influence on the computation of the graph characteristics. Third, as in all resting-state fMRI studies using graph analysis, partial voluming effects due to the relatively large fMRI voxels of 3 to 4 mm and the inclusion of misclassified CSF or white matter voxels into *Gnet* could potentially introduce artificial correlations that are not related to neuronal synchronization. As a result, they could in theory explain the found effects. To examine the effects of white matter and CSF voxels on the computed graph statistics an additional post-hoc analysis was performed, in which the connectivity graphs were formed out of all classified white matter (*Gwm*) and CSF (*Gcsf*) voxels. From these connectivity graphs the general graph characteristics were computed, in a similar way as described in the main analysis (figure 2.1). Both *Gwm* and *Gcsf* showed a high clustering-coefficient and a much higher path length than *Gnet*, typical for networks with a so-called 'regular' organization, lacking the existence of long distance connections critical for a *small-world* organization. In addition, the degree distribution of *Gwm* and *Gcsf* did not show the typical scale-free organization as found for *Gnet*. This post-hoc analysis suggests that white matter and CSF related correlations show a different organization in comparison to correlations between grey matter voxels and that they are likely to only minimally influence the computed graph characteristics of *Gnet*. Fourth, as with all cross-correlation methods, the association between points is based on linear effects. Other measures like s*ynchronization likelihood* have been successfully introduced as a measure of nonlinear coupling of EEG and MEG signals (Stam et al., 2003) and could make a valuable contribution to resting-state fMRI investigations. In addition, methods to calculate the network characteristics of weighted graphs have been suggested, as well as measures of global and local communication efficiency (Latora and Marchiori, 2001; Achard and Bullmore, 2007; Reijneveld et al., 2007; Stam and Reijneveld, 2007) and used as an effective method to control for disconnected nodes that are likely to arise with increasing cut-off thresholds (Ponten et al., 2007). In this study, the traditional definition of the clustering-coefficient was used (Watts and Strogatz, 1998; Achard and Bullmore, 2007; Stam and Reijneveld, 2007), but more advanced versions have been suggested. Soffer et al. (Soffer and Vazquez, 2005) showed that the

traditional definition is biased to the number of connections of a node and have suggested a non-biased definition. Future studies are aimed to investigate the use of these novel measures of network dynamics in a voxel-based approach.

In this study, the organization of functional connectivity in the human brain was examined on a voxel scale. Graph theory was used to investigate 3T resting-state fMRI recordings of 28 healthy subjects by forming individual networks out of all cortical and sub-cortical voxels, with connections between functionally connected voxels. The use of a voxel-wise approach allowed for the examination of inter-regional connectivity as well as intra-regional connectivity. Our results suggest a possible combined *small-world* and *scale-free* organization of the functionally connected human brain.

references

Achard S, Bullmore E (2007) Efficiency and cost of economical brain functional networks. PLoS Comput Biol 3:e17.

Achard S, Salvador R, Whitcher B, Suckling J, Bullmore E (2006) A resilient, low-frequency, small-world human brain functional network with highly connected association cortical hubs. J Neurosci 26:63-72.

Aertsen AM, Gerstein GL, Habib MK, Palm G (1989) Dynamics of neuronal firing correlation: modulation of "effective connectivity". J Neurophysiol 61:900-917.

Albert R, Barabasi AL (2000) Topology of evolving networks: local events and universality. Phys Rev Lett 85:5234-5237.

Albert R, Jeong H, Barabasi AL (2000) Error and attack tolerance of complex networks. Nature 406:378-382.

Barabasi AL, Albert R (1999) Emergence of scaling in random networks. Science 286:509-512.

Barabasi AL, Bonabeau E (2003) Scale-free networks. Sci Am 288:60-69.

Beckmann CF, DeLuca M, Devlin JT, Smith SM (2005) Investigations into resting-state connectivity using independent component analysis. Philos Trans R Soc Lond B Biol Sci 360:1001-1013.

Birn RM, Diamond JB, Smith MA, Bandettini PA (2006) Separating respiratory-variation-related fluctuations from neuronal-activity-related fluctuations in fMRI. Neuroimage 31:1536-1548.

Birn RM, Smith MA, Jones TB, Bandettini PA (2008) The respiration response function: the temporal dynamics of fMRI signal fluctuations related to changes in respiration. Neuroimage 40:644-654.

Biswal B, Yetkin FZ, Haughton VM, Hyde JS (1995) Functional connectivity in the motor cortex of resting human brain using echo-planar MRI. Magn Reson Med 34:537-541.

Biswal BB, Van Kylen J, Hyde JS (1997) Simultaneous assessment of flow and BOLD signals in resting-state functional connectivity maps. NMR Biomed 10:165-170.

Breakspear M, Terry JR, Friston KJ, Harris AW, Williams LM, Brown K, Brennan J, Gordon E (2003) A disturbance of nonlinear interdependence in scalp EEG of subjects with first episode schizophrenia. Neuroimage 20:466-478.

Buckner RL, Vincent JL (2007) Unrest at rest: Default activity and spontaneous network correlations. Neuroimage 37:1091-1096.

Buzsaki G, Draguhn A (2004) Neuronal oscillations in cortical networks. Science 304:1926-1929.

Callaway DS, Newman ME, Strogatz SH, Watts DJ (2000) Network robustness and fragility: percolation on random graphs. Phys Rev Lett 85:5468-5471.

Collins DL, Neelin P, Peters TM, Evans AC (1994) Automatic 3D intersubject registration of MR volumetric data in standardized Talairach space. J Comput Assist Tomogr 18:192-205.

Cordes D, Haughton VM, Arfanakis K, Wendt GJ, Turski PA, Moritz CH, Quigley MA, Meyerand ME (2000) Mapping functionally related regions of brain with functional connectivity MR imaging. AJNR Am J Neuroradiol 21:1636-1644.

Cordes D, Haughton VM, Arfanakis K, Carew JD, Turski PA, Moritz CH, Quigley MA, Meyerand ME (2001) Frequencies contributing to functional connectivity in the cerebral cortex in "resting-state" data. AJNR Am J Neuroradiol 22:1326-1333.

Damoiseaux JS, Rombouts SA, Barkhof F, Scheltens P, Stam CJ, Smith SM, Beckmann CF (2006) Consistent resting-state networks across healthy subjects. Proc Natl Acad Sci U S A 103:13848-13853.

Eguiluz VM, Chialvo DR, Cecchi GA, Baliki M, Apkarian AV (2005) Scale-free brain functional networks. Phys Rev Lett 94:018102.

Fox MD, Raichle ME (2007) Spontaneous fluctuations in brain activity observed with functional magnetic resonance imaging. Nat Rev Neurosci 8:700-711.

Fox MD, Snyder AZ, Vincent JL, Corbetta M, Van Essen DC, Raichle ME (2005) The human brain is intrinsically organized into dynamic, anticorrelated functional networks. Proc Natl Acad Sci U S A 102:9673-9678.

Friston KJ, Frith CD, Liddle PF, Frackowiak RS (1993) Functional connectivity: the principal-component analysis of large (PET) data sets. J Cereb Blood Flow Metab 13:5-14.

Goh KI, Kahng B, Kim D (2001) Universal behavior of load distribution in scale-free networks. Phys Rev Lett 87:278701.

Goh KI, Oh E, Jeong H, Kahng B, Kim D (2002) Classification of scale-free networks. Proc Natl Acad Sci U S A 99:12583-12588.

Golay X, Pruessmann KP, Weiger M, Crelier GR, Folkers PJ, Kollias SS, Boesiger P (2000) PRESTO-SENSE: an ultrafast whole-brain fMRI technique. Magn Reson Med 43:779-786.

Greicius MD, Krasnow B, Reiss AL, Menon V (2003) Functional connectivity in the resting brain: a network analysis of the default mode hypothesis. Proc Natl Acad Sci U S A 100:253-258.

Greicius MD, Supekar K, Menon V, Dougherty RF (2008) Resting-State Functional Connectivity Reflects Structural Connectivity in the Default Mode Network. Cereb Cortex.

Grigorov MG (2005) Global properties of biological networks. Drug Discov Today 10:365-372.

Gusnard DA, Raichle ME, Raichle ME (2001) Searching for a baseline: functional imaging and the resting human brain. Nat Rev Neurosci 2:685-694.

Hagmann P, Kurant M, Gigandet X, Thiran P, Wedeen VJ, Meuli R, Thiran JP (2007) Mapping human whole-brain structural networks with diffusion MRI. PLoS ONE 2:e597.

He Y, Chen ZJ, Evans AC (2007) Small-world anatomical networks in the human brain revealed by cortical thickness from MRI. Cereb Cortex 17:2407-2419.

Honey CJ, Kotter R, Breakspear M, Sporns O (2007) Network structure of cerebral cortex shapes functional connectivity on multiple time scales. Proc Natl Acad Sci U S A 104:10240-10245.

Horwitz B, Warner B, Fitzer J, Tagamets MA, Husain FT, Long TW (2005) Investigating the neural basis for functional and effective connectivity. Application to fMRI. Philos Trans R Soc Lond B Biol Sci 360:1093-1108.

Humphries MD, Gurney K, Prescott TJ (2006) The brainstem reticular formation is a small-world, not scale-free, network. Proc Biol Sci 273:503-511.

Kaiser M, Martin R, Andras P, Young MP (2007) Simulation of robustness against lesions of cortical networks. Eur J Neurosci 25:3185-3192.

Kiviniemi V, Kantola JH, Jauhiainen J, Hyvarinen A, Tervonen O (2003) Independent component analysis of nondeterministic fMRI signal sources. Neuroimage 19:253-260.

Latora V, Marchiori M (2001) Efficient behavior of small-world networks. Phys Rev Lett 87:198701.

Levina A, Herrmann JM, Geisel T (2007) Dynamical Synapses Causing Self-Organized Criticality in Neural Networks. Nature Physics 3:3.

Liu H, Liu Z, Liang M, Hao Y, Tan L, Kuang F, Yi Y, Xu L, Jiang T (2006) Decreased regional homogeneity in schizophrenia: a resting state functional magnetic resonance imaging study. Neuroreport 17:19-22.

Liu Y, Liang M, Zhou Y, He Y, Hao Y, Song M, Yu C, Liu H, Liu Z, Jiang T (2008) Disrupted small-world networks in schizophrenia. Brain 131:945.

Lowe MJ, Dzemidzic M, Lurito JT, Mathews VP, Phillips MD (2000) Correlations in low-frequency BOLD fluctuations reflect cortico-cortical connections. Neuroimage 12:582-587.

Lowe MJ, Beall EB, Sakaie KE, Koenig KA, Stone L, Marrie RA, Phillips MD (2008) Resting state sensorimotor functional connectivity in multiple sclerosis inversely correlates with transcallosal motor pathway transverse diffusivity. Hum Brain Mapp.

Mathias N, Gopal V (2001) Small worlds: how and why. Phys Rev E Stat Nonlin Soft Matter Phys 63:021117.

Micheloyannis S, Pachou E, Stam CJ, Breakspear M, Bitsios P, Vourkas M, Erimaki S, Zervakis M (2006) Small-world networks and disturbed functional connectivity in schizophrenia. Schizophr Res 87:60-66.

Neggers SF, Hermans EJ, Ramsey NF (2008) Enhanced sensitivity with fast three-dimensional blood-oxygen-level-dependent functional MRI: comparison of SENSE-PRESTO and 2D-EPI at 3 T. NMR Biomed:In Press.

Ponten SC, Bartolomei F, Stam CJ (2007) Small-world networks and epilepsy: graph theoretical analysis of intracerebrally recorded mesial temporal lobe seizures. Clin Neurophysiol 118:918-927.

Ramsey NF, van den Brink JS, van Muiswinkel AM, Folkers PJ, Moonen CT, Jansma JM, Kahn RS (1998) Phase navigator correction in 3D fMRI improves detection of brain activation: quantitative assessment with a graded motor activation procedure. Neuroimage 8:240-248.

Reijneveld JC, Ponten SC, Berendse HW, Stam CJ (2007) The application of graph theoretical analysis to complex networks in the brain. Clin Neurophysiol 118:2317-2331.

Rubinov M, Knock SA, Stam CJ, Micheloyannis S, Harris AW, Williams LM, Breakspear M (2007) Small-world properties of nonlinear brain activity in schizophrenia. Hum Brain Mapp.

Salvador R, Suckling J, Schwarzbauer C, Bullmore E (2005a) Undirected graphs of frequency-dependent functional connectivity in whole brain networks. Philos Trans R Soc Lond B Biol Sci 360:937-946.

Salvador R, Suckling J, Coleman MR, Pickard JD, Menon D, Bullmore E (2005b) Neurophysiological architecture of functional magnetic resonance images of human brain. Cereb Cortex 15:1332-1342.

Shmuel A, Leopold DA (2008) Neuronal correlates of spontaneous fluctuations in fMRI signals in monkey visual cortex: Implications for functional connectivity at rest. Hum Brain Mapp.

Soffer SN, Vazquez A (2005) Network clustering coefficient without degree-correlation biases. Phys Rev E Stat Nonlin Soft Matter Phys 71:057101.

Sporns O (2006) Small-world connectivity, motif composition, and complexity of fractal neuronal connections. Biosystems 85:55-64.

Sporns O, Zwi JD (2004) The small world of the cerebral cortex. Neuroinformatics 2:145-162.

Sporns O, Tononi G, Edelman GM (2000) Connectivity and complexity: the relationship between neuroanatomy and brain dynamics. Neural Netw 13:909-922.

Sporns O, Tononi G, Edelman GM (2002) Theoretical neuroanatomy and the connectivity of the cerebral cortex. Behav Brain Res 135:69-74.

Sporns O, Chialvo DR, Kaiser M, Hilgetag CC (2004) Organization, development and function of complex brain networks. Trends Cogn Sci 8:418-425.

Stam CJ (2004) Functional connectivity patterns of human magnetoencephalographic recordings: a 'small-world' network? Neurosci Lett 355:25-28.

Stam CJ, Reijneveld JC (2007) Graph theoretical analysis of complex networks in the brain. Nonlinear Biomed Phys 1:3.

Stam CJ, Breakspear M, van Cappellen van Walsum AM, van Dijk BW (2003) Nonlinear synchronization in EEG and whole-head MEG recordings of healthy subjects. Hum Brain Mapp 19:63-78.

Stam CJ, Jones BF, Nolte G, Breakspear M, Scheltens P (2007) Small-world networks and functional connectivity in Alzheimer's disease. Cereb Cortex 17:92-99.

Sun FT, Miller LM, D'Esposito M (2004) Measuring interregional functional connectivity using coherence and partial coherence analyses of fMRI data. Neuroimage 21:647-658.

Thirion B, Dodel S, Poline JB (2006) Detection of signal synchronizations in resting-state fMRI datasets. Neuroimage 29:321-327.
Toroczkai Z, Bassler KE (2004) Network dynamics: jamming is limited in scale-free systems. Nature 428:716.
Van den Heuvel MP, Mandl RC, Hulshoff Pol HE (2008) Normalized group clustering of resting-state fMRI data. PLoS ONE 3:e2001.
Watts DJ, Strogatz SH (1998) Collective dynamics of 'small-world' networks. Nature 393:440-442.
Wise RG, Ide K, Poulin MJ, Tracey I (2004) Resting fluctuations in arterial carbon dioxide induce significant low frequency variations in BOLD signal. Neuroimage 21:1652-1664.
Xiong J, Parsons LM, Gao JH, Fox PT (1999) Interregional connectivity to primary motor cortex revealed using MRI resting state images. Hum Brain Mapp 8:151-156.

supplementary information

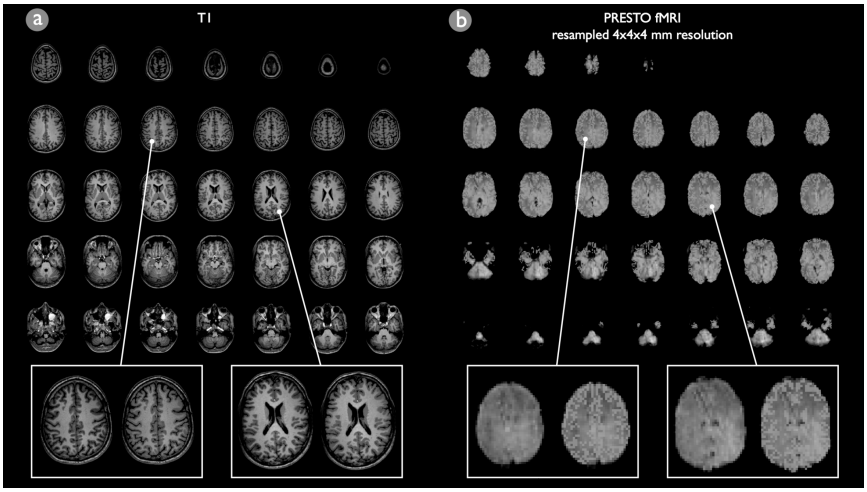

supplementary figure 2.1 cortical segmentation map Figure shows a typical cortical segmentation map of one of the subjects overlaid on the individual T1 image (***panel a***) and a 4x4x4 resliced version on one of the PRESTO fMRI images of this particular subject (***panel b***). For each individual dataset, the cortical segmentation was visually checked by overlapping the individual cortical segmentation map on the individual T1 image to verify a proper grey matter classification. No large misclassification of white matter and cerebral spinal fluid (CSF) voxels as gray matter voxels was found in any of the individual datasets. Color version online (van den Heuvel et al. Neuroimage 2008).

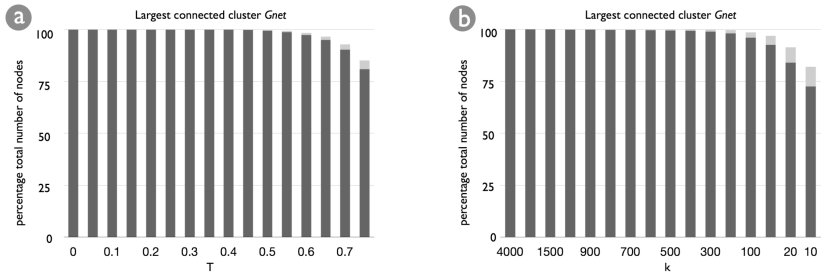

supplementary figure 2.2 largest connected cluster of nodes in *Gnet* For each individual dataset, a collection of connectivity graphs *Gnet* were formed by thresholding thresholding a connectivity matrix *M*, formed out of the temporal correlations between all possible voxel pairs. *M* was thresholded with a range of thresholds *T*, varying between 0 and 0.75 (with steps of 0.05). Increasing *T* would eventually lead to the removal of more and more edges, making *Gnet* more and more sparse. To verify that applying *T* would lead to the formation of one large connected component, rather than the formation of multiple relatively large but mutually disconnected components, the size of the largest connected cluster of *Gnet* was computed for all *T*. Figure 2.2a shows the largest connected cluster in *Gnet* in percentage of the total number of nodes, averaged over the 28 subjects. Green bars show the standard deviation over the group of subjects. For all thresholds *T* the largest connected cluster on average included more than 80% of all nodes in *Gnet*, with for $T \leqq 0.65$ even 90% and up, indicating that applying *T* indeed resulted in the formation of one large connected component with only a small number of disconnected voxels for all used thresholds of *T*. Figure 2.2b shows the largest connected cluster in *Gnet* for the range of fixed number of connections *k* in percentage of the total number of nodes in *Gnet*, averaged over the group of subjects. Similar to the range of *T*, for $4000 \leqq k \leqq 50$ the largest connected group of nodes consisted of more than 90% of the number of nodes in *Gnet*, indicating that *Gnet* mostly consisted out of one connected component. For $k = 20$ and $k = 10$ the largest connected group of nodes consisted of 83% and 72% of all nodes in *Gnet* respectively, averaged over the group of subjects. Green bars show the standard deviation over the group of 28 subjects. the removal of more and more edges, making *Gnet* more and more sparse. To verify that applying *T* would lead to the formation of one large connected component, rather than the formation of multiple relatively large but mutually disconnected components, the size of the largest connected cluster of *Gnet* was computed for all *T*. Figure 2.2a shows the largest connected cluster in *Gnet* in percentage of the total number of nodes, averaged over the 28 subjects. Green bars show the standard deviation over the group of subjects. For all thresholds *T* the largest connected cluster on average included more than 90% of all nodes in *Gnet*, indicating that applying *T* indeed resulted in the formation of one large connected component with only a small number of disconnected voxels for all used thresholds of *T*. Figure 2.2b shows the largest connected cluster in *Gnet* for the range of fixed number of connections k in percentage of the total number of nodes in *Gnet*, averaged

over the group of subjects. Similar to the range of T, for $4000 \leqq k \leqq 50$ the largest connected group of nodes consisted of more than 90% of the number of nodes in *Gnet*, indicating that *Gnet* mostly consisted out of one connected component. For k = 20 and k=10 the largest connected group of nodes consisted of 83% and 72% of all nodes in *Gnet* respectively, averaged over the group of subjects. Green bars show the standard deviation over the group of 28 subjects. Color version online (van den Heuvel et al. Neuroimage 2008).

chapter 3

normalized cut group clustering of resting-state fmri data

martijn van den heuvel, rené mandl, hilleke hulshoff pol

PLoS ONE 2008 3 (4) : e2001

Functional brain imaging studies have indicated that distinct anatomical brain regions can show coherent spontaneous neuronal activity during rest. Regions that show such correlated behavior are said to form resting-state networks (RSNs). RSNs have been investigated using seed-dependent functional connectivity maps and by a number of model-free methods. However, examining RSNs across a group of subjects is still a complex task and often involves human input in selecting meaningful networks. We report on a voxel based model-free normalized cut graph clustering approach with whole brain coverage for group analysis of resting-state data, in which the number of RSNs is computed as an optimal clustering fit of the data. Inter-voxel correlations of time-series are grouped at the individual level and the consistency of the resulting networks across subjects is clustered at the group level, defining the group RSNs. We scanned a group of 26 subjects at rest with a fast BOLD sensitive fMRI scanning protocol on a 3 Tesla MR scanner. An optimal group clustering fit revealed 7 RSNs. The 7 RSNs included motor/visual, auditory and attention networks and the frequently reported default mode network. The found RSNs showed large overlap with recently reported resting-state results and support the idea of the formation of spatially distinct RSNs during rest in the human brain.

introduction

Functional brain imaging studies have suggested that the brain is not inactive during rest, but rather shows a default state of activation (Biswal et al., 1995; Gusnard et al., 2001; Raichle et al., 2001; Greicius et al., 2003; De Luca et al., 2006). Low frequency oscillations (ranging from 0.01 to 0.1 Hz) of resting-state functional Magnetic Resonance Imaging (fMRI) time-series are known to show correlated patterns between anatomical separated brain regions (Biswal et al., 1995; Cordes et al., 2000; Fox and Raichle, 2007). These correlations are suggested to originate from coherency in the underlying neuronal activation patterns of these regions and believed to reflect functional connectivity. Regions that show this kind of coherent functional behavior are said to form a resting-state network (RSN). Multiple RSNs have been reported, including primary auditory, motor and sensory networks, attention networks and the default mode network (Lowe et al., 2000; Raichle et al., 2001; Damoiseaux et al., 2006; De Luca et al., 2006). Resting-state fMRI patterns are traditionally examined by correlating the rest recorded fMRI time-series of a single seed voxel against the time-series of all other voxels, resulting in a functional connectivity map (fcMap). A seed voxel is usually selected from an activation map of a separately acquired fMRI experiment. For example, when the seed voxel is based on activation in a motor task, the resting-state fcMap gives information about functionally connected regions involved in the motor network. Several studies mapping motor, visual, auditory and even cognitive networks have shown the potential of this seed-based resting-state analysis (Biswal et al., 1995; Biswal et al., 1997; Cordes et al., 2000; Cordes et al., 2001). However, the information of a fcMap is limited to the network associated with the selected seed voxel. In contrast, model-free methods enable the exploration of spatial and temporal activation patterns without the need of defining a specific model. Several model-free methods have been applied to individual (resting) PET and fMRI data, including principal component analysis (PCA) (Friston et al., 1993), independent component analysis (ICA)) (Kiviniemi et al., 2003; van de Ven et al., 2004; De Luca et al., 2006), hierarchical (Cordes et al., 2002) and Laplacian based clustering (Thirion et al., 2006).

A few model-free resting-state group methods have been introduced (Calhoun et al., 2001; Beckmann et al., 2005; Salvador et al., 2005b). However, group analysis of resting-state data is still a complex task and often involves human input in selecting the number of meaningful group networks. Here, we report on a model-free group graph clustering approach for selecting consistent functionally connected RSNs across a group of subjects. Our method works at the voxel level with whole brain coverage and includes a

procedure to determine the number of RSNs as an optimal fit of the data. The method involves the formation of individual and group functional connectivity graphs which are clustered to group voxels that show high functional connectivity in RSNs. For the clustering itself, the normalized cut (Ncut) graph clustering method of Shi and Malik (Shi and Malik, 2000) was used. The Ncut criterion is an unbiased measure of the disassociation between the subgroups of the data and minimizing this criterion directly leads to maximizing the total association within the subgroups. The Ncut method has the strong advantage of being less sensitive to outliers than other graph clustering methods. In essence, our RSN group selection method consists of a two stage process, combining clustering at the individual level with clustering at the group level. At the individual level, the inter-voxel functional connectivity of an individual fMRI dataset is expressed as the temporal coherence in the rest recorded BOLD time-series. This inter-voxel connectivity data is then clustered, resulting in individual clustermaps. At the group level, the consistency across the individual clustermaps is clustered and this determines the group RSNs. As a result, the RSNs directly reflect groups of voxels that consistently showed a high level of functional connectivity across the group of subjects. A group of 26 subjects was scanned on a 3 Tesla scanner with a fast fMRI protocol. Analysis of the acquired resting-state data was done with the two-stage Ncut group clustering approach and the resulting group RSNs are discussed on their functional relevance, overlap and differences with previous reported resting-state studies.

results

Spatial maps of the 7 clusters are shown in figure 3.1 and can be described as follows. Cluster *a* (figure 3.1a) shows a network of posterior cingulate/precuneus region (Brodmann Area (BA) 23/31), middle temporal gyrus (BA 39), inferior temporal gyrus (BA 21), inferior and superior parietal cortex (BA 40) and frontal regions, including both superior frontal gyrus (BA 8) and medial frontal gyrus (BA 11). Clusters *b* and *c* (figure 3.1b and 1c) show highly lateralized parietal-frontal networks in the left and right hemisphere, involving superior parietal lobule, inferior parietal lobule, supramarginal gyrus (BA 7/40), middle frontal gyrus and superior frontal gyrus (BA 8/9). Cluster *d* (figure 3.1d) shows the largest found network, consisting of postcentral gyrus (BA 3/1/2), precentral gyrus (BA 4), cingulate gyrus (BA 24) and lateral, medial and superior occipital gyrus and peristriate region (BA 17/18/19). Cluster *e* (figure 3.1e) involves bilateral insular and superior temporal cortex (BA 20/21/22) and a part of the cingulate gyrus (BA 24).

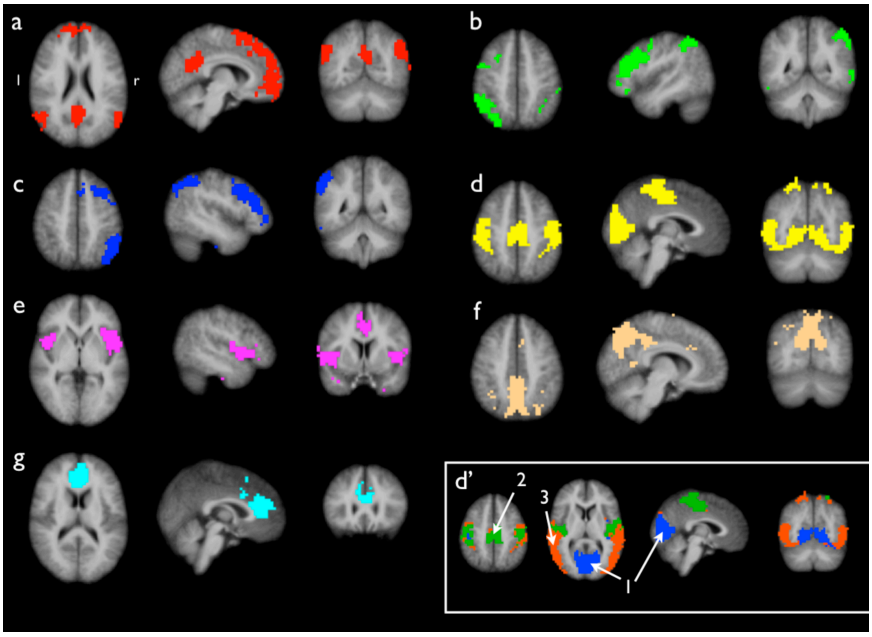

figure 3.1 group clustered resting-state networks Group clustering of 3 Tesla resting-state fMRI data of a group of 26 subjects revealed 7 resting-state networks (RSNs). 1a shows a functional connected network consisting of the posterior cingulate/precuneus, medial frontal regions and bilateral parietal/temporal regions, a RSN known as the default mode network. 1b and 1c show lateralized parietal-frontal networks, networks that are often reported in attention and memory processing. 1d shows a joint network of both sensorimotor and visual networks. Iteratively clustering partitioned this cluster in 3 sub-clusters, shown in clustermap d'. The results showed separate clusters for primary visual regions (cluster d'-1), primary sensorimotor regions (cluster d'-2) and extra-striate visual regions (cluster d'-3). 1e shows a network of bilateral insular regions and posterior cingulate cortex. 1f and 1g represent singular clusters consisting of, respectively, a posterior part of Brodmann Area 7 and an anterior part of the cingulate cortex. The clustered networks show resemblance with previous reported RSNs.

Cluster *f* (figure 3.1f) involves a singular region consisting of a posterior part of BA 7. Cluster *g* (figure 3.1g) involves a singular region covering a medial part of the medial frontal gyrus (BA 9) and an anterior part of the cingulate gyrus (BA 32).

Cluster *d* (figure 3.1d) overlapped several brain regions. Iteratively clustering the voxels in cluster *d* with the Ncut group clustering approach revealed 3 sub-clusters within this cluster. The results of this sub-clustering are shown in figure 3.1 (figure 3.1-d', lower right corner). Cluster *d'-1*

represents a sub-cluster consisting of striate and parastriate cortex (BA 17/18) (figure 3.1d'-1). Cluster *d'-2* shows a sub-cluster consisting of postcentral gyrus (BA 3/1/2), precentral gyrus (BA 4) and cingulate gyrus (BA 24) (figure 3.1d'-2). Cluster *d'-3* represents a sub-cluster consisting of lateral and superior occipital gyrus (BA 19) (figure 3.1d'-3).

discussion

We report on a group clustering method to select resting-state networks at a group level. Voxels with coherent resting-state time-series were grouped and disconnected from voxels showing a different time pattern, resulting in individual clustermaps. At the group level, the consistency across the individual clustermaps was computed and clustered, defining the group resting-state networks (RSNs). Normalized cut group clustering of 3 Tesla resting-state fMRI data of 26 subjects revealed 7 independent functional connected resting-state networks.

Group clustering resulted in resting-state networks (RSNs) of known functional relevance that show resemblance with recently reported resting-state group ICA results. Six out of seven of the found clusters show resemblance with the group ICA results of Beckmann et al. (Beckmann et al., 2005), De Luca et al. (De Luca et al., 2006) and Damoiseaux et al. (Damoiseaux et al., 2006), being cluster *a*, *b*, *c*, *d*, *e* and cluster *f*. Cluster *a* (figure 3.1a) represents a network of regions that is often referred to as the default mode network (Raichle et al., 2001; Greicius et al., 2003). The default mode network is consistently found in resting-state fMRI studies (Greicius et al., 2003; Fransson, 2005) and resting-state group ICA studies (Beckmann et al., 2005; Damoiseaux et al., 2006; De Luca et al., 2006). The default mode network is suggested to play an important role in core processes of human cognition (Gusnard et al., 2001; Greicius et al., 2003; Mason et al., 2007). Cluster *b* and *c* reflect lateralized parietal-frontal networks, which are often reported in attention and memory processing. Both networks are consistently found in resting-state studies (Beckmann et al., 2005; Damoiseaux et al., 2006; De Luca et al., 2006). Cluster *d* represents a combined network of regions involved in motor and visual processing. Cluster *e* shows a network consisting of bilateral insular regions and cingulate gyrus. This network is suggested to play an important role in the control of goal-directed behavior (Dosenbach et al., 2007) and salience processing (Seeley et al., 2007) and is often reported in RSN studies (Beckmann et al., 2005; Damoiseaux et al., 2006; De Luca et al., 2006). Two clusters, clusters *f* and *g* (figure 3.1f and 3.1g), consist of singular regions, which suggest that these clusters show an isolated pattern of neuronal

activity during rest. These results support the idea of complex functional connected RSNs underlying the architecture of the resting brain (Salvador et al., 2005a).

Interestingly, the group clustermaps also show important differences with previous reported resting-state studies. Previous studies have described up to 10 different RSNs (Damoiseaux et al., 2006), were in this study 7 RSNs were found. Most studies (Beckmann et al., 2005; Salvador et al., 2005b; Damoiseaux et al., 2006; De Luca et al., 2006) report the motor and visual regions to belong to two separate RSNs, while in this study they were grouped together in a single RSN (cluster *d*, figure 3.1d). In addition, primary visual and extra-striate visual regions have also been reported to form separated RSNs (Beckmann et al., 2005; Damoiseaux et al., 2007). Clustering motor and visual regions in a single RSN suggests that other RSNs are more differentiated in their level of functional connectivity than motor and visual regions and could imply that these regions are interconnected to quite some extent. This marks an important differentiation between the results of this study and previous studies (Beckmann et al., 2005; Salvador et al., 2005b; De Luca et al., 2006; Damoiseaux et al., 2007) and this difference is particular noteworthy as a number of studies have especially focused on the motor and visual system during rest and reported two separate networks (Biswal et al., 1995; Biswal et al., 1997; Cordes et al., 2000; Cordes et al., 2001). This suggested the existence of meaningful sub-RSNs within cluster *d.* The voxels in cluster *d* were therefore iteratively clustered using the Ncut clustering approach, partitioning cluster *d* in 3 sub-RSNs (see method section). This exploratory procedure resulted in 3 sub-clusters which are shown in figure 3.1d' (lower-right part of figure 3.1). Sub-clustering indeed resulted in two separate RSNs for primary visual regions (figure 3.1d'-1) and primary sensorimotor regions (figure 3.1d'-2), similar to previous group ICA (Beckmann et al., 2005; Damoiseaux et al., 2006; De Luca et al., 2006) and clustering studies (Salvador et al., 2005b). Furthermore, the extra-striate regions (figure 3.1d'-3) were clustered as a separate RSN, similar as reported by Damoiseaux et al. (Damoiseaux et al., 2006) and Beckmann et al. (Beckmann et al., 2005), although clustermap *d'-3* overlaps somewhat larger regions. These results suggest a valuable role for iteratively clustering in the Ncut group procedure and future studies are aimed to further explore such a multilevel Ncut clustering approach.

A number of other differences between the results of this study and previous studies are of interest. First, the singleton cluster *f* (figure 3.1f) was not found to be this prominent in other studies. Second, although most of the clustered RSNs represent regions of known functional relevance, cluster *g* (figure 3.1g) does not directly correspond to a known functional network.

Third, our results only partially overlap with the group results of Salvador et al. (Salvador et al., 2005a), who reports on a hierarchal graph clustering approach of resting-state fMRI. In their study, six main clusters were found, of which only the motor and visual clusters show some overlap with our combined motor/visual network (cluster *d*, figure 3.1d). The differences in clustering results may arise from the used voxel-wise approach in our study, in contrast to the averaged regional approach used by Salvador et al. In addition, in the study of Salvador et al. the group connectivity graph was constructed by averaging the individual regional-connectivity graphs, while in this study the group graph reflected the cluster-consistency over the individual clustering results.

Overall, despite differences between studies, we take the similarities between the clustered group networks and the previous reported group ICA components as a demonstration of the robust formation of functional networks when the brain is at rest. In this study, resting-state data was acquired in a different setting (on a 3 Tesla scanner and with a six times faster fMRI protocol) and analyzed with a novel group clustering approach, but this still resulted in the selection of known RSNs. The RSN similarities marks the potential of our normalized cut group clustering method in correctly detecting functionally connected RSNs in the resting brain.

The consistency of the proposed Ncut clustering group approach was studied by examining the results of multiple clusterings with different parameter settings (figure 3.2, 3.3 and 3.4). First, the cut-off threshold of the individual connectivity graph was varied for three settings (being 0.3, 0.4 and 0.5). This resulted in three different sets of individual clustering results which were clustered at the group level (Stage B). The group clustering showed to be only minor influenced by the individual cut-off threshold, as all 7 clusters of the 3 sets showed high overlap (figure 3.2). However, when the individual cut-off threshold was increased to 0.6 (and up) more and more paths were removed from the individual graphs and this did have an effect on the group results, showing less consistent group RSNs. Therefore the individual cut-off threshold was set to 0.4 in the main analysis. Second, the influence of the level of overclustering at the individual clustering stage (Stage A) on the final group clustering was examined by repeating the clustering with 5 settings of overclustering, ranging from 15 to 45. This resulted in 5 sets of group clusterings, all showing large overlap for all of the 7 clusters (figure 3), indicating that changing the level of individual overclustering did not change the nature of the group clustering results. As a third test, the influence of the group-graph complexity parameter on the group clustering was examined. The group graph was clustered with 5 settings of the group cut-off threshold around the found optimum of 9. The 5

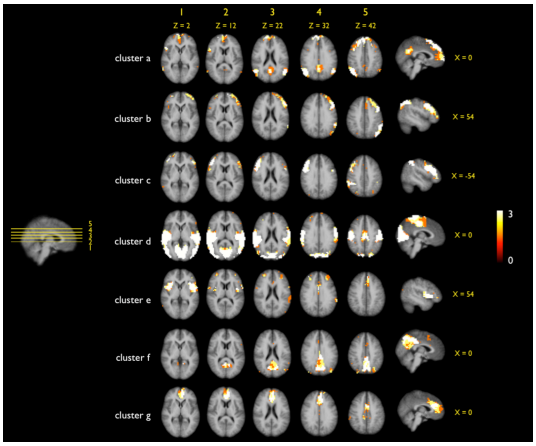
1
Z = 2
2
Z = 12
3
Z = 22
4
Z = 32
5
Z = 42
cluster a
cluster b
cluster c
cluster d
cluster e
cluster f
cluster g
X = 0
X = 54
X = -54
X = 0
X = 54
X = 0
X = 0
3
0

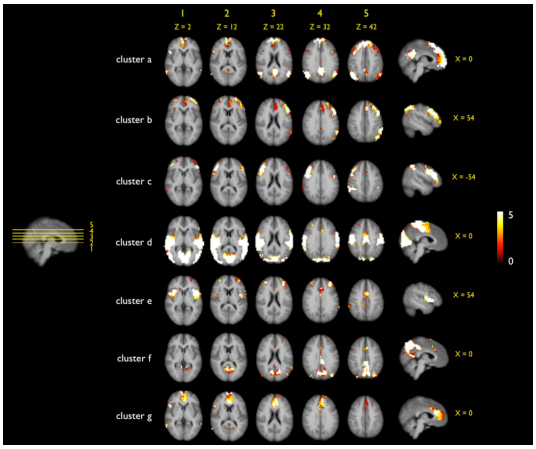
1
Z = 2
2
Z = 12
3
Z = 22
4
Z = 32
5
Z = 42
cluster a
cluster b
cluster c
cluster d
cluster e
cluster f
cluster g
X = 0
X = 54
X = -54
X = 0
X = 54
X = 0
X = 0
5
0

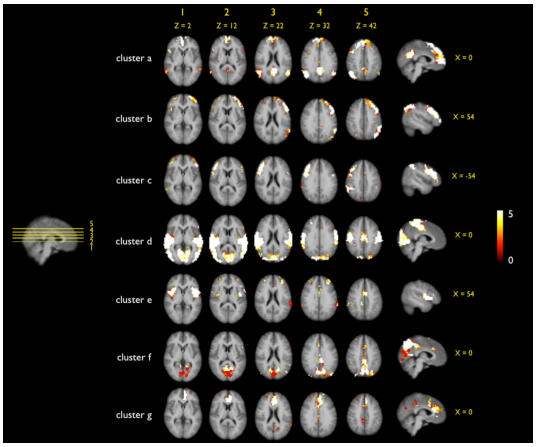
1
Z = 2
2
Z = 12
3
Z = 22
4
Z = 32
5
Z = 42
cluster a
cluster b
cluster c
cluster d
cluster e
cluster f
cluster g
X = 0
X = 54
X = -54
X = 0
X = 54
X = 0
X = 0
5
0

figure 3.2 overlap of multiple group clusterings of different sets of individual clustermaps, varying on the individual cut-off threshold At the individual clustering stage, the constructed individual connectivity graph was threshold with the set individual graph cut-off threshold rc before clustering. To examine the effect of rc on the final group clustering, the individual clustering procedure was repeated with 3 settings of rc, being 0.3, 0.4 and 0.5. The overclustering parameter was kept fixed on 20. Group clustering (graph complexity threshold set to 9; number of RSNs set to 7) was repeated with the 3 sets of individual clustering results, resulting in 3 group clusterings. For all of the 7 group clusters the overlap of these clustering solutions was computed. Figure clearly shows large overlap for all of the 7 group clusters, indicating that the setting of rc did not affect the final group clustering. However, when rc was increased to 0.6 and up, more and more paths were removed from the individual graph. This clearly affected the individual clustering and the group clustering, changing the spatially layout of the clusters (data not shown).

figure 3.3 overlap of multiple group clusterings of different sets of individual clustermaps, varying on the level of individual overclustering To test the assumed minor effect of overclustering at the individual level on the group clustering results, the individual clustering (Stage A) was repeated with varying overclustering settings (i.e., the number of clusters) and analyzed at the group level (Stage B). For each individual dataset, the individual clustering (stage A) was repeated with varying number of clusters (assumed to result in overclustering), ranging from 15 to 35 (with steps of 5). This resulted in 5 clustermaps per individual dataset. Next, the group clustering (stage B) was repeated with the 5 sets of individual clustermaps (graph complexity threshold set to 9; number of RSNs set to 7). For each of the 7 resulting group clusters, the 5 cluster solutions were summated, creating an overlap map (cluster a - g) with voxel values ranging up to a maximum of 5. The maximum of 5 indicated an overlap off all 5 cluster solutions. Figure shows highly similar cluster results over the 5 different group clusterings, as suggested by the large overlap for each of the 7 clusters. As expected, the results demonstrated that the overclustering at the individual level did not change the nature of the group clustering.

figure 3.4 overlap of multiple group clusterings with varying group graph complexity cut-off thresholds To verify that the optimization procedure considering the selection of the group graph complexity cut-off threshold resulted in a stable clustering, the group clustering was repeated with multiple settings of the graph complexity cut-off threshold. The group clustering stage (stage B) was repeated (using the individual clustermaps consisting of 20 clusters) with different settings for the group cut-off threshold varying around the found optimum of 9 (ranging from 7 to 11). The number of clusters was set to the found optimum of 7 (see main text). Next, for each of the 7 clusters, the 5 group cluster solutions were summated, creating an overlap map with voxels ranging up to a maximum of 5. The maximum of 5 indicated the overlap of all 5 clustering solutions. Figure shows large overlap between the 5 group clusterings, for all of the 7 clusters. This large overlap demonstrates that varying the cut-off threshold around the found optimum only minor influenced the group results, indicating that the automatic parameter setting procedure resulted in a stable clustering solution.

cluster solutions showed large similarity for all of the 7 group clusters (figure 3.4). This overlap suggests only a minor influence of the graph complexity threshold on the group clustering. Taken together, these results show that the used Ncut group clustering approach yield consistent results for clustering with different parameter settings. This indicates that our group clustering approach is robust for different settings of the cluster parameters. In addition, the overlap suggest that the clustered RSNs can be found consistently in a group of subjects, increasing the confidence in the found RSNs.

A number of model-free methods have been successfully introduced for the group wise selection of RSNs from resting-state fMRI. ICA based methods are perhaps the most commonly used (Calhoun et al., 2001; Beckmann et al., 2005) and have been reported to show large consistency (Correa et al., 2007; Ylipaavalniemi and Vigario, 2008). ICA methods search for a mixture of sources underlying the observed signal, with the assumption that the sources are statistically independent. An advantage of these methods is that they work at the voxel level and that the temporal signal of the independent components can be easily further examined and compared between groups. However, the interpretation of the ICA results may involve human input in selecting the anatomical meaningful networks from the total collection of components and this can be a complex task. New analysis methods are suggested to calculate the consistency across ICA solutions to provide additional information for a better interpretation of the results (Ylipaavalniemi and Vigario, 2008). Clustering methods have also been successfully used to investigate RSNs (Cordes et al., 2002; Salvador et al., 2005b). Salvador et al. (Salvador et al., 2005b) reported on hierarchical graph clustering of an averaged group connectivity matrix, clustering brain regions in six main groups. Advantages of this clustering method are the simplified selection of RSNs by controlling for the hierarchical levels of clustering and the straightforward interpretation of the results. However, most clustering approaches have clustered over brain regions, using a parcellation of the cortex in a number of fixed regions, making the spatial resolution of these methods limited to a regional scale. Clustering at the group level forms the core of our group clustering approach. Functional connectivity is represented on the voxel scale, enabling the examination of RSNs in detail, similar to group ICA methods (Calhoun et al., 2001; Beckmann et al., 2005). A strong asset is the data-driven computation of the number of RSNs, avoiding human input in defining the number of RSNs. Clustering purely implies the grouping of voxels that consistently show correlated time-series across a group of subjects making the results straightforward to interpret. However, in contrast to group ICA methods, the

temporal signals of the RSNs are not directly available for further processing, but this requires some level of post analysis like overlapping the clusters on the functional time-series and calculating the level of (partial) correlation between the RSN regions.

Graph clustering methods using minima criteria, among which hierarchal clustering and k-means clustering, tend to be sensitive to outliers in the dataset (Duda et al., 2001). Minima based clustering methods are generally very effective when clustering averaged time-series over regions, as noise over the time-series is averaged out. However, such clustering strategies are less effective in clustering voxels. The time-series of a single voxel could have a low signal to noise ratio and therefore easily show a rather distinct pattern from the rest of the dataset. As a result, the clustering of voxel-based data could result in grouping such an outlier or a small group of outliers as single clusters, ignoring the more global character of the data (Duda et al., 2001; Cordes et al., 2002). To overcome this problem, in this study the normalized cut clustering of Shi and Malik (Shi and Malik, 2000) was used. The normalized cut criterion measures both the total similarity within groups as well as the dissimilarity between groups, effectively penalizing the formation of small clusters and thereby stimulating the clustering of more global RSNs.

The neurophysiological meaning of resting-state networks remains unclear. It has been proposed that synchronization of neuronal oscillation patterns within neuronal networks may contribute to the regulation of information flow (Knight, 2007) supporting selection, consolidation and combination of learned information (Buzsaki and Draguhn, 2004), processes that are likely to be on-going during rest (Buckner and Vincent, 2007; Raichle and Snyder, 2007). Coherent oscillatory patterns during rest in RSNs may therefore be involved in the consolidation of past events and the preparation for future responses to stimuli (Buckner and Vincent, 2007; Raichle and Snyder, 2007). More specific, robust functional connections between the posterior and anterior cingulate cortex of the default mode network have been associated with integration of cognitive and emotional processing (Greicius et al., 2003).

Investigations into the resting-state of the brain may give us more insight into the foundation of the brains architecture and its dysfunction in brain disorders. It has been recently suggested that resting-state patterns may be affected in Alzheimer's disease (Greicius et al., 2004; Rombouts et al., 2005), depression (Greicius et al., 2007) and schizophrenia (Liang et al., 2006; Micheloyannis et al., 2006; Bluhm et al., 2007; Salvador et al., 2007; Williamson, 2007; Zhou et al., 2007). Our proposed group clustering method could contribute to this field of research. It allows for a direct comparison of

the spatial distribution of RSNs between patients and healthy controls. Furthermore, the used graph representation of connected voxels can be used to examine the organization of the functionally connected resting-state brain (Salvador et al., 2005b; Reijneveld et al., 2007) and possible disruptions in network organization in patients (Micheloyannis et al., 2006).

The described two-stage Ncut group clustering approach requires to set a number of parameters by the user before clustering, being the individual cut-off threshold, the level of individual overclustering and the group graph complexity threshold. In this study, the influence of the chosen parameter settings was tested and found to have only a minor influence on the group clustering (figure 3.2, 3.3 and 3.4). In addition, the number of group clusters, defining the total number of group RSNs, has to be defined. The described approach includes an exhaustive search procedure to find the group cluster parameters that resulted in an optimal clustering of the group data, by finding a clustering solution with a minimal normalized cut cost (Shi and Malik, 2000). The examined influence of the individual and group parameters on the final group clustering and the described optimization procedure might assist the user to set the required parameters.

Some limitations to this study have to be considered. Like in all clustering based resting-state methods, all cortical voxels must be placed in one of the RSNs. However, it can be argued that only parts of the brain participate in RSNs. Indeed, two of the found clustermaps show a solitary group of voxels, which suggest that these voxels do not participate in a network, but rather show an isolated pattern of neuronal activity during rest. Stronger pre-selection criteria may address this issue by removing voxels that show little to no significant connections from clustering. An additional limitation of using a clustering approach is that each voxel is exclusively assigned to one cluster. This may be incorrect for regions that participate in multiple RSNs, for example subcortical regions with relay functions like the thalamus. In this study we focused exclusively on the cortical areas, but it is of interest to examine subcortical contributions to RSNs. A more general limitation considers the assumption of cross-correlation between time-series reflecting functional connectivity. Two voxels showing a high cross-correlation between their time-series could be mediated by a third voxels time-series and not because they are (directly) functionally connected. The use of partial correlation or partial coherence has been suggested to account for these third party influences (Cordes et al., 2002; Stam, 2004; Sun et al., 2004; Salvador et al., 2005b).

We introduced a two-stage normalized cut based group clustering method to investigate the formation of resting-state networks in the human brain at a group level. Inter-voxel functional connectivity was clustered into

individual networks and consistency of these networks over the group of subjects determined the group RSNs. Group clustering of rest recorded 3 Tesla fMRI data of 26 subjects revealed resting-state networks of known functional relevance and included the often reported default mode network. Our results support the idea of the formation of spatially distinct RSNs during rest in the human brain.

materials and methods

datasets and preprocessing

Data was acquired using a 3 Tesla Philips Achieva Medical scanner (Philips Medical Systems, Best, The Netherlands) at the University Medical Center Utrecht, The Netherlands. 26 right handed healthy subjects with no psychiatric history participated in the study (age mean/std : 25/7.7; gender: 14 male, 12 female). All participants gave written consent prior to taking part in the study as approved by the medical ethics committee for research in humans (METC) of the University Medical Center Utrecht, the Netherlands. During the resting experiment the scanner room was darkened and the subjects were instructed to relax with their eyes closed, without falling asleep. Resting-state blood oxygenation level dependent (BOLD) signals were recorded during a period of 8 minutes using a fast fMRI sequence (3D-PRESTO pulse sequence with parallel imaging (Ramsey et al., 1998; Golay et al., 2000). Acquisition parameters: TR 21.75 ms, effective TE 32.4 ms (using a shifted echo); flip-angle 9 degrees; 1000 timeframes; FOV 256x256 mm, voxelsize 4 mm isotropic, 32 slices covering whole brain; total acquisition time per volume 0.5 sec). The short volume acquisition time of 500 ms allowed the sampling of information in the frequency domain up to 1 Hz. This minimized the possible backfolding (aliasing) of higher frequencies, such as cardiac and respiratory oscillations into the lower resting-state frequencies of interest (0.01 - 0.1 Hz). Directly after the acquisition of the functional time-series an additional PRESTO scan with better anatomical contrast using an increased flip angle of 25 degrees (FA25) was acquired for coregistration purposes. A T1 weighted image was acquired for anatomical reference (3D FFE pulse sequence. Acquisition parameters: TR=9.87 ms, TE=4.6 ms; flip-angle 8 degrees; SENSE reduction 1.7 (left-right) and 1.4 (anterior-posterior); FOV 240x240 mm, voxelsize 0.75x0.75x0.8 mm, 180 slices).

All preprocessing steps were done with the SPM2 software package (http://www.fil.ion.ucl.ac.uk). The functional scans were corrected for small head movements by realigning all functional scans to the last functional

scan. Realignment to the last functional scan ensured maximum spatial overlap with the FA25 scan at the start position of the registration, because the FA25 scan was acquired directly after the resting-state time-series. The functional time-series were coregistered to the FA25 image, by taking the last functional scan as a source. The T1 image was then coregistered to the FA25 image, providing spatial alignment between the functional time-series and the anatomical image. After realignment, the rest recorded functional time-series were bandpass filtered with a finite impulse response (FIR) bandpass filter with zero phase distortion (bandwidth 0.01 - 0.1 Hz) to eliminate low frequency noise (including slow scanner drifts) and influences of higher frequencies reflecting possible cardiac or respiratory oscillations (Cordes et al., 2001). Normalization parameters were estimated using the MNI 305 T1 brain (Collins et al., 1994) as a template and the T1 image as a source. All functional scans were then normalized to the standard space according to normalization parameters and resampled to a 4x4x4 mm resolution, enabling between subject comparisons. Cortex segmentation was done on the T1 image using the Freesurfer software package (http://surfer.nmr.mgh.harvard.edu/). Segmentation maps were normalized and resampled to a 4x4x4 mm resolution to spatially overlap the filtered time-series.

After preprocessing, the resting-state fMRI datasets were analyzed using the normalized cut group clustering method, consisting of two clustering stages (explained in detail below). At the individual level (Stage A, Individual clustering), voxels showing correlated BOLD activation patterns over time were clustered and defined an individual clustermap. Next, at the group level (Stage B, Group clustering) the consistency across the individual clustermaps was computed and clustered using the Ncut method, defining the group RSNs.

stage A: individual clustering

Clustering at the individual level (stage A) involved the grouping of voxels that showed coherent BOLD fMRI time signals. The individual clustering stage consisted of two steps (figure 3.5), the *formation of individual functional connectivity graph* (step A1) and the *clustering* of this graph (step A2).

step A1 formation of individual functional connectivity graph

Each fMRI dataset was represented as a fully connected undirected graph $G = (N, E)$, with nodes N representing the voxels in the dataset (all gray matter voxels) and the weighted edges *E* connecting each voxel pair (figure 3.5, step A1). This resulted in an individual graph of M nodes representing

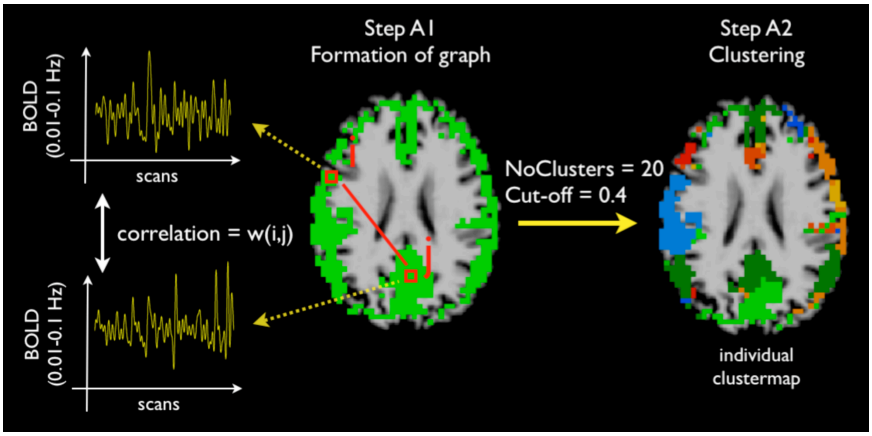

figure 3.5 individual clustering stage ***step A1 graph formation*** An individual graph was constructed, consisting of M cortical voxels and (M^2 -M)/2 edges connecting all voxel pairs. The weight *w(i,j)* of edge *e(i,j)* connecting voxel *i* and voxel *j* was computed as the correlation between the filtered time-series of voxel i and voxel *j*, reflecting the level of functional connectivity between the two voxels. ***step A2 clustering*** Prior to the clustering, a cut-off threshold *T* of 0.4 was applied to reduce the complexity of the graph and lower the computational load, setting all weights to zero that did not reach this threshold. Normalized cut clustering was used to partition the graph in a fixed number of 20 networks, grouping voxels that showed a high level of functional connectivity into networks, resulting in an individual clustermap.

the M cortical voxels with a total of $(M^2 - M)/2$ edges connecting each possible voxel pair. M varied between subjects from 8500 to 9500, depending on the individual cortical segmentation. The weights of the edges of the graph represented the level of functional connectivity between the voxels. The weight *w*(*i,j*) of edge *e*(*i,j*) connecting voxel *i* and voxel *j* in the graph was computed as the correlation between their filtered fMRI time-series. The individual functional connectivity graph was stored as a weighted connection matrix before clustering.

step A2 clustering

Next, the connectivity graph *G* was clustered in a number of sets consisting of groups of voxels that showed a high level of functional connectivity (figure 3.5). To partition graph *G* in a number of subsets the normalized cut-cost clustering method according to Shi and Malik (Shi and Malik, 2000) was used. By using a *graph cut method* for clustering a graph is partitioned in a number of subsets by removing edges from the graph that connect the

subsets, with the total cost of this operation defined as the sum of all the weights of the edges that have to be removed. The normalized cut value normalizes this cut cost by the fraction of all paths in that subset (for a more detailed description see supporting material). A direct advantage of the Ncut method is that, due to the normalization factor, the clustering is less sensitive to grouping outliers as individual subsets. The optimal partitioning of graph G is one that minimizes the Ncut cost and can be found by solving a generalized eigenvalue system representation of G (Shi and Malik, 2000). Clustering was done with the public available MATLAB implemented Ncutclustering_7 toolbox of Shi (http://www.cis.upenn.edu/~jshi/software).

To reduce the number of connecting edges in the connectivity graph and therefore reduce the graph complexity, a cut-off threshold *T* (Cordes et al., 2002) of 0.4 was applied, setting the weights of the edges that did not reach this threshold to zero. The effect of this individual cut-off threshold on the group clustering was examined by repeating the individual clustering stage with 3 different settings of *T*, being 0.3, 0.4 and 0.5, resulting in 3 clustermaps for each individual dataset. The group clustering stage (Stage B, see below) was then repeated with the 3 different sets of 26 individual clustermaps, resulting in 3 group clusterings. Varying the individual cut-off threshold *T* around 0.4 did not change the nature of the group clustering, as indicated by the overlap of the resulting group clusters (figure 3.2). Therefore, *T* was set to 0.4.

Clustering required a preset number of clusters to partition in. At start the number of RSNs was unknown. Setting the number of clusters lower than the true number of RSNs would result in an underclustering of the data, erroneously combining distinct RSNs. Setting a high number of clusters would probably result in an overclustering of the data, forcing networks to be divided in multiple subsets. However, if overclustering of the data would force a true RSN to be split in two or more subsets, the assignment of the voxels to one of the subsets would be random, as no correct splitting would be possible on basis of the data itself. Therefore, the devision into subsets would not change the shape or outline of the RSNs and would not affect the nature of the group clustering. To verify this assumed minor effect of individual overclustering on the group clustering, the individual clustering stage was repeated with the (overclustering) number of clusters ranging from 15 up to 35 (with steps of 5), resulting in a total of 5 clustermaps per individual dataset. Subsequently, the group clustering step (Stage B, see below) was repeated 5 times (using fixed group cluster parameters), with the 5 different sets of 26 individual clustermaps. As predicted, the 5 group clustermaps demonstrated large overlap, indicating

that overclustering at the individual level did not change the nature of the group results (figure 3.3).

To avoid incorrect underclustering of the data, the number of clusters was set to 20, double the number of 6 to 10 networks reported in previous fMRI resting-state studies. This was expected to result in harmless overclustering of the data. The individual graph was partitioned in 20 clusters using the Ncut clustering algorithm. Labeling the cortical voxels with their cluster number (ranging from 1 to 20) resulted in an individual clustermap. Small gaps in the individual clustermap were filled by using a majority voting algorithm with a minimum of 5 neighbors.

stage B: group clustering

In the group clustering stage the consistency across the 26 individual clustermaps was computed and clustered (Stage B, figure 3.6). The resulting group clustermap expressed networks that could be consistently found across the group of subjects. Group clustering consisted of 3 steps, *formation of the group graph* that reflected the RSN consistency across the group of subjects (step B1), *setting cluster parameters* (step B2) and *computing the group clustermap* (step B3).

step B1 formation of the group graph

Overlap of the normalized individual cortical segmentation maps resulted in a group cortical segmentation of 9014 gray matter voxels. From the 9014 cortical voxels a fully connected undirected group graph *Ggrp* was constructed with $(9014^2 - 9014)/2$ edges connecting all voxel pairs (figure 3.6, step B1). The weights of the edges were set to express the consistency of the cluster-similarity across the individual clustermaps and were computed as follows. In each individual clustermap (the outcome of the individual clustering stage), the cluster-similarity between two voxels was set to 1 if the two voxels were grouped in the same cluster and 0 otherwise. Then at the group level, the weight of the edge connecting those two voxels in the group graph was computed as the total summation of the cluster-similarity values across the individual clustermaps. More formally, weight $W(i,j)$ of edge $E(i,j)$ between voxel i and j in *Ggrp*, was defined as

$$W(i,j) = \sum_{S=1}^{N} clus_S(i,j) \qquad (3.1)$$

with N the number of subjects and $clus_S(i,j)$ being 1 if voxel i and j were in the same cluster in subject S and 0 otherwise. This definition of the weights of the group graph expressed between- subject cluster-similarity in such a

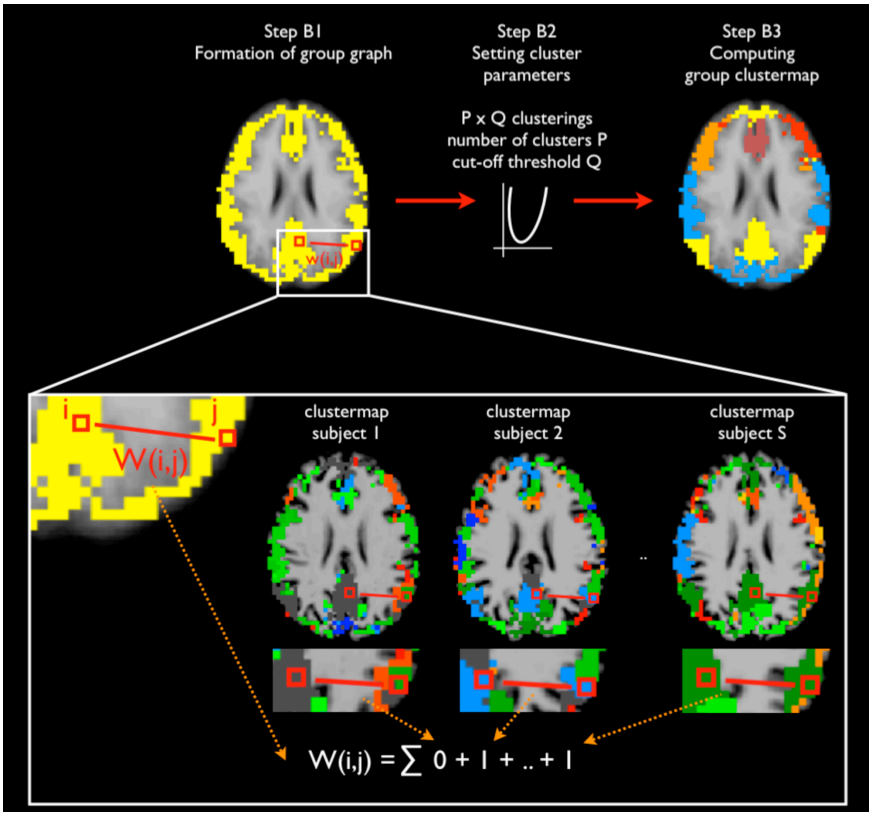

figure 3.6 group clustering stage ***step B1 formation of a group graph*** A group graph was constructed, consisting of the cortical voxels that resulted from the group averaged cortical segmentation map and edges connecting all possible voxel pairs. The weight *W(i,j)* of the edge connecting voxel *i* and voxel *j* reflected the cluster consistency across the group of subjects and was computed as follows. For each individual clustermap, the individual cluster-similarity between voxel *i* and *j* was defined as 1 if in the individual clustermap voxel i and voxel j were grouped in the same cluster and 0 otherwise. Figure box shows the clustermaps of subject 1 and 2 and the last subject (subject S). In subject 1 the voxels i and j were not clustered in the same cluster, hence the cluster-similarity between voxel *i* and voxel *j* was set to 0. In contrast, in subject 2 and in subject S voxel i and j were clustered in the same cluster and therefore the cluster-similarity values between these voxels in these subjects were set to 1. At the group level, *W(i,j)* was computed as the summation of the cluster-similarities between voxel i and voxel j over the group of S subjects. ***step B2 setting cluster parameters*** The group graph was clustered with increasing number of clusters P and increasing graph complexity cut-off thresholds Q. An optimal fit was computed as the clustering fit with the first minimum normalized cut cost value in descending direction of the number of P clusters, to maximize the number of meaningful clustered RSNs. ***step B3 computing group clustermap*** The cortical voxels were labeled according to the optimal clustering fit, resulting in the group clustermap. The group clustermap represents networks of voxels that were consistently clustered into the same resting-state network across the group of subjects.

way that high weight values reflected strong subject overlap. A high value of $W(i,j)$ would indicate that in a large proportion of the group of 26 subjects the two voxels i and j were clustered into the same cluster and therefore should probably belong to the same group RSN.

step B2 setting cluster parameters

At start of the group clustering stage the number of clusters (i.e. the number of RSNs) to partition *Ggrp* in was unknown. Furthermore, a graph complexity cut-off threshold was needed to be set to decrease the size of *Ggrp* in preparation for the clustering to reduce the computational load, setting the weights of the edges that did not reach the complexity cut-off threshold to zero. At start, the number of group clusters and the cut-off threshold were unknown and as a result could not be set correctly by the user. An optimal partitioning of *Ggrp* with respect to these 2 parameters was computed with the following procedure. First, *Ggrp* was clustered repetitively with different cut-off thresholds and with different values for the number of clusters (i.e. RSNs). For each of these clusterings the Ncut method was used and the Ncut cost to partition *Ggrp* was computed. This resulted in a *Ncut cost landscape* of size P x Q, with P the range of used numbers of clusters and Q the range of used graph complexity thresholds. The examined number of group clusters varied between 2 and 50 clusters and the graph complexity threshold varied between 5 and 25, resulting in a 49 x 21 Ncut cost landscape, containing 1029 group clustering solutions. Second, from this Ncut landscape the optimal clustering solution was selected. The Ncut cost of a clustering is defined as the summation of the weights of the edges that have to be removed to divide the group in multiple sets and directly reflects the quality of the clustering (Shi and Malik, 2000). Therefore, the optimal partitioning of *Ggrp* in an optimal number of clusters, was selected from the total collection of cluster solutions as a solution with a minimum Ncut cost. This minimum was selected by traveling through the Ncut cost landscape in descending direction of the number of clusters starting with 50 (i.e. from 50 to 2), partitioning the data in as much meaningful networks as possible and in ascending direction of the cut-off threshold (i.e up from 2 to 25), keeping the information in *Ggrp* as high as possible. This procedure resulted in an optimal partitioning of *Ggrp* in 7 clusters with a group cut-off threshold of 9.

step B3 computing group clustermap

The cluster labels resulting from the computed optimal clustering of *Ggrp* were assigned to the cortical voxels (figure 3.6, step B3). This resulted in a group clustermap of 7 RSNs.

To confirm that the optimization procedure resulted in a stable clustering fit of *Ggrp*, the overlap of the clustering solutions with a cut-off threshold varying around the found optimum of 9 was calculated. A range of -2 to 2 was chosen (i.e. 5 cut-off thresholds ranging from 7 to 11). To test the specific effect of the cut-off threshold on the group clustering the number of clusters was kept fixed for all 5 group clusterings to the found optimum of 7. The 5 computed group clustermaps showed large overlap for all of the 7 clusters, indicating that the optimization procedure resulted in a stable clustering (figure 3.4).

additional analysis, sub-clustering of cluster d

The largest clustered network (cluster *d*, figure 3.1) consisted of both sensorimotor and visual regions, combining these regions in a single RSN. To examine whether this cluster consisted of multiple sub-clusters, an iterative cluster procedure was added, sub-clustering the voxels in cluster *d* (figure 3.1d). This iterative clustering stage followed the exact procedure of the normalized group clustering approach, with both the individual clustering stage (Stage A) and group clustering stage (Stage B). First, individual connectivity graphs were formed out of the selected voxels and clustered. For the individual clustering a cut-off *T* of 0.4 was used and the level of overclustering was set to 10 clusters, being over twice the expected number of clusters, similar to the procedure followed in the main analysis (Stage A: Individual clustering, step A2). The individual clusterresults were combined at the group clustering stage, forming a new group graph, consisting of 4186 voxels (Stage B: Group clustering). This graph was then clustered with the graph-complexity threshold set to a value of 9 (similar to the main analysis) and the number of group clusters set to 3.

references

Beckmann CF, DeLuca M, Devlin JT, Smith SM (2005) Investigations into resting-state connectivity using independent component analysis. Philos Trans R Soc Lond B Biol Sci 360:1001-1013.

Biswal B, Yetkin FZ, Haughton VM, Hyde JS (1995) Functional connectivity in the motor cortex of resting human brain using echo-planar MRI. Magn Reson Med 34:537-541.

Biswal BB, Van Kylen J, Hyde JS (1997) Simultaneous assessment of flow and BOLD signals in resting-state functional connectivity maps. NMR Biomed 10:165-170.

Bluhm RL, Miller J, Lanius RA, Osuch EA, Boksman K, Neufeld R, Theberge J, Schaefer B, Williamson P (2007) Spontaneous Low-Frequency Fluctuations in the BOLD Signal in Schizophrenic Patients: Anomalies in the Default Network. Schizophr Bull 33:1004-1012.

Buckner RL, Vincent JL (2007) Unrest at rest: Default activity and spontaneous network correlations. Neuroimage 37:1091-1096.

Buzsaki G, Draguhn A (2004) Neuronal oscillations in cortical networks. Science 304:1926-1929.

Calhoun VD, Adali T, Pearlson GD, Pekar JJ (2001) A method for making group inferences from functional MRI data using independent component analysis. Hum Brain Mapp 14:140-151.

Collins DL, Neelin P, Peters TM, Evans AC (1994) Automatic 3D intersubject registration of MR volumetric data in standardized Talairach space. J Comput Assist Tomogr 18:192-205.

Cordes D, Haughton V, Carew JD, Arfanakis K, Maravilla K (2002) Hierarchical clustering to measure connectivity in fMRI resting-state data. Magn Reson Imaging 20:305-317.

Cordes D, Haughton VM, Arfanakis K, Wendt GJ, Turski PA, Moritz CH, Quigley MA, Meyerand ME (2000) Mapping functionally related regions of brain with functional connectivity MR imaging. AJNR Am J Neuroradiol 21:1636-1644.

Cordes D, Haughton VM, Arfanakis K, Carew JD, Turski PA, Moritz CH, Quigley MA, Meyerand ME (2001) Frequencies contributing to functional connectivity in the cerebral cortex in "resting-state" data. AJNR Am J Neuroradiol 22:1326-1333.

Correa N, Adali T, Calhoun VD (2007) Performance of blind source separation algorithms for fMRI analysis using a group ICA method. Magn Reson Imaging 25:684-694.

Damoiseaux JS, Rombouts SA, Barkhof F, Scheltens P, Stam CJ, Smith SM, Beckmann CF (2006) Consistent resting-state networks across healthy subjects. Proc Natl Acad Sci U S A 103:13848-13853.

Damoiseaux JS, Beckmann CF, Arigita EJ, Barkhof F, Scheltens P, Stam CJ, Smith SM, Rombouts SA (2007) Reduced resting-state brain activity in the "default network" in normal aging. Cereb Cortex.

De Luca M, Beckmann CF, De Stefano N, Matthews PM, Smith SM (2006) fMRI resting state networks define distinct modes of long-distance interactions in the human brain. Neuroimage 29:1359-1367.

Dosenbach NU, Fair DA, Miezin FM, Cohen AL, Wenger KK, Dosenbach RA, Fox MD, Snyder AZ, Vincent JL, Raichle ME, Schlaggar BL, Petersen SE (2007) Distinct brain networks for adaptive and stable task control in humans. Proc Natl Acad Sci U S A 104:11073-11078.

Duda RO, Hart PE, Stork DG (2001) Pattern Recognition, Second Edition Edition: John Wiley & Sons, Inc.

Fox MD, Raichle ME (2007) Spontaneous fluctuations in brain activity observed with functional magnetic resonance imaging. Nat Rev Neurosci 8:700-711.

Fransson P (2005) Spontaneous low-frequency BOLD signal fluctuations: an fMRI investigation of the resting-state default mode of brain function hypothesis. Hum Brain Mapp 26:15-29.

Friston KJ, Frith CD, Liddle PF, Frackowiak RS (1993) Functional connectivity: the principal-component analysis of large (PET) data sets. J Cereb Blood Flow Metab 13:5-14.

Golay X, Pruessmann KP, Weiger M, Crelier GR, Folkers PJ, Kollias SS, Boesiger P (2000) PRESTO-SENSE: an ultrafast whole-brain fMRI technique. Magn Reson Med 43:779-786.

Greicius MD, Krasnow B, Reiss AL, Menon V (2003) Functional connectivity in the resting brain: a network analysis of the default mode hypothesis. Proc Natl Acad Sci U S A 100:253-258.

Greicius MD, Srivastava G, Reiss AL, Menon V (2004) Default-mode network activity distinguishes Alzheimer's disease from healthy aging: evidence from functional MRI. Proc Natl Acad Sci U S A 101:4637-4642.

Greicius MD, Flores BH, Menon V, Glover GH, Solvason HB, Kenna H, Reiss AL, Schatzberg AF (2007) Resting-State Functional Connectivity in Major Depression: Abnormally Increased Contributions from Subgenual Cingulate Cortex and Thalamus. Biol Psychiatry 62:429-437.

Gusnard DA, Raichle ME, Raichle ME (2001) Searching for a baseline: functional imaging and the resting human brain. Nat Rev Neurosci 2:685-694.

Kiviniemi V, Kantola JH, Jauhiainen J, Hyvarinen A, Tervonen O (2003) Independent component analysis of nondeterministic fMRI signal sources. Neuroimage 19:253-260.

Knight RT (2007) Neuroscience. Neural networks debunk phrenology. Science 316:1578-1579.

Liang M, Zhou Y, Jiang T, Liu Z, Tian L, Liu H, Hao Y (2006) Widespread functional disconnectivity in schizophrenia with resting-state functional magnetic resonance imaging. Neuroreport 17:209-213.

Lowe MJ, Dzemidzic M, Lurito JT, Mathews VP, Phillips MD (2000) Correlations in low-frequency BOLD fluctuations reflect cortico-cortical connections. Neuroimage 12:582-587.

Mason MF, Norton MI, Van Horn JD, Wegner DM, Grafton ST, Macrae CN (2007) Wandering minds: the default network and stimulus-independent thought. Science 315:393-395.

Micheloyannis S, Pachou E, Stam CJ, Breakspear M, Bitsios P, Vourkas M, Erimaki S, Zervakis M (2006) Small-world networks and disturbed functional connectivity in schizophrenia. Schizophr Res 87:60-66.

Raichle ME, Snyder AZ (2007) A default mode of brain function: A brief history of an evolving idea. Neuroimage 37:1083-1090.

Raichle ME, MacLeod AM, Snyder AZ, Powers WJ, Gusnard DA, Shulman GL (2001) A default mode of brain function. Proc Natl Acad Sci U S A 98:676-682.

Ramsey NF, van den Brink JS, van Muiswinkel AM, Folkers PJ, Moonen CT, Jansma JM, Kahn RS (1998) Phase navigator correction in 3D fMRI improves detection of brain activation: quantitative assessment with a graded motor activation procedure. Neuroimage 8:240-248.

Reijneveld JC, Ponten SC, Berendse HW, Stam CJ (2007) The application of graph theoretical analysis to complex networks in the brain. Clin Neurophysiol 118:2317-2331.

Rombouts SA, Barkhof F, Goekoop R, Stam CJ, Scheltens P (2005) Altered resting state networks in mild cognitive impairment and mild Alzheimer's disease: an fMRI study. Hum Brain Mapp 26:231-239.

Salvador R, Suckling J, Schwarzbauer C, Bullmore E (2005a) Undirected graphs of frequency-dependent functional connectivity in whole brain networks. Philos Trans R Soc Lond B Biol Sci 360:937-946.

Salvador R, Suckling J, Coleman MR, Pickard JD, Menon D, Bullmore E (2005b) Neurophysiological architecture of functional magnetic resonance images of human brain. Cereb Cortex 15:1332-1342.

Salvador R, Martinez A, Pomarol-Clotet E, Sarro S, Suckling J, Bullmore E (2007) Frequency based mutual information measures between clusters of brain regions in functional magnetic resonance imaging. Neuroimage 35:83-88.

Seeley WW, Menon V, Schatzberg AF, Keller J, Glover GH, Kenna H, Reiss AL, Greicius MD (2007) Dissociable intrinsic connectivity networks for salience processing and executive control. J Neurosci 27:2349-2356.

Shi J, Malik J (2000) Normalized cuts and image segmentation. IEEE Transactions on pattern analysis and machine intelligence 22:17.

Stam CJ (2004) Functional connectivity patterns of human magnetoencephalographic recordings: a 'small-world' network? Neurosci Lett 355:25-28.

Sun FT, Miller LM, D'Esposito M (2004) Measuring interregional functional connectivity using coherence and partial coherence analyses of fMRI data. Neuroimage 21:647-658.
Thirion B, Dodel S, Poline JB (2006) Detection of signal synchronizations in resting-state fMRI datasets. Neuroimage 29:321-327.
van de Ven VG, Formisano E, Prvulovic D, Roeder CH, Linden DE (2004) Functional connectivity as revealed by spatial independent component analysis of fMRI measurements during rest. Hum Brain Mapp 22:165-178.
Williamson P (2007) Are Anticorrelated Networks in the Brain Relevant to Schizophrenia? Schizophr Bull 33:994-1003.
Ylipaavalniemi J, Vigario R (2008) Analyzing consistency of independent components: an fMRI illustration. Neuroimage 39:169-180.
Zhou Y, Liang M, Jiang T, Tian L, Liu Y, Liu Z, Liu H, Kuang F (2007) Functional dysconnectivity of the dorsolateral prefrontal cortex in first-episode schizophrenia using resting-state fMRI. Neurosci Lett 417:297-302.

supporting material

normalized cut cost

A graph is a mathematical object defined by G = (N,E), consisting of a collection of nodes N, a collection of edges E connecting the nodes, with $w(u,v)$ representing the weighted dependency between node u and v of edge $e(u,v)$. G can be cut into two disjoint subsets A and B with $A \cup B = N, A \cap B = \varnothing$, by removing the connecting edges between the nodes in A and the nodes in B, with a total cut cost of

$$cut(A,B) = \sum_{u \in A, v \in B} w(u,v) \qquad \text{(S.1)}$$

An optimized partitioning of G is one that minimizes the total cut cost S.1 (Shi and Malik, 2000). However, partitioning G in k subsets by minimizing S. 1 may result in grouping small sets of isolated nodes as subsets, as S.1 increases with the number of edges across A and B (Shi and Malik, 2000).

Shi and Malik introduced the *normalized cut cost* (*Ncut*), in which the cut cost of dividing G in subset A and B is defined as a fraction of the total weights of all the nodes in G of $cut(A,B)$:

$$Ncut(A,B) = \frac{cut(A,B)}{assoc(A,N)} + \frac{cut(A,B)}{assoc(B,N)} \tag{S.2}$$

with *assoc*(*A,N*) expressing the total collection of weights from nodes in subset A with all other nodes in G:

$$assoc(A,N) = \sum_{u \in A, t \in N} w(u,t) \tag{S.3}$$

From (S.2) it follows that grouping a small number of nodes as a subset will no longer give a low cut cost, as this will certainly be a large fraction of all the edges of that small subset to the other nodes in G. In a similar way, G can be grouped in *k* subgroups with the Ncut cost defined as:

$$Ncut_k = \frac{cut(A_1,N-A_1)}{assoc(A_1,N)} + \frac{cut(A_2,N-A_2)}{assoc(A_2,N)} + .. + \frac{cut(A_k,N-A_k)}{assoc(A_k,N)} \tag{S.4}$$

chapter 4

specific somatotopic organization of functional connections of the primary motor network during resting-state

martijn van den heuvel, hilleke hulshoff pol

human brain mapping 2009b, in press

Regions of the primary motor network are known to show a high level of spontaneous functional connectivity during rest. Resting-state fMRI studies have reported the left and right motor cortex to form a single resting-state network, without examining the specific organization of the functional connections between sub-regions of the primary motor network. The primary motor cortex has a somatotopic organization, clearly separating regions that control our feet from regions that control our fingers and other body parts. In this study, 3 Tesla resting-state fMRI time-series of 46 healthy subjects was acquired and for all sub-regions along the precentral gyrus the location of the maximum level of functional connectivity within the contralateral primary motor cortex was computed, together with whole brain functional connectivity maps,to examine a possible somatotopic organization of the functional connections of the motor network. Sub-regions of the primary motor cortex were found to be most strongly functionally linked to regions in the contralateral hemisphere with a similar spatial location along the contralateral primary motor cortex as the selected seed regions. Based on the knowledge of a somatopic organization of the primary motor network, these findings suggest that functional sub-regions of the motor network are one-on-one linked to their functional homolog in the contralateral hemisphere and organized in a somatotopic fashion. Examining the specific organization of the functional connections within the primary motor network could enhance our overall understanding of the organization of resting-state functional communication within the brain.

introduction

The pioneering neuroscience work of Penfield demonstrated that the motor regions along the precentral gyrus are organized in a somatotopic fashion, clearly separating motor regions that control our feet from motor regions that control our fingers or other parts of our body (Penfield and Boldrey, 1937; Penfield and Rasmussen, 1968; Rasmussen, 1977). A large number of studies have shown that the specific sub-regions motor regions of the right and left hemispheres of our brain are one-on-one structurally interconnected by cortico-cortical white matter pathways of the corpus callosum tract (Pandya et al., 1971; Wakana et al., 2004; Schmahmann and Pandya, 2006; Wahl et al., 2007; Doron and Gazzaniga, 2008). These structural connections have been suggested to play an important role in interhemispheric communication between the primary motor regions in the coordination of skills that involve bilateral motor regions, for example complex movements that involve both our right and left hand (Eliassen et al., 1999, 2000; Wiesendanger and Serrien, 2004). Primate studies have shown that the structural connections of the motor network are organized in a somatotopic organization and the existence of direct structural connections between left and right primary motor regions that are involved in the same motor function (Pandya et al., 1971; Rouiller et al., 1994; Liu et al., 2002). In addition, recent combined work has shown that such a somatotopic organization of the motor callosal fibers also exists in humans, as studied with fiber tractography using diffusion tensor imaging (Wahl et al., 2007). Interestingly, these structurally connected bilateral motor regions have also been reported to show a high level of functional connectivity during rest (Biswal et al., 1995; Cordes et al., 2000; Beckmann et al., 2005; Damoiseaux et al., 2006; Van den Heuvel et al., 2008b), suggesting that bilateral primary motor regions are not idle in the absence of performing a motor task, but rather show a vast amount of spontaneous neuronal activity that is highly synchronized between left and right hemispheric motor regions. This suggests a high level of ongoing interhemispheric communication during rest between primary motor regions (Biswal et al., 1995; Cordes et al., 2000). Although studies have demonstrated the existence of direct structural callosal connections between the sub-regions of left and right primary motor cortices, the organization of the functional connections between sub-regions of the primary motor network remains unknown.

Functional connectivity is known as the temporal dependence of neuronal activation between anatomically separate brain regions (Aertsen et al., 1989; Friston et al., 1993) and has been extensively investigated by measuring the coherence between resting-state functional Magnetic

Resonance Imaging (fMRI) time-series (Biswal et al., 1995; Xiong et al., 1999; Cordes et al., 2000; De Luca et al., 2005). Of special interest are the low frequency oscillations (<0.1 Hz) of resting-state time-series. These slow oscillations show a high level of coherence between multiple anatomically separate brain regions and are believed to reflect the existence of functional connections between these areas (Greicius et al., 2003; Fox and Raichle, 2007). These correlating resting-state patterns have been consistently found between regions of well-known functional networks, such as regions of the motor, visual and auditory network (Beckmann et al., 2005; Salvador et al., 2005b; Damoiseaux et al., 2006; De Luca et al., 2006; Van den Heuvel et al., 2008a). Further support for a neuronal basis of resting-state signals comes from recent studies indicating that spontaneous fMRI signals strongly correlate with concurrent fluctuations in neuronal spiking (Shmuel et al., 2006; Nir et al., 2008; Shmuel and Leopold, 2008).

The bilateral primary motor cortices have been consistently reported to show a high level of ongoing functional connectivity during rest (Calhoun et al., 2001; van de Ven et al., 2004; Beckmann et al., 2005; Damoiseaux et al., 2006; De Luca et al., 2006; Van den Heuvel et al., 2008b). However, group resting-state studies have mostly reported all primary motor regions to form a single resting-state network, but the existence of specific functional connections between sub-regions of the motor cortex have not yet been studied. Focusing on a high detailed mapping of the interhemispheric functional connections between these sub-regions could provide new insight about the specificity of the functional connections within the motor network and enhance our understanding of functional communication within the primary motor network during rest.

In this study, 3 Tesla resting-state fMRI time-series of 46 healthy participants was acquired to examine the topographic arrangement of the functional connections between the left and right primary motor sub-regions. First, for all seed regions in the left primary motor cortex the location of their strongest functional connection within the right motor cortex was computed, as an indicator of a possible somatotopic organization of the functional connections between the sub-regions of the motor network. Second, for all different motor sub-regions a voxel-wise functional connectivity map (fcMap) was computed to examine whole brain functional connectivity patterns.

methods

participants

46 healthy participants with no psychiatric history were included in this study (age mean/std : 27.7/9.1; gender: 26 male, 20 female, all right handed) after given written informed consent as approved by the medical ethics committee for research in humans (METC) of the University Medical Centre Utrecht, the Netherlands. During the resting experiment the scanner room was darkened and participants were instructed to relax with their eyes closed and to think of nothing in particular. Participants were asked not to fall asleep during the experiment, which was verified directly afterwards. Participants who had fallen asleep or reported to be close to falling asleep were excluded from the study, resulting in the described group of 46 participants.

data acquisition and preprocessing

Resting-State fMRI time-series were acquired on a 3 Tesla Philips Achieva Medical scanner (Philips Medical Systems, Best, The Netherlands) at the University Medical Center Utrecht, The Netherlands. Resting-State Blood Oxygenation Level Dependent (BOLD) signals were recorded during a period of 8 minutes using a fast fMRI sequence (3D-PRESTO pulse sequence with parallel imaging (Golay et al., 2000; Neggers et al., 2008). Acquisition parameters: TR 21.75 ms, effective TE 32.4 ms (using a shifted echo); SENSE p-reduction/s-reduction 2/2; flip-angle 9 degrees; 1000 timeframes; FOV 256x256 mm, voxelsize 4x4x4 mm isotropic, 32 slices covering whole brain; total acquisition time per volume 0.5 sec). The high temporal acquisition sampling rate was used to prevent the backfolding of higher frequencies of possible confounding cardiac (~ 0.8 - 1.0 Hz) and respiratory (~ 0.3 Hz) oscillation patterns into the lower resting-state frequencies of interest (0.01 - 0.1 Hz). Directly after the functional resting-state time-series an additional PRESTO scan with better anatomical contrast using an increased flip angle of 25 degrees was acquired for coregistration purposes. In addition, a T1 weighted image was acquired for anatomical reference (3D FFE pulse sequence. Acquisition parameters, TR=9.87 ms, TE=4.6 ms; SENSE reduction 1.7/1.4; flip-angle 8 degrees; FOV 240x240 mm, voxelsize 0.75x0.75x0.8mm, 180 slices).

preprocessing

All preprocessing steps were done with the SPM2 software package (http://www.fil.ion.ucl.ac.uk). Functional time-series were corrected for small head movements by realigning all scans to the last functional scan. Registration to

the last functional scan was used to maximize overlap with the high contrast functional scan. The functional time-series were coregistered to the high contrast functional image, by taking the last functional scan as a source. Next, the T1 image was coregistered to the high contrast functional image, to spatially match the resting-state fMRI time-series. A cortical segmentation was performed on the T1 image using the Freesurfer software package (http://surfer.nmr.mgh.harvard.edu/), providing an individual cortical segmentation and automatic parcellation of each hemisphere in 34 areas, including an individual segmentation of the left and right hemispheric precentral gyrus (Fischl et al., 2004). Normalization parameters were estimated by nonlinear registration of the T1 image to standard space, matching the T1 MNI-152 template brain. Next, all functional scans were normalized to match standard space to enable cross-subject comparison, by using the T1 normalization parameters. The functional images were spatially filtered with a full width half max smoothing kernel of 8 mm. Next, resting-state the time-series were bandpass filtered with a finite impulse response bandpass filter (bandwidth 0.01 - 0.1 Hz). Filtering was performed to select the low resting-state frequencies of interest (0.01-0.1 Hz) (Biswal et al., 1995; Cordes et al., 2001) and to eliminate low frequency noise (including slow scanner drifts of < 0.01 Hz) and influences of higher frequencies (> 0.1 - 1 Hz) reflecting possible cardiac or respiratory oscillations (Cordes et al., 2001). The individual cortical segmentation maps were normalized and resliced to a 4x4x4mm resolution to spatially overlap the resting-state fMRI time-series.

correlation analysis I, organization of interhemispheric functional motor connections at group level

A somatotopic organization of the functional connections of the primary motor regions was examined by computing the topographic arrangement of the regions that showed the maximum level of functional connectivity between all left and right primary motor voxels. For each seed voxel in the left primary motor cortex the location (i.e. voxel) with the highest level of functional connectivity within the right motor cortex was computed and averaged over the group of subjects. This was done in a 3 step analysis:

step 1 selection of seed voxels. From each of the individual normalized cortical segmentation maps the voxels in the left precentral gyrus were selected from the cortical segmentation map. Individual motor cortex segmentation maps were averaged over the group of subjects. Voxels that were assigned to the primary motor cortex anatomical map in 5 or more subjects were included in the groupmap of the primary motor cortex, resulting in a wide groupmap

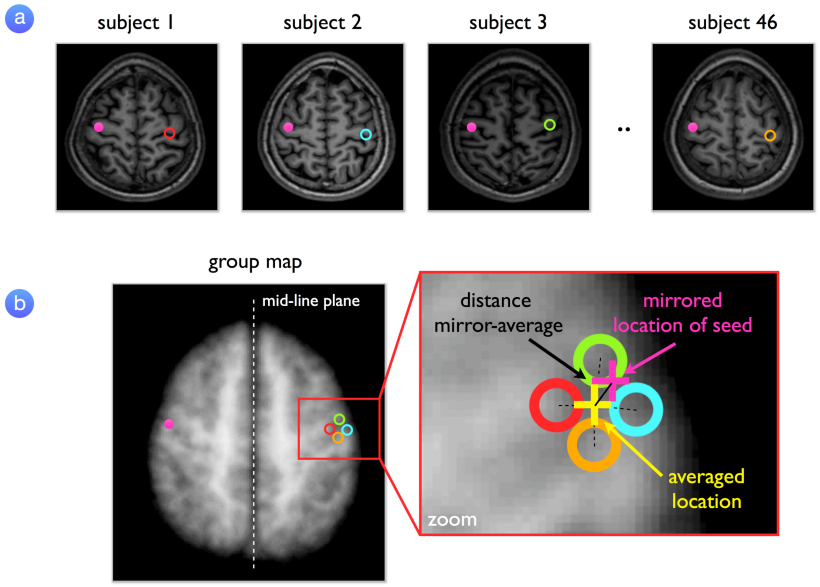

figure 4.1 computation of the averaged location of the strongest functional connection in the right motor cortex of a seed region located in the left primary motor cortex For all left motor seed regions (i.e. voxels) the location with the strongest functional connection (i.e highest correlation) was computed in all subjects. Figure 4.1a shows in 4 individual subjects the location of the seed voxel, indicated by the magenta filled circle and the individual location of the voxel in the right motor cortex that showed the highest level of functional connectivity with this seed voxel, indicated by a colored unfilled circle. Next, these individual locations were averaged over the group of subjects (figure 4.1b), marking the location in the right motor cortex that showed the highest functional connection with the seed voxel averaged over the group of subjects. In addition, for each seed voxel (yellow +), a mirrored location in the right hemisphere was computed (orange +), by mirroring the location of the seed voxel in the mid-line that separates the two hemispheres (dotted line). For each left-right connectivity pair, the distance between the mirrored location in the right motor cortex of the seed and the group averaged location with the strongest functionally connection was computed, as an indication of how close the computed location was located near a region in the right motor cortex with a similar motor function as the selected seed region (figure 4.1b). This procedure was repeated for all seed voxels (>1000) in the left motor cortex.

containing all seed regions (i.e. voxels) of the left primary motor cortex (~1000 seed voxels) and the voxels of the right primary motor cortex.

step 2 computing seed-based functional correlations with contralateral precentral gyrus. For each individual dataset, the resting-state time-series of each selected left motor seed voxel was correlated with the time-series of all voxels in the right primary motor cortex. This was repeated for all seed voxels in the left motor cortex.
step 3 group analysis: selection of location of highest functional connectivity at group level. For each individual dataset and for each seed voxel, the voxel in the right motor cortex that showed the highest level of functional connectivity (i.e. highest correlation) with the seed voxel in the left motor cortex was selected (figure 4.1a, magenta filled circle). This resulted in 46 flagged voxels in the right motor cortex for each left motor seed voxel over the group of subjects. The 46 flagged voxels indicated the individual locations that showed the strongest level of functional connectivity in the right motor cortex with the selected seed voxel in the left motor cortex (figure 4.1a unfilled circles). From these 46 voxels in the right motor cortex the average location over the group of subjects was computed (figure 4.1b, yellow +). This computed average location in the right motor cortex reflected the region that showed the strongest functional connection with the selected seed voxel in the left primary motor cortex averaged over the group of subjects.

This 3 step procedure resulted in a group-wise voxel-by-voxel mapping of the functional connections between the primary left and right motor cortex. Every seed voxel in the left motor cortex formed a matching pair with a corresponding location (i.e. voxel) in the right motor cortex that showed over the group of subjects the strongest functional connection (i.e. highest correlation between their resting-state time-series).

Next, for each left-right connectivity pair, a corresponding 'mirrored location' of the selected seed voxel in the right primary motor cortex was computed, as an indicator of how the strong the left-right functional connections would link regions with a similar motor function, for example left and right primary motor regions that respectively control our right and left hand. This mirrored location was computed by mirroring the coordinates of the left motor seed voxel in the mid-line plane that divides the two hemispheres (figure 4.1b, mirrored location indicated by magenta +). As the left and right motor regions follow a rather similar somatotopic mapping, the mirrored location would provide a proper estimation of a region in the contralateral right motor cortex with a similar motor function as the selected seed voxel located in the left primary motor cortex. For each of the left-right connectivity pairs, the Euclidian distance between the mirrored seed voxel and the group-averaged region that showed the highest level of functional connectivity was computed, as a measure of how the

region with the strongest functional connection in the right motor cortex was located near the same functional region as the seed voxel in the left motor cortex (figure 4.1, panel b). In addition, also at the individual level, the distance between the mirrored seed and the voxel that showed the highest level of functional connectivity was computed. Over all seed-voxels, this resulted in an individual distribution of distances for each subject. To asses inter-subject variance, these individual distributions were then averaged over the group of subjects.

In addition, to verify the interhemispheric functional connections between left and right primary motor regions, the correlation analysis (analysis I) was repeated in the exact same manner, but now for all seed voxels in the right primary motor cortex. For all voxels in the right motor cortex (>1000 seed voxels along the right motor cortex) this resulted in the identification of the location in the left motor cortex with the strongest functional connection with the selected right motor seed voxels.

To further test the statistical significance of the left-right connectivity pairs, a Monte Carlo simulation was performed to obtain the null-distribution of distances that could occur under the null-hypothesis. For each seed-voxel, the seed-specific null-distribution of each left-right connectivity pair was obtained by selecting 46 random location in the contralateral hemisphere (as if the individual left-right connections would be completely random) and the distance between the group-averaged location of these 46 locations and the mirrored seed was computed and repeating this for 10,000 iterations. Next, the real data was tested against the resulting null-distribution of random occurring distances, by assigning an overall adjusted p-value to each found real-data distance between the mirrored seed and the strongest functionally connected location in the contralateral hemisphere.

correlation analysis II, group-based voxel-wise seed connectivity maps of primary motor cortex

Analysis I provided information about the organization of the maximum level of functional connectivity between sub-regions of the left and right hemispheric primary motor cortices. To further examine the overall functional connectivity patterns of the primary motor regions and to provide additional information about the specificity of the functional connections, a second correlation analysis was performed in which for each seed voxel in the left motor cortex a group averaged functional connectivity map (fcMap) was computed. These fcMaps were computed in a 3-step procedure.

step 1 selection of seed voxels. The seed voxels in the left motor cortex were selected in a similar manner as in correlation analysis I, by averaging the

individual cortical segmentation maps over the group of subjects. This resulted in a group map of the seed voxels in the left primary motor cortex. As such, the collection of seed voxels was identical to the collection of analysis I (>1000 seed voxels).

step 2 computation of the seed-based fcMaps. For each of the group selected seed voxels of the left primary motor cortex, a matching fcMap was computed by correlating the resting-state fMRI time-series of the selected seed voxel with all other voxels in the brain. For each individual dataset, this resulted in a collection of seed based fcMaps, showing all functional connections of the multiple sub-regions of the left motor cortex.

step 3 group analysis: formation of group seed based fcMap. For each of the left primary motor seed voxels, the individual seed based fcMaps were averaged over the group of subjects. This resulted in a whole brain group fcMap for each of the seed regions (i.e. seed voxels) in the left hemispheric motor cortex.

To determine the statistical significance of the resulting seed based group fcMaps over the seed voxels and over the group of subjects, a nonparametric multiple comparisons procedure was conducted (Cordes et al., 2000) in a Monte Carlo simulation approach, holding strong control over type I errors (i.e. false positives). To compute the null statistic for the resting-state data, the time-series of a seed-voxel was randomized, by randomization of the phase of its complex Fourier components, not affecting the power spectrum of the time-series. Next, the seed specific null distribution of the correlation coefficients was computed by using a Monte Carlo (MC) simulation, in which all possible cross-correlations between the seed time-series after phase randomization and all other gray matter voxels were computed over a number of 10,000 MC iterations. This procedure defined a α=0.05 threshold (corrected for multiple comparisons) of those correlations that occurred with a $p < 0.05$ (Bonferroni corrected). Finally, the computed individual significant thresholds were averaged over all seed voxels and over all subjects. This Monte Carlo procedure resulted in a group threshold of α=0.05 (Bonferroni corrected) and all correlations of the group fcMap of the original seed time-series with all other voxels in the brain map were then tested against this threshold, marking supra-threshold seed-voxel resting-state fMRI correlations as significantly different different from the null distribution with an α=0.05 (Bonferroni corrected).

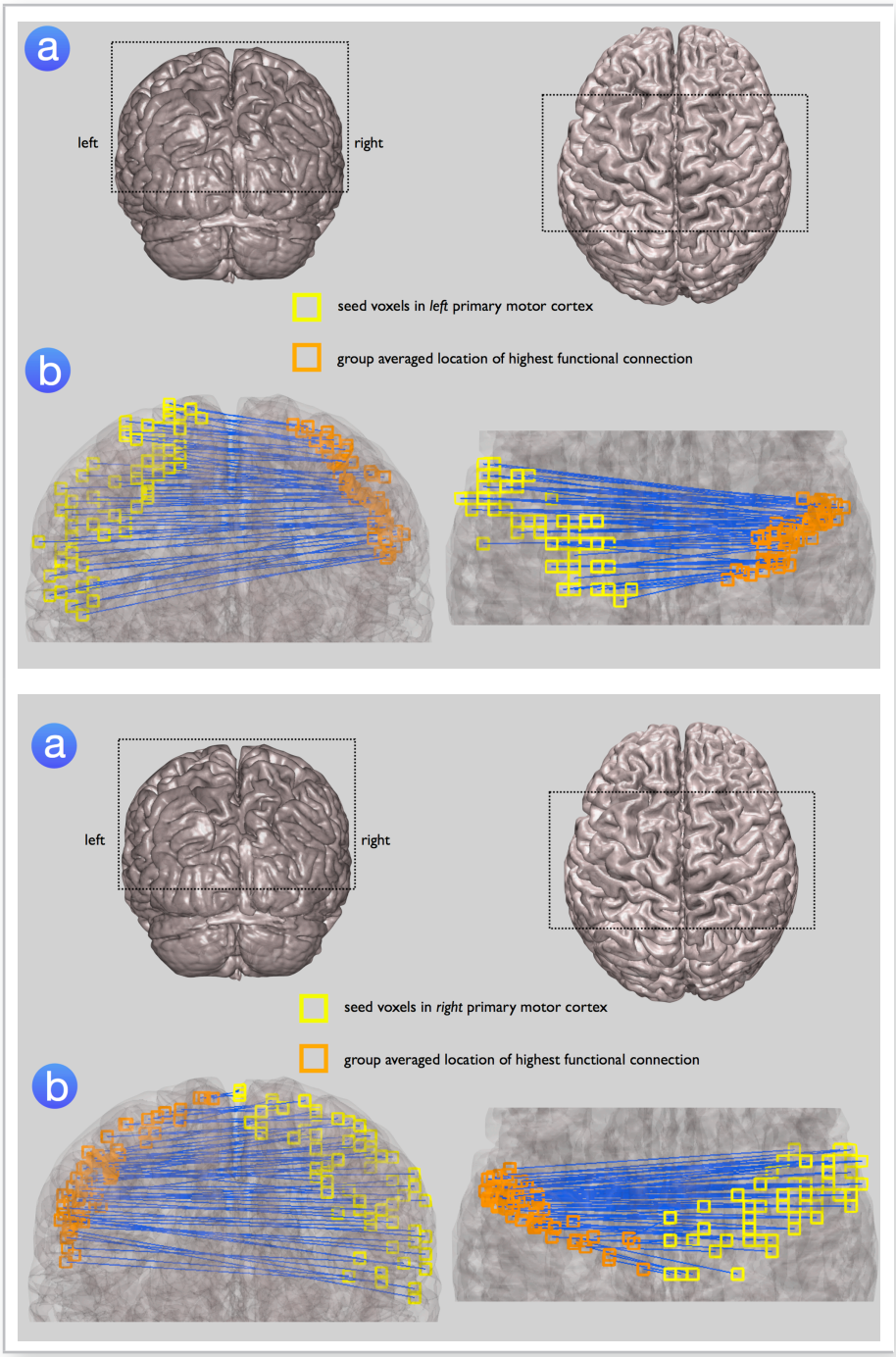
a
left
right
seed voxels in *left* primary motor cortex
group averaged location of highest functional connection
b
a
left
right
seed voxels in *right* primary motor cortex
group averaged location of highest functional connection
b

figure 4.2 connectivity pairs of left motor seed regions and their group averaged functionally linked regions in the contralateral motor cortex. Figure 4.2a illustrates a coronal and axial view of a 3D rendering of the anatomical scan. The dotted square marks the region shown in figure 4.2b. Left and right panel of figure 4.2b show the voxel-by-voxel seed regions in the left motor cortex (yellow squares) and the location of the region in the right motor cortex that showed the strongest level of functional connectivity (i.e. highest correlation between their resting-state time-series) averaged over the group of 46 subjects (orange squares). Each matching left-right connectivity pair is connected by a blue line. Figure shows 1 on every 20 left-right pairs (evenly distributed) to prevent cluttering of the image. Figure clearly demonstrates that the seed regions are most strongly functionally linked to their direct functional homolog in the right motor cortex.

figure 4.4 connectivity pairs of right hemispheric motor seed regions and their matching group averaged functional connections in the left primary motor cortex. To verify the organization of the functional connections between left and right primary motor regions (figure 4.2), the correlation analysis (analysis I) was repeated in the exact same manner, but now for all seed voxels in the right primary motor cortex. Figure 4.4a illustrates a coronal (left panel) and axial view (right panel) of a 3D rendering of the anatomical scan. Dotted square marks the region shown in figure 4.4b. The left and right panel of Figure 4b show the examined seed voxels along the right primary motor cortex (yellow boxes) and their matching location in the left primary motor cortex that showed the highest level of functional connectivity averaged over the group of 46 subjects (orange boxes). Matching right-left voxel pairs are connected by a blue connection. Figure 4.4 shows 1 on every 20 right-left pairs (evenly distributed). Figure 4.4 illustrates that sub-regions along the right motor cortex with a distinct motor function are strongly functionally connected to their direct functional homolog in the contralateral left primary motor cortex. The right-left matching voxel pairs show large similarity with the left-right voxel pairs shown in figure 4.2.

results

correlation analysis I, organization of interhemispheric functional motor connections at group level

Figure 4.2 shows the selected seed voxels in the left hemispheric primary motor cortex (yellow boxes) and the paired location in the right motor cortex (orange boxes) that showed the highest level of functional connectivity averaged over the group of 46 subjects. The left-right voxel pairs are displayed on an 3D rendering of the anatomical T1 image. The left panel of figure 4.2a shows a coronal view of the 3D rendering, the right panel shows an axial view of the rendering. The left panel of figure 4.2b shows a zoomed in version of the coronal view with the location of the seed voxels (yellow boxes) and their matching group averaged location in the right motor cortex (orange boxes) that showed the highest level of functional connectivity with the seed voxels. Figure 4.2 shows one on every 20 of the total number of computed connection pairs to prevent cluttering (evenly distributed over the total collection of seed regions). Each matching left-right pair is connected by a blue connection to clearly indicate the location of the matching voxel-pairs. In addition, the right panel of figure 4.2b shows the axial view of the matching left-right voxel pairs and the right panel. Note that the computed locations in the right motor cortex appear to be more 'packed together', i.e. tend to be clustered towards the center line of the cortex. This is likely to result from the fact that the maximum functionally connected location in the right motor cortex was computed as the average location of the maximally connected voxels over the group of 46 subjects. Individual voxel locations were restricted to be within the motor cortex and as a result the group averaged location, indicating the average location of the 46 individual locations, becomes slightly more located near the center-line of the cortex. The left-right connections of 9 exemplary individual datasets are shown in supplementary figure 4.1.

Figure 4.3a shows the distribution of the distance between the computed location of the highest connected region and the mirrored location of the seed voxel. Figure 4.3a shows that the mean distance between the computed group averaged location and the mirrored location in the right motor cortex was around 13.9 mm (SD: 7.6) as indicated by the mean of the distribution. This indicated that, on average, the distance between the region in the right motor cortex that showed the strongest functional connection over the group of subjects with a specific seed region in the left motor cortex and the region that reflected the right hemispheric functional homolog of the left motor seed region (i.e. the mirrored location) was on average only 3.5 fMRI voxels. As the group distribution does not follow a Gaussian function,

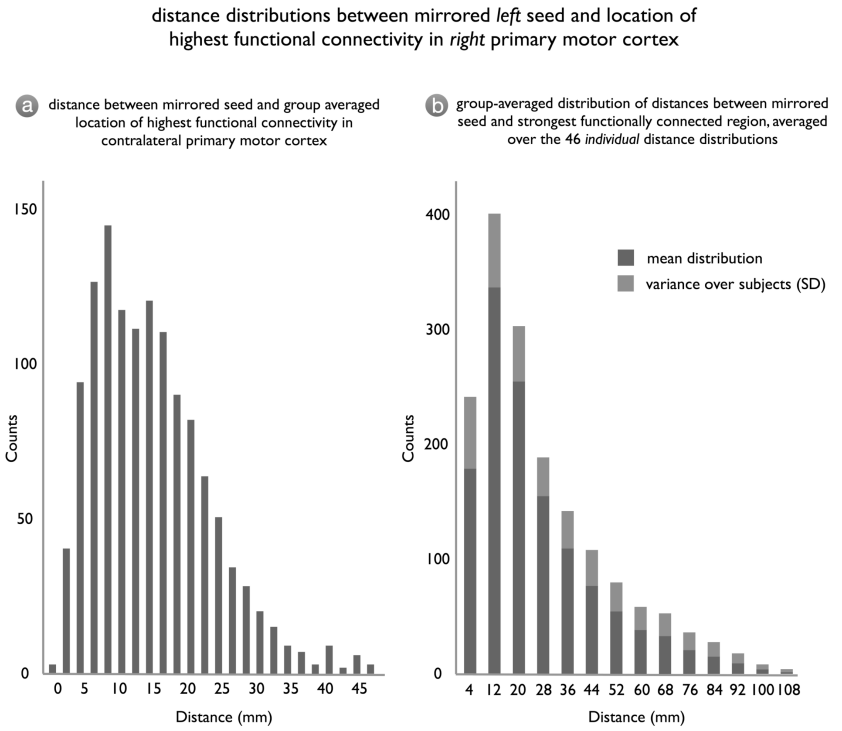

figure 4.3 distribution of the distance between the mirrored seed locations and the group averaged location of the region in the right motor cortex that showed the highest level of functional connectivity with the left motor seed regions The short mean distance of 13.9 mm (SD: 7.6, modus 8 mm) indicates that on average the distance between the computed location of the seed region and the region in the right motor cortex that showed the strongest level of functional connectivity with the left motor seed was around only 3.5 fMRI voxels. Figure 4.3b shows the group-averaged distribution, resulting from averaging the 46 individual distance distributions. Due to more signal variance at the individual level, at the individual level the average distance is larger than compared to the average distance to the group averaged location (figure 4.3a), but it is still relatively short. The mean distance at the individual level was around 25.6 mm (SD: 19), but as the distributions are clearly not Gaussian, the modus may be a better estimation of the mean distance, indicating a average distance between the mirrored seed and strongest functional location of only 12mm (~3-4 fMRI voxels). Together, figure 4.3a and 4.3b suggest that the regions of the motor cortex are strongly functionally linked to their direct functional homolog in the contralateral hemisphere.

the modus might be a better estimation of the average distance, indicating an even shorter average distance of ~8mm (2~3 fMRI voxels). Furthermore,

as an indication of inter-subject variance, also the distance between the mirrored seed and strongest functional location at the individual level was computed. These individual distributions were then averaged, resulting in a group averaged distribution, indicating the variance over the group of subjects, depicted by figure 4.3b. Interestingly, figure 4.3b shows that also at the individual level the distance between the mirrored seed and strongest functionally linked location was on average relatively short, with a mean of 25.6 mm (SD: 19). As the distribution is clearly not Gaussian, the average distance is likely better described by the modus, which indicates a short distance between the mirrored seed and strongest functionally linked region of ~12mm (3-4 fMRI voxels), which overlaps with the short group distance as indicated by the modus of the group distribution of ~8mm (~2-3 fMRI voxels) in figure 4.3a.

The statistical significance of the observed left-right connectivity pairs was examined by testing the found mirrored-seed distances against the null-distribution of mirrored-seed distances, obtained using a MC simulation (see Materials and Methods, Analysis I). On basis of this null-distribution, each left-right connection was assigned an overall adjusted p-value. Supplementary figure 4.2 shows the p-values of the left-right connectivity pairs of figure 4.2. This analysis indicated that almost all connectivity pairs (>92% of all tested connectivity pairs) were below the α=0.05 threshold. Moreover, even after applying strict Bonferroni correction to correct for multiple comparisons the majority of unique connectivity pairs (>72%) still showed a left-right orientation that was significantly different from random [$p<0.05$, Bonferroni corrected].

Furthermore, to verify the examined topology of interhemispheric left-right connections, the functional connections of all seed voxels in the right motor cortex were also computed, in the same way as the functional connections of the left motor regions were examined. The location of the maximum functionally connected regions in the left motor cortex and their matching right hemispheric seed regions are shown in figure 4.4. The right-left connectivity pairs showed strong overlapping results with the left-right connectivity pairs of the seed regions in the left primary motor cortex (figure 4.2).

correlation analysis II, group-based voxel-wise seed connectivity maps of primary motor cortex

A second analysis was performed in which for each seed voxel in the left motor cortex a whole brain group averaged fcMap was computed (by averaging the individual seed-based fcMaps) completely mapping the

functional connections of the primary motor cortex in high detail (i.e. voxel resolution). Figure 4.5 shows for 9 seed-regions located along key areas of the left motor homonculus their matching computed group averaged fcMap. Figure 4.5 shows for each of these 9 seed-regions their functional connections along the left and right hemispheres. For each of these 9 key regions, the seed location in the left motor cortex is marked with a filled black colored circle. The location of the region in the right hemisphere that showed the highest level of functional connectivity with the seed region is marked with a black colored arrow. To test for possible functional correlation map outliers, it was tested for each seed voxel, whether the average correlation of an individual fcMap was different from the average correlation over the group of subjects by more than 3 standard deviations. As expected, the number of outlier situations was very low, occurring at only 0.1% of all evaluated situations (over all seed voxels and all subjects). A post-hoc analysis indicated that removing these small number of outliers out of the group analysis had no effect on the nature of the results.

To determine the statistical significance of the group fcMaps a nonparametric multiple comparisons Monte Carlo procedure was used, determining the mean null distribution of the correlation coefficients over the group of subjects, strongly controlling for type I. This nonparametric multiple comparison Monte Carlo procedure determined a robust significance correlation threshold of 0.66 (SD : 0.068) with a $p < 0.05$ (Bonferroni corrected). Seed-specific fcMap correlations above this threshold were significantly different from the null-distribution and marked as statistically significant at a α=0.05 (Bonferroni corrected).

discussion

The main finding from this study is the existence of a specific somatotopic organization of the functional connections of the primary motor cortex during rest. Examining the specific organization of the functional connections within the primary motor network by measuring the level of synchronization between the spontaneous fMRI signals of a large number of sub-regions of the primary motor network suggest that the spontaneous resting-state fMRI signals of the sub-regions of the primary motor cortex are most strongly correlated with the time-series of specific sub-regions in the contralateral motor cortex that are located near the same spatial orientation as the selected seed sub-regions. As the primary motor network is well known to have a somatotopic organization, these findings strongly suggest that the sub-regions of the primary motor cortex are one-on-one functionally linked to their direct functional homolog in the contralateral motor cortex.

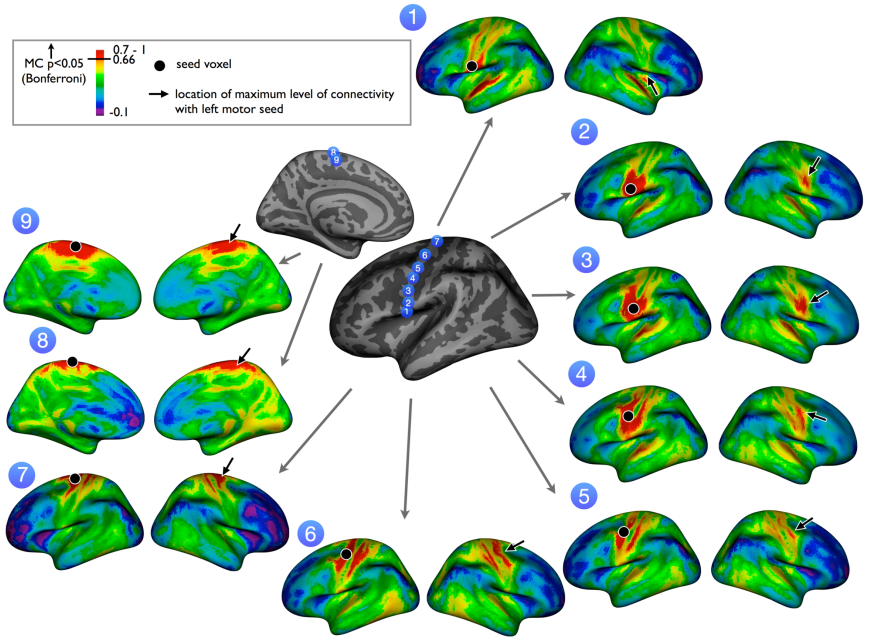

figure 4.5 group averaged functional connectivity maps of key regions along the left primary motor cortex Figure shows the group-averaged fcMaps of 9 seed regions located along key regions of the primary motor cortex. For each of the seed voxels in the left primary motor cortex and for each individual dataset a matching fcMap was computed by correlating the individual resting-state fMRI time-series of the seed voxel with all other cortical voxels. For each seed voxel, the group-averaged fcMap was computed by averaging the 46 individual seed-based fcMaps. This resulted in a group fcMap for each of all seed voxels (>1000) in the left primary motor cortex. Figure shows the fcMaps of 9 key regions on an inflated 3D rendering of the group averaged T1 image (the inflated rendering was created with the freesurfer software package). For each of the 9 maps, the location of the seed region is marked with a filled black circle and the location on the group-averaged fcMap that showed the highest level of functional connectivity with the seed voxel is marked with a black arrow. Using a nonparametric multiple comparisons Monte Carlo simulation a α = 0.05 (Bonferroni corrected) statistical threshold of 0.66 was determined (see Materials and Methods section). Figure demonstrates a high level of specificity of the functional connections of the somatotopic organized motor regions.

As such, our findings suggests the possible formation of functionally linked sub-networks within the motor resting-state network.

Spontaneous brain activity was measured with 3 Tesla resting-state fMRI recordings in a group of 46 healthy subjects. The functional connections between all left and right primary motor regions were examined

by correlating the resting-state time-series of all possible voxel-pairs located in the left and right motor precentral gyrus. For all sub-regions of the left motor cortex (>1000 seed voxels), the location in the right primary motor cortex with the highest level of functional connectivity was computed (analysis I) as well as matching whole-brain functional connectivity maps (fcMaps) (analysis II). The matching left-right connectivity pairs of analysis I are shown in figure 4.2, suggesting that the functional connections between the sub-regions of the primary motor cortex follow a specific somatotopic organization. As the left and right hemispheric motor regions are assumed to follow a similar somatotopic mapping along the primary motor cortex, the mirrored locations of the seed regions would provide a proper estimation of the regions in the contralateral hemisphere with a similar motor function as the seed voxels. The short average distance of around 14 mm (~3.5 voxels) between the mirrored seed and its group averaged functionally connected location suggests that the regions located along the precentral gyrus are strongly functionally connected to their direct functional homolog in the contralateral primary motor cortex (figures 4.3a and 4.3b). In addition, all computed right-left connections (taking all right motor voxel as seeds, see Method section) showed highly overlapping results with the computed left-right connectivity pairs (figure 4.4). Furthermore, the voxel-wise whole-brain fcMaps (analysis II) indicated that these functional connections are quite region specific. Panel 1 to 9 of figure 4.5 illustrate for 9 key seed regions located along the left motor cortex their matching group-averaged fcMAP. These fcMaps suggest a high level of specific inter-hemispheric functional connectivity between bilateral primary motor regions. Indeed, the fcMaps do not show other large connectivity hotspots in the contralateral motor cortex besides the regions located near the mirrored seed regions. Taken together, our results suggest that the cortical regions of the motor homunculus are one-on-one functionally connected to their direct functional homolog in the contralateral motor homunculus during rest. This means that interhemispheric functional connections between primary motor regions are highly ordered according to their motor function, functionally linking motor regions that control our right foot directly with regions that control our left foot and linking motor regions that control our right hand directly to motor regions that control our left hand.

The focus of our study was on the high detailed voxel-vise mapping of the functional connections of the bilateral somatotopic organized primary motor regions during rest. Task-dependent fMRI studies have extensively verified the results of Penfield, showing that distinct motor regions of our primary motor cortex become specifically activated when we perform a motor task, for example moving our fingers or other body parts (Kell et al.,

2005; Wahl et al., 2007; Newton et al., 2008). Several group resting-state fMRI studies have demonstrated that the regions of the primary motor network also show a vast amount of spontaneous neuronal activity in the absence of performing a task (i.e during rest) that is highly coherent between left and right hemispheric motor regions (Beckmann et al., 2005; Damoiseaux et al., 2006; De Luca et al., 2006; Van den Heuvel et al., 2008a; Van den Heuvel et al., 2008b). These group resting-state studies have focused on the selection of global resting-state networks and have reported all motor regions to form a single resting-state network. However, these studies have not examined the functional connections between sub-regions of the motor cortex with distinct motor functions. The results of our current study suggest that all motor regions do not just form a single large resting-state network. Instead, our results suggest that during rest distinct regions of the primary motor network with a specific motor function, like the regions that control our feet, hand or lips, form functionally linked interhemispheric sub-networks within the full resting-state motor network.

In this study, we used the relative traditional methodology of seed-based fcMaps (Biswal et al., 1995; Xiong et al., 1999; Cordes et al., 2000). Combining this fcMap methodology with a voxel-by-voxel mapping enabled a systematic mapping of the functional connections of a large number of seed regions (i.e. voxels) along the precentral gyrus. Most other resting-state studies have used a single seed or a small number of seed regions to examine interregional connectivity (Biswal et al., 1995; Lowe et al., 1996; Biswal et al., 1997; Lowe et al., 1998; Xiong et al., 1999; Cordes et al., 2000; Lowe et al., 2000; Cordes et al., 2001; Greicius et al., 2003; Fox et al., 2005; Fransson, 2005; Fox and Raichle, 2007). Of course, the proposed systematic voxel-based mapping allows for the examination of the functional connections of other cortical regions besides the primary motor regions. It potentially allows for a systematic mapping of the full functional connectivity architecture of the human brain. New methods like independent component analysis (ICA) (Beckmann et al., 2005; Damoiseaux et al., 2006; De Luca et al., 2006) and clustering based methods (Cordes et al., 2002; Van den Heuvel et al., 2008a) have shown the potential of examining whole brain voxel-wise functional connectivity patterns. In addition, the overall organization of whole-brain functional connectivity has been examined with resting-state electroencephalogram and magnetoencephalographam recordings (Breakspear et al., 2003; Stam et al., 2003; Stam, 2004), and with resting-state fMRI recordings on both a regional scale (Salvador et al., 2005a; Achard et al., 2006; Achard and Bullmore, 2007) as well as on a whole brain voxel-wise scale (Eguiluz et al., 2005; Van den Heuvel et al., 2008c); (Buckner et al., 2009). Interestingly, these studies have

shown that the functional brain as a whole is likely to be organized in small-world fashion (Achard et al., 2006; Van den Heuvel et al., 2008c; Bullmore and Sporns, 2009), indicating that local and global functional connections are organized in a highly efficient manner (Latora and Marchiori, 2001; Achard and Bullmore, 2007; Bullmore and Sporns, 2009). Examining these efficiently organized functional connections with a voxel-wise fcMap approach could provide a high detailed mapping of the functionally connected brain network.

Novel neuroimaging techniques can enable the examination of both the structural and functional connections of our brain. Diffusion Tensor Imaging (DTI) is a technique to determine the main diffusion direction of water molecules in brain tissue (Beaulieu and Allen, 1994; Basser et al., 2000) and allows for the reconstruction of the white matter pathways of the brain (Mori and van Zijl, 2002; Wakana et al., 2004; Schmahmann and Pandya, 2006; Wahl et al., 2007; Hagmann et al., 2008). A large number of studies have shown that the primary motor regions in the left and right hemispheres of our brain are structurally interconnected by the cortio-cortical white matter pathways of the corpus callosum (Pandya et al., 1971; Wakana et al., 2004; Schmahmann and Pandya, 2006; Wahl et al., 2007; Doron and Gazzaniga, 2008). These studies demonstrated that left and right primary motor regions are one-on-one structurally connected in both humans (Wahl et al., 2007) and primates (Schmahmann and Pandya, 2006). The results of our current study, showing the existence of a somatotopic organization of the interhemispheric functional connections between left and right motor regions are in support of these findings. Together, they suggest a direct relationship between the structural and functional connections between left and right primary motor regions of our brain. Indeed, structural corpus callosal tracts have been suggested to play an important role in interhemispheric communication, needed for the coordination of skills that involve both motor regions (Eliassen et al., 1999, 2000; Wiesendanger and Serrien, 2004). Moreover, recent studies combining DTI and resting-state fMRI have suggested a direct link between the structural and functional connections of our brain (Koch et al., 2002; Andrews-Hanna et al., 2007; Greicius et al., 2008; Hagmann et al., 2008; Van den Heuvel et al., 2008b; Van den Heuvel et al., 2009). For example, complete section of the corpus callosum has been reported to lead to loss of interhemispheric functional connectivity (Johnston et al., 2008). Furthermore, the microstructural organization of the white matter cingulum tract has been directly related to the level of functional connectivity between key regions of the so-called 'default mode network' (Van den Heuvel et al., 2008b). Concerning specific structural interhemisperic connections between primary motor regions, the

microstructural organization of corpus callosal tracts has been related to task-induced transcranial magnetic stimulation (TMS) inhibition effects between contralateral motor regions (Wahl et al., 2007). In addition, decreased levels of interhemispheric motor functional connectivity have been associated with the integrity measures of corpus callosal tracts in patients with multiple sclerosis (Lowe et al., 2008). The results of our current study suggest that the interhemispheric functional connections between bilateral motor regions are highly region specific. Therefore, it is of special interest to examine how the strength of these functional connections relate to the microstructural organization of specific white matter structural connections that connect these bilateral motor regions.

Some points have to be considered when interpreting our results. First, the exact neurophysiological underlying of resting-state fMRI BOLD signals is not fully understood. An increasing number of studies have suggested that the observed coherency between resting-state fMRI time-series of anatomically separate cortical regions is reflecting synchronization of the underlying neuronal activation patterns of these regions (Biswal et al., 1995; Greicius et al., 2003; Buckner and Vincent, 2007). This is supported by the notion that spontaneous BOLD fluctuations have been found to correlate with concurrent fluctuations in neuronal spiking, suggesting a direct link between resting-state BOLD signals and neuronal activity (Shmuel and Leopold, 2008). However, it has also been suggested that physiological signals like low-frequency respiratory oscillations (~0.3 Hz) or more higher frequent cardiac oscillations (0.8 - 1.0 Hz) could confound the BOLD time-series (Wise et al., 2004; Shmueli et al., 2007). In addition, possible slow patterns like variations in heart rate and interactions between cardiac and respiratory signals may affect the low resting-state frequencies of interest (Birn et al., 2006), making the resting-state correlations less specific. In this study, a high temporal fMRI acquisition protocol was used to minimize the possible backfolding of higher frequencies (0.3 - 1 Hz) into the resting-state frequencies of interest (0.01 - 0.1 Hz) (Cordes et al., 2001). Second, in this study we focused on the examination of functional connections between the sub-regions of the primary motor cortex. The average distance between the mirrored seed region and the strongest connected target region turned out to be on average very short (on average they were only 3.5 voxels separation, figure 4.3), indicating that functional sub-regions are most strongly functionally linked to a region with the same spatial location along the precentral gyrus in the contralateral hemisphere. As mentioned, it is well known that the left and right precentral gyrus have a somatotopic organization (Penfield and Boldrey, 1937; Penfield and Rasmussen, 1968; Rasmussen, 1977). Assuming that the left and right precentral gyrus in low

spatial detail follow a similar somatotopic organization, our results suggest that the sub-regions of the primary motor cortex are most strongly connected to their direct functional homolog in the contralateral motor cortex. However, as all seed areas and best connected target voxels in the other hemisphere were defined on anatomical and not on functional grounds, we cannot be completely sure about whether the seed and target did indeed have the exact same motor function. The topographical representation of motor cortex is known to be slightly variable between the left and right motor cortex due to for example handedness, resulting in a somewhat asymmetric representation of the functional sub-regions (Amunts et al., 1996; Amunts et al., 2000). Examining the specific location of each motor function using task related fMRI and selecting the seed voxels based on their function rather than on their anatomical location, could provide additional information about the organization of functional connections between sub-regions that share the exact similar motor function along the left and right motor cortex. However, unfortunately, using task related fMRI one is limited to the localization of only a minimal number of motor functions, as every function would require its own specific task and would require a separate fMRI experiment. Therefore, to map the overall organization of the functional connections between all sub-regions of the motor network we selected the seed voxels based on their anatomical location. To minimize the possible asymmetric variation in functional representation, the resting-state fMRI images were spatially smoothed to lessen local anatomical variation. Future studies of our lab are aimed to zoom in on key functional sub-regions along the primary motor cortex, using high-resolution task related fMRI acquired with high field MR to determine their exact location, and to map out the functional connections between these sub-regions in high detail.

Third, as can be clearly seen from figure 4.2 and 4.4 and briefly mentioned in the results section, the computed strongest functionally connected locations in the contralateral motor cortex appear to be more ‘packed together’, i.e. are slightly more localized near the center line of the cortex (figure 4.2 and 4.4). Although the seed voxels in the left primary motor cortex are clearly uniformly distributed along the left precentral gyrus, their matching group averaged strongest functionally connected regions in the right motor cortex tend to be more clustered towards the mid-line of the precentral gyrus. This effect was believed to result from the grouping of the strongest functionally linked locations across the individual datasets, following the procedure as depicted in figure 4.1. As a seed voxel is always linked to a voxel in the contralateral precentral gyrus, as the strongest functional connections in an individual dataset was restricted to be in the precentral gyrus, the computation of the average strongest

functionally linked location (figure 4.1) would always be more orientated near the center line of the group averaged precentral gyrus. However, as the effect appears to be systematic along the precentral sulcus an alternative explanation might include the existence of a possible mismatch between the neuronal and vascular signal, indicating a more fundamental issue of the resting-state fMRI measurement method. However, in our study, we believe that his is not the case. First, due to the nature of the PRESTO technique a small diffusion weighting is included in the acquisition, reducing the signal contribution of fast moving water molecules, making the PRESTO fMRI signal to be more related to signals coming from smaller vessels and the capillaries than to signals coming from the larger vessels of the brain (Neggers et al., 2008). Second, more importantly, the clustering effect as seen in the group analysis, was not shown in the individual data. Supplementary figure 4.1 shows individual left-right connectivity pairs, showing for 9 exemplary individual datasets the distribution of the seed voxels in left primary motor cortex with their matching strongest functional connected location in the contralateral hemisphere on the individual level. This suggest that the 'packing together' of the strongest functionally linked regions along the mid-line of the precentral gyrus is more likely to be a side-effect of the group averaging, rather than to a possible mismatch between the neuronal and vascular signals. Interestingly, supplementary figure 4.1 indicates that also on the individual level the existence of a specific organization of the functional connections in the primary motor network can be observed, suggesting that the found group-averaged organization has a robust character.

Fourth, as with all cross-correlation methods, the functional connections between left and right motor regions were based on linear effects between their resting-state time-series, missing possible temporal non-linear effects between these regions. Other coupling measures like synchronization likelihood have been successfully introduced to examine non-linear synchronization of brain signals (Stam et al., 2003) and could potentially make a valuable contribution to the field of resting-state fMRI research.

We report on a voxel-wise mapping of the interhemispheric functional connections of sub-regions within the primary motor network. Resting-state fMRI recordings of 46 healthy subjects were analyzed with a high detailed voxel-by-voxel fcMap approach, suggesting that the somatotopic organized regions of the primary motor cortex are strongly linked to their direct functional homolog in the contralateral hemisphere. Our results suggest the existence of a specific somatotopic organization of functional connections of primary motor regions during rest.

references

Achard S, Bullmore E (2007) Efficiency and cost of economical brain functional networks. PLoS Comput Biol 3:e17.

Achard S, Salvador R, Whitcher B, Suckling J, Bullmore E (2006) A resilient, low-frequency, small-world human brain functional network with highly connected association cortical hubs. J Neurosci 26:63-72.

Aertsen AM, Gerstein GL, Habib MK, Palm G (1989) Dynamics of neuronal firing correlation: modulation of "effective connectivity". J Neurophysiol 61:900-917.

Amunts K, Jancke L, Mohlberg H, Steinmetz H, Zilles K (2000) Interhemispheric asymmetry of the human motor cortex related to handedness and gender. Neuropsychologia 38:304-312.

Amunts K, Schlaug G, Schleicher A, Steinmetz H, Dabringhaus A, Roland PE, Zilles K (1996) Asymmetry in the human motor cortex and handedness. Neuroimage 4:216-222.

Andrews-Hanna JR, Snyder AZ, Vincent JL, Lustig C, Head D, Raichle ME, Buckner RL (2007) Disruption of large-scale brain systems in advanced aging. Neuron 56:924-935.

Basser PJ, Pajevic S, Pierpaoli C, Duda J, Aldroubi A (2000) In vivo fiber tractography using DT-MRI data. Magn Reson Med 44:625-632.

Beaulieu C, Allen PS (1994) Determinants of anisotropic water diffusion in nerves. Magn Reson Med 31:394-400.

Beckmann CF, DeLuca M, Devlin JT, Smith SM (2005) Investigations into resting-state connectivity using independent component analysis. Philos Trans R Soc Lond B Biol Sci 360:1001-1013.

Birn RM, Diamond JB, Smith MA, Bandettini PA (2006) Separating respiratory-variation-related fluctuations from neuronal-activity-related fluctuations in fMRI. Neuroimage 31:1536-1548.

Biswal B, Yetkin FZ, Haughton VM, Hyde JS (1995) Functional connectivity in the motor cortex of resting human brain using echo-planar MRI. Magn Reson Med 34:537-541.

Biswal BB, Van Kylen J, Hyde JS (1997) Simultaneous assessment of flow and BOLD signals in resting-state functional connectivity maps. NMR Biomed 10:165-170.

Breakspear M, Terry JR, Friston KJ, Harris AW, Williams LM, Brown K, Brennan J, Gordon E (2003) A disturbance of nonlinear interdependence in scalp EEG of subjects with first episode schizophrenia. Neuroimage 20:466-478.

Buckner RL, Vincent JL (2007) Unrest at rest: Default activity and spontaneous network correlations. Neuroimage 37:1091-1096.

Calhoun VD, Adali T, Pearlson GD, Pekar JJ (2001) A method for making group inferences from functional MRI data using independent component analysis. Hum Brain Mapp 14:140-151.

Cordes D, Haughton V, Carew JD, Arfanakis K, Maravilla K (2002) Hierarchical clustering to measure connectivity in fMRI resting-state data. Magn Reson Imaging 20:305-317.

Cordes D, Haughton VM, Arfanakis K, Wendt GJ, Turski PA, Moritz CH, Quigley MA, Meyerand ME (2000) Mapping functionally related regions of brain with functional connectivity MR imaging. AJNR Am J Neuroradiol 21:1636-1644.

Cordes D, Haughton VM, Arfanakis K, Carew JD, Turski PA, Moritz CH, Quigley MA, Meyerand ME (2001) Frequencies contributing to functional connectivity in the cerebral cortex in "resting-state" data. AJNR Am J Neuroradiol 22:1326-1333.

Damoiseaux JS, Rombouts SA, Barkhof F, Scheltens P, Stam CJ, Smith SM, Beckmann CF (2006) Consistent resting-state networks across healthy subjects. Proc Natl Acad Sci U S A 103:13848-13853.

De Luca M, Smith S, De Stefano N, Federico A, Matthews PM (2005) Blood oxygenation level dependent contrast resting state networks are relevant to functional activity in the neocortical sensorimotor system. Exp Brain Res 167:587-594.

De Luca M, Beckmann CF, De Stefano N, Matthews PM, Smith SM (2006) fMRI resting state networks define distinct modes of long-distance interactions in the human brain. Neuroimage 29:1359-1367.

Doron KW, Gazzaniga MS (2008) Neuroimaging techniques offer new perspectives on callosal transfer and interhemispheric communication. Cortex.

Eguiluz VM, Chialvo DR, Cecchi GA, Baliki M, Apkarian AV (2005) Scale-free brain functional networks. Phys Rev Lett 94:018102.

Eliassen JC, Baynes K, Gazzaniga MS (1999) Direction information coordinated via the posterior third of the corpus callosum during bimanual movements. Exp Brain Res 128:573-577.

Eliassen JC, Baynes K, Gazzaniga MS (2000) Anterior and posterior callosal contributions to simultaneous bimanual movements of the hands and fingers. Brain 123 Pt 12:2501-2511.

Fischl B, van der Kouwe A, Destrieux C, Halgren E, Segonne F, Salat DH, Busa E, Seidman LJ, Goldstein J, Kennedy D, Caviness V, Makris N, Rosen B, Dale AM (2004) Automatically parcellating the human cerebral cortex. Cereb Cortex 14:11-22.

Fox MD, Raichle ME (2007) Spontaneous fluctuations in brain activity observed with functional magnetic resonance imaging. Nat Rev Neurosci 8:700-711.

Fox MD, Snyder AZ, Vincent JL, Corbetta M, Van Essen DC, Raichle ME (2005) The human brain is intrinsically organized into dynamic, anticorrelated functional networks. Proc Natl Acad Sci U S A 102:9673-9678.

Fransson P (2005) Spontaneous low-frequency BOLD signal fluctuations: an fMRI investigation of the resting-state default mode of brain function hypothesis. Hum Brain Mapp 26:15-29.

Friston KJ, Frith CD, Liddle PF, Frackowiak RS (1993) Functional connectivity: the principal-component analysis of large (PET) data sets. J Cereb Blood Flow Metab 13:5-14.

Golay X, Pruessmann KP, Weiger M, Crelier GR, Folkers PJ, Kollias SS, Boesiger P (2000) PRESTO-SENSE: an ultrafast whole-brain fMRI technique. Magn Reson Med 43:779-786.

Greicius MD, Krasnow B, Reiss AL, Menon V (2003) Functional connectivity in the resting brain: a network analysis of the default mode hypothesis. Proc Natl Acad Sci U S A 100:253-258.

Greicius MD, Supekar K, Menon V, Dougherty RF (2008) Resting-State Functional Connectivity Reflects Structural Connectivity in the Default Mode Network. Cereb Cortex.

Hagmann P, Cammoun L, Gigandet X, Meuli R, Honey CJ, Wedeen VJ, Sporns O (2008) Mapping the Structural Core of Human Cerebral Cortex. PLoS Biol 6:e159.

Johnston JM, Vaishnavi SN, Smyth MD, Zhang D, He BJ, Zempel JM, Shimony JS, Snyder AZ, Raichle ME (2008) Loss of resting interhemispheric functional connectivity after complete section of the corpus callosum. J Neurosci 28:6453-6458.

Kell CA, von Kriegstein K, Rosler A, Kleinschmidt A, Laufs H (2005) The sensory cortical representation of the human penis: revisiting somatotopy in the male homunculus. J Neurosci 25:5984-5987.

Koch MA, Norris DG, Hund-Georgiadis M (2002) An investigation of functional and anatomical connectivity using magnetic resonance imaging. Neuroimage 16:241-250.

Latora V, Marchiori M (2001) Efficient behavior of small-world networks. Phys Rev Lett 87:198701.

Liu J, Morel A, Wannier T, Rouiller EM (2002) Origins of callosal projections to the supplementary motor area (SMA): a direct comparison between pre-SMA and SMA-proper in macaque monkeys. J Comp Neurol 443:71-85.

Lowe MJ, Mock BJ, Sorenson JA (1996) Resting State fMRI Signal Correlations in Multi-slice EPI. Neuroimage 3.

Lowe MJ, Mock BJ, Sorenson JA (1998) Functional connectivity in single and multislice echoplanar imaging using resting-state fluctuations. Neuroimage 7:119-132.

Lowe MJ, Dzemidzic M, Lurito JT, Mathews VP, Phillips MD (2000) Correlations in low-frequency BOLD fluctuations reflect cortico-cortical connections. Neuroimage 12:582-587.

Lowe MJ, Beall EB, Sakaie KE, Koenig KA, Stone L, Marrie RA, Phillips MD (2008) Resting state sensorimotor functional connectivity in multiple sclerosis inversely correlates with transcallosal motor pathway transverse diffusivity. Hum Brain Mapp 29:818-827.

Mori S, van Zijl PC (2002) Fiber tracking: principles and strategies - a technical review. NMR Biomed 15:468-480.

Newton JM, Dong Y, Hidler J, Plummer-D'Amato P, Marehbian J, Albistegui-Dubois RM, Woods RP, Dobkin BH (2008) Reliable assessment of lower limb motor representations with fMRI: Use of a novel MR compatible device for real-time monitoring of ankle, knee and hip torques. Neuroimage.

Nir Y, Mukamel R, Dinstein I, Privman E, Harel M, Fisch L, Gelbard-Sagiv H, Kipervasser S, Andelman F, Neufeld MY, Kramer U, Arieli A, Fried I, Malach R (2008) Interhemispheric correlations of slow spontaneous neuronal fluctuations revealed in human sensory cortex. Nat Neurosci.

Pandya DN, Karol EA, Heilbronn D (1971) The topographical distribution of interhemispheric projections in the corpus callosum of the rhesus monkey. Brain Res 32:31-43.

Penfield W, Boldrey E (1937) Somatic motor and sensory representation in the cerebral cortex of man as studied by electrical stimulation. Brain 60:54.

Penfield W, Rasmussen T (1968) The cerebral cortex of man: A clinical study of localization of function.

Rasmussen TB (1977) Wilder Penfield: his legacy to neurology. Surgical treatment of epilepsy. Can Med Assoc J 116:1369-1370.

Rouiller EM, Babalian A, Kazennikov O, Moret V, Yu XH, Wiesendanger M (1994) Transcallosal connections of the distal forelimb representations of the primary and supplementary motor cortical areas in macaque monkeys. Exp Brain Res 102:227-243.

Salvador R, Suckling J, Schwarzbauer C, Bullmore E (2005a) Undirected graphs of frequency-dependent functional connectivity in whole brain networks. Philos Trans R Soc Lond B Biol Sci 360:937-946.

Salvador R, Suckling J, Coleman MR, Pickard JD, Menon D, Bullmore E (2005b) Neurophysiological architecture of functional magnetic resonance images of human brain. Cereb Cortex 15:1332-1342.

Schmahmann JD, Pandya DN (2006) Fiber pathways of the brain. In, pp 485-496: Oxford University Press.

Shmuel A, Leopold DA (2008) Neuronal correlates of spontaneous fluctuations in fMRI signals in monkey visual cortex: Implications for functional connectivity at rest. Hum Brain Mapp 29:751-761.

Shmuel A, Augath M, Oeltermann A, Logothetis NK (2006) Negative functional MRI response correlates with decreases in neuronal activity in monkey visual area V1. Nat Neurosci 9:569-577.

Shmueli K, van Gelderen P, de Zwart JA, Horovitz SG, Fukunaga M, Jansma JM, Duyn JH (2007) Low-frequency fluctuations in the cardiac rate as a source of variance in the resting-state fMRI BOLD signal. Neuroimage 38:306-320.

Stam CJ (2004) Functional connectivity patterns of human magnetoencephalographic recordings: a 'small-world' network? Neurosci Lett 355:25-28.

Stam CJ, Breakspear M, van Cappellen van Walsum AM, van Dijk BW (2003) Nonlinear synchronization in EEG and whole-head MEG recordings of healthy subjects. Hum Brain Mapp 19:63-78.

van de Ven VG, Formisano E, Prvulovic D, Roeder CH, Linden DE (2004) Functional connectivity as revealed by spatial independent component analysis of fMRI measurements during rest. Hum Brain Mapp 22:165-178.

Van den Heuvel MP, Mandl RC, Hulshoff Pol HE (2008a) Normalized group clustering of resting-state fMRI data. PLoS ONE 3:e2001.

Van den Heuvel MP, Stam CJ, Boersma M, Hulshoff Pol HE (2008b) Small-world and scale-free organization of voxel based resting-state functional connectivity in the human brain. Neuroimage 43:11.

Van den Heuvel MP, Mandl RC, Luigjes J, Hulshoff Pol HE (2008c) Microstructural organization of the cingulum tract and the level of default mode functional connectivity. J Neurosci 28:7.

Van den Heuvel MP, Mandl RCW, Kahn RS, Hulshoff Pol HE (2009) Functionally linked resting state networks reflect the underlying structural connectivity architecture of the human brain. In Press.

Wahl M, Lauterbach-Soon B, Hattingen E, Jung P, Singer O, Volz S, Klein JC, Steinmetz H, Ziemann U (2007) Human motor corpus callosum: topography, somatotopy, and link between microstructure and function. J Neurosci 27:12132-12138.

Wakana S, Jiang H, Nagae-Poetscher LM, van Zijl PC, Mori S (2004) Fiber tract-based atlas of human white matter anatomy. Radiology 230:77-87.

Wiesendanger M, Serrien DJ (2004) The quest to understand bimanual coordination. Prog Brain Res 143:491-505.

Wise RG, Ide K, Poulin MJ, Tracey I (2004) Resting fluctuations in arterial carbon dioxide induce significant low frequency variations in BOLD signal. Neuroimage 21:1652-1664.

Xiong J, Parsons LM, Gao JH, Fox PT (1999) Interregional connectivity to primary motor cortex revealed using MRI resting state images. Hum Brain Mapp 8:151-156.

supplementary information

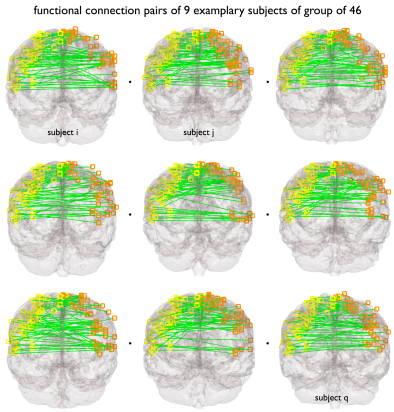

supplementary figure 4.1

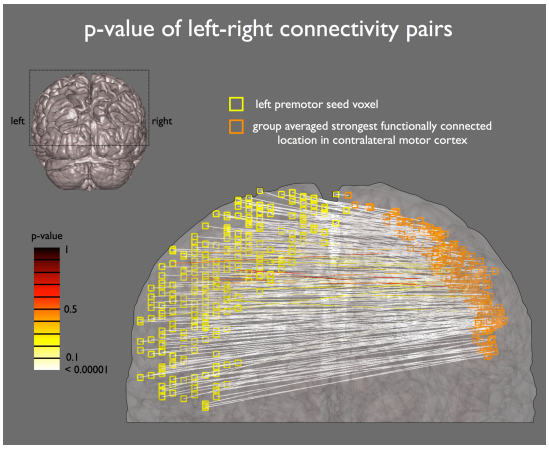

supplementary figure 4.2

supplementary figure 4.1 individual connectivity pairs of left primary motor seeds and strongest functionally connected connected voxels in the contralateral right primary motor regions Figure shows of 9 exemplary subjects from the total group of 46 subjects their individual organization of the functional connections of the primary motor network. For each of the seed voxels evenly distributed along the left primary motor cortex, the individual time-series of the seed was correlated with all voxels along the contralateral primary motor cortex and the voxel with the strongest functional connection was selected, forming a left-right connectivity pair. Figure shows for 9 exemplary subjects their matching left-right connectivity pairs, with the seed voxels along the left primary motor cortex depicted by yellow squares, their matching strongest functional connected location in the contralateral hemisphere as a orange square, with a green connection between each matching left-right pair. Every 1 on 25 seed voxels and their matching strongest functional connection are showed in the figures to prevent cluttering. Figure illustrates that also in the individual data a specific organization between the left and right primary motor regions is present, suggesting a somatopic organization of the functional connections within the primary motor network. Please note that these individual datasets also provide important information about the observed clustering of the group locations along the mid-line of the contralateral motor cortex, as can be observed in figure 2 and 4 in the main text. As supplementary figure 1 shows, the effect of the clustering of the group-averaged location of the strongest functionally connected region with the selected left seed voxel towards the mid-line of the contralateral primary motor cortex, is not present in the individual data. This suggest that the clustering-effect in the group data is more a side effect of averaging of individual locations over the group of subjects, rather than a possible mismatch between neuronal and vascular signals.

supplementary figure 4.2 p-values of the null-hypothesis that the group averaged strongest functional connected left-right pair could emerge from random In analysis I, in a Monte Carlo simulation, for each computed left-right strongest functionally connected voxel-pair it was tested whether this voxel-pair could also emerge from when the strongest functionally connected locations in the individual datasets were random placed over the contralateral primary motor cortex, rather than following a specific organization. For this, for each left-right seed - strongest functionally connected group location, 46 random locations were selected along the contralateral precentral gyrus, as if the individual functionally connected regions would have no specific organization. Next, a group average location of these 46 non-specific locations were computed, similar as the procedure followed in figure 1. For each seed-voxel, the selection of 46 random locations and the group averaging was repeated 10000 times and for each simulation the distance between the group-averaged non-specific location and the mirrored location of the seed was computed (similar as depicted in figure 1). For each seed-voxel, this Monte Carlo simulation resulted in a null-distribution of possible distances that could occur just by chance. Next, the real data, i.e. the distance between the matching left-right connectivity pair and the mirrored seed location (as shown in figure 3) was tested against this distribution, testing whether the found distance could occur with a certainly probability under the null-hypothesis (i.e. no specific organization). This resulted in an adjusted p-value for each of the left-right connectivity pairs. supplementary figure 2 shows for the left-right connectivity pairs their p-value. Panel b shows 1 on every 10 connections. Figure shows that far most all connections have a p-value < 0.05 (uncorrected). Moreover, even after applying strict Bonferroni correction to correct for multiple comparisons the majority of unique connectivity pairs (>72%) still showed a left-right orientation that was significantly different from random [$p<0.05$, Bonferroni corrected]. Please not that only a small number of connections in the central part of the primary motor cortex showed a p-value > 0.05, i.e. a non-significant left-right connectivity pair. However, the high p-value of these pairs is likely to result form the fact that their mirrored location was close to the average group-averaged random location. Averaging 46 random locations often result in a location in this direction, making it very difficult to make the matching left-right connectivity pairs in these locations to obtain a low p-value. Indeed, examining the distance between the mirrored seed and strongest functional location of these seeds, showed that also these strongly functionally connected locations were also only 8-12 mm off from their mirrored seed location, similar to all other left-right voxel pairs in the superior and inferior part of the primary motor cortex.

chapter 5

functionally linked resting-state networks reflect the underlying structural connectivity architecture of the human brain

martijn van den heuvel, rené mandl, rené kahn, hilleke hulshoff pol

human brain mapping 2009a, epub ahead of print

During rest, multiple cortical brain regions are functionally linked forming resting-state networks. This high level of functional connectivity within resting-state networks suggests the existence of direct neuroanatomical connections between these functionally linked brain regions to facilitate the ongoing interregional neuronal communication. White matter tracts are the structural highways of our brain, enabling information to travel quickly from one brain region to another region. In this study, we examined both the functional and structural connections of the human brain in a group of 26 healthy subjects, combining 3 Tesla resting-state functional Magnetic Resonance Imaging time-series with Diffusion Tensor Imaging scans. Nine consistently found functionally linked resting-state networks were retrieved from the resting-state data. The Diffusion Tensor Imaging scans were used to reconstruct the white matter pathways between the functionally linked brain areas of these resting-state networks. Our results show that well-known anatomical white matter tracts interconnect at least 8 of the 9 commonly found resting-state networks, including the default mode network, the core network, primary motor and visual network and two lateralized parietal-frontal networks. Our results suggest that the functionally linked resting-state networks reflect the underlying structural connectivity architecture of the human brain.

introduction

Our brain is never idle. Even when we are at rest, a large number of anatomically separated brain areas show a vast amount of spontaneous neuronal activity and are functionally linked to each other (Biswal et al., 1995; Gusnard et al., 2001; Greicius et al., 2003). Regions that show such synchronized behavior during rest are said to form resting-state networks (RSNs) (Greicius et al., 2003; Beckmann et al., 2005; Damoiseaux et al., 2006; Van den Heuvel et al., 2008a; Van den Heuvel et al., 2008c). The high level of functional connectivity between RSN regions suggests the existence of direct anatomical pathways between these brain areas to facilitate this high level of ongoing interregional communication during rest. In this study, we examined the structural connectivity architecture of functionally linked RSNs.

The synchronization of neuronal activity between anatomically separate brain regions is known as functional connectivity (Aertsen et al., 1989; Friston et al., 1993; Biswal et al., 1995; Lowe et al., 2000) and has been investigated by examining the coherence of resting-state functional Magnetic Resonance Imaging time-series (Biswal et al., 1995; Xiong et al., 1999; Lowe et al., 2000). Of special interest are the low frequency oscillations (0.01 - 0.1 Hz) of resting-state fMRI BOLD time-series, which show a strong correlation between RSN regions during rest (Biswal et al., 1995; Lowe et al., 1996; Xiong et al., 1999; Cordes et al., 2000; Lowe et al., 2000; Damoiseaux et al., 2006). There is an ongoing debate about whether these coherent patterns predominantly originate from physiological signals, like cardiac or respiratory oscillations (Wise et al., 2004; Shmueli et al., 2007) or whether they truly reflect synchronization of intrinsic neuronal activity. The latter view is supported by the notion that most of these coherent patterns have been found between regions that are known to share a common behavioral or cognitive function (Biswal et al., 1995; Xiong et al., 1999; Damoiseaux et al., 2006). Furthermore, resting-state BOLD fluctuations have been reported to strongly correlate with concurrent fluctuations in neuronal spiking (Shmuel and Leopold, 2008), linking resting-state fMRI time-series directly to neuronal activation and synchronization (Shmuel and Leopold, 2008). In addition, a recent study has shown that slow modulations in neuronal spiking are linked to spontaneous fMRI fluctuations in the human sensory cortex (Nir et al., 2008). In this context, it is believed that the coherence between the resting-state fMRI time-series of anatomically separate cortical regions reflects, at least in part, a high level of functional connectivity between these brain areas.

A number of group studies have reported the consistent formation of RSNs during rest (Beckmann et al., 2005; Salvador et al., 2005b; Damoiseaux et al., 2006; De Luca et al., 2006; Van den Heuvel et al., 2008a; Van den Heuvel et al., 2008c). The most commonly found RSNs include the 'default mode network' that links precuneus/posterior cingulate cortex with medial frontal regions and bilateral inferior parietal regions (Gusnard et al., 2001; Greicius et al., 2003; Damoiseaux et al., 2006; Fox and Raichle, 2007), the 'core network' linking bilateral insular regions and anterior cingulate cortex (Dosenbach et al., 2007), two lateralized parietal-frontal networks that are often associated with attention and networks that overlap primary sensorimotor and (extra-striate) visual systems (Biswal et al., 1995; Lowe et al., 1998; Xiong et al., 1999; Lowe et al., 2000; Beckmann et al., 2005; Damoiseaux et al., 2006). Activation of the default mode network and the core network have been suggested to play an important role in core processes of human cognition (Gusnard et al., 2001; Fox and Raichle, 2007), including mind wandering (Mason et al., 2007), goal-directed behavior (Dosenbach et al., 2007) and relating oneself to the outside world (Gusnard et al., 2001).

The high level of functional connectivity within RSNs suggests the existence of direct anatomical connections between these brain areas to support the ongoing information transfer between these regions during rest. White matter pathways are the structural connections of our brain and can be investigated using Diffusion Tensor Imaging (DTI). DTI is a technique to determine the main diffusion direction of water molecules in brain tissue (Beaulieu and Allen, 1994; Basser et al., 2000), enabling the reconstruction of the white matter pathways of the brain (Mori and van Zijl, 2002). Indeed, Greicius et al. (Greicius et al., 2008) demonstrated the existence of direct structural white matter pathways between the regions of the functional default mode network, suggesting an important role for the cingulum tract in connecting the active regions of the default mode network. Indeed, in a recent study we reported a direct association between the microstructural organization of the interconnecting cingulum tract and the level of default mode functional connectivity (Van den Heuvel et al., 2008c). Furthermore, Lowe et al. (Lowe et al., 2008) recently demonstrated in patients with multiple sclerosis that disease related decreases of functional connectivity between left and right primary motor regions are inversely correlated with the structural integrity of corpus callosum tracts. In addition, section of the corpus callosum has been reported to result in complete loss of interhemispheric resting-state functional connectivity (Johnston et al., 2008). These studies support the view that anatomical white matter pathways play an important role in resting-state synchronization. Taken together, they

suggest a direct link between structural and functional connectivity in the human brain (Koch et al., 2002; Greicius et al., 2008; Hagmann et al., 2008, 2007; Johnston et al., 2008; Lowe et al., 2008; Van den Heuvel et al., 2008c). However, it is unknown whether functional RSNs are truly 'hard-wired' in the brain. In other words, are the functionally linked regions of known RSNs directly interconnected by anatomical white matter pathways? If the high level of observed fMRI coherence indeed reflects neuronal synchronization between RSN regions, one would expect an underlying anatomical infrastructure to facilitate the ongoing interregional communication between RSN regions during rest. In this study, we examined the existence of structural white matter bundles between the functionally connected regions of known RSNs as evidence for an anatomical dependence of resting-state networks. We acquired resting-state fMRI BOLD time-series in 26 healthy subjects on a 3 Tesla MR scanner, together with high resolution DTI scans to reconstruct the white matter tracts of the brain. Nine consistently found RSNs were retrieved from the resting-state data. The existence of direct structural connections between the functionally linked RSN regions was examined by combining the RSN maps with DTI based fiber tracking.

materials and methods

subjects

26 healthy subjects (age mean: 25, SD: 7.7, 14 male, 12 female) participated in this study after given written consent as approved by the medical ethics committee for research in humans of the University Medical Centre Utrecht, the Netherlands. Resting-state functional Magnetic Resonance Imaging (resting-state fMRI) and Diffusion Tensor Imaging (DTI) data were acquired on a 3 Tesla Philips Achieva Medical Scanner. During the resting-state recordings, the subjects were instructed to relax, keep their eyes closed without falling asleep and to think of nothing in particular. Subjects who reported to have fallen asleep or reported to be close to fallen asleep were excluded and a new subject was included as a replacement, resulting in the described group of 26 subjects.

image acquisition

Resting-state Blood Oxygenation Level Dependent (BOLD) signals were recorded during a period of 8 minutes using a fast fMRI sequence (3D PRESTOSENSE p/s-reduction 2/2, TR/TE = 22/32 ms using shifted echo, slice orientation: sagittal, flip-angle 9 degrees, dynamic scan time 0.5 sec, voxel-size 4 x 4 x 4mm, FOV = 128 x 256 x 256 mm, reconstruction matrix =

32 x 64 x 64 covering whole brain). The short volume acquisition time of 500 ms allowed proper sampling of information in the frequency domain up to 1 Hz. This minimized the possible back-folding of possible confounding effects of higher frequencies, such as respiratory and cardiac oscillations (~0.3 Hz and >0.8 Hz, respectively), into the lower frequencies of interest (0.01 - 0.1 Hz) (Cordes et al., 2001). Functional PRESTO images have a relative low anatomical contrast compared to an anatomical T1 image. Therefore, directly after the functional time-series an additional high contrast PRESTO image was acquired, with identical scanning parameters but with a higher anatomical contrast (i.e. a better contrast between white and grey matter), which was obtained by increasing the flip angle to 25 degrees. This additional high contrast PRESTO image was acquired to improve the coregistration of the resting-state time-series with the T1 image.

In the same scanning session, 2 DTI sets each consisting of 30 weighted diffusion scans and 5 unweighted B=0 scans (b=0 s/mm2) were acquired (DTI-MR using parallel imaging SENSE p-reduction 3; high angular gradientset of 30 different weighted directions (Jones et al., 1999; Jones, 2004), TR/TE = 7035/68 ms, voxel-size 2 x 2 x 2 mm, FOV = 240 x 240 x 150 mm, reconstruction matrix = 120 x 120 x 75 covering whole brain, b=0 s/mm2 for the unweighted scans and b=1000 s/mm2 for the weighted scans, second set with reversed k-space read-out). In addition, an anatomical T1 weighted image (3D FFE using parallel imaging; TR/TE = 10/4.6ms, flip-angle 8 degrees, slice orientation: sagittal, 0.75 x 0.75 x 0.8 mm voxelsize, FOV = 160 x 240 x 240 mm, reconstruction matrix = 200 x 320 x 320 covering whole brain) was acquired for anatomical reference.

image preprocessing

Preprocessing of the resting-state fMRI data was performed with the SPM2 software package (http://www.fil.ion.ucl.ac.uk). Functional scans were corrected for small head movements by realigning all functional scans to the last scan. Next, the functional time-series and the T1 image were co-registered with the high-contrast functional scan, enabling overlap between the functional resting-state time-series and the T1 image. Cortical voxels were selected based on a cortical segmentation of the T1 image, which was performed with the freely available Freesurfer software package (http://surfer.nmr.mgh.harvard.edu/). The T1 image was spatially normalized (nonlinear) to match the MNI 305 T1 template brain (Collins et al., 1994) and the fMRI time-series and the cortical segmentation map were normalized (nonlinear) to standard space by using the normalization parameters of the T1 image.

To select the low resting-state frequencies of interest (0.01 – 0.1 Hz) (Biswal et al., 1995; Biswal et al., 1997; Cordes et al., 2001), the rest recorded fMRI time-series were bandpass filtered with a finite impulse response (FIR) bandpass filter with zero phase distortion (bandwidth 0.01 - 0.1 Hz). Filtering eliminated low frequency noise (including slow scanner drifts) and influences of higher frequencies reflecting cardiac and respiratory signals (Cordes et al., 2001).

Preprocessing of the DTI data was performed with the diffusion toolbox of Andersson et al. (Andersson and Skare, 2002; Andersson et al., 2003) and in-house developed software. For each of the 2 DTI sets, the 5 unweighted B=0 were averaged. In total, this resulted in 2 averaged unweighted B=0 images. Next, susceptibility distortions, which are often reported in single-shot EPI images (Andersson et al., 2003), were corrected by combining the two DTI datasets. This correction was performed by computing a field distortion map based on the 2 averaged unweighted B=0 images, which were acquired with an opposite k-space read-out direction (Andersson et al., 2003). The resulting field map was then applied to the 2 sets of 30 weighted images, resulting in a single set of 30 weighted directions (Andersson et al., 2003). The DTI images were corrected for small head movements by realigning all weighted scans to the unweighted B=0 image (Andersson and Skare, 2002). Within each voxel, the diffusion profile was fitted a tensor using a robust tensor fit method based on M-estimators (Chang et al., 2005). Next, the main diffusion direction within each voxel was selected as the principal eigenvector, determined by the eigenvalue decomposition of the fitted tensor (Mori et al., 1999; Mori and van Zijl, 2002). For each individual DTI dataset, the *Fiber Assignment by Continuous Tracking* (FACT) (Mori et al., 1999; Mori and van Zijl, 2002) algorithm was used to reconstruct the total collection of white matter tracts of the brain, often called *fibers* or *tracts* (Mori et al., 2002). 27 seeds were started in each voxel. Fiber tracking was stopped when the fiber reached a voxel with a FA value lower than 0.1, when the trajectory of the traced fiber exceeded the brain or when the eigenvector had an average angle of > 45 degrees with the main diffusion direction of neighboring voxels.

selection of functionally linked resting-state networks

RSNs were retrieved from the resting-state data using the *normalized cut group clustering* method, as validated earlier (Van den Heuvel et al., 2008a). In brief, this voxel-based clustering method involved the grouping of voxels that consistently showed a high level of functional connectivity over the group of subjects. The *normalized cut group clustering* method consists of 2 clustering stages, being (1) the individual clustering stage and (2) the group

clustering stage. First, at stage 1, from each individual dataset a graph $G = (V,E)$ was formed, with V the collection of points (called nodes or vertices) and E the collection of edges (or connections) between the nodes of the graph. The graph was formed out of all cortical voxels (i.e. the nodes V), selected from the individual cortical segmentation maps. The weights of the connections E between all voxel pairs were computed as the zero-lag temporal correlation between the time-series of the voxels, reflecting their level of voxel-wise functional connectivity. For example, the weight $w(i,j)$ of edge $e(i,j)$ between voxel i and voxel j was computed as the correlation between the resting-state time-series of voxel i and voxel j. Next, the resulting individual connectivity graph G was thresholded, setting all connections to 0 that did not reach the set threshold of 0.4 and all connections to 1 that exceeded the threshold. As such, G was defined as an unweighted unidirectional graph with connections between those voxels that showed a high level of functional connectivity. Next, the resulting individual connectivity graph was clustered, using the normalized cut graph clustering algorithm (Shi and Malik, 2000). This resulted in the grouping of functionally linked voxels into resting-state networks. Second, at the group level (stage 2), the consistency of the individual clustering results was computed to determine which voxels consistently showed a high level of functional connectivity over the group of subjects. First, the consistency of the individual clustering results was represented as a *group graph*. The connections between the voxels in the group graph (i.e. the voxels of the group averaged anatomical image) were defined as the *cluster-consistency* over the group of subjects. This was done by defining $w(i,j)$ of edge $e(i,j)$ between voxel i and j in the *group graph* as the total number of times voxel i and j were clustered into the same cluster over the group of subjects. As such, a high weight $w(i,j)$ expressed that in a high number of subjects voxel i and j showed a high level of functional connectivity and were therefore clustered into the same RSN, indicating that over the group of subjects these voxels were likely to belong to the same RSN. As a result, the weights of the *group graph* expressed which voxels consistently showed a high level of functional connectivity over the group of subjects. Second, the resulting group graph was clustered, clustering the voxels into group RSNs that consistently showed a high level of functional connectivity over the group of subjects and grouping voxels into different RSNs that showed a low level of functional connectivity over the group of subjects. Using the *normalized cut group clustering* procedure, the optimal number of group clusters (i.e. the number of group RSNs) is determined as an optimal clustering fit of the *group graph*, based on minimizing the total *normalized cut cost* to partition the graph into separate networks. As a result, the number of group RSNs was

determined automatically, avoiding manual selection of RSNs (Van den Heuvel et al., 2008a).

Group clustering revealed 9 RSNs (figure 5.2a), including the default mode network (figure 5.2a, RSN a, red regions), two lateralized parietal-frontal networks consisting of superior parietal and superior frontal regions (figure 5.2a, RSN b and c, green and blue regions), a network consisting of primary motor regions (figure 5.2a, RSN d, dark green regions), a network consisting of primary visual regions (figure 5.2a, RSNd, dark blue regions), a network consisting of extra-striate visual regions (figure 5.2a, RSNd, orange regions), a network overlapping bilateral insular regions and anterior cingulate cortex (ACC) (figure 5.2a, RSN e, pink regions) and two singular networks consisting of bilateral medial frontal cortex (figure 5.2a, RSN f, light blue regions) and posterior precuneus regions (figure 5.2a, RSN g, light brown regions). Please see the results section and table 5.1 for a full description of the RSN regions.

structural connections between functionally linked resting-state network regions

To examine the existence of structural connections between the functionally linked RSN regions the DTI fiber data was combined with the 9 RSN clustermaps. The selection of interconnecting anatomical tracts between RSN regions was performed in a 3-step procedure, illustrated in figure 5.1. First, for each individual dataset, the total collection of reconstructed fibers was selected (figure 5.1a). Second, from each of the 9 RSNs, a first region of interest (ROI) was appointed and from the total collection of reconstructed fibers the tracts that reached this first ROI were selected (figure 5.1b). To improve the penetration of the reconstructed tracts into the RSN regions of interest, the ROIs were dilated with a maximum of 4 mm (i.e. 1 fMRI voxel). Third, a second ROI was selected from the RSN clustermap (figure 5.1c) and from the resulting fibers of the previous step, only the tracts that also reached the second ROI were selected. This procedure resulted in the tracts that connected both ROIs (figure 5.1c). Next, as this procedure was completed for all subjects, the individual interconnecting tracts were normalized to match standard space (MNI 305) using the normalization parameters of the B=0 image and combined over the group of subjects. Individual tracts were combined by bundling the individual tracts over the group of subjects, such that the total collection of tracts reflected all the tracts between ROIa and ROIb of subject 1 to subject 26 (figure 5.1d).

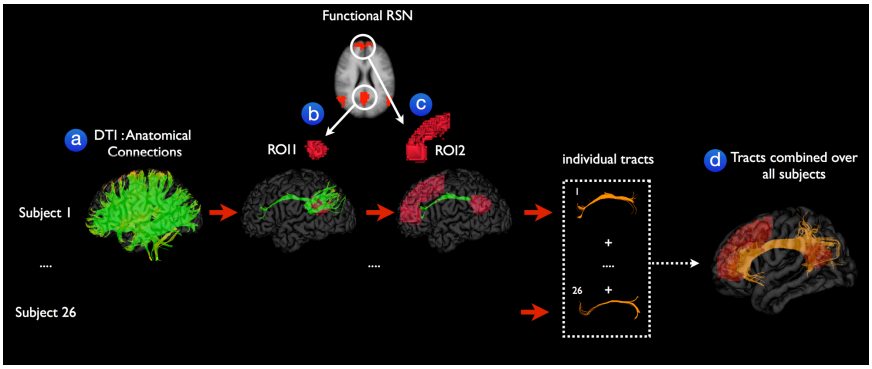

figure 5.1 structural connections between functionally connected resting-state network regions The existence of possible anatomical white matter tracts between functionally connected resting-state network (RSN) regions was examined in a 3-step procedure. First, for each individual, the DTI data was used to reconstruct the white matter tracts of the human brain, called fibers or tracts (***step a***). Second, for each of the 9 functionally connected RSNs, a first region of interest (ROI) was selected and from the total collection of fibers, the tracts that reached the first ROI were selected (***step b***). Third, a second ROI was retrieved from the RSN clustermap and from the resulting tracts of the previous step, only the tracts that reached this second ROI were selected (***step c***). For illustration purposes, the individual interconnecting tracts were normalized to match standard space (MNI 305) and combined over the group of subjects. The combined tracts represented the existence of a direct anatomical white matter connection between the functionally connected regions of a known resting-state network.

group consistency maps

To examine the consistency of the interconnecting white matter pathways between RSN regions over the group of subjects, for each interconnecting tract within each RSN a *group consistency flag map* was computed. This group consistency flag map served as an indicator of which white matter regions were consistently crossed over the group of subjects by the interconnecting fiber tracts. This was done in a 3 step procedure. First, for each individual dataset, the interconnecting fibers between the two selected RSN regions were selected and an individual 3D volume was created, flagging those voxels that were crossed by the interconnecting fibers. Voxels that were crossed by 1 or more fibers were flagged with a value of 1, resulting in an individual binary flag map. Second, in the group stage, the individual flag maps were summated providing a *group consistency flag map*, indicating the overlap of the found interconnecting tracts over the group of subjects. As such, white matter regions that are consistently crossed by the

interconnecting fibers over the group of subjects are indicated with a high voxel value. This procedure was repeated for all RSNs.

results

resting-state networks

Normalized cut group clustering of the resting-state fMRI time-series of the 26 subjects revealed 9 RSNs, as validated earlier (Van den Heuvel et al., 2008b). These functionally linked networks included the *default mode network*, the *core network*, two lateralized parietal-frontal networks, primary motor, primary visual, extra-striate visual network and two singular networks consisting of bilateral medial frontal regions and posterior parietal cortical regions. The 9 RSNs are shown in figure 5.2 (panel a). RSN a (figure 5.2a, RSN a) shows the default mode network (Gusnard et al., 2001; Raichle et al., 2001; Greicius et al., 2003; Raichle and Snyder, 2007) overlapping posterior cingulate/precuneus region (Brodmann Area (BA) 23/31), inferior and superior parietal cortex (BA 39/40), superior frontal gyrus (BA 8) and medial frontal gyrus (BA 8/9/10/11) (Damoiseaux et al., 2006). RSN b and c (figure 5.2a, RSN b and c) reflect lateralized parietal-frontal networks in the left and right hemisphere, including cortical regions of the superior parietal lobule, supramarginal gyrus (BA 40) and the middle and superior frontal gyrus (BA 8/9). RSN d (figure 5.2a, RSN d) consisted of postcentral gyrus (BA 3/1/2), precentral gyrus (BA 4), cingulate gyrus (BA 24) and lateral, medial and superior occipital gyrus and peristriate regions (BA 17/18/19). The motor and visual regions of RSNd were originally clustered as a single RSN (Van den Heuvel et al., 2008b), suggesting a high level of functional connectivity between primary motor and primary (extra-striate) visual regions. Most other studies have reported the motor and visual networks as two separate RSNs, although a recent study has provided supporting evidence for a high level of functional connectivity between motor and visual regions by also reporting these regions as a single RSN (Vincent et al., 2008). To examine the existence of sub-networks within this combined motor/visual network, a second level clustering was performed on the voxels in the combined motor/visual RSN (RSNd) (Van den Heuvel et al., 2008a). As expected, this resulted in the clustering of separate sub-networks for the primary motor, primary visual and extra-striate visual regions. These sub-networks are shown in RSN d of figure 5.2a, including a separate primary sensorimotor network (figure 5.2a, RSN d, green cluster), a visual network (figure 5.2a, RSN d, blue cluster) and a network consisting of bilateral extra-striate visual regions (figure 5.2a, RSNd, orange cluster) (Biswal et al., 1995; Xiong et al.,

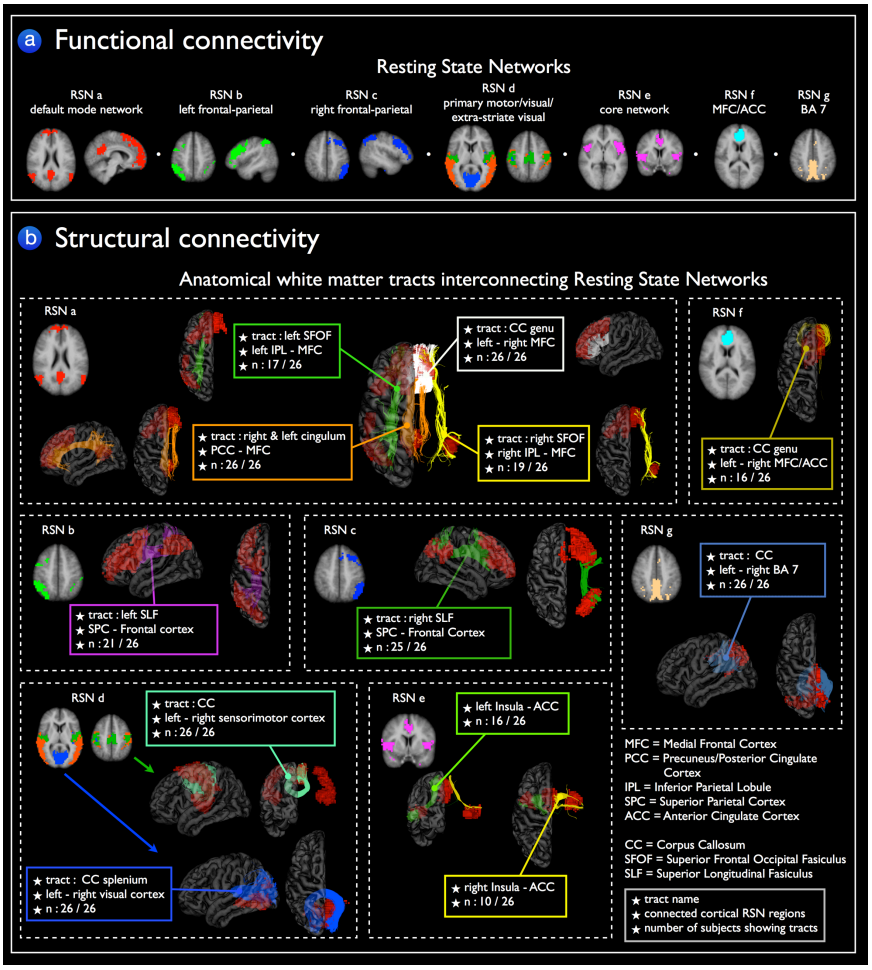

figure 5.2 structural connections of the functionally linked resting-state networks Group clustering of the resting-state fMRI data revealed 9 resting-state networks (RSNs) of functionally linked cortical regions (***panel a***). Fiber tracking DTI data revealed interconnecting white matter pathways in 8 of these 9 RSNs in a substantial proportion of the group of subjects (***panel b***). ***panel a functional connectivity***: resting-state networks. The 9 networks included the default mode network (RSN a, red network), two lateralized parietal-frontal networks (RSN b green network and RSN c blue network), primary motor, visual and extra-striate visual networks (RSN d, green, blue and orange networks, respectively), the core network consisting of bilateral insular regions and regions overlapping the anterior cingulate cortex (RSN e pink network) and two networks consisting of bilateral regions overlapping medial frontal cortex/anterior cingulate cortex (RSN f light blue network) and regions overlapping left and right posterior precuneus (BA 7) (RSN g light brown network). ***panel b structural connectivity:*** Anatomical white matter tracts interconnecting resting-state

figure 5.2 (continuing)
networks. Fiber tracking DTI data revealed interconnecting white matter pathways in 8 of the 9 RSNs in a substantial proportion of the group of subjects. The cingulum tract, bilateral superior frontal occipital fasciculus (SFOF), and the genu of the corpus callosum (CC) were found to interconnect the regions of the default mode network (RSN a orange, green/yellow and white tracts, respectively). The functionally linked regions of the lateralized parietal-frontal networks were found to be interconnected by the superior longitudinal fasciculus (SLF) (RSN b purple tracts, RSN c green tracts). Legend continued on next page. Corpus callosum (CC) tracts interconnected the regions of the motor network (RSN d mint green fibers) and the regions of the visual network (RSN d blue tracts). Left and right insular regions and anterior cingulate cortex of the core network were found to be interconnected by white matter tracts (RSN e, green and yellow tracts, respectively) in part of the group of subjects. Finally, the bilateral regions of the two singular networks RSN f and RSN g were found to be interconnected by corpus callosum tracts (RSN f dark yellow tracts and RSN g grey blue tracts). Fiber information boxes provide information about the name of the interconnecting tract, the functionally linked cortical regions and the number of N subjects of the group of 26 subjects that showed these interconnecting tracts (N/26).

1999; Salvador et al., 2005b; Damoiseaux et al., 2006). Furthermore, RSN e (figure 5.2a, RSN e) shows the so-called *core network* (Dosenbach et al., 2007) consisting of bilateral insular and superior temporal cortex (BA 22) and a part of the cingulate gyrus (BA 24). RSN f (figure 5.2a, RSN f) overlaps bilateral regions of the medial frontal gyrus (BA 9) and an anterior part of the cingulate gyrus (BA 32) (Damoiseaux et al., 2006). Finally, RSN g (figure 5.2a, RSN g) consisted of a singular region overlapping a posterior part of bilateral precuneus (BA 7).

anatomical white matter tracts interconnecting resting-state networks

Well-known anatomical white matter tracts (Vogt and Pandya, 1987; Wakana et al., 2004; Schmahmann and Pandya, 2006; Schmahmann et al., 2007) were found to interconnect 8 of the 9 functionally linked RSNs across the group of subjects. Figure 5.2a and 5.2b shows a general overview of all RSNs and the white matter tracts that were found to interconnect the RSN regions. Figure 5.3 to 5.7 show the RSNs and the interconnecting tracts in more detail, together with the matching *group consistency flag maps*. In addition, table 5.1 describes the functionally linked regions of the 9 RSNs (RSN a to g) and the interconnecting white matter tracts that were found to interconnect the RSN regions.

RSN a. Figure 5.3 shows the interconnecting tracts of the regions of the so-called *default mode network* (Gusnard et al., 2001; Raichle et al., 2001;

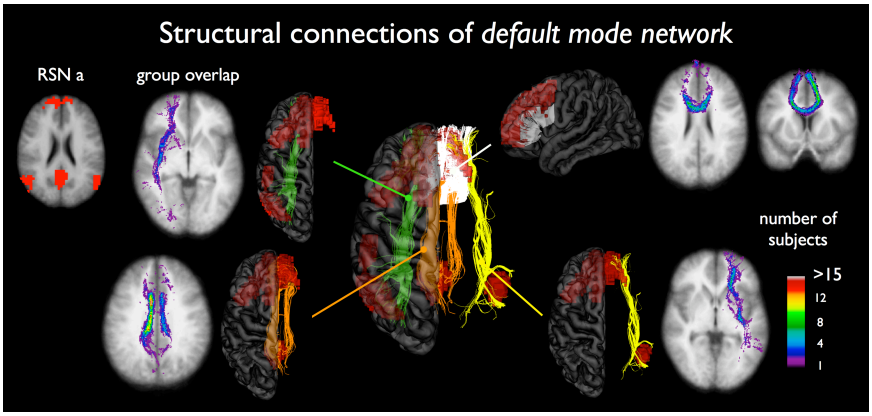

figure 5.3 structural white matter tracts between regions of the default mode network (RSN a) Figure shows that the cingulum tract (orange tracts, 26 out of 26 subjects showing interconnecting tracts), the left and right inferior/superior frontal-occipital fasciculus (green 17/26 and yellow tracts 19/26) and the genu of the corpus callosum (26/26 subjects) play an important role in interconnecting the regions of the default mode network. The matching group consistency flag maps show large overlap over the group of subjects, especially for the cingulum (maximum consistency voxel values of 15) and genu tracts (voxel values of 12). The group consistency flag maps indicate for each voxel how many subjects of the group of 26 subjects showed interconnecting tracts between the two RSN regions that touched this particular white matter region. Please note that no spatial smoothing was applied to the group consistency flagmaps.

Greicius et al., 2003; Raichle and Snyder, 2007). The *cingulum* tract (figure 5.3, RSN a orange tracts, 26 out of 26 subjects showed interconnecting fibers (26/26)) (Greicius et al., 2008), the left and right *inferior/superior frontal-occipital fasciculus* (green and yellow tracts, 17/26 and 19/26) and the *genu* of the *corpus callosum* (white tracts, 26/26) were found to interconnect the active areas within the default mode network. The matching *group consistency flag maps* suggest a high level of consistency of the interconnecting tracts over the group of subjects. The consistency flag maps show high voxel values for the center line of the *cingulum*, i.e. group consistency voxel values of over 15 were found, indicating that the trajectories of the interconnecting tracts of more than 15 subjects of the group of 26 all crossed overlapping voxels. Similarly, the group consistency maps for the *genu* tract showed high consistency voxel values (i.e. >12), also indicating a high level of consistency over the group of subjects. Please note that no spatial smoothing was applied to the group consistency flag maps.

RSN b and c. The two lateralized parietal-frontal RSNs were found to be interconnected by the left and right structural *superior longitudinal fasciculus* (Wakana et al., 2004) (figure 5.4, RSN b purple tracts, 21/26 and RSN c dark green tracts, 25/26). The group consistency flag maps of these interconnecting tracts are shown in figure 5.4, suggesting a high level of consistency of the interconnecting tracts over the group of subjects (showing group consistency voxel values of over 15 in both left and right hemispheric tracts).

RSN d. Tracts of the *body* of the *corpus callosum* were found to interconnect the primary sensorimotor network (figure 5, RSN d mint green tracts, 26/26) and tracts crossing the *splenium* of the *corpus callosum* were found to interconnect the regions of the primary visual network (RSN d blue tracts, 26/26). Similar to the other RSNs these interconnecting tracts were found with a high level of consistency over the group of subjects, indicated by group consistency voxel values of over 15 (figure 5). No interconnecting tracts were found between the extra-striate visual regions (figure 5.2a, RSNd, orange network).

RSN e. In part of the group of subjects (16 out of 26 and 10 out of the group of 26 subjects, respectively) white matter tracts were found to interconnect the regions of the *core network* (figure 6, RSN e, green and yellow tracts) (Vogt and Pandya, 1987). Figure 5.6 shows the interconnecting tracts between the left and right insular regions and the anterior cingulate cortex and the matching group consistency flag maps of the found tracts (group consistency values of 5 and 3 respectively).

RSN f and g. Fibers passing the *genu* of the *corpus callosum* were found to interconnect the left and right prefrontal cortical regions of RSN f, shown in figure 5.6 (RSN f, dark yellow tracts) in 16 out of the 26 subjects (maximum group consistency values of 15). Finally, interhemispheric *corpus callosum* tracts were found to interconnect the left and right posterior precuneus regions of RSN g (figure 5.6, RSN g grey blue tracts, 26 out 26 subjects showing tracts, maximum group consistency values of 12).

discussion

Multiple brain regions are functionally linked to each other during rest, forming *resting-state networks* (RSNs) (Biswal et al., 1995; Greicius et al., 2003; Fox and Raichle, 2007). This study demonstrates that almost all of these functionally linked RSNs are interconnected by anatomical white matter tracts (Wakana et al., 2004). Our findings strongly suggest that functionally linked resting-state networks have an underlying structural core.

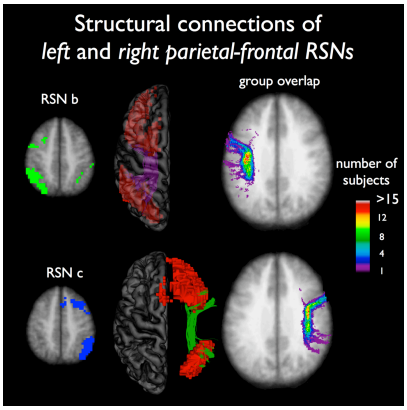

figure 5.4 structural white matter connections between regions of the two lateralized parietal-frontal networks (RSN b and c) Figure shows an important role for the left and right superior parietal fasciculus to interconnect the functionally linked middle/superior frontal and superior parietal regions in the left (21 of 26 subjects showed interconnecting tracts) and right hemisphere (25 of 26 subjects showed interconnecting tracts). The group consistency maps show large overlap over the group of subjects (maximum group consistency voxel values of over 15).

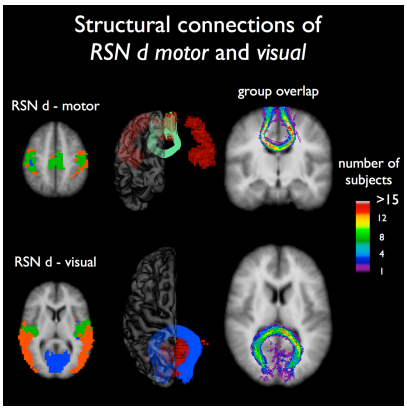

figure 5.5 interconnecting tracts between regions of the primary motor and primary visual resting-state network (RSNd) Figure shows an important role for corpus callosum tracts to interconnect the regions of the primary motor (green RSN, 26 of 26 subjects showing tracts) and primary visual resting-state network (blue RSN, all 26 subjects showing tracts). The group consistency flag maps show a large consistency of the found interconnecting tracts over the group of 26 subjects (maximum consistency values of over 15).

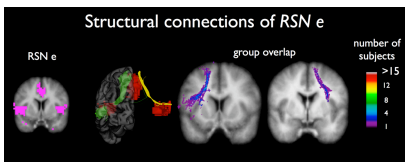

figure 5.6 interconnecting tracts between regions of the core network (RSN e) Fiber tracking revealed interconnecting tracts between the ACC region and the left/right insular regions of RSN e) in part of the subjects (respectively 16 out of 26 and 10 out of 26). Group consistency maps showed a high variation of the interconnecting tracts over the group of subjects, indicated by the maximum consistency voxel values of 5 and 3 respectively.

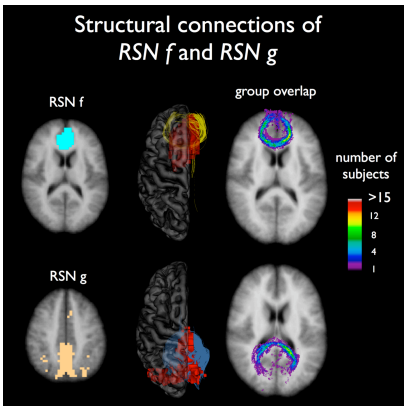

figure 5.7 interconnecting tracts between homogeneous brain regions of RSN f and RSN g Corpus callosum tracts were found to interconnect the bilateral medial frontal regions of RSN f (16 of 26 subjects showed tracts) and the bilateral posterior precuneus regions of RSN g (all 26 subjects showed interconnecting tracts), with a high level of consistency over the group of subjects (maximum consistency values of 15 and 12 respectively).

The 9 examined RSNs are commonly found in resting-state group studies (Beckmann et al., 2005; Salvador et al., 2005b; Damoiseaux et al., 2006; De Luca et al., 2006) (figure 5.2a). In particular, 8 of the 9 group clustered RSNs show one-on-one overlap with the 10 group ICA components reported by Damoiseaux et al. (Damoiseaux et al., 2006), including the *default mode network* (RSN a), the lateralized parietal-frontal networks (RSN b and c), the primary motor, visual and extra-striate visual sub-networks (RSN d), the *core network* consisting of bilateral insular and ACC regions (RSN e) and the network overlapping bilateral posterior medial frontal regions (RSN f). Only the network consisting of posterior precuneus regions (RSN g) was not reported by Damoiseaux et al. The high overlap between the found RSNs of our study and the networks found by Damoiseaux et al. provide strong evidence for the robust formation of functional RSNs in the human brain during rest.

The focus of our study was on the identification of white matter tracts between functionally linked RSN regions. Well-known white matter tracts (Wakana et al., 2004) were found to interconnect the functionally linked regions in 8 out of 9 commonly found RSNs. Specifically, we found an important role for the *tracts of the cingulum, inferior/superior frontal-occipital fasciculus* and *genu of the corpus callosum* (Wakana et al., 2004) in interconnecting the active regions of the default mode network (figure 5.3). The *group consistency flag maps*, reflecting the overlap of the found interconnecting tracts over the group of subjects suggest a high level of consistency of these tracts over the group of subjects, especially for the cingulum and genu tracts (figure 5.3). These results are supported by recent findings, demonstrating an important interconnecting role for the cingulum tract in the default mode network (Greicius et al., 2008). Furthermore, the left and right *superior longitudinal fasciculus* (Wakana et al., 2004) were found to interconnect the two lateralized parietal-frontal RSNs (figure 5.4). In addition, distinct interhemispheric *corpus callosal* tracts (Wakana et al., 2004) were found to interconnect the regions of the primary motor network (Lowe et al., 2008) and the regions of the visual network with a high level of consistency over the group of subjects (figure 5). Furthermore, *corpus callosal* tracts were found to interconnect the regions of the two singular resting-state networks, overlapping bilateral prefrontal and posterior precuneus regions (figure 7).

5 of the 9 clustered group RSNs consist of homologous regions, being the primary motor, primary visual, extra-striate visual and the RSNs consisting of bilateral prefrontal (RSN f) and posterior precuneus regions (RSN g). Given that most homologous regions are interconnected by corpus callosal tracts, the existence of direct structural connections between these

RSN regions was expected. However, the other 4 RSNs, including the default mode network, core network and the two parietal-frontal networks do not solely consist of homologous regions, but rather consist of lateralized brain regions. Therefore, the existence of interconnecting white matter tracts between these functionally linked RSN regions strongly supports the notion of a structural core of RSNs in the human brain.

White matter pathways are bundles of huge numbers of axons that connect large neuronal populations over long distances (Vogt and Pandya, 1987; Wakana et al., 2004; Schmahmann and Pandya, 2006; Schmahmann et al., 2007). They are the structural information highways of our brain, enabling information to travel quickly from one region to another. The notion that functionally linked RSN regions are directly interconnected by these structural highways suggests that RSN activity and synchronization indeed reflect ongoing information integration between anatomically separate regions during rest (Greicius et al., 2003; Greicius et al., 2008). This supports the view that RSNs are meaningful networks (Gusnard et al., 2001; Greicius et al., 2003; Dosenbach et al., 2007; Fox and Raichle, 2007; Mason et al., 2007).

Our results do not directly provide information about the functional relevance of RSNs, but other studies have indicated that activity of at least the default mode network and the core network may play an important role in human cognition. Regions of the core network have been associated with the processing of salient stimuli (Seeley et al., 2007) and goal-directed behavior (Dosenbach et al., 2007) and activation of the default mode network has been linked to mind-wandering (Mason et al., 2007), relating oneself to the outside world (Gusnard et al., 2001) and integration of cognitive and emotional processing (Greicius et al., 2003). These cognitive processes are likely to continue during rest (Gusnard et al., 2001; Greicius et al., 2003) and anatomical white matter pathways between these functionally linked RSN regions could facilitate the ongoing information integration between these regions.

Functional connections between multiple cortical brain regions were examined by computing the correlation between fMRI time-series measured during rest, expressing functional connections between brain regions (Salvador et al., 2005a; Achard et al., 2006; Van den Heuvel et al., 2008c). However, when correlation is used as a measure of functional connectivity, it is unclear whether a high level of functional connectivity between two regions is reflecting *direct* communication between these regions, or whether these regions are *indirectly* linked through a third party region. As DTI only measures the *direct* structural connections between brain regions and resting-state fMRI may express both *direct* and *indirect* connections the functional

resting state network	name	functionally linked regions	structural connections
RSN a	default mode network	MFC (left, right) PCC left IPL right IPL	genu of corpus callosum cingulum left superior fronto-occipital fasciculus right superior fronto-occipital fasciculus
RSN b	left parietal-frontal	left SPC left SFC	left superior longitudinal fasciculus
RSN c	right parietal-frontal	right SPC right SFC	right superior longitudinal fasciculus
RSN d	primary motor	left motor right motor	body of corpus callosum
	primary visual	left visual right visual	splenium of corpus callosum
	extra-striate visual	left extra-striate right extra-striate	
RSN e	core network	left insular cortex right insular cortex ACC	
RSN f	posterior medial frontal network	left MFC right MFC	genu of corpus callosum
RSN g	posterior precuneus network	left posterior prec right posterior prec	corpus callosum

table 5.1 functional and structural connections of resting-state networks Table describes the functionally linked regions of the 9 clustered RSNs (a - g) and the interconnecting structural white matter pathways shown in figure 5.2b and figure 5.3 - 5.7. MFC = medial frontal cortex, PCC = precuneus/posterior cingulate cortex, IPL = inferior parietal lobule, SFC = superior frontal cortex, SPC = superior parietal cortex, ACC = anterior cingulate cortex, prec = precuneus.

and structural connectivity results may only partially overlap. The results of our study demonstrate that a large number of functionally linked RSN regions are directly structurally interconnected. This suggests that a large number of the functional connections between RSN regions are likely to reflect *direct* connections, as at least the structural infrastructure is present to support direct functional synchronization between these regions. *Partial correlation* has been successfully used to measure the unique level of functional connectivity between two brain regions, by factoring out the

influence of third-party regions, expressing only the direct functional connections between two regions (Salvador et al., 2005a; Achard et al., 2006; Liu et al., 2008; Van den Heuvel et al., 2008c). Future studies of our lab are aimed to specifically examine the direct functional and structural connections between RSN regions (Van den Heuvel et al., 2008c).

Supporting evidence for a structural core of functional RSNs comes from studies who report on decreased functional connectivity in combination with studies how report on degenerative effects of the microstructural organization of white matter tracts. Aging has been related to reduced resting-state activity (Damoiseaux et al., 2007) as well as decreased levels of fractional anisotropy of white matter (Makris et al., 2007; Schneiderman et al., 2007; Yoon et al., 2007). Reduced activity of the default mode network has been directly related to an altered microstructural organization of the cingulum tract in advanced aging, as well as decreased levels of cognitive performance (Andrews-Hanna et al., 2007). In addition, disease related decreases of functional connectivity in patients with multiple sclerosis have been associated with decreased structural integrity of corpus callosum fibers (Lowe et al., 2008). Furthermore, patients with psychiatric diseases, such as schizophrenia, that are known to have (progressive) structural gray matter change (Hulshoff Pol et al., 2001; Hulshoff Pol and Kahn, 2008) have been reported to show both altered resting-state activity (Liang et al., 2006; Liu et al., 2006; Bluhm et al., 2007; Salvador et al., 2007; Liu et al., 2008) as well as altered organization of white matter (Sun et al., 2003; Hulshoff Pol et al., 2004; Kubicki et al., 2005; Kubicki et al., 2007; Nestor et al., 2007).

Our findings suggest that functionally linked RSNs have an underlying structural connectivity core. The functionally linked RSNs are represented as separate networks that consist of distinct brain regions showing a high level of coherence between their resting-state fMRI time-series. Almost all of the commonly reported RSNs were found to be directly interconnected by known white matter tracts. In this context, it is reasonable to speculate about the idea that direct structural connections between two anatomically separate brain regions may be a precondition for large brain regions to be (direct) functionally linked. As such, our findings support the notion that white matter pathways may be crucial to support the ongoing neuronal communication between anatomically separated brain regions during rest (Greicius et al., 2008; Hagmann et al., 2008; Van den Heuvel et al., 2008c). However, this does not imply that all structural connected regions should show a high level of functional connectivity during rest. Furthermore, our study suggest the existence of white matter connections between large brain regions of widespread networks. This does not

implicate that local functional connectivity is exclusively related to the existence of structural connections between these regions (Koch et al., 2002).

Nine RSNs were found in our study. However, we by no means try to suggest that our functional brain consists of independent functional networks. Rather, we strongly believe that our brain is an integrated dynamic network (Achard and Bullmore, 2007; Hagmann et al., 2007; Hagmann et al., 2008; Van den Heuvel et al., 2008b), with a vast amount of interaction between multiple RSNs and the existence of both functional and structural connections between RSNs (Hagmann et al., 2007; Hagmann et al., 2008; Sridharan et al., 2008; Vincent et al., 2008). Our study adds to the accumulating evidence that our brain is an integrated network of interconnected regions (Stam, 2004; Achard and Bullmore, 2007; Hagmann et al., 2008; Liu et al., 2008; Van den Heuvel et al., 2008b). Recent studies have shown that the brain network has a so-called *small-world* architecture (Stam, 2004; Micheloyannis et al., 2006; Achard and Bullmore, 2007; Stam et al., 2007; Hagmann et al., 2008; Van den Heuvel et al., 2008b), meaning that its functional and structural connections are organized in an highly efficient manner (Achard and Bullmore, 2007; Hagmann et al., 2007; Hagmann et al., 2008). Small-world networks are known to have a high level of both local and global efficiency (Latora and Marchiori 2001; Achard and Bullmore 2007), suggesting that information can be efficiently processed locally and then quickly transported to remote regions for further processing. Our results suggest that the cortico-cortical white matter pathways of our brain play an important role in the efficient integration of information within functionally linked RSNs during rest.

We used deterministic fiber tracking (Mori et al., 1999; Mori and van Zijl, 2002) to examine the existence of white matter pathways between functionally linked RSN regions. An alternative approach would be the use of probabilistic fiber tracking. Probabilistic fiber tracking, as implemented in the FSL software package, measures the probability that a seed region is connected to a second region. Probabilistic fiber tracking has the advantage that individual connectivity probability maps can be compared between subjects, enabling a statistical group analysis. However, probabilistic fiber tracking does not directly measure the true structural connections between brain regions, but rather the probability that two regions are connected (Jones, 2008). As the focus of our study was on the identification of the structural white matter pathways between RSN regions, deterministic fiber tracking was used.

Some limitations have to be considered when interpreting the results of this study. First, not all subjects showed interconnecting tracts between all RSN regions. A limited number of subjects showed interconnecting tracts

between the regions of the core network (i.e. 10 and 16 out of the 26 subjects showed interconnecting tracts) and between the bilateral regions of RSN f (figure 5.2b, RSN f, brown tracts, 10/16). In addition, no interconnecting tracts were found between the two bilateral insular regions of the core network (figure 5.2a, RSN e) and between the regions of the extra-striate visual network (figure 5.2a, RSN d orange regions). The inability to track fibers between these regions could be related to the difficulty of reconstructing tracts that cross other white matter bundles (Wakana et al., 2004). This is coherent with other studies who report on the difficulty of reconstructing interhemispheric callosal white matter tracts (Basser et al., 2000; Wakana et al., 2004). Furthermore, fiber tracking only revealed white matter tracts between parts of the RSN regions. The interconnecting tracts shown suggest that only sub-parts of the ROIs are structurally interconnected. This might indicate that functionally linked RSNs are structurally interconnected in a somewhat hierarchical fashion, meaning that only sub-parts of a RSN region are directly structurally connected to the other regions of the network and that the other sub-parts of the ROI are in turn connected to these structural connectivity hubs. However, our findings do not provide direct evidence for this. The inability of finding fibers between all parts of two functionally linked ROIs could also be related to the limitations of the used fiber tracking method. Large fiber bundles disperse just before they enter the cortex, which could affect the directionality measurement in the white matter (i.e. lower FA) and hence affect the fiber tracking. Second, individual interconnecting tracts between the functionally linked RSN regions were selected based on group ROIs, which were selected from a group clustering of the resting-state data (figure 5.2a). An alternative approach would be the use of individual ROIs instead of group ROIs to better account for individual anatomical differences of the human brain. However, little is known about individual differences in RSN formation. Until now most resting-state studies have focused on the identification of RSNs across subjects (Beckmann et al., 2005; Damoiseaux et al., 2006). As the focus of our study was on the identification of possible interconnecting structural tracts between regions of known RSNs, group ROIs were used to minimize the possible effects of unknown individual differences in RSN formation. However, it is of high interest to examine whether individual differences in functional connectivity between RSN regions is related to individual variation of the interconnecting white matter pathways of the human brain. Third, in this study we focused on cortical regions of RSNs and the existence of cortico-cortical structural connections between these regions. However, sub-cortical regions have also been reported to be involved in RSNs (Greicius et al., 2003; Beckmann et al., 2005; Damoiseaux et

al., 2006). Examining the functional and structural connections of sub-cortical regions is of high interest. For example, intrinsic functional connections between the thalamus and cortical regions have been reported to be highly region specific (Zhang et al., 2008) and tend to show strong overlap with the structural projections of the thalamus (Behrens et al., 2003). Fourth, our study shows the existence of interconnecting structural pathways between a large number of functionally linked RSN regions. However, in theory, our data could also be explained by the fact that the fiber tracking reveals structural connections between any two arbitrary brain regions. However, given the special small-world organization of the structural connections of the brain (Hagmann et al., 2007; Hagmann et al., 2008) we believe that this alternative explanation is highly unlikely. A small-world organization indicates that not every brain region is connected to every other region in the brain, but rather that the number of white matter pathways is limited (Watts and Strogatz, 1998; Hagmann et al., 2008). There has to be noted that we do not suggest that our brain consists of fully independent functionally and structurally connected networks. Rather, our brain is likely to be a fully integrated network (Achard et al., 2006; Hagmann et al., 2008; Van den Heuvel et al., 2008b), indicating the existence of both functional and structural connections *between* RSN networks. Future studies are needed to examine these inter-RSN connections.

The main finding from this study is the existence of structural white matter connections between the functionally linked regions of resting-state networks. 26 healthy subjects were scanned with 3 Tesla resting-state fMRI recordings and DTI scans to examine both the functional and structural connections of the human brain. Almost all of the commonly reported functional resting-state networks were found to be interconnected by known structural white matter tracts. Our results suggest that functionally linked resting-state networks reflect the underlying structural connectivity architecture of the human brain.

references

Achard S, Bullmore E (2007) Efficiency and cost of economical brain functional networks. PLoS Comput Biol 3:e17.

Achard S, Salvador R, Whitcher B, Suckling J, Bullmore E (2006) A resilient, low-frequency, small-world human brain functional network with highly connected association cortical hubs. J Neurosci 26:63-72.

Aertsen AM, Gerstein GL, Habib MK, Palm G (1989) Dynamics of neuronal firing correlation: modulation of "effective connectivity". J Neurophysiol 61:900-917.

Andersson JL, Skare S (2002) A model-based method for retrospective correction of geometric distortions in diffusion-weighted EPI. Neuroimage 16:177-199.

Andersson JL, Skare S, Ashburner J (2003) How to correct susceptibility distortions in spin-echo echo-planar images: application to diffusion tensor imaging. Neuroimage 20:870-888.

Andrews-Hanna JR, Snyder AZ, Vincent JL, Lustig C, Head D, Raichle ME, Buckner RL (2007) Disruption of large-scale brain systems in advanced aging. Neuron 56:924-935.

Basser PJ, Pajevic S, Pierpaoli C, Duda J, Aldroubi A (2000) In vivo fiber tractography using DT-MRI data. Magn Reson Med 44:625-632.

Beaulieu C, Allen PS (1994) Water diffusion in the giant axon of the squid: implications for diffusion-weighted MRI of the nervous system. Magn Reson Med 32:579-583.

Beckmann CF, DeLuca M, Devlin JT, Smith SM (2005) Investigations into resting-state connectivity using independent component analysis. Philos Trans R Soc Lond B Biol Sci 360:1001-1013.

Behrens TE, Johansen-Berg H, Woolrich MW, Smith SM, Wheeler-Kingshott CA, Boulby PA, Barker GJ, Sillery EL, Sheehan K, Ciccarelli O, Thompson AJ, Brady JM, Matthews PM (2003) Non-invasive mapping of connections between human thalamus and cortex using diffusion imaging. Nat Neurosci 6:750-757.

Biswal B, Yetkin FZ, Haughton VM, Hyde JS (1995) Functional connectivity in the motor cortex of resting human brain using echo-planar MRI. Magn Reson Med 34:537-541.

Biswal BB, Van Kylen J, Hyde JS (1997) Simultaneous assessment of flow and BOLD signals in resting-state functional connectivity maps. NMR Biomed 10:165-170.

Bluhm RL, Miller J, Lanius RA, Osuch EA, Boksman K, Neufeld R, Theberge J, Schaefer B, Williamson P (2007) Spontaneous Low-Frequency Fluctuations in the BOLD Signal in Schizophrenic Patients: Anomalies in the Default Network. Schizophr Bull 33:1004-1012.

Chang LC, Jones DK, Pierpaoli C (2005) RESTORE: robust estimation of tensors by outlier rejection. Magn Reson Med 53:1088-1095.

Collins DL, Neelin P, Peters TM, Evans AC (1994) Automatic 3D intersubject registration of MR volumetric data in standardized Talairach space. J Comput Assist Tomogr 18:192-205.

Cordes D, Haughton VM, Arfanakis K, Wendt GJ, Turski PA, Moritz CH, Quigley MA, Meyerand ME (2000) Mapping functionally related regions of brain with functional connectivity MR imaging. AJNR Am J Neuroradiol 21:1636-1644.

Cordes D, Haughton VM, Arfanakis K, Carew JD, Turski PA, Moritz CH, Quigley MA, Meyerand ME (2001) Frequencies contributing to functional connectivity in the cerebral cortex in "resting-state" data. AJNR Am J Neuroradiol 22:1326-1333.

Damoiseaux JS, Rombouts SA, Barkhof F, Scheltens P, Stam CJ, Smith SM, Beckmann CF (2006) Consistent resting-state networks across healthy subjects. Proc Natl Acad Sci U S A 103:13848-13853.

Damoiseaux JS, Beckmann CF, Arigita EJ, Barkhof F, Scheltens P, Stam CJ, Smith SM, Rombouts SA (2007) Reduced resting-state brain activity in the "default network" in normal aging. Cereb Cortex.

De Luca M, Beckmann CF, De Stefano N, Matthews PM, Smith SM (2006) fMRI resting state networks define distinct modes of long-distance interactions in the human brain. Neuroimage 29:1359-1367.

Dosenbach NU, Fair DA, Miezin FM, Cohen AL, Wenger KK, Dosenbach RA, Fox MD, Snyder AZ, Vincent JL, Raichle ME, Schlaggar BL, Petersen SE (2007) Distinct brain networks for adaptive and stable task control in humans. Proc Natl Acad Sci U S A 104:11073-11078.

Fox MD, Raichle ME (2007) Spontaneous fluctuations in brain activity observed with functional magnetic resonance imaging. Nat Rev Neurosci 8:700-711.

Friston KJ, Frith CD, Liddle PF, Frackowiak RS (1993) Functional connectivity: the principal-component analysis of large (PET) data sets. J Cereb Blood Flow Metab 13:5-14.

Greicius MD, Krasnow B, Reiss AL, Menon V (2003) Functional connectivity in the resting brain: a network analysis of the default mode hypothesis. Proc Natl Acad Sci U S A 100:253-258.

Greicius MD, Supekar K, Menon V, Dougherty RF (2008) Resting-State Functional Connectivity Reflects Structural Connectivity in the Default Mode Network. Cereb Cortex.

Gusnard DA, Raichle ME, Raichle ME (2001) Searching for a baseline: functional imaging and the resting human brain. Nat Rev Neurosci 2:685-694.

Hagmann P, Kurant M, Gigandet X, Thiran P, Wedeen VJ, Meuli R, Thiran JP (2007) Mapping human whole-brain structural networks with diffusion MRI. PLoS ONE 2:e597.

Hagmann P, Cammoun L, Gigandet X, Meuli R, Honey CJ, Wedeen VJ, Sporns O (2008) Mapping the Structural Core of Human Cerebral Cortex. PLoS Biol 6:e159.

Hulshoff Pol HE, Kahn RS (2008) What happens after the first episode? A review of progressive brain changes in chronically ill patients with schizophrenia. Schizophr Bull 34:354-366.

Hulshoff Pol HE, Schnack HG, Mandl RC, Cahn W, Collins DL, Evans AC, Kahn RS (2004) Focal white matter density changes in schizophrenia: reduced inter-hemispheric connectivity. Neuroimage 21:27-35.

Hulshoff Pol HE, Schnack HG, Mandl RC, van Haren NE, Koning H, Collins DL, Evans AC, Kahn RS (2001) Focal gray matter density changes in schizophrenia. Arch Gen Psychiatry 58:1118-1125.

Johnston JM, Vaishnavi SN, Smyth MD, Zhang D, He BJ, Zempel JM, Shimony JS, Snyder AZ, Raichle ME (2008) Loss of resting interhemispheric functional connectivity after complete section of the corpus callosum. J Neurosci 28:6453-6458.

Jones DK (2004) The effect of gradient sampling schemes on measures derived from diffusion tensor MRI: a Monte Carlo study. Magn Reson Med 51:807-815.

Jones DK (2008) Studying connections in the living human brain with diffusion MRI. Cortex 44:936-952.

Jones DK, Horsfield MA, Simmons A (1999) Optimal strategies for measuring diffusion in anisotropic systems by magnetic resonance imaging. Magn Reson Med 42:515-525.

Koch MA, Norris DG, Hund-Georgiadis M (2002) An investigation of functional and anatomical connectivity using magnetic resonance imaging. Neuroimage 16:241-250.

Kubicki M, McCarley R, Westin CF, Park HJ, Maier S, Kikinis R, Jolesz FA, Shenton ME (2007) A review of diffusion tensor imaging studies in schizophrenia. J Psychiatr Res 41:15-30.

Kubicki M, Park H, Westin CF, Nestor PG, Mulkern RV, Maier SE, Niznikiewicz M, Connor EE, Levitt JJ, Frumin M, Kikinis R, Jolesz FA, McCarley RW, Shenton ME (2005) DTI and MTR abnormalities in schizophrenia: analysis of white matter integrity. Neuroimage 26:1109-1118.

Liang M, Zhou Y, Jiang T, Liu Z, Tian L, Liu H, Hao Y (2006) Widespread functional disconnectivity in schizophrenia with resting-state functional magnetic resonance imaging. Neuroreport 17:209-213.

Liu H, Liu Z, Liang M, Hao Y, Tan L, Kuang F, Yi Y, Xu L, Jiang T (2006) Decreased regional homogeneity in schizophrenia: a resting state functional magnetic resonance imaging study. Neuroreport 17:19-22.

Liu Y, Liang M, Zhou Y, He Y, Hao Y, Song M, Yu C, Liu H, Liu Z, Jiang T (2008) Disrupted small-world networks in schizophrenia. Brain 131:945.

Lowe MJ, Mock BJ, Sorenson JA (1996) Resting State fMRI Signal Correlations in Multi-slice EPI. Neuroimage 3.

Lowe MJ, Mock BJ, Sorenson JA (1998) Functional connectivity in single and multislice echoplanar imaging using resting-state fluctuations. Neuroimage 7:119-132.

Lowe MJ, Dzemidzic M, Lurito JT, Mathews VP, Phillips MD (2000) Correlations in low-frequency BOLD fluctuations reflect cortico-cortical connections. Neuroimage 12:582-587.

Lowe MJ, Beall EB, Sakaie KE, Koenig KA, Stone L, Marrie RA, Phillips MD (2008) Resting state sensorimotor functional connectivity in multiple sclerosis inversely correlates with transcallosal motor pathway transverse diffusivity. Hum Brain Mapp 29:818-827.

Makris N, Papadimitriou GM, van der Kouwe A, Kennedy DN, Hodge SM, Dale AM, Benner T, Wald LL, Wu O, Tuch DS, Caviness VS, Moore TL, Killiany RJ, Moss MB, Rosene DL (2007) Frontal connections and cognitive changes in normal aging rhesus monkeys: a DTI study. Neurobiol Aging 28:1556-1567.

Mason MF, Norton MI, Van Horn JD, Wegner DM, Grafton ST, Macrae CN (2007) Wandering minds: the default network and stimulus-independent thought. Science 315:393-395.

Micheloyannis S, Pachou E, Stam CJ, Breakspear M, Bitsios P, Vourkas M, Erimaki S, Zervakis M (2006) Small-world networks and disturbed functional connectivity in schizophrenia. Schizophr Res 87:60-66.

Mori S, van Zijl PC (2002) Fiber tracking: principles and strategies - a technical review. NMR Biomed 15:468-480.

Mori S, Crain BJ, Chacko VP, van Zijl PC (1999) Three-dimensional tracking of axonal projections in the brain by magnetic resonance imaging. Ann Neurol 45:265-269.

Mori S, Kaufmann WE, Davatzikos C, Stieltjes B, Amodei L, Fredericksen K, Pearlson GD, Melhem ER, Solaiyappan M, Raymond GV, Moser HW, van Zijl PC (2002) Imaging cortical association tracts in the human brain using diffusion-tensor-based axonal tracking. Magn Reson Med 47:215-223.

Nestor PG, Kubicki M, Spencer KM, Niznikiewicz M, McCarley RW, Shenton ME (2007) Attentional networks and cingulum bundle in chronic schizophrenia. Schizophr Res 90:308-315.

Nir Y, Mukamel R, Dinstein I, Privman E, Harel M, Fisch L, Gelbard-Sagiv H, Kipervasser S, Andelman F, Neufeld MY, Kramer U, Arieli A, Fried I, Malach R (2008) Interhemispheric correlations of slow spontaneous neuronal fluctuations revealed in human sensory cortex. Nat Neurosci.

Raichle ME, Snyder AZ (2007) A default mode of brain function: A brief history of an evolving idea. Neuroimage 37:1083-1090.

Raichle ME, MacLeod AM, Snyder AZ, Powers WJ, Gusnard DA, Shulman GL (2001) A default mode of brain function. Proc Natl Acad Sci U S A 98:676-682.

Salvador R, Suckling J, Schwarzbauer C, Bullmore E (2005a) Undirected graphs of frequency-dependent functional connectivity in whole brain networks. Philos Trans R Soc Lond B Biol Sci 360:937-946.

Salvador R, Suckling J, Coleman MR, Pickard JD, Menon D, Bullmore E (2005b) Neurophysiological architecture of functional magnetic resonance images of human brain. Cereb Cortex 15:1332-1342.

Salvador R, Martinez A, Pomarol-Clotet E, Sarro S, Suckling J, Bullmore E (2007) Frequency based mutual information measures between clusters of brain regions in functional magnetic resonance imaging. Neuroimage 35:83-88.

Schmahmann JD, Pandya DN (2006) Fiber pathways of the brain. In, pp 485-496: Oxford University Press.

Schmahmann JD, Pandya DN, Wang R, Dai G, D'Arceuil HE, de Crespigny AJ, Wedeen VJ (2007) Association fibre pathways of the brain: parallel observations from diffusion spectrum imaging and autoradiography. Brain 130:630-653.

Schneiderman JS, Buchsbaum MS, Haznedar MM, Hazlett EA, Brickman AM, Shihabuddin L, Brand JG, Torosjan Y, Newmark RE, Tang C, Aronowitz J, Paul-Odouard R, Byne W, Hof PR (2007) Diffusion tensor anisotropy in adolescents and adults. Neuropsychobiology 55:96-111.

Seeley WW, Menon V, Schatzberg AF, Keller J, Glover GH, Kenna H, Reiss AL, Greicius MD (2007) Dissociable intrinsic connectivity networks for salience processing and executive control. J Neurosci 27:2349-2356.

Shi J, Malik J (2000) Normalized cuts and image segmentation. IEEE Transactions on pattern analysis and machine intelligence 22:17.

Shmuel A, Leopold DA (2008) Neuronal correlates of spontaneous fluctuations in fMRI signals in monkey visual cortex: Implications for functional connectivity at rest. Hum Brain Mapp 29:751-761.

Shmueli K, van Gelderen P, de Zwart JA, Horovitz SG, Fukunaga M, Jansma JM, Duyn JH (2007) Low-frequency fluctuations in the cardiac rate as a source of variance in the resting-state fMRI BOLD signal. Neuroimage 38:306-320.

Sridharan D, Levitin DJ, Menon V (2008) A critical role for the right fronto-insular cortex in switching between central-executive and default-mode networks. Proc Natl Acad Sci U S A 105:12569-12574.

Stam CJ (2004) Functional connectivity patterns of human magnetoencephalographic recordings: a 'small-world' network? Neurosci Lett 355:25-28.

Stam CJ, Jones BF, Nolte G, Breakspear M, Scheltens P (2007) Small-world networks and functional connectivity in Alzheimer's disease. Cereb Cortex 17:92-99.

Sun Z, Wang F, Cui L, Breeze J, Du X, Wang X, Cong Z, Zhang H, Li B, Hong N, Zhang D (2003) Abnormal anterior cingulum in patients with schizophrenia: a diffusion tensor imaging study. Neuroreport 14:1833-1836.

Van den Heuvel MP, Mandl RC, Hulshoff Pol HE (2008a) Normalized group clustering of resting-state fMRI data. PLoS ONE 3:e2001.

Van den Heuvel MP, Stam CJ, Boersma M, Hulshoff Pol HE (2008b) Small-world and scale-free organization of voxel based resting-state functional connectivity in the human brain. Neuroimage In Press.

Van den Heuvel MP, Mandl RC, Luigjes J, Hulshoff Pol HE (2008c) Microstructural organization of the cingulum tract and the level of default mode functional connectivity. J Neurosci 28:7.

Vincent JL, Kahn I, Snyder AZ, Raichle ME, Buckner RL (2008) Evidence for a Frontoparietal Control System Revealed by Intrinsic Functional Connectivity. J Neurophysiol.

Vogt BA, Pandya DN (1987) Cingulate cortex of the rhesus monkey: II. Cortical afferents. J Comp Neurol 262:271-289.

Wakana S, Jiang H, Nagae-Poetscher LM, van Zijl PC, Mori S (2004) Fiber tract-based atlas of human white matter anatomy. Radiology 230:77-87.

Watts DJ, Strogatz SH (1998) Collective dynamics of 'small-world' networks. Nature 393:440-442.

Wise RG, Ide K, Poulin MJ, Tracey I (2004) Resting fluctuations in arterial carbon dioxide induce significant low frequency variations in BOLD signal. Neuroimage 21:1652-1664.

Xiong J, Parsons LM, Gao JH, Fox PT (1999) Interregional connectivity to primary motor cortex revealed using MRI resting state images. Hum Brain Mapp 8:151-156.

Yoon B, Shim YS, Lee KS, Shon YM, Yang DW (2007) Region-specific changes of cerebral white matter during normal aging: A diffusion-tensor analysis. Arch Gerontol Geriatr.

Zhang D, Snyder AZ, Fox MD, Sansbury MW, Shimony JS, Raichle ME (2008) Intrinsic Functional Relations between Human Cerebral Cortex and Thalamus. J Neurophysiol.

chapter 6

microstructural organization of the cingulum tract and the level of default mode functional connectivity

martijn van den heuvel, rené mandl, judith luigjes, hilleke hulshoff pol

journal of neuroscience 2008 43 (28)

The default mode network is a functionally connected network of brain regions that show highly synchronized intrinsic neuronal activation during rest. However, less is known about the structural connections of this network, which could play an important role in the observed functional connectivity patterns. In this study, we examined the microstructural organization of the cingulum tract in relation to the level of resting-state default mode functional synchronization. *resting-state functional magnetic resonance imaging* and *diffusion tensor imaging* data of 45 healthy subjects was acquired on a 3 Tesla scanner. Both structural and functional connectivity of the default mode network were examined. In all subjects, the cingulum tract was identified from the total collection of reconstructed tracts to interconnect the precuneus / posterior cingulate cortex and medial frontal cortex, key regions of the default mode network. A significant positive correlation was found between the average *fractional anisotropy* value of the cingulum tract and the level of functional connectivity between the precuneus / posterior cingulate cortex and medial frontal cortex. Our results suggest a direct relationship between the structural and functional connectivity measures of the default mode network and contribute to the understanding of default mode network connectivity.

introduction

Multiple cortical and sub-cortical regions show coherent time-series during rest and are suggested to form resting-state networks (Damoiseaux et al., 2006; Van den Heuvel et al., 2008). In particular, a set of regions called the default mode network (Raichle et al., 2001; Greicius et al., 2003) has been reported to show high levels of intrinsic neuronal activity during rest (Gusnard et al., 2001; Greicius et al., 2003; Raichle and Snyder, 2007). The most often reported and most influential regions of this network are the precuneus / posterior cingulate cortex (PCC), involved in responding to salient stimuli in the world around us (Gusnard et al., 2001; Corbetta et al., 2000) and medial frontal cortex (MFC), involved in emotional processing and the monitoring of one's mental state (Northoff and Bermpohl, 2004; Northoff et al., 2006; Schmitz and Johnson, 2007). Neuronal activation patterns of the PCC and MFC have been reported to be highly coherent during rest (Greicius et al., 2003; Fox and Raichle, 2007), indicating a high level of functional connectivity (Biswal et al., 1995) and ongoing communication between the PCC and MFC during rest. This supports the idea of the default mode network as a cohesive brain network that may be involved in important functions of human cognition (Gusnard et al., 2001; Greicius et al., 2003; Mason et al., 2007).

However, less is known about the structural connections of the default mode network. The cingulum bundle is a collection of white matter tracts that connect regions of the frontal lobe with the precuneus, posterior cingulate cortex, hippocampus and parahippocampus (Wakana et al., 2004; Schmahmann et al., 2007; Lawes et al., 2008). These termination regions show large overlap with key regions of the default mode network. Indeed, Greicius et al. recently reported that the PCC and MFC regions of the default mode network are connected by the cingulum tract (Greicius et al., 2008). These results suggest an anatomical basis of the default mode network and raise the question about a possible association between the structural and functional connectivity measures of the default mode network. We hypothesize that an association exists between the microstructural organization of the cingulum tract and the level of default mode functional connectivity. Examining this association could add to the understanding of default mode network connectivity. In this study, resting-state functional Magnetic Resonance Imaging (fMRI) recordings and Diffusion Tensor Imaging (DTI) scans were acquired on a 3 Tesla MR scanner in 45 subjects. The unique level of functional connectivity between the PCC and MFC regions of the default mode network was computed as the partial correlation between their resting-state time-series. Cingulum tracts interconnecting the

PCC and MFC were reconstructed using the DTI scans and fractional anisotropy (FA) values of these tracts were calculated as an indication of white matter integrity (Kim et al., 2007). Over the group of subjects, the mean FA value of the cingulum tract was correlated with the level of functional connectivity between the PCC and MFC regions of the default mode network.

materials and methods

subjects

45 healthy subjects (mean age: 24.8 years, SD: 4.8, 25 male, 20 female) participated in this study after giving written consent as approved by the medical ethics committee for research in humans (METC) of the University Medical Centre Utrecht, the Netherlands. All subjects underwent a 45 minute scanning session. During the resting-state recordings, subjects were instructed to relax, keep their eyes closed without falling asleep and to think of nothing in particular.

image acquisition

Resting-state functional Magnetic Resonance Imaging (resting-state fMRI) and Diffusion Tensor Imaging (DTI) data were acquired on a 3 Tesla Philips Achieva Medical Scanner (Philips Medical Systems, Best, The Netherlands) at the University Medical Center Utrecht, The Netherlands. During the rest experiment, resting-state blood oxygenation level dependent (BOLD) signals were recorded during a period of 8 minutes using a fast fMRI sequence (3D PRESTOSENSE p/s-reduction 2/2 (Golay et al., 2000; Neggers et al., 2008); TR/TE 22 ms/32 ms using shifted echo, flip-angle 9 degrees; dynamic scan time 0.5 sec, 1000 timeframes; FOV 256x256 mm, 4 mm isotropic voxel size, 32 slice volume covering the whole brain). Directly after the fMRI time-series an additional functional scan was acquired with identical parameters, but with a high anatomical contrast due to an increased flip-angle of 25 degrees. This additional high contrast functional scan was acquired to improve the co-registration of the functional images with the anatomical image. In the same scanning session DTI scans were acquired (DTI-MR using parallel imaging SENSE p-reduction 3; 5 unweighted B=0 scans, high angular gradient set of 30 weighted directions (Jones, 2004; Jones et al., 1999), TR = 7035 ms, TE = 68 ms, EPI factor 35; FOV 240x240mm, 2 mm isotropic voxelsize, 75 slices covering the whole brain). In total, 2 DTI sets of 30 weighted diffusion scans with different weighting directions (b = 1000 s/mm2) and 5 unweighted B0 scans (b = 0 s/mm2) were acquired. The second

DTI set was acquired with a reversed k-space read-out direction (Anterior direction) in comparison to the first set (Posterior direction) (Andersson et al., 2003). In addition, a T1 weighted image (3D FFE using parallel imaging; TR/TE 10ms/4.6ms; FOV 240x240mm, 200 slices, 0.75mm isotropic voxelsize) was acquired for anatomical reference of the functional time-series and structural DTI scans.

image preprocessing

fMRI preprocessing was performed with the SPM2 software package (http://www.fil.ion.ucl.ac.uk). The functional scans were corrected for small head movements by realigning all scans to the last functional scan. Both the T1 image and the functional scans were co-registered with the high contrast functional scan, to enable spatial overlap between the functional time-series and the T1 image. Cortical voxels were selected based on a cortical segmentation of the T1 image. Cortical segmentation was performed with the widely used and freely available Freesurfer software package (http://surfer.nmr.mgh.harvard.edu/). The T1 image was normalized to match the MNI 305 T1 template brain (Collins et al., 1994). Next, the fMRI time-series and cortical segmentation map were normalized to standard space by using the normalization parameters of the T1 image. The normalized cortical segmentation map was resliced to the spatial resolution of the fMRI images.

DTI preprocessing was performed with the diffusion toolbox of Andersson et al. (Andersson and Skare, 2002) and in-house developed software. First, susceptibility distortions, often reported in single-shot EPI images, were corrected by combining the 2 sets of DTI images. A field distortion map was computed based on the two set-averaged unweighted B=0 images and applied to the weighted images (Andersson et al., 2003), resulting in a single set of corrected scans, which were realigned with the corrected B=0 image (Andersson and Skare, 2002). Within each voxel, the diffusion profile was fitted a tensor using a robust tensor fit method based on M-estimators (Chang et al., 2005) and the main diffusion direction within each voxel was selected as the principal eigenvector, determined by the eigenvalue decomposition of the fitted tensor. The *Fiber Assignment by Continuous Tracking (*FACT) algorithm (Mori et al., 1999; Mori and van Zijl, 2002) was used to reconstruct the white matter tracts of the brain. In each voxel, 27 fiber seeds were started. Fiber tracking was stopped when the fiber touched a voxel with a FA value lower than 0.1 or when it had an average angle change between the neighboring eigenvectors of more than 45 degrees or when the trajectory of the traced fiber exceeded the brain. Only fibers with a minimum length of 50 mm were considered. Next, the B=0 image was registered (linear) to the anatomical image and normalized using the

normalization parameters of the T1 image, to overlap with the normalized resting-state fMRI time-series.

selection of default mode network

Resting-state networks (RSNs) across the group of subjects were selected with the voxel-based *normalized cut group clustering* approach, described in detail elsewhere (Van den Heuvel et al., 2008). This method involves the clustering of voxels that show a high level of functional connectivity consistently over a group of subjects. In brief, for each individual dataset, the resting-state fMRI dataset was represented as a network that was constructed out of all cortical voxels with weighted connections between all voxel pairs. Cortical voxels were identified from the individual cortical segmentation map. The weights of the connections between the voxels in the network were computed as the zero-lag temporal correlation between the filtered resting-state time-series. The resulting connectivity graph was then clustered, resulting in the grouping of voxels that showed a high level of functional connectivity. Next, the overlap of the individual voxel-wise clustering results defined a *group graph*, with weighted connections between the cortical voxels reflecting the level of consistency of the clustering results over the group of subjects. The voxels in the group graph were selected from the group cortical segmentation map, which resulted from overlapping the individual cortical segmentation maps. The group graph was clustered, clustering voxels into resting-state networks that showed a high level of functional connectivity consistently over the group of subjects. Using the normalized cut group clustering approach, the number of RSN clusters are defined as an optimal clustering fit of the group graph, which is defined as a clustering fit that minimizes the total cost of partitioning the graph into separate networks (Van den Heuvel et al., 2008). This optimization procedure resulted in an optimal clustering fit of the data in 7 RSNs (figure 6.1). Group clustering revealed the extensively described default mode network (Raichle et al., 2001; Greicius et al., 2003), overlapping the PCC (Brodmann Area (BA) 23/31), bilateral middle/superior temporal gyrus (BA 21/39) and inferior/superior parietal cortex (SPC) (BA 39/40), and frontal cortices, including both superior frontal cortex (BA 8/9) and MFC (BA 10/11). The other clustered RSNs included two lateralized frontal-parietal networks, a motor/sensory/auditory network, a network consisting of insula and anterior cingulate cortex and two singular networks that overlapped the medial frontal gyrus and a posterior part of BA 7 (figure 6.1). The clustered RSNs showed resemblance with the resting-state networks found by previous studies reporting on the group-wise selection of resting-

state networks (Beckmann et al., 2005; Damoiseaux et al., 2006; De Luca et al., 2006; Van den Heuvel et al., 2008).

functional connectivity

For each of the individual datasets, the functional connectivity between the PCC and MFC was calculated as follows. First, the PCC and MFC were selected from the default mode network clustermap (figure 6.1a). Next, the fMRI time-series of all voxels were filtered using a bandpass filter, extracting the low resting-state frequencies of interest (0.01 - 0.08 Hz) (Achard et al., 2006; Biswal et al., 1995; Biswal et al., 1997; Cordes et al., 2001). The representative time-series of the PCC and MFC were obtained by averaging the time-series of the voxels within these regions. The level of functional connectivity between the PCC and MFC regions was computed as a *partial correlation* between their filtered time-series, controlling for third-party influences of other RSN regions (Stam, 2004; Sun et al., 2004; Salvador et al. 2005; Achard et al., 2006; Liu et al., 2008). Besides the default mode network, the group clustering revealed 6 other resting-state networks, which in total consisted of 13 anatomically separate regions. For each of these 13 other RSN regions and the two bilateral SPC regions of the default mode network, representative time-series were computed by averaging the time-series of all voxels within this particular RSN region (Liu et al., 2008). The partial correlation between the time-series of the PCC and MFC was computed by correlating the resting-state time-series of the PCC and MFC, factoring out the contributions of the time-series of the other 13 RSN regions and the two bilateral superior parietal cortex (SPC) regions of the default mode network (figure 6.1a). This procedure was similar to the methodology used in previous studies examining functional connectivity between brain regions (Achard et al., 2006; Liu et al., 2008; Salvador et al., 2005). In these studies the brain was partitioned into a fixed number of regions based on a predefined anatomical template, normally around 90 regions and partial correlations between the time-series of each pair of regions was computed by factoring out the contributions of the time-series of the other 88 regions. In our study, the third-party regions were defined as the brain regions of the other RSNs (figure 6.1) that resulted from the group clustering. The use of a *partial correlation* ensured the examination of the *specific* level of functional connectivity between the PCC and MFC (Achard et al., 2006; Liu et al., 2008; Salvador et al., 2005). To verify this specificity, the *non-partial correlation* coefficient between the filtered time-series of the PCC and MFC was computed, correlating the fMRI time-series of the PCC and MFC, without factoring out the contributions of the other RSN regions. In addition, to examine the level of overall default mode functional connectivity, the time-

series of the PCC and MFC regions were correlated, factoring out the third-party effects of the other RSN regions (figure 6.1, network b-g), but *not* the effects of the two SPC regions of the default mode network (figure 6.1). Finally, a Fisher's r-to-z transformation was used to improve the normality of the partial correlation coefficients (Fox and Raichle, 2007; Salvador et al., 2005). The partial correlation Fisher's z coefficient reflected the unique level of functional connectivity between the PCC and MFC of the default mode network (Achard et al., 2006; Salvador et al., 2005).

selection of interconnecting tracts

It was verified for each individual dataset whether or not the two PCC and MFC regions of interest were interconnected with white matter tracts. First, to overlap the regions of interest with the individual structural DTI data, the default mode network clustermap was registered to the individual unweighted B=0 image (using the reversed normalization and registration parameters generated in the matching of B=0 and T1 images). Next, from the total collection of reconstructed tracts, the tracts that touched both the PCC and the MFC were selected, using a three step procedure (figure 6.2). From the total collection of reconstructed tracts (figure 6.2, step 1), the tracts that touched the PCC were selected (figure 6.2, step 2). Next, from the resulting tracts, the tracts that touched the MFC were selected (figure 6.2, step 3). To enable group comparison, the resulting tracts were normalized using the registration and normalization parameters of the B=0 image. The mean FA value of the resulting tracts, an estimate of the microstructural organization within these white matter tracts (Beaulieu, 2002), was calculated by averaging the FA values of the points along the selected left and right hemispheric tracts. This procedure was repeated for each individual dataset, obtaining a mean FA value for the connecting tracts in each subject. In addition, for each individual DTI dataset the mean FA value of the total collection of fibers in the brain was computed.

association between structural and functional connectivity

The association between the level of structural connectivity and the level of functional connectivity of the default mode network was computed by correlating the mean FA value of the connecting tracts with the unique level of functional connectivity (Fisher's z score) between the PCC and MFC over the group of subjects. Possible age effects were regressed out of the FA and functional connectivity measures separately, as recent studies have demonstrated that normal aging is associated with both decreased microstructural organization (i.e. lower FA values) of the cingulum tract

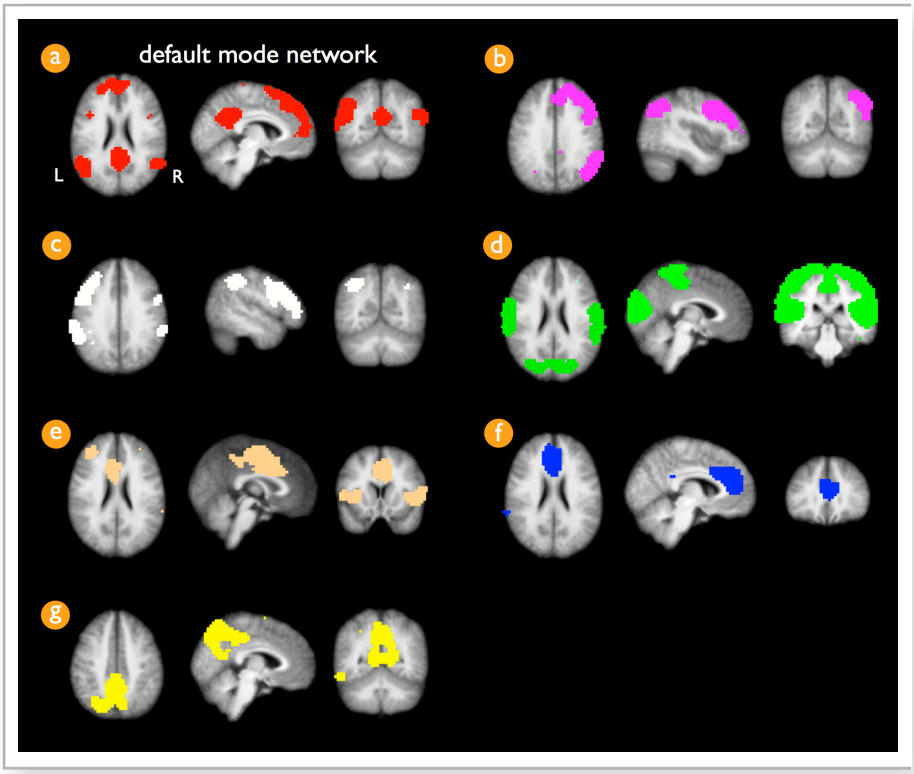

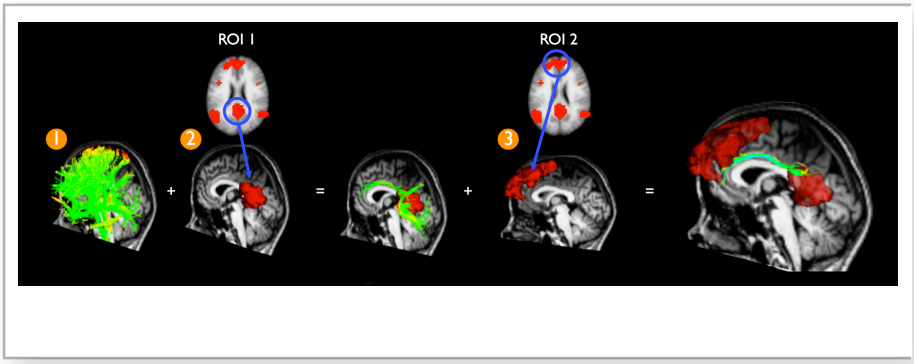

(Andrews-Hanna et al., 2007) and decreased levels of default mode functional connectivity (Andrews-Hanna et al., 2007; Damoiseaux et al., 2007). In addition, an alternative approach to correct for aging effects was examined by taking age as a covariate in assessing the correlation between default mode functional connectivity and mean cingulum FA values. Furthermore, to examine whether the association between mean FA and

figure 6.1 group clustered resting-state networks Normalized cut group clustering of the resting-state time series of the group of 45 subjects revealed seven resting-state networks. ***Cluster a*** (***a***) shows the default mode network, consisting of frontal regions, including superior frontal gyrus (BA 8/9) and medial frontal gyrus (BA 10/11) and precuneus/posterior cingulate cortex (BA 23/31) and bilateral regions overlapping middle/superior temporal tyrus (BA 21/39) and inferior/superior parietal cortex (BA 39/40). ***Clusters b*** and ***c*** (***b***, ***c***) show lateralized frontoparietal networks in the right and left hemisphere, overlapping regions in the superior parietal lobule, inferior parietal lobule, supramarginal gyrus (BA 40), and medial and superior frontal gyrus (BA 8/9). ***Cluster d*** (***d***) shows a combined network of both visual and motor regions, consisting of medial, lateral, and superior occipital gyrus and peristriate regions (BA 17/18/19), precentral (BA 4), and postcentral gyrus (BA 3/1/2). ***Cluster e*** (***e***) shows a network of cingulate gyrus (BA 24) and bilateral insular and superior temporal gyrus (BA 13/22), a network that is also commonly found in resting-state studies. ***Cluster f*** (***f***) involves a singular region consisting of a medial part of the medial frontal gyrus (BA 9) and cingulate gyrus (BA 32). ***Cluster g*** (***g***) involves a singular region consisting of a posterior part of BA 7. L, left; R, right.

figure 6.2 selection of tracts that interconnect the regions of the default mode network In each individual dataset, interconnecting tracts between the PCC and MFC of the default mode network were selected as follows. First, the FACT algorithm was used to trace the total collection of tracts in the human brain. 27 fiber seeds were started in all voxels of the brain, reconstructing the total collection of fibers (***step 1***). Second, the PCC was selected from the default mode network clustermap (figure 6.1a). Fibers that touched the PCC region were selected (***step 2***). Third, the MFC was selected from the default mode network clustermap and from the resulting fibers of step 2 the fibers that touched the MFC regions were selected (***step 3***). This procedure resulted in the fibers that touched both regions of interest, selecting the fibers that interconnect the PCC and MFC of the default mode network.

default mode functional connectivity was specific to the interconnecting cingulum tracts or instead was related to a more global effect, two additional analyses were performed. One, the level of functional connectivity between the PCC and MFC regions was correlated with the mean FA value of the total collection of reconstructed fibers in the brain. Two, the functional connectivity levels of the other clustered RSNs were correlated with the

mean FA value of the cingulum tract. Group clustering revealed 6 additional RSNs, with 4 RSNs consisting of two or more anatomically separate cortical regions (figure 6.1). In total, these 4 RSNs consisted of 11 regions. Functional connectivity measures of these RSNs were computed in a similar manner as the computation of the level of functional connectivity of the default mode network. The level of functional connectivity was defined as the partial correlation between the filtered resting-state time-series of the regions of the selected RSN, correcting for third-party effects of the time-series of the regions of the other clustered RSNs. The resulting partial correlation coefficient was correlated with the mean FA value of the cingulum, after controlling for age on both measures.

results

Normalized cut group clustering of the resting-state fMRI data revealed 7 resting-state networks, including the often reported default mode network (figure 6.1, cluster a). The level of overall default mode connectivity (i.e. the correlation between the PCC and MFC, factoring out the effects of the other RSNs, but not the two SPC regions) was significantly non-zero over the group of subjects (mean: 0.51, SD: 0.23, $p < 0.001$). The level of *unique* default mode functional connectivity between the PCC and MFC was found to be significant non-zero over the group of subjects (mean: 0.19, SD: 0.24, $p < 0.001$). All 45 subjects showed interconnecting tracts between the PCC and MFC of the default mode network. The normalized connecting tracts of all 45 subjects are shown in figure 6.3, together with the PCC and MFC regions of interest from the default mode network clustermap. The selected connecting tracts reflected the left and right cingulum fiber bundle (Lawes et al., 2008; Wakana et al., 2004). The average FA value of the cingulum tracts over the group of subjects was 0.52 (SD: 0.05). Correlating the *non-partial correlation coefficient* between the PCC and MFC time-series with the mean FA value of the cingulum tracts revealed a positive, but non-significant association ($r = 0.18$, $p = 0.17$, mean: 0.18, SD: 0.33, corrected for age). Correlating the level of overall default mode functional connectivity with the FA value of the cingulum tract revealed a positive trend ($r = 0.23$, $p = 0.07$, corrected for age). Correlating the *partial correlation coefficient* as a measure of the *unique* level of default mode PCC - MFC functional connectivity with the mean FA value of the cingulum tracts revealed a significant positive association ($r = 0.29$, $p < 0.05$, figure 6.4), after controlling for age on each measure. The association between default mode functional connectivity and mean cingulum FA values was also examined by taking age as a covariate when assessing the correlation of mean cingulum FA and resting-state

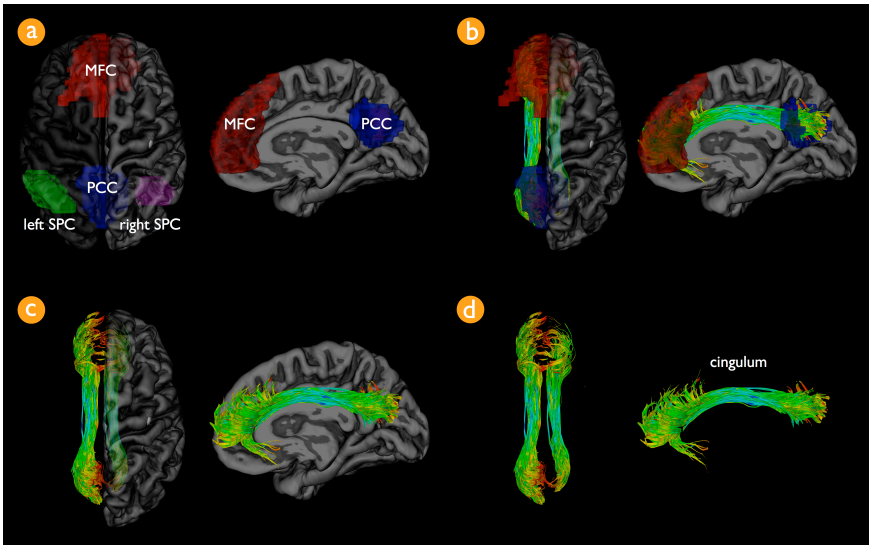

figure 6.3 cingulum tract connects precuneus and posterior cingulate cortex and medial frontal cortex of the default mode network Figure 6.3a shows the regions of interest of the default mode network on a 3D rendering of the averaged normalized T1 scan. The default mode network was selected by using a normalized cut group clustering approach of the resting-state data. Clustering revealed the default mode network, including the precuneus / posterior cingulate cortex (PCC, blue region of interest), medial frontal cortex (MFC, red region of interest) and bilateral superior parietal cortex (SPC, green and magenta regions). Figure 6.3b, c and d show the interconnecting tracts between the PCC and MFC regions over all subjects combined. Figure 6.3b shows both the tracts together with the PCC (blue) and MFC (red) regions of the default mode network projected on the averaged normalized anatomical brain of the group of subjects.

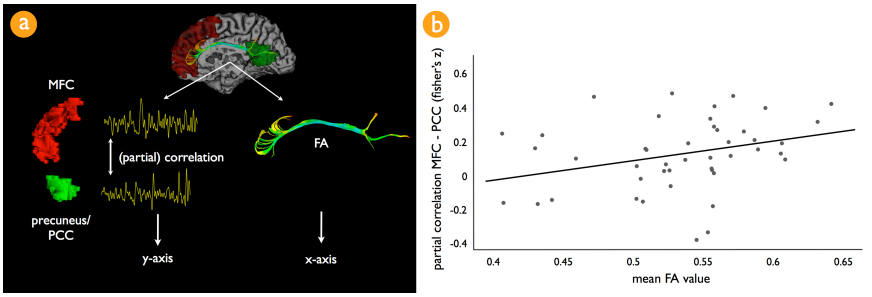

figure 6.4 association between the level of default mode functional connectivity and the microstructural organization of the cingulum tract Figure 6.4a illustrates the analysis that was used to compute the level of functional and structural connectivity

figure 6.4 (continuing)
between the regions of interest from the default mode network. In each individual dataset, the spatially averaged filtered rest-recorded time-series (0.01 - 0.08 Hz) of the PCC and MFC of the default mode network clustermap were correlated, correcting for third-party effects. This resulted in a partial correlation between the PCC and MFC regions (legend continues on next page), which reflected the unique level of functional connectivity between these two key regions of the default mode network. The normality of the partial correlation coefficient was improved by using a Fisher's r-to-z transformation. For each individual dataset, the mean FA value of the found interconnecting cingulum tract was calculated, by averaging the FA values along all points of the found interconnecting tracts. Correlating the level of default mode functional connectivity and mean cingulum FA revealed a significant positive correlation, correcting for age ($r = 0.29$, $p < 0.05$) (figure 6.4b). This suggests a direct positive association between the microstructural organization of the cingulum tract and the level of functional connectivity of the default mode network during rest. Note that the partial correlation between the PCC and MFC regions represented the partial correlation between these regions, factoring out the pair-wise correlations between the time-series of the other resting-state network regions, including the two lateralized superior parietal regions of the default mode network. This relationship was found to be specific for the cingulum tract, as no significant association was found between the partial correlation between the PCC and MFC and the mean FA value of the total collection of reconstructed tracts in the brain. Furthermore, functional connectivity measures between the regions of the other clustered resting-state networks (figure 6.1, network b - g) did not show a significant association with the mean FA value of the cingulum tract.

functional connectivity measures. This alternative approach also revealed a significant association between default mode functional connectivity and mean cingulum FA (total $r^2 = 0.12$, $p < 0.05$). Furthermore, the association between the level of default mode functional connectivity and FA measures was found to be specific to the cingulum since no significant association was found between the level of default mode functional connectivity and the mean FA value of the total collection of reconstructed tracts in the brain (i.e. all other white matter tracts in the brain) ($r = 0.12$, $p = 0.37$). In addition, no significant correlation was found between the mean FA value of the cingulum tract and the level of functional connectivity between the regions of the other RSNs (RSN b, figure 6.1b, $r = -0.16$, $p = 0.29$; RSN c, figure 6.1c, $r = -0.11$, $p = 0.43$; RSN d, figure 6.1d, left - right primary motor/sensory cortex, $r = 0.05$, $p=0.74$; RSN d, figure 6.1d, left - right primary visual cortex, $r = 0.16$, $p = 0.33$, RSN e, figure 6.1e, left - right inferior/superior temporal cortex $r = 0.08$, $p = 0.61$; RSN e, figure 6.1e, left inferior/superior temporal cortex - anterior cingulate gyrus, $r = 0.03$, $p = 0.85$; RSN e, figure 6.1e, right inferior/superior temporal cortex - anterior cingulate gyrus, $r = 0.17$, $p =$

0.26). No significant association was found between mean cingulum FA values and age ($r = -0.05$, $p = 0.73$) or the level of default mode functional connectivity and age ($r = 0.06$, $p = 0.68$), which is likely to result from the relative young age of the subjects that were included in this study (mean age: 24.8 years, SD: 4.8).

discussion

The main finding of this study is that the microstructural organization (fractional anisotropy) of the interconnecting cingulum tract was found to be directly associated with the level of functional connectivity of the default mode network. We combined resting-state functional MRI and structural DTI in a group of 45 subjects on a 3 Tesla MR scanner. The cingulum tract was confirmed to interconnect the precuneus / posterior cingulate cortex (PCC) and medial frontal cortex (MFC) of the default mode network in all subjects (figure 6.3). Furthermore, the mean FA value of the cingulum tract was positively correlated with the level of unique correlation between the resting-state fMRI time-series of the PCC and MFC of the default mode network (figure 6.4). These results suggest a specific association between the microstructural organization of the cingulum tract and the level of default mode functional connectivity. Our findings suggest an important role of the cingulum tract in the default mode network.

The observed interconnecting role of the cingulum tract in the default mode network is consistent with studies demonstrating that the cingulum tract forms a direct neuroanatomical link between the precuneus and medial frontal cortex (Wakana et al., 2004; Schmahmann et al., 2007; Lawes et al., 2008). Our results are coherent with the recent study of Greicius et al. reporting on an important role of the cingulum tract in interconnecting PCC and MFC of the default mode network (Greicius et al., 2008). This direct anatomical connection reflects a vast number of axonal connections between the PCC and MFC, responsible for the facilitation of neuronal communication between these regions. This communication is likely to be ongoing during rest as suggested by the high level of neuronal activity (Gusnard et al., 2001; Raichle et al., 2001; Damoiseaux et al., 2007; Raichle and Snyder, 2007) and the observed high level of resting-state synchronization between the PCC and MFC (Greicius et al., 2003; Damoiseaux et al., 2007). Furthermore, our results show that the temporal coherency between the activation patterns of the PCC and MFC regions is specifically related to the microstructural organization (i.e. FA value) of the cingulum. It is believed that the major contribution to the directional dependent diffusion signal is due to axonal membranes hindering the

diffusion process of water molecules (Beaulieu, 2002) and increased FA values may be associated with a more dense packing of axonal fibers. In this context, it is reasonable to speculate about a positive relationship between the microstructural organization of white matter tracts, reflected by the FA value, and the level of default mode neuronal communication. A possible interpretation of our results is that a higher level of microstructural organization of the cingulum tract is associated with increased communication between PCC and MFC of the default mode network during rest.

Supporting evidence for our findings comes from studies reporting on decreased default mode functional connectivity in combination with studies reporting on degenerative brain abnormalities in the cingulum bundle. Alzheimer patients show a decreased level of functional connectivity within the default mode network (Greicius et al., 2004; Rombouts et al., 2005) as well as reduced FA values in the cingulum tract (Xie et al., 2005; Zhang et al., 2007). In addition, normal aging has been associated with decreased resting-state activation within the default mode network (Andrews-Hanna et al., 2007; Damoiseaux et al., 2007) and with lower FA values of the cingulum (Schneiderman et al., 2007; Yoon et al., 2007; Makris et al., 2007). Furthermore, decreased default mode functional connectivity (Friston, 1999; Liang et al., 2006; Micheloyannis et al., 2006; Salvador et al., 2007; Williamson, 2007; Liu et al., 2008; Bluhm et al., 2007) and reduced microstructural organization of the cingulum tract (Sun et al., 2003; Nestor et al., 2007) have been suggested to play an important role in schizophrenia.

The results of this study can be interpreted as supporting evidence for a general association between structural and functional connectivity in the human brain (Koch et al. 2002; Toosy et al., 2004; Greicius et al., 2008). A number of recent studies have suggested a direct link between white matter organization and fMRI BOLD activation patterns. FA values of splenial fibers have been associated with BOLD activation in the primary visual regions (Toosy et al., 2004) and inter-hemispheric synchronization in the developing brain (Fornari et al., 2007). Furthermore, complete section of the corpos callosum has been reported to result in loss of interhemispheric resting-state functional connectivity (Johnston et al., 2008).

What does it mean when subjects show a higher level of resting-state default mode neuronal activation and synchronization? The results of our study cannot be used to draw conclusions about the functional relevance of the default mode network. However, other studies have suggested that increased recruitment of the default mode network is related to the tendency of a person's mind to wander (Mason et al., 2007) and it may be linked to the integration of cognitive and emotional processing (Greicius et al., 2003) and

relating oneself to the outside world (Gusnard et al., 2001). These processes are likely to be ongoing during rest and to involve the integration of multiple cognitive functions. Structural pathways interconnecting the regions of default mode network may facilitate this kind of functional integration. It is of interest to further examine the observed structural-functional relationship and its effect on cognitive and emotional processes that are related to default mode activation (Andrews-Hanna et al., 2007).

The level of overall default mode functional connectivity was significantly non-zero over the group of 45 subjects (Salvador et al., 2005; Greicius et al., 2003; Beckmann et al., 2005; De Luca et al., 2006; Damoiseaux et al., 2007; Van den Heuvel et al., 2008). Interestingly, the *unique* level of default mode functional connectivity between the PCC and MFC (i.e. controlling for the third-party influences of the two superior parietal cortex (SPC) regions) was found to be negative in 10 of the 45 subjects, with 2 subjects showing a partial correlation lower than -0.2 (figure 6.4). Negative levels of default mode connectivity have been related to advanced aging (Andrews-Hanna et al., 2007). However, such an effect could not be concluded from our results. The 10 subjects who showed a negative level of connectivity were not significantly older than the 35 subjects who showed a positive level of default mode connectivity. This is likely to result from the relatively young age of the included group of subjects (mean age 24.8 years). Most other resting-state studies have reported only positive levels of default mode connectivity in young adults (Greicius et al., 2003). However, these studies have mainly focused on the level of *overall* default mode connectivity, defined as a *straight* correlation between the resting-state time-series of the PCC and MFC. In this study, we focused on the level of *unique* default mode connectivity between the PCC and MFC (by factoring out the contribution of the two SPC regions), as these are the two regions of the default mode network that are specifically connected by the cingulum. Indeed, supporting the results of previous resting-state studies, the level of overall default mode connectivity was found to be positive in all 45 subjects (mean: 0.51). Future studies are needed to examine the meaning of these specific negative synchronization patterns and how they relate to cognitive processes that involve default mode network activity. In this study, negative synchronization patterns between the PCC and MFC were interpreted as lower levels of default mode functional connectivity.

Some limitations of this study have to be taken into account when interpreting its results. The PCC and MFC regions are the most often reported regions of the default mode network. Therefore, the focus of this study was on the tracts that interconnected these two regions of the default mode network. As mentioned, bilateral parietal and temporal cortices have

also been found to participate in the default mode network (Raichle et al., 2001; Greicius et al., 2003; Fox et al., 2005; Damoiseaux et al., 2006) (figure 6.3). However, tracts connecting these regions are likely to cross other white matter pathways, making the reconstruction of these tracts more difficult. Future studies are aimed to examine these tracts using other methods of representing the diffusion signal in combination with other tractography algorithms. Furthermore, the level of functional connectivity is expressed as a (partial) correlation between the rest-recorded BOLD time-series, believed to result from synchronization of neuronal activation (Biswal et al., 1997; Cordes et al., 2001; Greicius et al., 2003; Salvador et al., 2005; Buckner and Vincent, 2007). However, it has been suggested that physiological temporal patterns, including respiratory and cardiac oscillations could confound the BOLD signal (Wise et al., 2004), making the resting-state correlations less specific. We used a high temporal fMRI acquisition sequence to minimize these effects (Cordes et al., 2001).

In this study, we found a significant role for the cingulum tract in the default mode network in interconnecting the precuneus / posterior cingulate cortex and medial frontal cortex, key regions of the default mode network. Higher fractional anisotropy values of the cingulum were found to be associated with increased default mode functional connectivity, suggesting a direct association between the microstructural organization of the cingulum tract and the level of neuronal synchronization between key regions of the default mode network. Our results suggest an important role for the cingulum tract in default mode functional connectivity.

references

Achard S, Salvador R, Whitcher B, Suckling J, Bullmore E (2006) A resilient, low-frequency, small-world human brain functional network with highly connected association cortical hubs. J Neurosci 26:63-72.

Andersson JL, Skare S (2002) A model-based method for retrospective correction of geometric distortions in diffusion-weighted EPI. Neuroimage 16:177-199.

Andersson JL, Skare S, Ashburner J (2003) How to correct susceptibility distortions in spin-echo echo-planar images: application to diffusion tensor imaging. Neuroimage 20:870-888.

Andrews-Hanna JR, Snyder AZ, Vincent JL, Lustig C, Head D, Raichle ME, Buckner RL (2007) Disruption of large-scale brain systems in advanced aging. Neuron 56:924-935.

Beaulieu C (2002) The basis of anisotropic water diffusion in the nervous system - a technical review. NMR Biomed 15:435-455.

Beckmann CF, DeLuca M, Devlin JT, Smith SM (2005) Investigations into resting-state connectivity using independent component analysis. Philos Trans R Soc Lond B Biol Sci 360:1001-1013.

Biswal B, Yetkin FZ, Haughton VM, Hyde JS (1995) Functional connectivity in the motor cortex of resting human brain using echo-planar MRI. Magn Reson Med 34:537-541.

Biswal BB, Van Kylen J, Hyde JS (1997) Simultaneous assessment of flow and BOLD signals in resting-state functional connectivity maps. NMR Biomed 10:165-170.

Bluhm RL, Miller J, Lanius RA, Osuch EA, Boksman K, Neufeld R, Theberge J, Schaefer B, Williamson P (2007) Spontaneous Low-Frequency Fluctuations in the BOLD Signal in Schizophrenic Patients: Anomalies in the Default Network. Schizophr Bull 33:1004-1012.

Buckner RL, Vincent JL (2007) Unrest at rest: Default activity and spontaneous network correlations. Neuroimage 37:1091-1096.

Chang LC, Jones DK, Pierpaoli C (2005) RESTORE: robust estimation of tensors by outlier rejection. Magn Reson Med 53:1088-1095.

Collins DL, Neelin P, Peters TM, Evans AC (1994) Automatic 3D intersubject registration of MR volumetric data in standardized Talairach space. J Comput Assist Tomogr 18:192-205.

Corbetta M, Kincade JM, Ollinger JM, McAvoy MP, Shulman GL (2000) Voluntary orienting is dissociated from target detection in human posterior parietal cortex. Nat Neurosci 3:292-297.

Cordes D, Haughton VM, Arfanakis K, Carew JD, Turski PA, Moritz CH, Quigley MA, Meyerand ME (2001) Frequencies contributing to functional connectivity in the cerebral cortex in "resting-state" data. AJNR Am J Neuroradiol 22:1326-1333.

Damoiseaux JS, Rombouts SA, Barkhof F, Scheltens P, Stam CJ, Smith SM, Beckmann CF (2006) Consistent resting-state networks across healthy subjects. Proc Natl Acad Sci U S A 103:13848-13853.

Damoiseaux JS, Beckmann CF, Arigita EJ, Barkhof F, Scheltens P, Stam CJ, Smith SM, Rombouts SA (2007) Reduced resting-state brain activity in the "default network" in normal aging. Cereb Cortex.

De Luca M, Beckmann CF, De Stefano N, Matthews PM, Smith SM (2006) fMRI resting state networks define distinct modes of long-distance interactions in the human brain. Neuroimage 29:1359-1367.

Fornari E, Knyazeva MG, Meuli R, Maeder P (2007) Myelination shapes functional activity in the developing brain. Neuroimage 38:511-518.

Fox MD, Raichle ME (2007) Spontaneous fluctuations in brain activity observed with functional magnetic resonance imaging. Nat Rev Neurosci 8:700-711.

Fox MD, Snyder AZ, Vincent JL, Corbetta M, Van Essen DC, Raichle ME (2005) The human brain is intrinsically organized into dynamic, anticorrelated functional networks. Proc Natl Acad Sci U S A 102:9673-9678.

Friston KJ (1999) Schizophrenia and the disconnection hypothesis. Acta Psychiatr Scand Suppl 395:68-79.

Golay X, Pruessmann KP, Weiger M, Crelier GR, Folkers PJ, Kollias SS, Boesiger P (2000) PRESTO-SENSE: an ultrafast whole-brain fMRI technique. Magn Reson Med 43:779-786.

Greicius MD, Krasnow B, Reiss AL, Menon V (2003) Functional connectivity in the resting brain: a network analysis of the default mode hypothesis. Proc Natl Acad Sci U S A 100:253-258.

Greicius MD, Srivastava G, Reiss AL, Menon V (2004) Default-mode network activity distinguishes Alzheimer's disease from healthy aging: evidence from functional MRI. Proc Natl Acad Sci U S A 101:4637-4642.

Greicius MD, Supekar K, Menon V, Dougherty RF (2008) Resting-State Functional Connectivity Reflects Structural Connectivity in the Default Mode Network. Cereb Cortex.

Gusnard DA, Raichle ME, Raichle ME (2001) Searching for a baseline: functional imaging and the resting human brain. Nat Rev Neurosci 2:685-694.

Johnston JM, Vaishnavi SN, Smyth MD, Zhang D, He BJ, Zempel JM, Shimony JS, Snyder AZ, Raichle ME (2008) Loss of resting interhemispheric functional connectivity after complete section of the corpus callosum. J Neurosci 28:6453-6458.

Jones DK (2004) The effect of gradient sampling schemes on measures derived from diffusion tensor MRI: a Monte Carlo study. Magn Reson Med 51:807-815.

Jones DK, Horsfield MA, Simmons A (1999) Optimal strategies for measuring diffusion in anisotropic systems by magnetic resonance imaging. Magn Reson Med 42:515-525.

Kim JH, Loy DN, Liang HF, Trinkaus K, Schmidt RE, Song SK (2007) Noninvasive diffusion tensor imaging of evolving white matter pathology in a mouse model of acute spinal cord injury. Magn Reson Med 58:253-260.

Koch MA, Norris DG, Hund-Georgiadis M (2002) An investigation of functional and anatomical connectivity using magnetic resonance imaging. Neuroimage 16:241-250.

Lawes IN, Barrick TR, Murugam V, Spierings N, Evans DR, Song M, Clark CA (2008) Atlas-based segmentation of white matter tracts of the

human brain using diffusion tensor tractography and comparison with classical dissection. Neuroimage 39:62-79.
Liang M, Zhou Y, Jiang T, Liu Z, Tian L, Liu H, Hao Y (2006) Widespread functional disconnectivity in schizophrenia with resting-state functional magnetic resonance imaging. Neuroreport 17:209-213.
Liu Y, Liang M, Zhou Y, He Y, Hao Y, Song M, Yu C, Liu H, Liu Z, Jiang T (2008) Disrupted small-world networks in schizophrenia. Brain 131:945.
Makris N, Papadimitriou GM, van der Kouwe A, Kennedy DN, Hodge SM, Dale AM, Benner T, Wald LL, Wu O, Tuch DS, Caviness VS, Moore TL, Killiany RJ, Moss MB, Rosene DL (2007) Frontal connections and cognitive changes in normal aging rhesus monkeys: a DTI study. Neurobiol Aging 28:1556-1567.
Mason MF, Norton MI, Van Horn JD, Wegner DM, Grafton ST, Macrae CN (2007) Wandering minds: the default network and stimulus-independent thought. Science 315:393-395.
Micheloyannis S, Pachou E, Stam CJ, Breakspear M, Bitsios P, Vourkas M, Erimaki S, Zervakis M (2006) Small-world networks and disturbed functional connectivity in schizophrenia. Schizophr Res 87:60-66.
Mori S, van Zijl PC (2002) Fiber tracking: principles and strategies - a technical review. NMR Biomed 15:468-480.
Mori S, Crain BJ, Chacko VP, van Zijl PC (1999) Three-dimensional tracking of axonal projections in the brain by magnetic resonance imaging. Ann Neurol 45:265-269.
Neggers SF, Hermans EJ, Ramsey NF (2008) Enhanced sensitivity with fast three-dimensional blood-oxygen-level-dependent functional MRI: comparison of SENSE-PRESTO and 2D-EPI at 3 T. NMR Biomed:In Press.
Nestor PG, Kubicki M, Spencer KM, Niznikiewicz M, McCarley RW, Shenton ME (2007) Attentional networks and cingulum bundle in chronic schizophrenia. Schizophr Res 90:308-315.
Northoff G, Bermpohl F (2004) Cortical midline structures and the self. Trends Cogn Sci 8:102-107.
Northoff G, Heinzel A, de Greck M, Bermpohl F, Dobrowolny H, Panksepp J (2006) Self-referential processing in our brain--a meta-analysis of imaging studies on the self. Neuroimage 31:440-457.
Raichle ME, Snyder AZ (2007) A default mode of brain function: A brief history of an evolving idea. Neuroimage 37:1083-1090.
Raichle ME, MacLeod AM, Snyder AZ, Powers WJ, Gusnard DA, Shulman GL (2001) A default mode of brain function. Proc Natl Acad Sci U S A 98:676-682.

Rombouts SA, Barkhof F, Goekoop R, Stam CJ, Scheltens P (2005) Altered resting state networks in mild cognitive impairment and mild Alzheimer's disease: an fMRI study. Hum Brain Mapp 26:231-239.

Salvador R, Suckling J, Coleman MR, Pickard JD, Menon D, Bullmore E (2005) Neurophysiological architecture of functional magnetic resonance images of human brain. Cereb Cortex 15:1332-1342.

Salvador R, Martinez A, Pomarol-Clotet E, Sarro S, Suckling J, Bullmore E (2007) Frequency based mutual information measures between clusters of brain regions in functional magnetic resonance imaging. Neuroimage 35:83-88.

Schmahmann JD, Pandya DN, Wang R, Dai G, D'Arceuil HE, de Crespigny AJ, Wedeen VJ (2007) Association fibre pathways of the brain: parallel observations from diffusion spectrum imaging and autoradiography. Brain 130:630-653.

Schmitz TW, Johnson SC (2007) Relevance to self: A brief review and framework of neural systems underlying appraisal. Neurosci Biobehav Rev 31:585-596.

Schneiderman JS, Buchsbaum MS, Haznedar MM, Hazlett EA, Brickman AM, Shihabuddin L, Brand JG, Torosjan Y, Newmark RE, Tang C, Aronowitz J, Paul-Odouard R, Byne W, Hof PR (2007) Diffusion tensor anisotropy in adolescents and adults. Neuropsychobiology 55:96-111.

Stam CJ (2004) Functional connectivity patterns of human magnetoencephalographic recordings: a 'small-world' network? Neurosci Lett 355:25-28.

Sun FT, Miller LM, D'Esposito M (2004) Measuring interregional functional connectivity using coherence and partial coherence analyses of fMRI data. Neuroimage 21:647-658.

Sun Z, Wang F, Cui L, Breeze J, Du X, Wang X, Cong Z, Zhang H, Li B, Hong N, Zhang D (2003) Abnormal anterior cingulum in patients with schizophrenia: a diffusion tensor imaging study. Neuroreport 14:1833-1836.

Toosy AT, Ciccarelli O, Parker GJ, Wheeler-Kingshott CA, Miller DH, Thompson AJ (2004) Characterizing function-structure relationships in the human visual system with functional MRI and diffusion tensor imaging. Neuroimage 21:1452-1463.

Van den Heuvel MP, Mandl RC, Hulshoff Pol HE (2008) Normalized group clustering of resting-state fMRI data. PLoS ONE 3:e2001

Wakana S, Jiang H, Nagae-Poetscher LM, van Zijl PC, Mori S (2004) Fiber tract-based atlas of human white matter anatomy. Radiology 230:77-87.

Williamson P (2007) Are Anticorrelated Networks in the Brain Relevant to Schizophrenia? Schizophr Bull 33:994-1003.

Wise RG, Ide K, Poulin MJ, Tracey I (2004) Resting fluctuations in arterial carbon dioxide induce significant low frequency variations in BOLD signal. Neuroimage 21:1652-1664.

Xie S, Xiao JX, Wang YH, Wu HK, Gong GL, Jiang XX (2005) Evaluation of bilateral cingulum with tractography in patients with Alzheimer's disease. Neuroreport 16:1275-1278.

Yoon B, Shim YS, Lee KS, Shon YM, Yang DW (2007) Region-specific changes of cerebral white matter during normal aging: A diffusion-tensor analysis. Arch Gerontol Geriatr.

Zhang Y, Schuff N, Jahng GH, Bayne W, Mori S, Schad L, Mueller S, Du AT, Kramer JH, Yaffe K, Chui H, Jagust WJ, Miller BL, Weiner MW (2007) Diffusion tensor imaging of cingulum fibers in mild cognitive impairment and Alzheimer disease. Neurology 68:13-19.

chapter 7

efficiency of functional brain networks and intellectual performance

martijn van den heuvel, cornelis stam, rené kahn, hilleke hulshoff pol

journal of neuroscience 2009 29 (23)

Our brain is a complex network in which information is continuously processed and transported between spatially distributed but functionally linked regions. These ongoing neuronal processes enable us to respond quickly and flexibly to the complex situations that we encounter in daily life. Recent studies have shown that the functional connections of the brain network are organized in a highly efficient *small-world* manner, indicating a high level of local neighborhood clustering, together with the existence of more long-distance connections that ensure a high level global communication efficiency within the overall network. Such an efficient network architecture of our functional brain raises the question about a possible association between how efficient the regions of our brain are functionally connected and our level of intelligence. Examining the overall organization of the brain network using graph analysis, we show a strong negative association between the normalized characteristic path length *lambda* of the resting-state brain network (expressing the level of global communication efficiency) and IQ. This suggests that intelligence is likely to be related to how efficiently our brain integrates information between multiple brain regions. Most pronounced effects between *normalized path length* and IQ were found in frontal and parietal regions. This suggests that intelligence is likely to be related to how efficient these frontal and parietal regions are able to integrate the information between the different functional regions of the brain. Our findings suggest that smarter brains have a more direct and therefore more efficient access to information across the brain network.

introduction

Our brain is a complex network of interconnected regions (Sporns et al., 2004; Achard et al., 2006; Fox and Raichle, 2007; Stam and Reijneveld, 2007; Hagmann et al., 2008; Van den Heuvel et al., 2008c; Buckner et al., 2009; Honey et al., 2009; Van den Heuvel et al., 2009). Within this brain network, information is constantly processed and integrated between specialized, spatially distributed but functionally linked brain regions with coherent temporal dynamics (Sporns et al., 2000). This integration of information is a never ending process that goes on even when we are at rest (Biswal et al., 1995; Gusnard et al., 2001; Raichle et al., 2001; Greicius et al., 2003; Damoiseaux et al., 2006; Fox and Raichle, 2007; Van den Heuvel et al., 2008a). This ongoing integration of information enables us to evaluate the world around us and to respond quickly and flexibly to complex situations. Interestingly, recent studies have shown that the functional connections of the brain network are organized in a highly efficient *small-world* fashion (Sporns et al., 2004; Stam, 2004; Eguiluz et al., 2005; Achard et al., 2006; Van den Heuvel et al., 2008b). A s*mall-world* organization of the brain network suggests a high level of local neighborhood clustering, responsible for efficient *local* information processing, together with the existence of several long-distance connections that ensure a high level of *global* communication efficiency across the network and integration of information between the different regions of the brain (Watts and Strogatz, 1998; Latora and Marchiori, 2001; Stam and Reijneveld, 2007; Bullmore and Sporns, 2009). Such an efficient organization of our brain network raises the question about a possible relationship between the level of how efficiently the functional connections of our brain are placed and individual differences in intelligence. Neuroimaging studies have linked intelligence to the developmental course of specific high order brain regions (Shaw et al., 2006), total brain volume (Posthuma et al., 2002), focal brain structure (Thompson et al., 2001; Haier et al., 2004; Colom et al., 2006; Hulshoff Pol et al., 2006; Colom et al., 2007; Choi et al., 2008), microstructural organization of white matter (Chiang et al., 2009) and the functional dynamics of specific high cognitive brain regions (Duncan et al., 2000; Gray et al., 2003; Choi et al., 2008; Song et al., 2008). However, it remains unknown how intelligence is related to the overall connectivity network architecture of our brain. The aim of this study was to examine how human intelligence is related to the overall organization of the functional brain network.

Gender (Male/Female)	14/5
Age, years (mean ± SD)	29 ± 7.8
Full Scale IQ	121 ± 11.9
Verbal IQ	121 ± 9.5
Verbal Comprehension Index	119 ± 9.5
Working Memory Index	117 ± 11.9
Performance IQ	117 ± 12.6
Perceptual Organization Index	115 ± 11.2
Processing Speed Index	112 ± 15.1

table 7.1 demographic and IQ data Age and IQ scores are displayed as mean ± SD.

	FIQ	VIQ	PIQ	VCI	WMI	POI
VIQ	0.91					
PIQ	0.91	0.66				
VCI	0.75	0.88	0.52			
WMI	0.72	0.67	0.61	0.36		
POI	0.78	0.57	0.84	0.53	0.51	
PSI	0.63	0.53	0.65	0.41	0.39	0.40

table 7.2 correlations between IQ (sub-)scores FIQ = Full scale Intelligence Quotient (IQ), VIQ = Verbal IQ, PIQ = Performance IQ, VCI = Verbal Comprehension Index, WMI = Working Memory Index, POI = Perceptual Organization Index, PSI = Processing Speed Index.

materials and methods

subjects

19 healthy subjects without a psychiatric history (age mean/std : 29/7.8 ; gender: 14 male, 5 female, table 7.1) participated in this study after providing written informed consent as approved by the medical ethics committee for research in humans (METC) of the University Medical Center Utrecht, The Netherlands.

intelligence scores

The Intelligence Quotient of the participants was measured with the Dutch version of the Wechsler Adult Intelligence Scale III (WAIS-III) test. The WAIS test gives a standardized Full scale Intelligence Quotient, in this paper referred to as IQ, based on a number of subtests that assess the level of verbal (Verbal IQ, VIQ) and non-verbal knowledge and reasoning

(Performance IQ, PIQ) of the participants. Table 7.1 describes the IQ data and table 7.2 describes the correlations between the IQ scores.

data acquisition

The functional connections of the brain network were examined by measuring the correlations between the spontaneous brain signals of the different regions of the brain during rest (Aertsen et al., 1989; Friston et al., 1993; Biswal et al., 1995; Salvador et al., 2005; Achard et al., 2006; Damoiseaux et al., 2006). Resting-state fMRI time-series of each participant was acquired for a period of 8 minutes on a 3 Tesla Magnetic Resonance Imaging scanner (3D PRESTO, acquisition parameters: TR/TE 22ms/32ms using shifted echo, flipangle of 9 degrees; SENSE p/s reduction 2/2; a dynamic scantime of 0.5 sec, 1000 timeframes, total duration 8 minutes; FOV 256x256 mm, voxelsize 4x4x4mm, 32 slices covering whole brain (Van den Heuvel et al., 2008a) (supplemental material). During this resting-state period, the level of spontaneous brain activity of all cortical and sub-cortical brain regions (i.e. voxels) was measured.

preprocessing

Before the graph analysis, the fMRI data was preprocessed (please see supplemental material for a detailed description). In summary, resting-state fMRI time-series were realigned with the last functional scan to correct for possible small head movements and co-registered with the T1 image, for anatomical overlap. Next, the T1 and realigned resting-state time-series were normalized to standard space, using the normalization parameters of the T1 image. Finally, the resting-state time-series were band-pass filtered (0.01 - 0.1 Hz).

graph analysis

The organization of the functional brain network was examined using graph theory (Achard et al., 2006; Stam and Reijneveld, 2007; Bullmore and Sporns, 2009), as validated earlier (Van den Heuvel et al., 2008b). Please see supplemental material for a detailed description of the performed graph analysis. In summary, from each of the individual filtered resting-state fMRI BOLD time-series an individual functional brain network was formed out of all the cortical and sub-cortical brain voxels (~9500 voxels, called nodes) with connections between all functionally linked voxels. The level of functional connectivity between any two voxels *i* and *j* was defined as the zero-lag correlation between their voxel-wise resting-state BOLD time-series and voxel *i* and *j* were defined as functionally linked when their zero-lag

correlation reached above a threshold *T* (ranging from 0.05 to 0.5) (Biswal et al., 1995; Achard et al., 2006; Van den Heuvel et al., 2008a; Van den Heuvel et al., 2008b). Computing the level of functional connectivity between all voxel pairs and thresholding these connectivity values resulted in the formation of an interconnected functional connectivity graph for each individual dataset, representing the functional brain network (supplemental figure 7.1). From these functional brain networks a number of key characteristics that describe the overall organization of a network were computed, including the *clustering-coefficient C* and *characteristic path length L* (Watts and Strogatz, 1998). The clustering-coefficient *C* is given by the ratio between the number of connections between the direct neighbors of a node and the total number of possible connections between these neighbors and provides information about the level of local connectedness within a network. In addition, the characteristic path length *L* of a network gives the average number of connections that have to be crossed to travel from each node to every other node in the network and provides information about the level of global communication efficiency of a network.

Networks with a so-called *small-world* organization have a clustering-coefficient *C* that is much higher than the clustering-coefficient of a comparable random organized network, but still with a short characteristic path length *L* that is similar to that of an equivalent random organized network (Watts and Strogatz, 1998). Formally, *small-world* networks show a ratio *gamma* defined as C / C^{random} of >>1 and a ratio *lambda* defined as L / L^{random} of ~1 (Watts and Strogatz, 1998; Stam and Reijneveld, 2007), with C^{random} and L^{random} the clustering-coefficient and characteristic path length of a random organized network of similar size (Watts and Strogatz, 1998; Sporns et al., 2004). Together, *gamma* and *lambda* provide important information about the level of *local* and *global* connectivity *efficiency* of a network. A high *gamma* reflects a high level of *local* neighborhood clustering within a network and a short normalized travel distance *lambda* expresses a high level of *global* communication efficiency within a network (Watts and Strogatz, 1998; Sporns et al., 2004; Bullmore and Sporns, 2009).

association between network organization and intelligence

To examine the relationship between the organization of the brain network and intelligence, the computed *lambda* and *gamma* values of the individual brain networks were correlated with the measured full scale IQ scores of the participants. In addition, to examine whether intelligence is related to the overall number of connections of the brain network, also the total number of connections *k* was correlated with the individual IQ scores.

To point out which specific brain regions have the strongest association between global network organization and IQ an exploratory analysis was conducted, in which the normalized path length of each individual node (i.e. voxel) was correlated with IQ separately (supplemental material). The individual normalized path length of a node reflects how close this node is connected to the other nodes of the network, providing information about how efficient this node is connected to rest of the network. First, for each individual dataset, the normalized path length of each node was computed. Second, for all voxels separately, the normalized path length of voxel *i* was correlated with the measured IQ scores over the group of subjects. This resulted in a correlation-coefficient map indicating which voxels showed a significant association between the full scale IQ scores and *normalized path length*. An exploratory threshold of 0.05 (uncorrected for multiple comparisons) was used to mark brain regions that showed a significant association between their *normalized path length* and IQ.

results

The functional brain networks showed a clear small-world organization for $0.3 \leqq T \leqq 0.5$ (figure 7.1a-d), expressed by $L \sim L^{random}$ and *lambda* ~ 1 for $T \leq 0.5$ and $C >> C^{random}$ and *gamma* >>1 for $T \geqq 0.3$ [one-sample t-test, all $p < \alpha$ of 0.01, Bonferroni corrected for multiple comparisons of *T*, df = 18], indicating a small-world organization (Sporns et al., 2004; Stam, 2004; Achard et al., 2006; Van den Heuvel et al., 2008b).

Next, the association between brain network organization and individual variation in intelligence was examined by correlating the full scale IQ scores with the *lambda* and *gamma* values of the individual brain networks within the clear small-world range of $0.3 \leq T \leq 0.5$. For higher *T*, a significant negative association was found between the normalized characteristic path length *lambda* and IQ [linear regression, $T = 0.45$, $r = -0.54$, $p = 0.010$, df = 18 (figure 7.2a); $T = 0.5$, $r = -0.57$, $p = 0.017$, df = 18 (figure 7.2b), which is significant considering an α of 0.05 after Bonferroni correction for multiple comparisons of *T*; regressions corrected for age] (figure 7.2 a-b, supplemental figure 7.3 a-c). It is important to note that the observed association between *lambda* and IQ could not be related to possible variation in overall connectivity, as the IQ scores showed no correlation with the total number of connections *k* of the brain network (supplemental figure 7.3 g-i). or the distribution of *k*. No significant correlation was found between the clustering-coefficient *gamma* and IQ (figure 7.2 c-d).

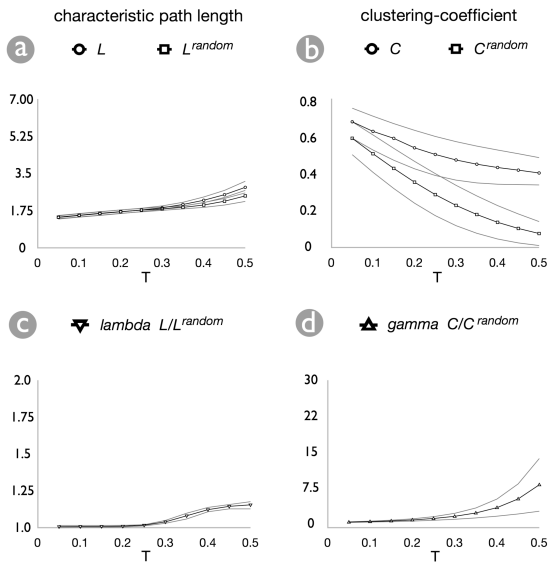

figure 7.1 group averaged characteristic path length and clustering-coefficient Panel a and b show the results of the characteristic path length L and L^{random} (***panel a***) and the results of clustering-coefficient C and matching C^{random} (***panel b***) for cut-off thresholds $0.05 \leqq T \leqq 0.5$. The clustering-coefficient C reflects the level of local neighborhood clustering and the normalized path length L reflects the average travel distance between all nodes of the network. L^{random} and C^{random} reflect the characteristic path length and clustering-coefficient of a comparable random network. L was found to be around the same as L^{random} for $T \leqq 0.5$ and C was found to be $> C^{random}$ for $T \geqq 0.3$ [two-sample t-test, df = 36, all $p < \alpha$ of 0.01, Bonferroni corrected for multiple comparisons of T]. ***Panel c*** and ***d*** show matching lambda (L/L^{random}) and gamma (C/C^{random}) values for all T. The functional brain networks showed a clear small-world organization, expressed by *lambda* ~1 (panel c) and *gamma* >>1 (panel d) for $T \geqq 0.3$ [one-sample t-test, df = 18, all $p < \alpha$ of 0.01, Bonferroni corrected for multiple comparisons of T].

To further probe which specific brain regions have the strongest association between global network organization and IQ, the normalized path length of each individual node (i.e. voxel) was correlated with the full scale IQ scores separately. Figure 7.3 shows the correlation coefficients of those voxels that showed a significant correlation between their normalized path length and IQ [linear regression, df = 18, $p < 0.05$ uncorrected for multiple comparisons, corrected for age]. The most prominent effects between full scale IQ and normalized path length were found in *medial prefrontal gyrus* [Brodmann Area 9/10, r = -0.75, p = 0.001, df = 18, yellow box], *precuneus/posterior cingulate gyrus* [BA 7, r = -0.55, p = 0.014, df = 18, orange box] and bilateral *inferior parietal regions* [BA 39/40, r = -0.72, p =

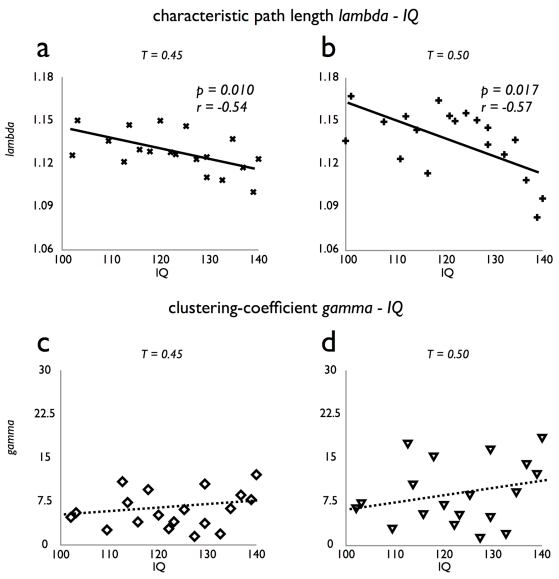

figure 7.2 For networks within the small-world range (T = 0.45, T = 0.50), the normalized characteristic path length *lambda* was found to be negatively correlated with IQ, as shown in ***panel a*** and ***b*** [linear regression, df = 18; T = 0.45, r = -0.54, p = 0.010 (panel a); T = 0.5, r = -0.57, p = 0.017 (panel b), significant for a α of 0.05, Bonferroni corrected for multiple comparisons of T]. IQ was found not to be significantly associated with the normalized clustering-coefficient gamma (***panel c*** and ***d*** for T = 0.45 and T = 0.5 respectively). All associations were corrected for possible age effects, by factoring out age out of *lambda* and *gamma*, before assessing the correlation between IQ and lambda, gamma. The strong negative association between *lambda* and IQ suggests a strong positive association between the level of global communication efficiency within the brain network and intelligence.

0.001, df = 18, red box]. Also regions overlapping left *superior temporal* [BA 22/40, r= -0.69, p = 0.014, df = 18] and left inferior frontal [BA 44/45, r = -0.68, p = 0.012, df = 18] showed a significant negative correlation between normalized path length and full scale IQ.

discussion

The main finding of this study is the existence of a strong association between the level of global communication efficiency of the functional brain network and intellectual performance. Examining the overall network architecture of functional brain networks, we showed that the normalized characteristic path length *lambda* was strongly negatively associated with full scale IQ (figure 7.2 a-b). The characteristic path length *lambda* indicates how close all the nodes of the networks are connected to each other globally and

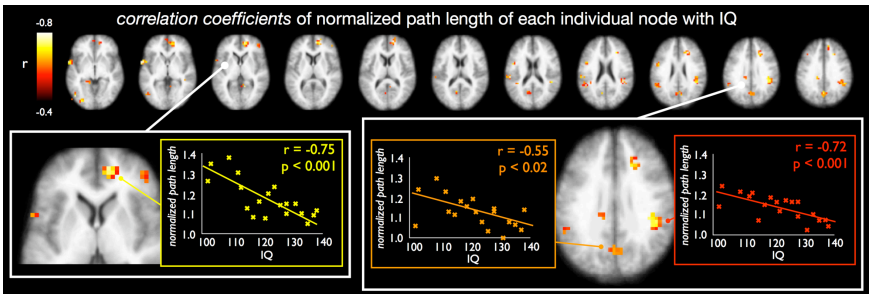

figure 7.3 Most prominent effects between IQ and the level of global connectivity efficiency (as expressed by a shorter node specific normalized path length) were found to be located in medial prefrontal cortex (yellow box), bilateral inferior parietal cortex (red box) and precuneus / posterior cingulate regions (orange box) of the functional brain network. Shown are correlation coefficient values of those voxels that had a significant negative association between IQ and normalized path length for T = 0.45 [linear regression, $p < 0.05$ uncorrected for multiple comparisons, df = 18, corrected for age].

a shorter *lambda* reflects a higher level of overall communication efficiency between the regions of the network. As such, our findings indicate a strong positive association between the level of global communication efficiency within the brain network and intelligence. In other words, more efficiently functionally connected brains show a higher level of intelligence.

The normalized clustering-coefficient *gamma* was found not to be significantly associated with IQ, suggesting that intelligence is not directly related to the level of local information processing. Moreover, the total number of connections *k* of the network was not associated with IQ, suggesting that intelligence is also not directly related to the total number of functional connections of our brain. The strong association between overall normalized characteristic path length *lambda* and IQ suggests that human intelligence is more related to how *efficient* the global connections of our brain are organized and how efficient information can be integrated globally between the different regions of the brain network.

The strongest associations between full scale IQ and individual normalized path length were found in *medial prefrontal gyrus, precuneus/ posterior cingulate gyrus* and bilateral *inferior parietal* regions (figure 7.3). Recently, these regions have been reported to form functional hubs within the cortical brain network (Buckner et al., 2009). This is important, as efficient hub nodes are more likely to have a stronger effect on global network efficiency than less connected peripheral nodes. The structural

dynamics of these brain regions have been previously linked to intelligence (Haier et al., 2004; Hulshoff Pol et al., 2006; Shaw et al., 2006) (Colom et al., 2007; Jung and Haier, 2007). Interestingly, these frontal and parietal regions overlap the often reported *default mode network* (Raichle et al., 2001; Greicius et al., 2003; Damoiseaux et al., 2006; Buckner et al., 2008; Van den Heuvel et al., 2008c; Van den Heuvel et al., 2009), a dynamic resting-state network which is suggested to play a key role in processes of human cognition, like the integration of cognitive and emotional processes (Greicius et al., 2003), monitoring the world around us (Gusnard et al., 2001) and mind-wandering (Mason et al., 2007). In addition, strong associations between normalized path length and full scale IQ were found in left *superior temporal* and *inferior frontal gyrus*, regions that are known to play a key role in language processing (figure 7.3).

To further examine the association between lambda and IQ, a post-hoc analysis was performed in which we examined the association between normalized characteristic path length lambda and the sub-scales of the WAIS test, including Verbal (VIQ) and Performance IQ (PIQ) and Verbal Comprehension (VCI), Working Memory (WMI), Perceptual Organization (POI) and Processing Speed (PSI) indices (table 7.1 and table 7.2). Lambda was found to be mostly related to PIQ and POI sub-scores [linear regression, PIQ: $r = -0.63$, $p = 0.004$, $df = 18$, POI: $r = -0.50$, $p = 0.029$, $df = 18$] (supplemental figure 7.4). Furthermore, a second exploratory post-hoc analysis was performed, examining the association between normalized path length of each individual node and IQ sub-scores. As expected, strongest regional effects between IQ sub-scales and normalized path length were found for POI and PIQ scores [linear regression, $r < -0.4$, $p < 0.05$ uncorrected, $df = 18$] (supplemental figure 7.5).

Interestingly, graph analysis of large-scale anatomical networks of the primate cerebral cortex has shown before that long-range pathways play a crucial role for maintaining short processing paths across the network (Kaiser and Hilgetag, 2006). Short path length promotes high computational efficiency and is thus likely to be an important factor, together with wiring minimization (Chklovskii et al., 2002; Chen et al., 2006), for shaping cortical connectivity (Kaiser and Hilgetag, 2006). Our study may add to this discussion, as our results indicate that a short path length is crucial in efficient information processing and leading towards a high IQ. This suggests that functional brain networks are optimized towards processing speed and a high level of efficient global information integration between the multiple regions and functional sub-networks of the brain network.

A recent study has also shown a direct link between the structural connectivity architecture of the brain network and intellectual performance,

reporting on a positive association between the microstructural organization of white matter and intelligence (Chiang et al., 2009). Among other white matter tracts, the white matter organization of the cingulum tract (as reflected by the level of fractional anisotropy measured with Diffusion Tensor Imaging) was found to be positively associated with IQ. Interestingly, the cingulum bundle has been suggested to play an important role in structurally interconnecting the functionally linked medial frontal cortex and precuneus regions of the default mode network (Greicius et al., 2008; Van den Heuvel et al., 2008c). Our current results, showing a negative association between the normalized path length of these regions and IQ (figure 7.3), suggest that besides the level of structural connectivity, also the level of functional communication efficiency of these regions is related to intellectual performance. Furthermore, white matter organization was found to be most prominently related to PIQ and POI sub-scales (Chiang et al., 2009). This supports our findings, showing a strong negative association between lambda and POI and PIQ sub-scores (supplemental figure 4 and 5). In addition, common genetic factors were found to mediate the association between IQ and structural connectivity (Chiang et al., 2009), indicating a genetic contribution to the brain's architecture (Posthuma et al., 2002; Hulshoff Pol et al., 2006). Recent studies have suggested a high level of heritability of both the level of local (i.e. *C*) and global (i.e. *L*) interconnectedness of the brain network as measured with electroencephalogram recordings (Smit et al., 2008). The results of our current study show a strong association between human intelligence and the level of global interconnectedness of the brain network. Therefore, future studies are needed to examine if common genes mediate the association between functional and structural brain network organization and intelligence. However, although the brain's structural and functional networks are certainly linked, their exact relationship remains unclear (Bullmore and Sporns, 2009). Indeed, the reported positive association between the white matter fractional anisotropy of the posterior thalamic radiation and intelligence (Chiang et al., 2009) was not reflected in the level of functional communication efficiency of the thalamus.

It is interesting to note that the reported correlations between network measures and IQ are with respect to resting-state functional connectivity and not to task-related connectivity. The data reflects the level of efficient organization of the functional brain network during a resting-state and not the efficiency of functional connectivity between brain regions during the performance of specific cognitive tasks that enter into the IQ score. As such, our data suggest that the efficiency of intrinsic resting-state functional connectivity patterns is predictive of cognitive performance.

We examined the existence of a relationship between the efficient organization of the brain network and human intelligence using graph analysis and 3 Tesla resting-state fMRI recordings. Our results suggest that a short path length is crucial for efficient information processing across the brain network and leading towards a high IQ. Our findings may aid to the understanding of a neural basis of intelligence, suggesting that smarter brains have a more direct and therefore more efficient access to information across the functional brain network.

references

Achard S, Salvador R, Whitcher B, Suckling J, Bullmore E (2006) A resilient, low-frequency, small-world human brain functional network with highly connected association cortical hubs. J Neurosci 26:63-72.

Aertsen AM, Gerstein GL, Habib MK, Palm G (1989) Dynamics of neuronal firing correlation: modulation of "effective connectivity". J Neurophysiol 61:900-917.

Biswal B, Yetkin FZ, Haughton VM, Hyde JS (1995) Functional connectivity in the motor cortex of resting human brain using echo-planar MRI. Magn Reson Med 34:537-541.

Buckner RL, Andrews-Hanna JR, Schacter DL (2008) The brain's default network: anatomy, function, and relevance to disease. Ann N Y Acad Sci 1124:1-38.

Buckner RL, Sepulcre J, Talukdar T, Krienen FM, Liu H, Hedden T, Andrews-Hanna JR, Sperling RA, Johnson KA (2009) Cortical hubs revealed by intrinsic functional connectivity: mapping, assessment of stability, and relation to Alzheimer's disease. J Neurosci 29:1860-1873.

Bullmore E, Sporns O (2009) Complex brain networks: graph theoretical analysis of structural and functional systems. Nat Rev Neurosci 10:186-198.

Chen BL, Hall DH, Chklovskii DB (2006) Wiring optimization can relate neuronal structure and function. Proc Natl Acad Sci U S A 103:4723-4728.

Chiang MC, Barysheva M, Shattuck DW, Lee AD, Madsen SK, Avedissian C, Klunder AD, Toga AW, McMahon KL, de Zubicaray GI, Wright MJ, Srivastava A, Balov N, Thompson PM (2009) Genetics of brain fiber architecture and intellectual performance. J Neurosci 29:2212-2224.

Chklovskii DB, Schikorski T, Stevens CF (2002) Wiring optimization in cortical circuits. Neuron 34:341-347.

Choi YY, Shamosh NA, Cho SH, DeYoung CG, Lee MJ, Lee JM, Kim SI, Cho ZH, Kim K, Gray JR, Lee KH (2008) Multiple bases of human intelligence revealed by cortical thickness and neural activation. J Neurosci 28:10323-10329.

Colom R, Jung RE, Haier RJ (2006) Distributed brain sites for the g-factor of intelligence. Neuroimage 31:1359-1365.

Colom R, Jung RE, Haier RJ (2007) General intelligence and memory span: evidence for a common neuroanatomic framework. Cogn Neuropsychol 24:867-878.

Damoiseaux JS, Rombouts SA, Barkhof F, Scheltens P, Stam CJ, Smith SM, Beckmann CF (2006) Consistent resting-state networks across healthy subjects. Proc Natl Acad Sci U S A 103:13848-13853.

Duncan J, Seitz RJ, Kolodny J, Bor D, Herzog H, Ahmed A, Newell FN, Emslie H (2000) A neural basis for general intelligence. Science 289:457-460.

Eguiluz VM, Chialvo DR, Cecchi GA, Baliki M, Apkarian AV (2005) Scale-free brain functional networks. Phys Rev Lett 94:018102.

Fox MD, Raichle ME (2007) Spontaneous fluctuations in brain activity observed with functional magnetic resonance imaging. Nat Rev Neurosci 8:700-711.

Friston KJ, Frith CD, Liddle PF, Frackowiak RS (1993) Functional connectivity: the principal-component analysis of large (PET) data sets. J Cereb Blood Flow Metab 13:5-14.

Gray JR, Chabris CF, Braver TS (2003) Neural mechanisms of general fluid intelligence. Nat Neurosci 6:316-322.

Greicius MD, Krasnow B, Reiss AL, Menon V (2003) Functional connectivity in the resting brain: a network analysis of the default mode hypothesis. Proc Natl Acad Sci U S A 100:253-258.

Greicius MD, Supekar K, Menon V, Dougherty RF (2008) Resting-State Functional Connectivity Reflects Structural Connectivity in the Default Mode Network. Cereb Cortex.

Gusnard DA, Raichle ME, Raichle ME (2001) Searching for a baseline: functional imaging and the resting human brain. Nat Rev Neurosci 2:685-694.

Hagmann P, Cammoun L, Gigandet X, Meuli R, Honey CJ, Wedeen VJ, Sporns O (2008) Mapping the Structural Core of Human Cerebral Cortex. PLoS Biol 6:e159.

Haier RJ, Jung RE, Yeo RA, Head K, Alkire MT (2004) Structural brain variation and general intelligence. Neuroimage 23:425-433.

Honey CJ, Sporns O, Cammoun L, Gigandet X, Thiran JP, Meuli R, Hagmann P (2009) Predicting human resting-state functional connectivity from structural connectivity. Proc Natl Acad Sci U S A 106:2035-2040.

Hulshoff Pol HE, Schnack HG, Posthuma D, Mandl RC, Baare WF, van Oel C, van Haren NE, Collins DL, Evans AC, Amunts K, Burgel U, Zilles K, de Geus E, Boomsma DI, Kahn RS (2006) Genetic contributions to human brain morphology and intelligence. J Neurosci 26:10235-10242.

Jung RE, Haier RJ (2007) The Parieto-Frontal Integration Theory (P-FIT) of intelligence: converging neuroimaging evidence. Behav Brain Sci 30:135-154; discussion 154-187.

Kaiser M, Hilgetag CC (2006) Nonoptimal component placement, but short processing paths, due to long-distance projections in neural systems. PLoS Comput Biol 2:e95.

Latora V, Marchiori M (2001) Efficient behavior of small-world networks. Phys Rev Lett 87:198701.

Mason MF, Norton MI, Van Horn JD, Wegner DM, Grafton ST, Macrae CN (2007) Wandering minds: the default network and stimulus-independent thought. Science 315:393-395.

Posthuma D, De Geus EJ, Baare WF, Hulshoff Pol HE, Kahn RS, Boomsma DI (2002) The association between brain volume and intelligence is of genetic origin. Nat Neurosci 5:83-84.

Raichle ME, MacLeod AM, Snyder AZ, Powers WJ, Gusnard DA, Shulman GL (2001) A default mode of brain function. Proc Natl Acad Sci U S A 98:676-682.

Salvador R, Suckling J, Coleman MR, Pickard JD, Menon D, Bullmore E (2005) Neurophysiological architecture of functional magnetic resonance images of human brain. Cereb Cortex 15:1332-1342.

Shaw P, Greenstein D, Lerch J, Clasen L, Lenroot R, Gogtay N, Evans A, Rapoport J, Giedd J (2006) Intellectual ability and cortical development in children and adolescents. Nature 440:676-679.

Smit DJ, Stam CJ, Posthuma D, Boomsma DI, de Geus EJ (2008) Heritability of "small-world" networks in the brain: a graph theoretical analysis of resting-state EEG functional connectivity. Hum Brain Mapp 29:1368-1378.

Song M, Zhou Y, Li J, Liu Y, Tian L, Yu C, Jiang T (2008) Brain spontaneous functional connectivity and intelligence. Neuroimage 41:1168-1176.

Sporns O, Tononi G, Edelman GM (2000) Connectivity and complexity: the relationship between neuroanatomy and brain dynamics. Neural Netw 13:909-922.

Sporns O, Chialvo DR, Kaiser M, Hilgetag CC (2004) Organization, development and function of complex brain networks. Trends Cogn Sci 8:418-425.

Stam CJ (2004) Functional connectivity patterns of human magnetoencephalographic recordings: a 'small-world' network? Neurosci Lett 355:25-28.

Stam CJ, Reijneveld JC (2007) Graph theoretical analysis of complex networks in the brain. Nonlinear Biomed Phys 1:3.

Thompson PM, Cannon TD, Narr KL, van Erp T, Poutanen VP, Huttunen M, Lonnqvist J, Standertskjold-Nordenstam CG, Kaprio J, Khaledy M, Dail R, Zoumalan CI, Toga AW (2001) Genetic influences on brain structure. Nat Neurosci 4:1253-1258.

Van den Heuvel MP, Mandl RC, Hulshoff Pol HE (2008a) Normalized group clustering of resting-state fMRI data. PLoS ONE 3:e2001.

Van den Heuvel MP, Stam CJ, Boersma M, Hulshoff Pol HE (2008b) Small-world and scale-free organization of voxel based resting-state functional connectivity in the human brain. Neuroimage 43:11.

Van den Heuvel MP, Mandl RC, Luigjes J, Hulshoff Pol HE (2008c) Microstructural organization of the cingulum tract and the level of default mode functional connectivity. J Neurosci 28:7.

Van den Heuvel MP, Mandl RCW, Kahn RS, Hulshoff Pol HE (2009) Functionally linked resting-state networks reflect the underlying structural connectivity architecture of the human brain. Hum Brain Mapp In Press.

Watts DJ, Strogatz SH (1998) Collective dynamics of 'small-world' networks. Nature 393:440-442.

supplemental materials and methods

resting-state fmri

Our brain is a complex dynamic system in which information is continuously processed and transferred between brain regions with highly correlated functional dynamics (Sporns et al., 2000; Sporns et al., 2004). These coherent dynamics are believed to reflect the existence of functional connections between these regions. Functional connectivity is defined as the temporal coherency between neuronal brain signals of anatomically separated brain regions (Aertsen et al., 1989; Friston et al., 1993) and is widely investigated by measuring the correlation between resting-state Blood Oxygen Level Dependent functional Magnetic Resonance Imaging time-series (Biswal et al., 1995; Cordes et al., 2000; Lowe et al., 2000;

Beckmann et al., 2005; Achard et al., 2006; Damoiseaux et al., 2006; Van den Heuvel et al., 2008a).

During rest, brain regions produce a vast amount of spontaneous neuronal activity (Raichle et al., 2001; Raichle and Snyder, 2007) which can be measured with these resting-state BOLD fMRI recordings (Biswal et al., 1995; Salvador et al., 2005b; Damoiseaux et al., 2006). Of special interest are the low frequency oscillations (~0.01 - 0.1Hz) of the fMRI time-series measured during rest. These slow moving temporal patterns show a high level of correlation between multiple anatomically separated brain regions (Biswal et al., 1995; Cordes et al., 2000; Lowe et al., 2000), especially between brain regions that are involved in the same function, for example primary motor, visual and auditory regions. The exact neurophysiological basis of these low frequency correlations is not yet fully understood. There is an ongoing debate about whether resting-state BOLD correlations predominantly originate from respiratory and cardiac oscillations (Wise et al., 2004; Shmueli et al., 2007) or whether these correlating time-series are related to true synchronization of the neuronal activation patterns of brain regions, observed through a hemodynamic response function (Gusnard et al., 2001; Greicius et al., 2003; Buckner and Vincent, 2007). This latter view is supported by recent observations that report that resting-state BOLD time-series show a high correlation with concurrent fluctuations in neuronal spiking, suggesting a direct link between resting-state time-lag BOLD signals and intrinsic neuronal activity (Nir et al., 2008; Shmuel and Leopold, 2008). Furthermore, as mentioned, most of these coherent BOLD patterns have been found between regions of known functional networks, for example the motor and visual network and known high order cognitive networks (Biswal et al., 1995; Biswal et al., 1997; Cordes et al., 2001; Beckmann et al., 2005; Salvador et al., 2005a ; Damoiseaux et al., 2006; Van den Heuvel et al., 2008a). In addition, resting-state BOLD time-series of cortical regions have been reported to be mainly dominated by lower frequencies (<0.1 Hz), with only a minimal contribution of higher cardiac and respiratory oscillations (Cordes et al., 2000; Cordes et al., 2001). In this context, it is believed that the observed coherence between resting-state BOLD fluctuations of anatomically separate regions do, at least in part, originate from synchronized intrinsic neuronal activity of these regions and reflect a high level of functional connectivity between these brain areas (Biswal et al., 1995; Gusnard et al., 2001; Fox and Raichle, 2007; Greicius et al., 2008).

data acquisition

subjects

19 healthy subjects without a psychiatric history (age mean/std : 29/7.8 ; gender: 14 male, 5 female) participated in this study after providing written informed consent as approved by the medial ethics committee for research in humans (METC) of the University Medical Center Utrecht, The Netherlands.

intelligence scores

The Intelligence Quotient (IQ) of the participants was measured with the Dutch version of the Wechsler Adult Intelligence Scale III (WAIS-III) test. The WAIS test gives a standardized full scale IQ score based on a number of subtests that assess the level of verbal and non-verbal knowledge and reasoning of the participants. Each sub-test of the WAIS provided a raw score and from these raw-scores the Verbal Comprehension Index (VCI), Working Memory Index (WMI), Perceptual Organization Index (POI) and Processing Speed Index (PSI) index scores, Verbal IQ (VIQ), Performance IQ (PIQ) and Full-Scale IQ (FIQ) were derived. table 7.1 and 7.2 of the main text describe the index-scores, VIQ, PIQ and FIQ scores (table 7.1) together with the correlations between the index-scores and IQ-scores (table 7.2).

resting-state paradigm

During the resting-state fMRI scans, the scanner room was darkened. Subjects were instructed to relax with their eyes closed and to think of nothing in particular without falling asleep, which was verified directly after the 8 minute scanning session. None of the 19 included subjects reported to have fallen asleep or to be close to falling asleep.

mr acquisition

Resting-state functional Magnetic Resonance Imaging time-series were acquired on a 3 Tesla Phillips Achieva Medical scanner (Philips Medical Systems, Best, The Netherlands) at the University Medical Center Utrecht, The Netherlands. Resting-state Blood Oxygenation Level Dependent (BOLD) signals were recorded during a period of 8 minutes using a fast fMRI sequence (3D PRESTO (Golay et al., 2000), acquisition parameters: TR/TE 22ms/32ms using shifted echo, flipangle of 9 degrees; SENSE p/s reduction 2/2; a dynamic scantime of 0.5 sec, 1000 timeframes, total duration 8 minutes; FOV 256x256 mm, voxelsize 4x4x4mm, 32 slices covering whole brain). A high temporal acquisition of 2 Hz was used to minimize aliasing effects of high frequent respiratory and cardiac oscillations (respectively ~0.3

Hz and ~0.9-1.0 Hz) into the low resting-state frequencies of interest (0.01 - 0.1 Hz). PRESTO fMRI scans have a low anatomical contrast in comparison with a T1 image. Therefore, directly after the functional resting-state time-series an additional PRESTO scan with similar scanning parameters, but with a higher anatomical contrast was acquired by increasing the flipangle to 25 degrees. This additional high contrast PRESTO scan was made to improve the co-registration of the functional time-series with the T1 image. Directly after the resting-state time-series, a T1 weighted image was acquired for anatomical reference (3D FFE, acquisition parameters: TR/TE 10ms/4.6ms, SENSE p/s reduction 1.7/1.4; FOV 256x256 mm, voxelsize 0.75x0.75x0.8mm, 200 slices).

preprocessing

All fMRI preprocessing steps were done with the SPM2 software package (http://www.fil.ion.ucl.ac.uk). First, small head motion effects during the resting experiment were corrected by realigning the fMRI time-series to the last functional scan. Registration to the last functional scan was used to maximize the spatial overlap of the fMRI time-series with the high anatomical contrast functional scan. Second, both the functional time-series and anatomical T1 scan were coregistered to the high contrast functional scan, to provide spatial alignment between the resting-state time-series and the anatomical image. Third, an automatic cortical segmentation procedure was performed on the T1 image to select all cortical and sub-cortical gray matter voxels of the brain. Cortical segmentation was performed with the freely available Freesurfer software package (http://surfer.nmr.mgh.harvard.edu/). Cortical segmentation maps were resliced to a 4x4x4mm resolution to overlap with the resting-state time-series. Fourth, the individual functional time-series and matching cortical segmentation map were normalized to standard MNI 305 space, using the parameters of the normalization of the T1 image to the MNI 305 T1 brain (Collins et al., 1994). Fifth, the low resting-state frequencies of interest were selected by filtering the resting-state time-series with a finite impulse response (FIR) filter with a bandwidth of 0.01 - 0.1 Hz. The relatively high sampling-rate of the used resting-state fMRI protocol (i.e. 2 Hz) enabled the proper sampling of cardiac and respiratory signals. As a result, band-pass filtering minimized the influence of low frequency MR scanner noise (e.g. slow scanner drifts, typical < 0.01 Hz) and high frequent cardiac or respiratory oscillations up to 1 Hz (> 0.1 - 1 Hz) (Cordes et al., 2001).

graph analysis

The organization of the functional connections of the brain network was examined using a graph theoretical approach, as validated earlier (Van den Heuvel et al., 2008b). All steps of the graph analysis are illustrated in supplemental figure 7.1 and described in detail below. In summary, graph analysis involved the construction of a functional connected brain network *G* for each individual dataset, consisting of all gray matter sub-cortical and cortical voxels and connections between all functionally linked voxels. From these functional networks, key graph characteristics were computed that describe the architecture of the network, including the *clustering-coefficient C*, providing information about the level of *local* connectedness of the network and characteristic *path length L*, which provides information about the level of *global* communication efficiency of a network (Watts and Strogatz, 1998; Latora and Marchiori, 2001). *C* and *L* are typically compared to the clustering-coefficient C^{random} and characteristic path length L^{random} of comparable random organized networks, with the same number of connections and the same distribution of connections as *G*. For each *G*, up to 20 comparable random networks were formed and the overall C^{random} and L^{random} were defined as the average *clustering-coefficient* and characteristic *path length* of these random organized networks. The ratios *gamma*, defined as C / C^{random} and *lambda*, defined as L / L^{random} were computed and averaged over the group of subjects to verify a small-world organization of functional brain networks (Watts and Strogatz, 1998). Next, to examine the association between the organization of the brain network and inter-subject differences in intelligence the *gamma* and *lambda* scores of the individual brain networks were correlated with the individual IQ scores of the participants. Finally, to point out which nodes in the brain network showed the strongest relationship between network organization and intelligence, voxel-wise IQ correlation maps were computed, pointing out those nodes (i.e. voxels) of the functional brain network that showed the strongest correlation with IQ scores over the group of subjects. A detailed step-by-step description of the graph analysis is given below and is illustrated in supplemental figure 7.1.

graph construction

For each individual functional dataset, a connectivity graph $G = (V,E)$ was formed, with *V* the collection of N grey matter voxels and *E* the collection of edges (also called connections) between the voxels. The number of points N of the constructed functional brain graph varied around 9500 across the groups of subjects. The zero-lag temporal correlations between all possible voxel-pairs (i.e. ~9500x9500) was computed, reflecting the level of inter-

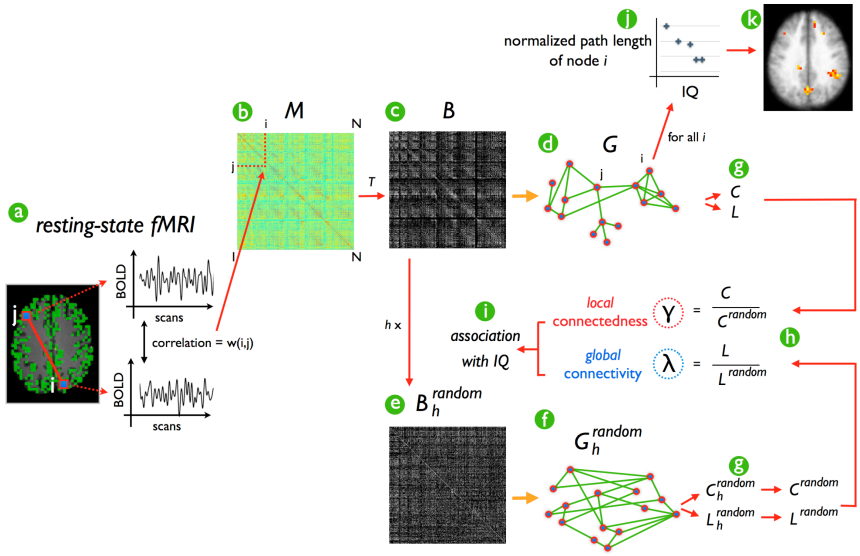

supplemental figure 7.1 graph analysis procedure Figure illustrates the individual steps of the performed graph analysis. For each individual resting-state fMRI dataset a graph $G = (V,E)$ was formed with V the collection of sub-cortical and cortical voxels and E the collection of connections between all voxels. First, the level of functional connectivity between voxel i and j was computed by correlating the resting-state BOLD time-series of voxel i and j (***panel a***) and placed in a connectivity matrix M (***panel b***). Next, M was threshold by threshold T, setting all connections to 1 that did reach T and all connections to 0 that did not reach T, transforming M into a binary valued connectivity matrix B (***panel c***). B directly reflected an unidirectional unweighted graph G, representing the functionally connected brain network (***panel d***). B was randomized resulting in B_h^{random} (***panel e***), which represented a randomized graph G_h^{random} (***panel f***). In total, h random graphs were formed, with h set to 20 for $0.40 \leqq T \leqq 0.5$, to 10 for $0.2 \leqq T < 0.40$ and to 5 for $T < 0.2$. Of all formed graphs G and G_h^{random}, the clustering-coefficient and characteristic path length were computed (***panel g***). C^{random} and L^{random} were computed by averaging the clustering-coefficients and path lengths of the h random graphs (***panel g***). Next, gamma (i.e. C / C^{random}) and lambda (i.e L / L^{random}) were computed (***panel h***) and associated with IQ (***panel i***) to examine the association between intelligence and the connectivity architecture of the functional brain network. Finally, to point out which brain regions showed the strongest association between normalized path length and IQ, the normalized path length of each node i of G was correlated with IQ over the group of subjects (***panel j*** *and* ***k***).

voxel functional connectivity (supplemental figure 7.1a). Voxel-wise correlations were stored as a correlation matrix *M* with cell *M(i,j)* holding the zero-lag temporal correlation between the fMRI time-series of voxel *i* and voxel *j* (supplemental figure 7.1b). A binary valued matrix *B* was formed by thresholding *M* by a threshold *T*, putting all cells of *M* to 1 that exceeded the threshold and all cells to 0 that did not exceed this threshold (supplemental figure 7.1c). Thresholding *M* directly resulted in the formation of an unweighted unidirectional graph *G*, with *V* reflecting all sub-cortical and cortical points (i.e. voxels) and *E* the functional connections between the voxels. In this study, *T* was varied for multiple settings between 0.05 and 0.5, with steps of 0.05. Increasing *T* too much would eventually lead to disconnecting a number of voxels from *G* and this could have an effect on the computed graph characteristics (i.e. clustering-coefficient *C* and characteristic path length *L*). Therefore, the maximum *T* was set to 0.5, to minimize the number of disconnecting nodes in *G* and to ensure that the largest interconnected cluster included more than 95% of the number of nodes in *G* over the group of subjects (Van den Heuvel et al., 2008b).

network characteristics

Next, the clustering-coefficient *C* and characteristic path length *L* of *G* were computed (supplemental figure 7.1g) to examine the overall connectivity architecture of the functional brain network.

The clustering-coefficient C_i of node *i* expresses the level of connectedness of the direct neighbors of node *i*. C_i gives information on how strong node *i* and its direct neighbors form a clustered sub-network within the total network. C_i of voxel *i* is defined as (Watts and Strogatz, 1998; Sporns et al., 2004):

$$C_i = \frac{\#\,edges\ in G_i}{\frac{1}{2}k_i(k_i-1)} \qquad (7.1)$$

with G_i the sub-graph of neighbors of voxel *i* and k_i the number of edges of voxel *i*.

In words, C_i is defined as the ratio of the number of edges between its neighbors of voxel *i* and the total number of possible edges between the neighbors. In turn, the overall clustering-coefficient *C* of *G* is defined as the average of C_i over all voxels *i* in *G* (Watts and Strogatz, 1998; Sporns et al., 2004) :

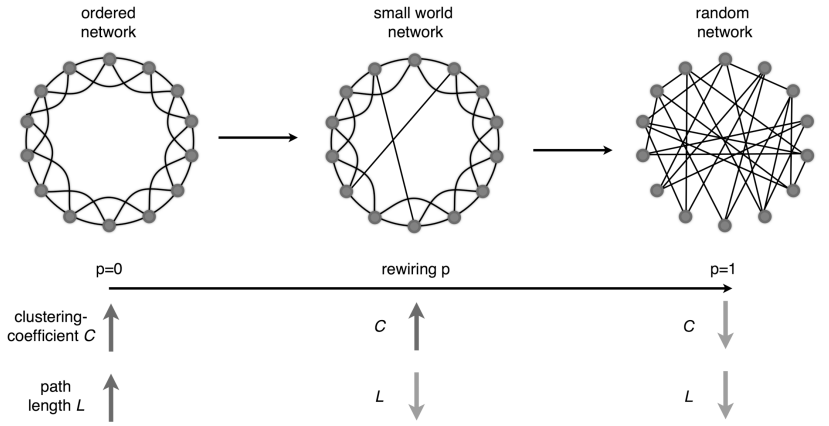

supplemental figure 7.2 regular, small-world and random networks Figure illustrates the relationships between ordered, small-world and random networks (Watts and Strogatz, 1998). On the left side an regular network is shown, with vertices (blue/red points) and the connections (black lines) between the vertices. Regular networks have a high level of local clustering (i.e. high *C*) but an average long travel distance between all the nodes (i.e. a high characteristic path length *L*). The high *C* and high *L* indicate that an regular network has a high level of local organization. Let *p* be a probability that the connection between point *i* and point j is randomly rewired. When $p = 1$, all connections in the network are randomly rewired, resulting in a fully random network (network shown at the right side). In contrast to regular networks, random networks have a more global character, indicated by a low level of clustering (i.e. low *C*) and a short average travel distance (i.e. low *L*). Interestingly, Watts and Strogatz (Watts and Strogatz, 1998) showed that for a low rewiring probability *p*, a so-called *small-world* network is formed. Small-world networks (network shown in the middle) have an intermediate character, showing a high level of clustering (i.e. high *C*), but still with a short characteristic path length (i.e. low *L*) similar to that of a random network .

$$C = \frac{1}{N}\sum_{i \in G} C_i \qquad (7.2)$$

The definition of C_i (formula 1) is undefined when the number of neighbors of node *i* is zero or one, which happens when node *i* is disconnected from the graph or when node *i* is a so-called *leaf* node (i.e. when node *i* has only one connection). In that case C_i was defined as 0. However, as mentioned by Kaiser the contributing effect of disconnected nodes and leaf nodes on *C* is likely to increase when the to be examined network becomes more and more sparse, biasing *C* to a mixture of neighborhood clustering and edge density

(Kaiser, 2008). In our study, the effect of the disconnected nodes and leaf nodes on *C* was believed to be minimal as the number of disconnected nodes was kept to a absolute minimum by using low cut-off thresholds *T*. To verify this minimal effect, an alternative definition of *C* was used in which all nodes with less than two connections (i.e. disconnected nodes and leaf nodes) were removed, before computing *C* (Kaiser, 2008). As expected due to the low number of disconnected nodes and leaf nodes in *G* (due to the relative low *T*), this did not change our findings. This overlaps with our previous findings on the influence of disconnected nodes in functional brain networks with high *T* (Van den Heuvel et al., 2008b).

Furthermore, the characteristic path length *L* of a graph is defined as the averaged minimal distance (in number of edges) between each possible node pair in the graph. The average characteristic path length *L* expresses how well the graph is connected globally. Formally, *L* is given by:

$$L = \frac{1}{N(N-1)} \sum_{i \neq j, i, j \in G} d(i,j) \qquad (7.3)$$

with distance *d(i,j)* the minimal number of edges that have to be crossed to travel from node *i* to node *j*, for *i* and *j* in *G* and N the number of nodes in *G*. Before computing *L*, possible disconnected nodes were removed from *G*. Due to the low number of disconnected nodes in *G* this was believed to have only a very minimal effect on the computation of *L* (Van den Heuvel et al., 2008b).

Taken together, the clustering-coefficient *C* and characteristic path length *L* of a graph express key characteristics of the examined network. *C* and *L* indicate whether a network is connected in an *regular*, *small-world* or *random* fashion (Watts and Strogatz, 1998) (supplemental figure 7.2). Regular networks show a high level of clustering *C* and a high characteristic path length *L* (supplemental figure 7.2a). This in contrast to *random* networks, which typically show a low level of clustering and a short average characteristic path length, reflected by low *C* and low *L* (supplemental figure 7.2c). The high *C* of a regular network indicates that functional neighbors within the network are high connected, but the high *L* indicates that it takes a high number of steps to travel to more distant nodes in the network. In contrast, random networks have a more global character, indicated by the low path length *L* and the low *C*. The low *C* indicates a limited formation of neighborhood connectedness and the low *L* indicates that on average the number of edges that have to be crossed to another point in the graph is relatively low. Regular and random networks are each the end points of a network spectrum. Defining a probability *p* that a connection from a regular

network is randomly rewired will shift a network from an ordered organization to a more random organization with increasing *p* (Watts and Strogatz, 1998). Increasing the rewiring probability *p* a network becomes more and more randomly organized (supplemental figure 7.2). So-called *small-world networks* have an intermediate organization, showing a high level formation of sub-graphs in the network, but still with an average short characteristic path length of around the same length as the characteristic path length of random organized networks, ensuring an optimal level of global connectivity (Watts and Strogatz, 1998; Latora and Marchiori, 2001). As such, *small-world* networks typically show a clustering-coefficient that is much higher than that of a random network, but still with a characteristic path length that is around the same order of that of a random network. More formally, a network has a small-world organization when $C >> C^{random}$ and $L \sim L^{random}$ (Watts and Strogatz, 1998), with C^{random} and L^{random} defined as the clustering-coefficient and characteristic path length of a comparable random network G^{random} of similar size (Sporns et al., 2004; Sporns, 2006) and connectivity distribution (Sporns and Zwi, 2004; Stam and Reijneveld, 2007).

The local and global connectivity properties of a network are typically expressed by the ratio *gamma* γ between *C* and C^{random} and *lambda* λ between *L* and L^{random} (supplemental figure 7.1h). Small-world networks have a *gamma* of >1 and *lambda* of ~1 (Sporns and Zwi, 2004; Stam and Reijneveld, 2007). γ and λ are formally given by:

$$\gamma = \frac{C}{C^{random}} \tag{7.4}$$

$$\lambda = \frac{L}{L^{random}} \tag{7.5}$$

Besides the graph characteristics *C*, *L*, *gamma* and *lambda* also the average number of connections *k* of each *G* was examined as an indication of the overall level of connectivity of the individual functional brain network (Van den Heuvel et al., 2008b).

comparable random networks

For normalization of *C* and *L*, for each thresholded *G* a number of *h* comparable random graphs G_h^{random} were formed, by randomizing the binary connectivity matrix *B* (supplemental figure 7.1e). It has been suggested that for a correct statistical comparison of two networks the connectivity distribution of the two networks have to be similar (Sporns and

Zwi, 2004). Therefore, G_h^{random} was formed by randomizing the connections of *G*, keeping the total number of connections of node *i* fixed (Van den Heuvel et al., 2008b), resulting in a random graph G_h^{random} with a degree distribution similar to that of *G* (supplemental figure 7.1f).

L^{random} For each of the resulting G_h^{random} the clustering-coefficient C_h^{random} and characteristic path length L_h^{random} were computed (supplemental figure 7.1g). Next, and C^{random} were determined as the average of the computed graph characteristics of the *h* random graphs:

$$C^{random} = \frac{1}{h}\sum C_h^{random} \tag{7.6}$$

$$L^{random} = \frac{1}{h}\sum L_h^{random} \tag{7.7}$$

The number of random networks *h* was set to 20 for $0.40 \leqq T \leqq 0.50$, to 10 for $0.20 \leqq T < 0.40$ and to 5 for $T < 0.20$, to reduce the computational load.

group averaged graph characteristics

For each setting of *T* (ranging from 0.05 to 0.5, steps of 0.05), the performed graph analysis (supplemental figure 7.1a-h) resulted in clustering-coefficient *C*, characteristic path length *L*, comparable C^{random}, L^{random} and *gamma* and *lambda* values for each of the individual functional connectivity brain networks *G*. To examine an overall possible small-world organization of the functional brain, the graph characteristics were averaged over the group of 19 subjects.

association between graph characteristics and IQ

To examine a possible association between the overall architecture of the functional brain network and intelligence, individual *gamma* and *lambda* values were correlated with individual IQ scores (supplemental figure 7.1i). *Gamma* and *lambda* are directly related to the level of *global* and *local* communication efficiency of a network (Latora and Marchiori, 2001). A high *gamma* reflects a high level of *local* connectedness in the network, ensuring a high level of local communication efficiency. In addition, a low *lambda* reflects an average short path length between any two nodes in the network, expressing a high level of global communication efficiency within the network.

For the small-world organized networks G of $0.40 \leqq T \leqq 0.50$, the association between the individual IQ scores and the computed graph characteristics *gamma* and *lambda* was computed. Correlations between gamma/lambda values and IQ scores were corrected for possible age effects by regressing out age out of the *gamma* and *lambda* scores.

correlation coefficient maps

To point out which regions in the functional brain network showed the strongest association between *path length* and IQ, an exploratory post-hoc analysis was performed, in which voxel-wise correlation-coefficient maps for the nodes in G of $T = 0.45$ were computed (supplemental figure 7.1k). This was done in a 3-step procedure. *Step 1.* For each individual dataset, for each node i in the individual functional brain network G, voxel i (i.e node i) was flagged with its *normalized path length*. This resulted in an individual spatial *normalized path length* map. Voxel-wise path length values were expressed as individual *normalized path length* values, to correct for mean effects on the individual path length scores. The *normalized path length* of node i in the network was computed as:

$$normalized\_path\_length_i = \frac{L_i}{L^{random}} \tag{7.8}$$

In this way, the *normalized path length* of node i was computed in a similar manner as the computation of overall *lambda*. *Step 2.* To increase cross-subject overlap between the individual cortical segmentation maps, individual *Lmaps* were dilated, by flagging voxel j with the mean *normalized path length* of voxels directly touching voxel j. *Step 3*. For all voxels that overlapped the group of subjects, the *normalized path length* of each node i in the functional brain network was correlated with individual IQ scores. An exploratory threshold of $p < 0.05$ [uncorrected for multiple comparisons] was used to examine which regions in the brain showed a significant correlation between normalized path length and IQ. To minimize the number of false positives, only clusters that consisted of 8 or more spatially adjacent voxels of $p < 0.05$ were considered as significant. To examine the effect size of the regions in the brain network that showed the strongest relationship between normalized path length and IQ, a correlation coefficient *rmap* was formed by flagging all significant nodes with their matching correlation coefficient *r*-values. Figure 7.3 of the main text shows the group correlation-coefficient *rmap* of $T = 0.45$.

supplemental results

characteristic path length and clustering-coefficient

The group averaged L, L^{random}, C, C^{random}, *lambda* and *gamma* are shown in figure 7.1 of the main text and clearly indicate a small-world organization of functional brain networks for $T \geq 0.3$. The characteristic path length L was found not to be different from L^{random} (panel a) and for $T \geq 0.3$ the clustering-coefficient C turned out to be $>> C^{random}$ and for $T \leqq 0.5$ (panel b) [two-sample t-test, df = 36, all $p < \alpha$ of 0.01, Bonferroni corrected for multiple comparisons of T]. This was reflected by *lambda* ~1 $T \leqq 0.5$ (panel c) and by *gamma* >1 for $T \geq 0.3$ [one-sample t-test, df =18, $p < 0.01$, Bonferroni corrected] (panel d). These results clearly suggest a small-world organization of the functional human brain, supporting the findings of recent studies showing a small-world organization of the brain network on both a regional (Sporns and Zwi, 2004; Stam, 2004; Achard et al., 2006; Achard and Bullmore, 2007; Sporns et al., 2007) and a voxel scale (Eguiluz et al., 2005; Van den Heuvel et al., 2008b).

association of graph characteristics and IQ

To examine the relationship between the connectivity architecture of the brain network and inter-subject variation in intelligence, the individual graph characteristic *lambda* and *gamma* scores were correlated with the individual IQ scores for G within the small-world range of $0.3 \leqq T \leqq 0.5$.

Interestingly, a negative association was found between *lambda* and IQ, suggesting a positive relationship between the global level of connectivity in the brain network and intelligence [linear regression, df=18; $T = 0.45$, $r = -0.54$, $p = 0.010$ (figure 7.2a); $T = 0.5$, $r = -0.57$, $p = 0.017$ (figure 7.2b), which is significant considering a α of 0.01 after Bonferroni correction for multiple comparisons of T; regressions corrected for age]. No association was found between the level of local clustering and intelligence, as reflected by the lack of association between *gamma* and IQ scores. The associations between overall *lambda* and *gamma* and IQ are shown in figure 7.2 of the main text and in supplemental figure 7.3a-f. Furthermore, to examine whether the individual overall number of connections k of the brain network were related to intelligence, k was correlated with the IQ scores in a similar manner as the *lambda* and *gamma* scores. No association was found between k and IQ scores (corrected for age, supplemental figure 7.3h-j). Considering the clear association between IQ and *lambda*, this suggests that intelligence is not related to the absolute number of connections of our brain network or how these connections are *organized* at the local level, but more related to

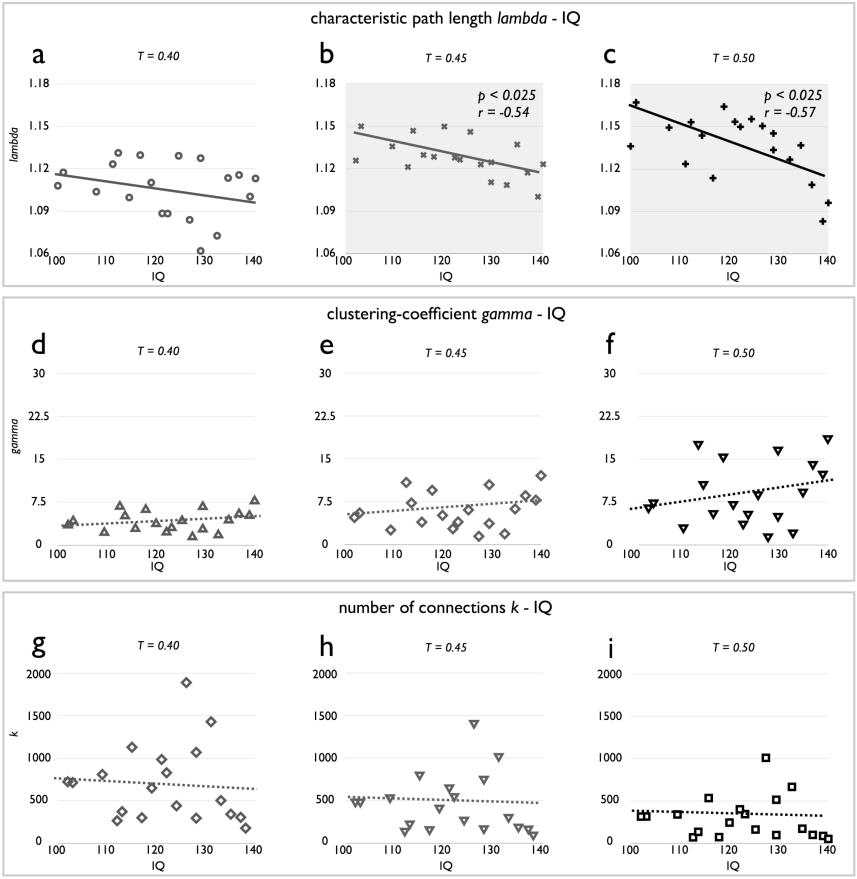

supplemental figure 7.3 associations between characteristic path length lambda, clustering-coefficient gamma and number of connections *k* and IQ For networks within the clear small-world range a significant correlation was found between the overall normalized characteristic path length lambda and IQ [linear regression, df = 18; *T* = 0.45, r = -0.54, p = 0.010 (***panel b***); *T* = 0.5, r = -0.57, p = 0.017 (panel c), corrected for age], suggesting a positive association between the level of global communication efficiency within the functional brain network and intelligence. No significant association was found between the level of local clustering gamma and IQ (***panel d***,***e***, ***f***) nor the number of connections k and IQ (supplemental figure 7.3 g,h,i). Taken the results of *lambda*, *gamma* and *k* together, our findings suggest that intelligence is not directly related to the overall number of connections of the brain network, or how these connections are organized at the local level within the many functional sub-networks of our brain, but rather to how efficient information is integrated globally between different regions of the brain. These results indicate that smarter brains have a more direct and therefore more efficient access to information across the global brain network.

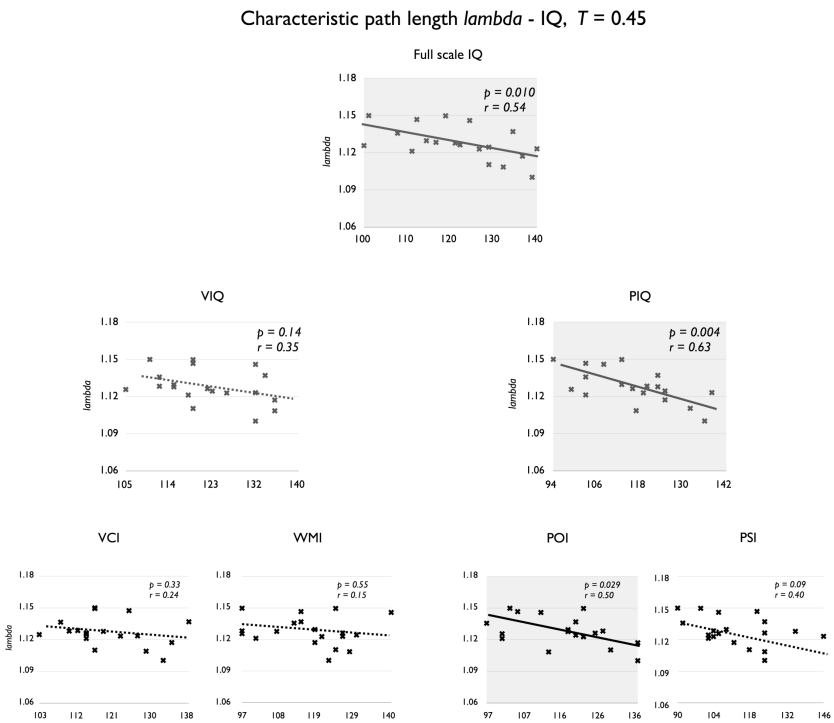

supplemental figure 7.4 associations between characteristic path length *lambda* and IQ sub-scales Upper panel shows for the cut-off threshold $T = 0.45$, the significant association between full scale IQ and normalized characteristic path length *lambda* of the functional brain network [linear regression, p = 0.010, df = 18, corrected for age]. Middle panels show the association between Verbal IQ (VIQ) and Performance IQ (PIQ) and characteristic path length. PIQ was found to be significantly correlated with lambda [linear regression, p = 0.004, df = 18, corrected for age]. Lower panels show the association between lambda and VCI, WMI, POI and PSI index scores. *Lambda* was found to be significantly negatively associated with POI [linear regression, p = 0.004, df = 18, corrected for age].

how efficient the global connections of our brain are organized.

correlation coefficient rmaps of normalized path length with IQ

For the small-world brain network G of $T = 0.45$ the individual computed *normalized path length* values of each node i (i.e. voxel i) of the network were correlated with the individual IQ scores separately. The resulting correlation coefficient *rmap* is shown in figure 7.3 of the main text. The strongest

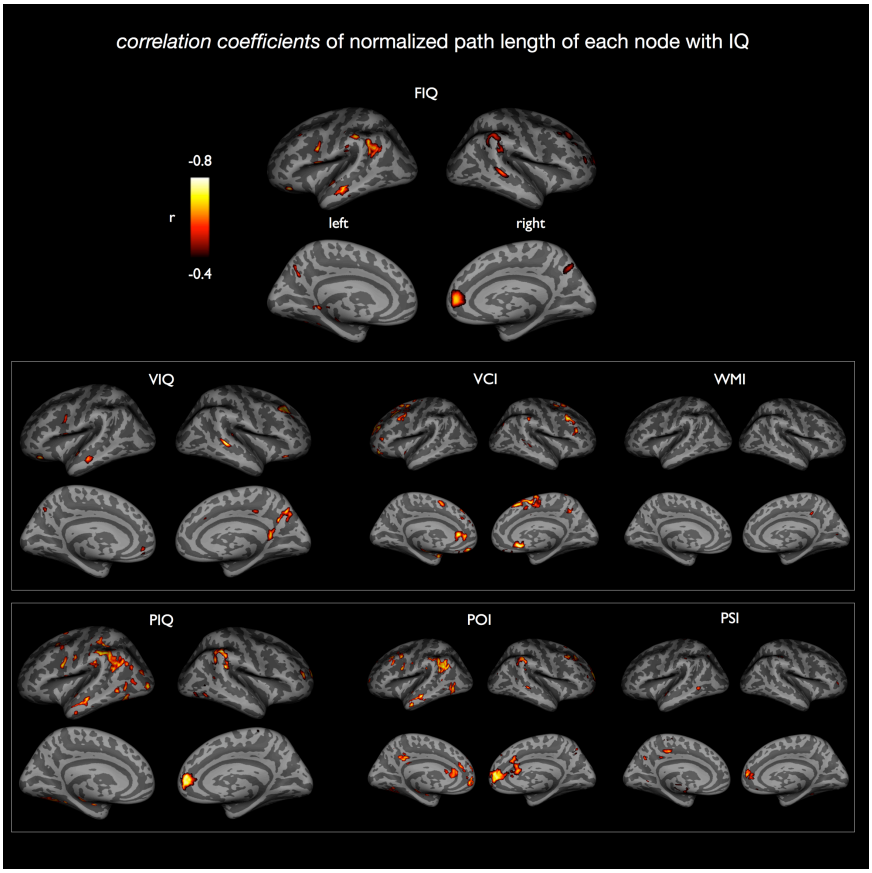

supplemental figure 7.5 regional specific patterns between normalized path length of each node and IQ subscales Figure shows the regional specific patterns between the path length of each node and the full scale IQ, Verbal IQ (VIQ), Performance IQ (PIQ), Verbal Comprehension Index (VCI), Working Memory Index (WMI), Perceptual Organization Index (POI) and Processing Speed Index (PSI), plotted on a 3D rendering of the average T1 image over the group of subjects. As expected from the association between IQ sub-scores and the overall characteristic path length lambda (supplemental figure 4) the strongest effects were found on PIQ and POI. Shown are correlation coefficient values of those voxels that had a significant negative association between IQ sub-scores and node-specific L [$T = 0.45$, $p < 0.05$ uncorrected for multiple comparisons, df=18, corrected for age].

associations between IQ and normalized path length were found in medial frontal (BA 9/10, r = -0.75, $p < 0.001$ age corrected, yellow box), precuneus/posterior anterior cingulate cortex (BA 7, r = -0.55, $p < 0.02$ age corrected, orange box), and inferior parietal cortex (BA 39/40, r = -0.72, $p < 0.001$ age

corrected, red box). These findings suggest that increased intelligence may be related to increased efficiency of frontal and parietal regions to access information of other sub-networks in the functional brain network. This suggest that inter-subject differences in intelligence may be related to how efficient high order frontal and parietal regions can integrate information of the other functional sub-networks within the brain network. Also regions overlapping left *superior temporal* [BA 22/40, r= -0.69, p = 0.014, df = 18] and left inferior frontal [BA 44/45, r = -0.68, p = 0.012, df = 18] showed a significant negative correlation between normalized path length and full scale IQ.

additional references supplemental materials and methods

Achard S, Salvador R, Whitcher B, Suckling J, Bullmore E (2006) A resilient, low-frequency, small-world human brain functional network with highly connected association cortical hubs. J Neurosci 26:63-72.

Beckmann CF, DeLuca M, Devlin JT, Smith SM (2005) Investigations into resting-state connectivity using independent component analysis. Philos Trans R Soc Lond B Biol Sci 360:1001-1013.

Biswal BB, Van Kylen J, Hyde JS (1997) Simultaneous assessment of flow and BOLD signals in resting-state functional connectivity maps. NMR Biomed 10:165-170.

Buckner RL, Vincent JL (2007) Unrest at rest: Default activity and spontaneous network correlations. Neuroimage 37:1091-1096.

Collins DL, Neelin P, Peters TM, Evans AC (1994) Automatic 3D intersubject registration of MR volumetric data in standardized Talairach space. J Comput Assist Tomogr 18:192-205.

Cordes D, Haughton VM, Arfanakis K, Wendt GJ, Turski PA, Moritz CH, Quigley MA, Meyerand ME (2000) Mapping functionally related regions of brain with functional connectivity MR imaging. AJNR Am J Neuroradiol 21:1636-1644.

Cordes D, Haughton VM, Arfanakis K, Carew JD, Turski PA, Moritz CH, Quigley MA, Meyerand ME (2001) Frequencies contributing to functional connectivity in the cerebral cortex in "resting-state" data. AJNR Am J Neuroradiol 22:1326-1333.

Eguiluz VM, Chialvo DR, Cecchi GA, Baliki M, Apkarian AV (2005) Scale-free brain functional networks. Phys Rev Lett 94:018102.

Golay X, Pruessmann KP, Weiger M, Crelier GR, Folkers PJ, Kollias SS, Boesiger P (2000) PRESTO-SENSE: an ultrafast whole-brain fMRI technique. Magn Reson Med 43:779-786.

Kaiser M (2008) Mean clustering coefficients: the role of isolated nodes and leafs on clustering measures for small-world networks. New Journal of Physics 10.

Lowe MJ, Dzemidzic M, Lurito JT, Mathews VP, Phillips MD (2000) Correlations in low-frequency BOLD fluctuations reflect cortico-cortical connections. Neuroimage 12:582-587.

Nir Y, Mukamel R, Dinstein I, Privman E, Harel M, Fisch L, Gelbard-Sagiv H, Kipervasser S, Andelman F, Neufeld MY, Kramer U, Arieli A, Fried I, Malach R (2008) Interhemispheric correlations of slow spontaneous neuronal fluctuations revealed in human sensory cortex. Nat Neurosci.

Raichle ME, Snyder AZ (2007) A default mode of brain function: A brief history of an evolving idea. Neuroimage 37:1083-1090.

Salvador R, Suckling J, Schwarzbauer C, Bullmore E (2005a) Undirected graphs of frequency-dependent functional connectivity in whole brain networks. Philos Trans R Soc Lond B Biol Sci 360:937-946.

Shmuel A, Leopold DA (2008) Neuronal correlates of spontaneous fluctuations in fMRI signals in monkey visual cortex: Implications for functional connectivity at rest. Hum Brain Mapp.

Shmueli K, van Gelderen P, de Zwart JA, Horovitz SG, Fukunaga M, Jansma JM, Duyn JH (2007) Low-frequency fluctuations in the cardiac rate as a source of variance in the resting-state fMRI BOLD signal. Neuroimage 38:306-320.

Sporns O (2006) Small-world connectivity, motif composition, and complexity of fractal neuronal connections. Biosystems 85:55-64.

Sporns O, Honey CJ, Kotter R (2007) Identification and classification of hubs in brain networks. PLoS ONE 2:e1049.

Sporns O, Chialvo DR, Kaiser M, Hilgetag CC (2004) Organization, development and function of complex brain networks. Trends Cogn Sci 8:418-425.

Wise RG, Ide K, Poulin MJ, Tracey I (2004) Resting fluctuations in arterial carbon dioxide induce significant low frequency variations in BOLD signal. Neuroimage 21:1652-1664.

chapter 8

summary and discussion

In this final chapter the main findings of this thesis are summarized. Some general conclusions will be discussed, together with a number of suggestions for future research and how we think that the proposed graph analysis techniques maybe helpful in examining functional cortical network alterations in psychiatric and neurological diseases, as well as how it is evident to form an important tool to examine brain development. Furthermore, a number of methodological issues concerning the use of graph analysis techniques on resting-state fMRI will be discussed.

The main aim of this thesis was to examine the network architecture of the functional brain. Our brain consists of a large number of functionally linked regions, each with their own function and task, that together form a dynamic and complex network. Within this network, information is continuously processed and transported between regions with coherent temporal dynamics, processes that are always on, even when we are 'at rest'. Our studies suggest that these functional connections are organized in a highly robust and efficient *small-world, scale-free* and *modular* fashion. Such an architecture indicates that our brain has a high level of local connectedness with the formation of functional sub-networks, that are in turn linked together by more 'long-distance' connections that ensure a high level of global communication efficiency across the full network (**chapters 2** and **3**). In this thesis, we focused on the two key characteristics that define this small-world modular organization. First, we examined the formation of functional sub-networks and how they are structurally anchored into our brain. Second, we examined the existence of a possible association between the level of efficient wiring of the global connections of our brain network and our cognitive capabilities. To examine the modularity of the functional brain network we proposed a novel graph based group clustering approach for the selection of *resting-state networks* called *normalized cut group clustering* (**chapter 3**) and we examined the existence of a somatotopic organization of the functional connections within the primary motor network (**chapter 4**). Furthermore, the existence of a structural core of resting-state networks

(**chapters 5** and **6**) was examined and how the 'quality' of this structural core is related to the level of functional connectivity in the *default mode network* (**chapter 6**). Focusing on the high level of global efficiency of the brain network as revealed by its small-world organization, we show that intellectual performance is strongly associated to the level of efficient wiring of the functional connections across the brain network (**chapter 7**).

summary of findings

In the past 5 years, a number of pioneering studies have suggested that our functional brain is organized in a highly efficient *small-world* and *modular* fashion (Sporns et al., 2004; Sporns and Zwi, 2004; Eguiluz et al., 2005; Achard et al., 2006; Sporns et al., 2007; Stam et al., 2007; Stam and Reijneveld, 2007; Bullmore and Sporns, 2009). Most of the resting-state fMRI network studies have examined the functional brain network as a collection of interconnected brain regions, based on a predefined anatomical template. These studies have focused on examining the inter-regional functional connectivity, but have not taken into account intra-regional communication. Examining the brain network at a voxel level, which is the native resolution of fMRI recordings, could provide important information about the organization of the functional connections of the brain network in high spatial detail. Therefore, in this thesis, we examined the organization of the functional brain network by defining the brain network as a collection of voxels, rather than using a predefined regional template defining the brain as a network of a small number of brain regions.

small-world and scale-free organization of the brain network

Our studies indicate a small-world organization of the functional brain network (**chapter 2** and **7**), reflected by a high normalized clustering-coefficient *gamma* and a short normalized characteristic path length *lambda* (Van den Heuvel et al., 2008c, 2009b). These results support the findings of pioneering MEG (Stam, 2004) and region based fMRI studies (Salvador et al., 2005b; Achard et al., 2006). However, these resting-state neuroimaging studies have been less conclusive about a possible *scale-free* organization of the functional brain network. Real-world biological scale-free networks have been characterized by a power-law degree distribution with an exponent close to 2, which marks the existence of a small number of so-called hub-nodes that have many more connections than the averaged node in the network, taking a special central role in the overall network. Resting-state studies using a regional approach have suggested a small-world, but not a

scale-free organization of the functional brain network (Achard et al., 2006). Interestingly, our findings based on a voxel-wise approach did mark a possible scale-free organization of the functional brain network, as indicated by a suggested power-law scaling of the degree distribution of the functional brain network at higher cut-off thresholds *T.* These findings strongly support the voxel-based results of Equiluz et al., reporting on a scale-free organization of the brain network during task-induced fMRI (Eguiluz et al., 2005). Our results suggest a combined small-world and scale-free organization of the brain network, marking the importance of using a voxel-wise approach in examining the functional brain network.

What is the functional implication of such an efficient small-world and scale-free organization of our functional brain network? One interpretation of our results may be that our brain is organized in an highly efficient fashion (Mathias and Gopal, 2001) in which information can be processed by highly clustered sub-networks that each have their own function and task, and in which, in turn, information can be efficiently transported between different sub-networks for further processing (Sporns et al., 2004; Sporns and Zwi, 2004). The high level of local neighborhood clustering ensures a high level of robustness to random failure of individual nodes in the network (Kaiser et al., 2007) and the short overall node-to-node distance, as reflected by the short *characteristic path length* of the small-world brain network, shows that the functional travel distance between brain regions is surprisingly short (Watts and Strogatz, 1998). Such a short travel distance reflects a high level of global communication efficiency and information integration within the brain network (Latora and Marchiori, 2001; Sporns et al., 2004; Stam and Reijneveld, 2007; Bullmore and Sporns, 2009). Interestingly, a possible scale-free organization might suggest that the inter-network communication is mediated by a small number of strongly and efficiently connected hub regions. A scale-free topology ensures an efficient transport of information between the different nodes of the network, with a minimum of congestion problems (Toroczkai and Bassler, 2004; Grigorov, 2005) together with a high level of robustness to random attack (Albert et al., 2000; Callaway et al., 2000). Taken together, our voxel-based approach suggests a combined *small-world* and *scale-free* organization of the functional brain network. Such an organization might ensure a highly efficient network architecture of functional communication in the human brain, forming an optimal balance between a maximum level of local and global functional communication efficiency, together with a low level of wiring of connections (Mathias and Gopal, 2001; Chklovskii et al., 2002; Barabasi and Bonabeau, 2003; Chen et al., 2006).

modularity

normalized cut group clustering

In the subsequent chapters, we examined the level of *modularity* of the functional brain network with the use of a novel clustering approach. The formation of strongly intraconnected sub-networks within the full brain network was examined, often referred to as the formation of *resting-state networks* (**chapters 3** and **4**) and how these functionally linked sub-networks are structurally anchored into the brain (**chapters 5** and **6**). In **chapter 3** we proposed a graph clustering method, called *normalized cut group clustering*, for the selection of functional resting-state networks from resting-state fMRI data across a group of subjects (Van den Heuvel et al., 2008a). Most resting-state fMRI studies have used a predefined seed model to examine the functional connections of a particular brain region. Although a simple and powerful method, seed-based techniques are limited in examining only the functional connections of the chosen seed, without providing any information about the other functional connections of the brain network. In contrast, a few model-free group analysis strategies have been suggested, most of them based on *Independent Component Analysis (ICA)*, enabling the examination of the formation of resting-state networks across a group of subjects without the need of selecting a model-dependent seed region (Calhoun et al., 2001; Beckmann et al., 2005; Salvador et al., 2005a; De Luca et al., 2006). However, group wise model-free selection of resting-state networks using ICA remains a complex task. It often requires manual intervention and manual interpretation to select the meaningful components from the total collection of components, relying on the researcher to determine which components reflect functional networks and which components reflect physiological or scanner noise. Furthermore, ICA results are often perceived as difficult to interpret as it remains unclear what exactly a component is representing in relationship to the results of the more classical functional connectivity seed method. In **chapter 3** we proposed a graph based model-free clustering method, in which the number of resting-state group networks is based on an optimal clustering fit of functional brain networks across a group of subjects (Van den Heuvel et al., 2008a). Our proposed method, called *normalized cut group clustering*, consists of two subsequent stages, combining clustering at an *individual level* with clustering at a *group level*. At the individual level, the functional brain network was formed out of all cortical gray matter voxels with connections between functionally linked voxels and clustered into groups that show a high number of connections between the voxels within a cluster and a low number of connections between voxels in different clusters. Over-clustering

was used to control for the unknown number of individual networks. Next, at the group level, these individual clustering results were combined by forming a *group graph*, consisting of all grey matter voxels and connections between voxels that reflected the level of cluster-similarity across the group of subjects. Clustering the resulting *group graph* directly reflected the grouping of voxels that showed a high level of functional connectivity consistently over the group of subjects. A strong advantage of our proposed clustering method is that it includes the option to determine the number of group clusters, i.e. the number of group resting-state networks, as an optimal clustering fit of the data, minimizing the influence of manual intervention. Furthermore, the resulting group clustermaps are easy to interpret as they directly reflect the grouping of voxels that consistently showed a high level of functional connectivity. This has the advantage that they are more easy to compare with more traditional seed based resting-state results. In short, we proposed a group clustering graph based method that groups voxels that consistently show a high level of functional connectivity across the brain networks of a group of subjects.

resting-state networks

The normalized cut group clustering approach revealed 9 resting-state networks (RSNs), suggesting a high level of modularity of the functional brain network during rest (Van den Heuvel et al., 2008a). These RSNs included the *primary motor network*, the *visual network*, an *extra-striate visual network*, a network overlapping insular and anterior cingulate cortex, two lateralized *parietal-frontal networks*, the *default mode network*, consisting of posterior cingulate cortex/precuneus (PCC), medial frontal cortex (MFC) and bilateral inferior/superior parietal lobule (IPL/SPL) regions and two singular networks consisting of medial frontal regions and posterior precuneus regions respectively. Eight of these networks show direct one-on-one overlap with the networks reported by benchmark RSN papers (Beckmann et al., 2005; Salvador et al., 2005a; Damoiseaux et al., 2006). The high overlap between the RSN maps of these studies and our clustering results was taken as an indication of the robust formation of resting-state networks in the functional brain at a resting-state.

Interestingly, at first, the normalized cut group clustering grouped the primary motor and visual regions into a single resting-state network, rather than two separate networks as reported by other group resting-state studies (Beckmann et al., 2005; Salvador et al., 2005b; Damoiseaux et al., 2006; De Luca et al., 2006). These results indicated a relative high level of functional connectivity between the primary motor and primary visual regions during rest. Indeed, a recent paper supports our findings of a high

level of motor-visual resting-state connectivity, also reporting the primary motor and primary visual regions as a single group component (Vincent et al., 2008). Nevertheless, most other studies have reported these networks as two separate clusters and re-clustering the combined motor-visual network indeed revealed the existence of functionally linked sub-networks for the primary motor and primary visual regions, supporting previous studies (Beckmann et al., 2005; Damoiseaux et al., 2006).

The re-clustering of the combined motor/visual network into two separate motor and visual networks, raised the question about further subdivision of the specific regions of the primary motor network into sub-clusters, each with their own specialized function. Until now, all group resting-state studies have reported all primary motor regions to form a single resting-state network (Beckmann et al., 2005; Salvador et al., 2005b; Damoiseaux et al., 2006), including our own study (**chapter 3**, Van den Heuvel, 2008a), without distinguishing between the different functions of the sub-regions of the primary motor network. It is well known that the motor network is not a homogenous network, but rather consists of many sub-regions, each responsible for a specific motor function. However, less is known about the functional connections of these sub-regions during rest and whether they, according to their function, form functional resting-state sub-networks within the full primary motor resting-state network. In **chapter 4**, the examination of the organization of the functional connections of a large number of sub-regions of the motor network revealed that the functional sub-regions of the primary motor cortex are most strongly one-on-one functionally linked to their functional homolog in the contralateral hemisphere. Although all group resting-state studies until now have reported the primary motor regions to form a single resting-state network, our study strongly suggest that the resting-state primary motor network, and likely other resting-state networks as well, do not just form a single network but rather consist out of multiple functionally linked sub-networks. In summary, the results of **chapter 3** and **4** indicate a high level of modularity of the functional brain network. Clustering of resting-state fMRI data at the individual and group level revealed the formation of 9 resting-state networks, suggesting a possible modular organization of the functional brain network.

structural core of functionally linked resting-state networks

But how is all this ongoing neuronal synchronization between these anatomically separate brain regions possible? A number of group studies have shown the formation of functionally linked networks during rest, indicating that brain regions are not silent during rest but rather show a vast

amount of spontaneous synchronized brain activity. However, less is known about the structural basis of these functionally linked resting-state networks. If the observed coherence between resting-state signals truly reflects a high level of ongoing neuronal communication during rest than we would expect the existence of structural connections between these regions to support this ongoing information transfer. Indeed, in **chapter 5** we showed that well-known white matter bundles structurally interconnect functionally linked resting-state networks regions, demonstrating the existence of a structural core of functional resting-state networks (Van den Heuvel et al., 2009a). Specifically, we showed an important role for the *cingulum* tract, the left and right *inferior/superior frontal-occipital fasciculus* and the *genu* of the *corpus callosum* to connect the active areas within the default mode network and the left and right *superior longitudinal fasciculus* to connect the regions of the two lateralized parietal-frontal networks. Furthermore, *corpus callosum* tracts were found to interconnect the regions of the resting-state primary sensorimotor and visual networks and the left and right posterior precuneus regions and prefrontal cortical regions. Previous studies have shown a direct link between functional and structural connectivity on a local scale and within specific networks (Koch et al., 2002; Greicius et al., 2008; Lowe et al., 2008). Our findings clearly support these studies, showing a more general character of linked functional and structural connectivity in the human brain, showing as first that all known resting-state networks are structurally anchored into the human brain. As such, our findings provide supporting evidence for a direct link between resting-state functional connectivity and white-matter structural connectivity in the human brain (Hagmann et al., 2008). Moreover, our studies indicate the existence of a structural core of resting-state networks.

structural basis of the default mode network

In particular, our data suggested an important role for the white-matter *cingulum* tract to interconnect the active regions of the *default mode network*. The cingulum tract is known to play an important role in interconnecting the functionally linked medial frontal cortex (MFC) and posterior cingulate/precuneus cortex (PCC) of the default mode network (Greicius et al., 2008, **chapter 5**), but it remained unknown how these two forms of connectivity are exactly linked. Examining this structural-functional relationship would provide important information about a direct link between the brain's functional and structural connections. In the past few years the default mode network has gained special interest of the neuroscience community, as it has been suggested to play an important role in core processes of human cognition, like the integration of cognitive and emotional processing

(Greicius et al., 2003), mind-wandering (Mason et al., 2007) and self-related thoughts (Gusnard et al., 2001; Buckner et al., 2008). Interestingly, aberrant default mode network connectivity has been found in patients with alzheimer's disease (Greicius et al., 2004; Rombouts et al., 2009) and schizophrenia (Liu et al., 2006; Bluhm et al., 2007) (Zhou et al., 2007a) (Broyd et al., 2008). In **chapter 6** we zoomed in on the role of the cingulum tract in the default mode network (**chapter 5**) and showed that not only the regions of the default mode network are structurally interconnected by the cingulum, but also that the microstructural organization of these interconnecting white matter tracts are directly related to the level of functional default mode connectivity. Interestingly, this was the first study to show a direct relationship between the microstructural organization of white matter connections and the level of resting-state functional connectivity, providing an important association between the structural and functional topology of the brain network. Within our study, we demonstrated, by combining DTI with resting-state fMRI, that the fractional anisotropy (FA) of the cingulum tract is positively associated with the level of unique functional connectivity between the PCC and MFC, key regions of the default mode network. Although it is not fully clear how FA values are related to the microstructure and to, in a certain extent, myelination of white matter, it is widely believed that FA values provide important information about the overall microstructural organization of white matter. In this context, we speculate about the idea that a higher level of organization of the cingulum tract is directly associated with a higher level of neuronal communication between the structurally and functionally interconnected brain regions of the default mode network (Van den Heuvel et al., 2008b). Our study indicate a key role for the cingulum tract in structurally interconnecting the default mode network, showing a direct link between it's microstructural organization and the level of default mode functional communication during rest.

brain efficiency and intellectual performance

So, we now know that our brain is a highly efficiently organized network, but 'how efficient is it'? The observed small-world modular organization of the functional brain network suggests a high level of local neighborhood clustering, which has been the focus of **chapter 2** to **6**. Besides the high level of neighborhood clustering, a key characteristic of the small-world organization of the brain network is it's short average functional travel distance between any two regions of the network (Sporns and Zwi, 2004; Stam, 2004; Salvador et al., 2005b; Achard et al., 2006). This average short travel distance suggests a high level of global communication efficiency

across the brain network (Eguiluz et al., 2005; Salvador et al., 2005b; Achard et al., 2006). So, functional brain networks are efficiently organized, but how is this level of communication efficiency linked to the brain's output, referring to our level of cognitive performance? Neuroimaging studies have linked human intellectual performance to the developmental course of specific high order brain regions (Shaw et al., 2006), total brain volume (Posthuma et al., 2002), focal brain structure (Thompson et al., 2001; Haier et al., 2004; Hulshoff Pol et al., 2006; Choi et al., 2008), brain fiber architecture (Chiang et al., 2009) and the functional dynamics of specific high cognitive brain regions (Duncan et al., 2000; Gray et al., 2003; Choi et al., 2008; Song et al., 2008), but it remains unknown how human intelligence is related to the overall topology of the functional brain network. In **chapter 7**, using voxel-wise graph analysis, we explored the overall organization of functional brain networks using resting-state fMRI recordings in relationship to the level of intellectual performance of the participants, as measured by the full scale Intelligence Quotient (IQ). Interestingly, we observed a strong negative association between the normalized path length lambda and IQ, demonstrating a strong positive link between the level of overall global communication efficiency within the brain network and intellectual performance (Van den Heuvel et al, 2009b). Support for our findings comes from resting-state magnetoencephalography (MEG) recordings, showing that higher educated participants have on average a lower path length than lower educated subjects (Micheloyannis et al., 2006). Furthermore, a very recent study also have showed a link between structural efficiency and intellectual performance (Li et al., 2009), providing strong support for our functional findings.

In our study, IQ was found not to be correlated with the normalized clustering-coefficient *gamma* or the total number of connections *k* of the network. This suggests that smarter brains do not necessarily have a higher level of *local* communication efficiency or a higher number of connections. Taken the results of *lambda, gamma* and *k* together, our findings suggest that our level of intelligence is associated to how *efficient* the functional connections of our brain are placed and to a lesser extent to the absolute overall level of communication within the network or to how strong the individual functional sub-networks are connected locally. In short, our findings suggest that the most efficiently globally organized brain networks belong to the most intelligent people (Van den Heuvel et al, 2009b).

Interestingly, as our data is solely based on resting-state connectivity data, and not based on fMRI recordings during the performance of a specific cognitive task that enters into the IQ score, our results suggest that intelligence is linked to the level of organization of the resting-state patterns

of the human brain. This suggest that human intelligence is not only related to how well a specific cognitive task can be performed, but also to how efficient the *intrinsic* functional connections of the brain are wired. As such, resting-state functional connectivity patterns may be predictive for cognitive performance. Such a resting-state network view of intelligence provides a new insight in the neuronal basis of intelligence.

As our study was based on the proposed voxel-wise representation of the brain network (**chapter 2**), we were able to examine the specific role of each node in the network in relationship to the IQ scores in high spatial detail. Most pronounced effects between IQ and normalized path length were found in the *medial frontal cortex* and *inferior parietal regions*, regions that tend to overlap with the *default mode network*. Interestingly, a recent study has indicated a direct positive association between the FA value of the cingulum tract and IQ (Chiang et al., 2009), suggesting a positive association between the quality of the structural connectivity architecture of the brain network and IQ. This is particular interesting as our results of **chapter 5** and **6** suggest that the cingulum plays an important role in structurally interconnecting the regions of the default mode network (Greicius et al., 2008; Van den Heuvel et al., 2008b; Van den Heuvel et al., 2009). The structural findings of Chiang et al. support our hypothesis that the observed association between the path length of these regions and IQ may indicate that a short path length of frontal and parietal regions plays a crucial role in efficient information processing across the brain network. Furthermore, also significant effects between full scale IQ and normalized path length were found within *superior temporal gyrus* and *inferior frontal gyrus*, regions that are often linked to language processing, overlapping *wernicke's* and *broca's areas*. These regional specific effects suggest that high-order cognitive regions of smarter brains have a more direct and therefore more efficient access to information across the brain network.

Interestingly, the critical role of a short path length in cortical networks has been noted before, showing that structural cortical networks are optimized towards a short average travel distance, due to the existence of important long-distance projections (Kaiser and Hilgetag, 2006). In this context, our results suggest that a short path length is crucial in efficient information processing and leading towards a high IQ. This suggests that functional brain networks may be optimized towards a high processing speed and efficient global information integration between the different regions of the network.

For decades, neuroscientists have been examining where in the brain intelligence may reside. Our study, suggests that the answer might be that it is everywhere. Previous studies have linked intelligence to the

morphological properties of specific gray and white matter regions, but it remained unknown whether and if so how human intelligence was related to the overall network organization of the functional brain. Our study, using graph analysis and resting-state fMRI demonstrates a direct relationship between the level of global communication efficiency across the functional brain network and intellectual performance. The strong negative association between IQ and path length suggest that a higher level of intellectual performance is related to a higher level of efficient information integration across the brain network. Our study suggests that the most efficiently organized brain networks belong to the most intelligent people.

conclusion

What can we learn from these studies? Well, clearly, our brain is a complex dynamic network. Although brain regions can have a specialized function and form functional sub-networks, all regions are in some way directly or indirectly functionally linked to each other, forming one efficiently organized integrative network. Highly connected hub-nodes are likely to play an important role in this efficient communication, as indicated by a possible scale-free organization. The possible small-world and scale-free organization marks an efficient and robust organization of the functional connections of the brain network. As all studies are based on resting-state fMRI data, they suggest that brain regions do not only communicate during the performance of their specific function, but that these regions continue to communicate to each other during rest. Our data suggest a high level of modularity of the brain network, indicating that during rest, brain regions form highly clustered resting-state networks, that tend to strongly overlap with known functional networks. This ongoing intrinsic intranetwork communication is likely to be facilitated by white matter pathways that structurally interconnect these brain regions, enabling fast ongoing neuronal communication between different regions of the network. Especially, the level of functional resting-state communication between brain regions is associated with the microstructural organization of the interconnecting white matter pathways. In turn, these resting-state networks are connected together, forming the full functional brain network. Interestingly, our findings showed that the level of how efficiently the global functional connections are placed across the brain network is predictive for our level of intellectual performance. Taken together, our findings suggest that our brain is a network of functionally and structurally linked regions, with an organization towards a high level of fast and efficient information processing and information integration.

discussion and future directions

Reading these results and conclusions will probably raise a lot of questions. We would like to discuss a number of issues of which we believe that they deserve special attention and future research.

it is a network, but what kind of network?

The main aim of this thesis was to examine the overall network organization of the functional brain. In contrast to previous studies, a voxel-wise approach was used, providing a new platform in which the brain network can be examined on a much higher resolution as done before. In our studies, we used the relative classic measures of clustering-coefficient and path length to examine the interregional and intraregional functional connectivity layout of the functional brain. The use of these classic network measures makes our results relative easy to interpret. The down-side of the use of these measures is that they are relative 'crude' measures of connectivity, providing only information about overall measures of local and global connectedness of the graph. Fortunately, the use of a voxel-wise approach allowed for a more exploratory examination of the normalized path length of each brain node (i.e. voxel) individually, providing important information about the more specific role of each brain region in the overall network (**chapter 7**). Interestingly, the proposed voxel-wise approach would be ideally to further combine with more advanced connectivity measures to examine the role of each specific brain region in the overall network. The possible scale-free organization of the functional brain network at a voxel level suggests the existence of highly connected hub-regions that take a central role and play an important role in the level of efficient communication within the network (Barabasi and Bonabeau, 2003). More specific graph measures have been introduced to identify and classify hub-nodes. *Centrality* measures mark the central role of each node in the network by defining how much of the total level of efficient information transports passes through a certain region. Hub-nodes tend to show a high level of *betweenness centrality*, as they form a bridge between the shortest travel distance between a large number of nodes in the network. From this definition it is easy to see that removing a hub-node is likely to increase the overall travel distance and therefore heavily affect the level of communication efficiency within the network. These more specific network measures give information about the more specific role of each node in the network and provide important information about the specific architecture of our brain (Sporns et al., 2007; Bassett et al., 2008; Buckner et al., 2009). They may form an interesting target area to better understand possible

altered connectivity in brain diseases, especially as targeted attack to hub-nodes is known to heavily decrease efficient global network communication (Albert et al., 2000; Goh et al., 2002). Furthermore, hub-node classification measures can be combined with participation measures to further probe the specific role of a hub-node. A hub-node can be classified as an intra-cluster provincial hub, connecting local nodes together into a clustered sub-network, or it can form a bridge between multiple sub-networks, forming a so-called inter-cluster connector hub. *Participation-index* measures have been successfully used to classify hub-regions in local structural networks (Sporns et al., 2007) and it would be interesting to explore the use of these measures to identify inter- and intra- resting-state network communication. In addition, other more advanced complex network measures have been suggested (Bullmore and Sporns, 2009), including *Assortativity*, *Efficiency* and *Synchronizability* measures. Furthermore, in this thesis we used clustering as an indication of modularity of the brain network. Recently, direct *modularity* measures have been successfully used to identify functional modules within brain networks, showing a strong modular organization of the functional brain network at rest (Ferrarini et al., 2009; Meunier et al., 2009; Chen et al., 2008). Interestingly, these results tend to overlap with the clustered RSNs, as revealed by the normalized cut group clustering approach (Chen et al., 2008). Furthermore, also *motif participation* has been successfully used to identify sub-groups within structural cortical networks (Sporns et al., 2007). Taken together, these advanced network measures may reveal new important information about the organization about the functional brain network, especially in a voxel-wise approach. Current studies of our lab are focused on examining how these advanced network measures can be used in a voxel-wise setting to examine the specific role of crucial nodes in the network in high spatial detail.

Such an examination brings up new challenges on the computational side, but also on the theoretical side, starting with how we define functional connectivity. In our studies, we used the simple measure of correlation, which is easy to understand, but other more sophisticated measures of functional coupling have been suggested, including partial correlation (Salvador et al., 2005b; Achard et al., 2006)(**chapter 6**) and non-linear coupling measures like *Synchronization Likelihood* (Stam et al., 2003). However, besides the issue of using which measure to use for functional connectivity, we may also need to re-think our definition of *functionally connected*. In most studies, a fixed threshold T or fixed number of k is used to define whether or not two voxels are connected, but this may not always overlap with the definition of a hub-node. In general, a hub-node is defined as a node with a large number of connections. However, in our current

definition of connectivity, this would mean that this node would have shown a high level of correlation between its time-series and the time-series of a large number of other nodes. But how can a connector hub, which is defined as a node that links multiple independent sub-networks together, show a high level of correlation with both the time-series of nodes of two unconnected sub-networks, especially when using slow fluctuating time patterns as in rs-fMRI? The use of very fast data collection, weighted graphs and/or dynamic connectivity measures (i.e. varying over time) may shed new light on this, as well as defining the number of connections of a node by normalizing it to its maximum level of connectivity. Future studies are aimed to explore these new measures.

indirect versus direct connections

In this thesis we defined the existence of functional connections between cortical voxels as the level of correlation between their resting-state fMRI time-series (Biswal et al., 1995; Cordes et al., 2001; Fox and Raichle, 2007), expressing the level of ongoing neuronal synchronization between these regions during rest (Nir et al., 2008; Shmuel and Leopold, 2008). However, when using *correlation* as a measure of functional connectivity, it remains unclear whether a high level of functional connectivity is reflecting *direct* or *indirect* communication between these regions. Correlating time-series can indicate that two brain regions are directly linked to each other, but a high level of correlation can also be mediated through means of a third region, reflecting indirect communication between the two target regions. As a result, measuring the level of coherent behavior between two regions by correlating their functional time-series could reflect both direct as well as indirect communication. In contrast, white matter pathways only reflect *direct* connections between brain regions. In **chapters 5** and **6**, Diffusion Tensor Imaging (DTI) was used to examine the structural core of functional resting-state networks, reconstructing the large white matter bundles of the brain that interconnect RSN regions. As DTI measures the *direct* structural connections between two brain regions and resting-state fMRI analysis may express both *direct* and *indirect* connections, the structural and functional connectivity results might only partially overlap. However, the results of **chapter 5** suggest that a large number of functionally linked RSN regions are directly structurally interconnected by white matter bundles. Interestingly, the existence of direct structural connections between these regions may suggests that a large number of the large-scale functional connections between RSN regions are likely to reflect *direct* functional connections, as at least the structural infrastructure is present to support direct neuronal communication. One way to focus on only the *direct* functional connections

of the brain network might be the use of *partial* correlation. Using partial correlation, the level of coherent behavior between the time-series of two regions is corrected for possible third-party effects on both of the regions, reflecting the level of unique functional connectivity between brain regions (Salvador et al., 2005b; Achard et al., 2006; Liu et al., 2008) (**chapter 6**). Comparing the *direct* functional and *direct* structural connections of the brain might provide more specific information about the relationship between the functional connections that connect regions into resting-state networks and the structural basis of these functional connections.

However, all of this remains quite a bit speculative as we do not know for sure whether the structural connections between RSN regions are actually used to facilitate the observed ongoing functional connectivity between brain regions during rest. It is believed that the measured (partial) correlation between the resting-state fMRI BOLD time-series of RSN regions reflects ongoing neuronal synchronization between these regions and a high level of ongoing (direct) functional connectivity (**chapters 2**,**3** and **4**). Indeed, our studies indicate the existence of structural white matter connections between RSN regions and this supports this idea of ongoing neuronal communication, as the reconstructed fiber connections reflect the existence of direct axonal connections between the synchronized neuronal populations. However, we do not know for sure whether these structural connections are actually used to transport information between RSN regions during rest. To answer the question whether the structural connections of our brain are actually used for the transport of ongoing neuronal communication between the RSN regions during rest we need to measure the activation of the interconnecting white matter bundles. Using fMRI it is possible to measure the activation patterns of grey matter, but until recently, it remained unclear how to measure activation of the interconnecting white matter tracts between gray matter regions *in vivo* using MR. Fortunately, very recently a new pioneering method has been proposed that assesses activation of white matter fibers by measuring morphological changes in diffusion profile of fiber bundles that occurs during transport of information along a white matter bundle (Mandl et al., 2008a). This new method, that is appropriately called *functional DTI,* enables the measurement of neuronal communication between resting-state network regions during rest. Especially, this new method could provide us with information about whether the found structural connections between RSN regions (**chapters 5** and **6**) are actually used to transport information between these regions during rest, believed to be needed for the synchronization of their activity patterns. As a welcome bonus, demonstrating that neuronal information is actually transported between RSN regions during rest would provide

supporting evidence for the idea that resting-state networks reflect meaningful functional brain networks. Therefore, in our opinion, future studies examining the neuronal communication between RSN regions during rest are of utmost importance.

functional versus structural networks

A related topic refers to the direct relationship between structural networks and functional networks. As discussed, several studies have shown a small-world organization of the functional brain network (Sporns and Zwi, 2004; Stam, 2004; Salvador et al., 2005a; Achard et al., 2006; Achard and Bullmore, 2007) (**chapter 2**). Also structural brain networks have been shown to be organized following a small-world fashion (Hagmann et al., 2007; He et al., 2007; Hagmann et al., 2008), which may indicate that such an organization forms a more general aspect of the brain. Furthermore, a few studies have shown a direct relationship between the functional and structural connections of the human brain, both during resting-state (Greicius et al., 2003) (**chapters 5** and **6**) and task performance (Toosy et al., 2004) as well as the other way around, showing a direct relationship between the organization of the structural connections of our brain and the functional behavior of the regions they connect (Koch et al., 2002) (Hagmann et al., 2007; Honey et al., 2009). These studies suggest a strong overlap between the functional and structural organization of the brain network. Indeed, the structural organization of a network is known to have a direct influence on its level of robustness, its capability to integrate information and to its level of local and global communication efficiency (Latora and Marchiori, 2001; Mathias and Gopal, 2001; Buzsaki and Draguhn, 2004; Grigorov, 2005; Achard and Bullmore, 2007). Moreover, at the neuronal level, the rule of wiring optimization has been suggested to be linked to both neuronal structure and function (Chklovskii, 2004; Chen et al., 2006). However, our brain is an ultra complex piece of machinery and although its functional and structural organization are definitely linked, we by no means try to suggest that it is a one-on-one relationship. Moreover, they are likely to differ on several points. A highly efficient small-world organized *structural* network can still produce random *functional* activity and connectivity and, vice versa, a random organized *structural* network is still able to show a high level of efficient *functional* communication. As an analogy, structural highways can be efficiently located between cities, but that does not mean that the traffic between these cities is also efficient, some roads can be empty, some can be jammed. The other way around is also true, inefficiently placed roads could still be used for effective transport. In summary, although it is evident that the functional and structural connectivity organizations of the brain are

linked, their exact relationship remains unknown. This calls for future structural and functional network studies to examine how the structural brain network is able to support the fast changing functional activation patterns of the brain network (Bullmore and Sporns, 2009).

resting-state versus task-state

One topic that needs special attention describes the issue of the relationship between our brain during resting-state and during active state. In this thesis, we have represented the functional brain network as a network of brain regions with functional connections between those regions that show a high level of *resting-state* functional connectivity. However, this is an extreme simplification of reality. Our brain is of course not always in a resting-state, but is often involved in the performance of a specific task, for example while we do our daily job, read the newspaper, drink coffee, lunch or drive home. How is the examined resting-state organization of our brain network related to these active states? This thesis does not provide direct information about this topic, but there is room for some speculative ideas. As discussed, one class of resting-state synchronizations is likely to reflect ongoing neuronal activation and synchronization related to specific ongoing cognitive processes during rest. Spontaneous activity within the *default mode network* is suggested to reflect the integration of cognitive and emotional processes (Greicius et al., 2003), mind-wandering (Mason et al., 2007) and self-related thoughts (Gusnard et al., 2001; Buckner et al., 2008), processes that are likely to continue during the absence of specific task. Interestingly, our results suggest that these ongoing functional connectivity patterns may be predictive for cognitive performance (**chapter 7**, Van den Heuvel et al. 2009b). Furthermore, a second class of coherent resting-state fluctuations might reflect spontaneous firing of neuronal populations that are linked by large bundles of axons. As such, resting-state synchronization reflects the intrinsic functional connections of the brain network. Neurons are known to continuously fire even in the absence of performing a task, continuously sending information to other neurons. This ongoing functional connectivity might be there to keep communication channels open for whenever information transfer is needed, keeping connected regions in a high state of readiness. In this way, ongoing resting-state functional connectivity could be like the 'sleep state' of your laptop. Although your laptop continues to use energy while it is in a sleep state, it is better than shutting it down every time we do not directly need it, as it is much faster up and ready for the times we do need it. Resting-state functional connections might reflect ongoing information integration needed for the existence and maintenance of

functional connections between specialized brain regions that can be used whenever a specific task is performed. Support for this idea comes from the findings that most of the resting-state networks (showing the more global functional connections of our brain) reflect networks of regions that share a common function and are known to often work together, like the cortical regions of the primary motor and primary visual systems, but also regions of attentional networks (Salvador et al., 2005b; Damoiseaux et al., 2006) (**chapter 3**). Keeping these functional systems in an active state of readiness may help to improve their performance and their reaction time. Indeed, a recent study has suggested that long term motor training significantly increases resting-state activity within primary motor regions (Xiong et al., 2008). Moreover, as training progresses, long-term structural connections might improve between these regions, which may include a higher level of microstructural organization and maybe a more dense myelinization of the interconnecting white matter bundles, to facilitate the increased ongoing neuronal communication. Indeed, studies have shown a direct relationship between the microstructural organization of white matter and task-related activation (Toosy et al., 2004). However, as said, all of this remains highly speculative and needs some solid proof.

methodological considerations

Some general methodological issues have to be considered when interpreting the results of our studies. The most important issues concern the origin of the resting-state fMRI signal and applying graph analysis techniques to functional neuroimaging MR data.

First, in this thesis we have used resting-state fMRI recordings to measure the functional connections of the human brain. However, as was mentioned in the introduction, the true neuronal basis of the resting-state fMRI signal is not yet fully understood. There is still an ongoing debate about whether the observed correlations between the resting-state fMRI signal reflect true neuronal synchronization, or whether these correlations arise from confounding physiological sources, like cardiac and respiratory signals. Cardiac and respiratory signals have an oscillating pattern which is known to have a direct effect on the measured fMRI BOLD signal. These oscillating patterns could influence the BOLD signal of two anatomically separate brain regions in a similar way and as a result may introduce artificial correlation between the time-series of these regions (Wise et al., 2004; Birn et al., 2006; Shmueli et al., 2007; Birn et al., 2008; Chang et al., 2009; van Buuren et al., 2009). Support for a possible neuronal basis of resting-state fMRI signals comes from studies who report that these cardiac and

respiratory oscillations have a different frequency pattern and therefore a different frequency related influence on resting-state correlations than the low resting-state frequencies of interest (0.01 - 0.1 Hz) (Cordes et al., 2000; Cordes et al., 2001). These studies showed that resting-state correlations between different gray matter brain regions are mainly dominated by lower frequencies (< 0.1 Hz) and only influenced to a minor extent by the contribution of higher cardiac and respiratory oscillations (> 0.3 Hz) (Cordes et al., 2000; Cordes et al., 2001). Moreover, filtering out cardiac and respiratory oscillations has been shown to still result in high temporal correlations between regions of the default mode network (van Buuren et al., 2009). In addition, most of the correlations are found within known functional networks (Damoiseaux et al., 2006) (chapter 3), supporting the notion that resting-state signals reflect meaningful oscillations. Furthermore, recent studies, combining fMRI with single cell recordings, have linked resting-state fMRI recordings directly to concurrent fluctuations of spontaneous neuronal firing, suggesting a direct link between resting-state fMRI signals and spontaneous neuronal activity. As a result, the general consensus is shifting more to the issue to what extent these patterns might be confounded by other sources of non-neural oscillations, like cardiac and respiratory oscillations, rather than if resting-state fMRI patterns reflect ongoing neuronal synchronization between anatomically separated brain regions at all. In our studies, a high acquisition frequency (2 scans every 1 second) was used, to effectively minimize the possible backfolding of distinct physiological signals into the resting-state frequencies of interest and enabling the proper filtering of these possible confounding effects before assessing voxel-wise connectivity (Cordes et al., 2000; Cordes et al., 2001). In summary, it is now widely believed and generally accepted that the coherence between resting-state fMRI recordings, at least in part, reflects ongoing spontaneous neuronal activity and functional connectivity of brain regions during rest. In this context, in this thesis the correlation between resting-state fMRI time-series was taken as a measure of voxel-wise functional connectivity.

A second issue is related to the used voxel-wise approach. In this thesis, we examined the overall organization of the functional brain network using graph analysis. The functional brain was represented as a network of all gray matter voxels (cortical and sub-cortical) with functional connections between those voxels that showed a high level of resting-state functional connectivity. As mentioned, most other studies have used a regional approach, using a predefined parcellation of the cortex in a relative small number of brain regions. However, a regional approach requires an arbitrary definition of these brain regions which could have an effect on the graph

characteristics. Indeed, a recent study demonstrated that using a different brain atlas will have a direct effect on the network organization of brain networks. Different parcellation strategies resulted in different topological parameters of the functional brain network (Wang et al., 2008). We used a voxel-wise approach, defining the functional brain as a network of interconnected gray matter voxels. As both a regional approach and voxel-wise approach revealed a small-world organization of the functional brain network, the use of a regional or voxel-wise approach does not seem to differ concerning the brain's small-world organization. However, things might be different when examining a possible scale-free organization. As mentioned, resting-state fMRI network studies using a regional approach have argued against a scale-free organization of the brain network. However, in contrast, our data did suggest a possible scale-free organization of the functional brain network at a high spatial voxel resolution. As such, a voxel-wise approach may provide additional information about the fundamental organization of the brain network (Eguiluz et al., 2005)(**chapter 2**). Furthermore, a high-resolution voxel-wise approach might provide additional information in comparison to a regional approach, especially concerning spatial localization of node dependent effects. A voxel-wise approach enables to examine the brain network in more spatial detail (**chapter 4**) and might provide us with a new insight in the special role of specific brain regions in the overall organization of the brain network (**chapter 7**) and provide information about the specific role of critical hub-nodes in the network.

However, there is no such thing as a free lunch. First, increasing the number of nodes of a network will also heavily increase the computational time of the network statistics. With ever increasing computer memory, increasing computational speed and clever algorithms to compute key graph characteristics this is likely to be solved over time, but for now it needs to be taken into account when designing a voxel-wise network study. Second, in our study, voxel-wise brain networks were formed of all gray matter voxels, selected on the basis of a cortical segmentation of the anatomical image. However, a large number of fMRI voxels is likely to contain at least for some part also white matter, an effect known as partial voluming. This is due to the relative large size of the fMRI voxels of 4 mm isotropic in relation to the thickness of gray matter cortex of ~2-3 mm. In theory, the inclusion of white matter might have an effect on the measured cortical resting-state fMRI BOLD signal and in turn on the computation of the small-world and scale-free properties of the cortical brain network. In **chapter 2** we performed a post-hoc analysis examining the organization of white matter and cerebral spinal fluid (CSF) voxels. This post-hoc analysis indicated that white matter

and CSF related correlations show a different organization in comparison to correlations between grey matter voxels and therefore are likely to only minimally influence the computed graph characteristics of the brain network. In addition, a related topic is that fMRI recordings have an intrinsic level of smoothness and this could introduce artificial inter-voxel correlations that are not related to neuronal activity. As a result, spatial smoothness could lead to an overestimation of the local inter-voxel correlations in the brain network and introduce a bias in the computation of the graph characteristics. However, incorporating spatial smoothness in the formation of the comparable random graphs did not change the nature of our findings, indicating that spatial smoothness is likely to only play a minor role on the computed small-world organization of the brain network (**chapter 2**).

Please note that the suggested effect of partial voluming (including the inclusion of white matter voxels) and to a lesser extent the effect of spatial smoothing do not only concern our voxel-wise network approach, but is also highly relevant for regional approaches. Moreover, partial voluming may play even a bigger problem in a group-based regional approach than in a subject-based voxel-wise approach. Using a fixed group-based anatomical template is likely to include a large number of white matter voxels directly into the estimation of the representative time-series of a region. This in contrast to our subject-based voxel-wise approach in which individual cortical segmentations were used to define the gray matter nodes of the networks.

Furthermore, a related topic refers to the 'size' of the graph, meaning the number of nodes and connections of the brain network. Using a voxel-wise approach defined the brain network in a much higher number of nodes, increasing the spatial resolution from ~90 regions to ~9500 voxels. However, scale-free properties are normally only reported of substantial large networks consisting of a large number of nodes (Barabasi and Bonabeau, 2003), like for example the world wide web etc (Albert et al., 2000), as it requires a very large number of nodes and connections to have nodes that have many more times the number of connections than an average node of the network. Therefore, it may be questionable to examine the scale-free properties of networks with a small size. This includes the regional studies, examining small networks of 90 brain regions, but likely also our voxel-wise approach of 'only' 10000 nodes. Although a voxel-wise examination of the brain network tends to suggest a possible scale-free organization of our brain for high threshold T, also in our studies the network size is still very small compared to networks like the WWW, which (in 2009) counted well over a 100 million websites and well over 500 million documents (indexed in

2001)(wikipedia). Future studies are needed to examine whether we can map the scale-free properties of the brain network on a small voxel scale using high resolution fMRI acquired at ultra-high field strengths.

examining connectivity diseases

schizophrenia

The studies in this thesis have been focused on examining the topology of the healthy brain network. However, it is important to note that these studies have been conducted with the purpose to explore the development of new methods for the examination of altered activity patterns and hypothesized disconnectivity effects in brain diseases. Our main focus is on schizophrenia, a severe psychiatric disease that is characterized by delusions and hallucinations, loss of emotion and disrupted thinking and behavior. Schizophrenia has been suggested to be a disconnection disease and widespread functional disconnectivity between brain regions has been considered to underly cognitive dysfunction in schizophrenia (Friston and Frith, 1995; Andreasen et al., 1998; Friston, 1998; Kim et al., 2003; Kim et al., 2005; Bluhm et al., 2007; Zhou et al., 2007a). Examining the default state and the organization of the functional brain network of schizophrenic patients could provide new information about impaired brain communication and functional disconnectivity in schizophrenia. Schizophrenia is known to have aberrant effects on gray and white matter (Hulshoff Pol et al., 2001; Hulshoff Pol et al., 2004; van Haren et al., 2007), overlapping regions of the default mode network. Indeed, aberrant default mode functional connectivity has been shown to play a role in schizophrenia, reporting on a decrease in functional connectivity between medial frontal cortex and precuneus, key regions of this network (Bluhm et al., 2007; Whitfield-Gabrieli et al., 2009). Interestingly, also altered levels of white matter integrity has been reported in schizophrenia (Kubicki et al., 2002; Kubicki et al., 2005a; Kubicki et al., 2005b; Kubicki et al., 2007; Mandl et al., 2008b), including decreased levels of microstructural organization in the cingulum tract (Sun et al., 2003; Nestor et al., 2007). In particular, as the cingulum tract is known to interconnect the MFC and PCC regions of the default mode network (Greicius et al., 2008) (**chapter 6**), decreased levels of default mode functional connectivity and decreased organization of the cingulum could play an interactive role in schizophrenia. Interestingly, a recent study has reported hyperactivity and hyperconnectivity of the default mode network in first-episode schizophrenic patients. Although these findings seem to contrast at first glance with the earlier reported decreased levels of default mode functional

connectivity in schizophrenia (Bluhm et al., 2007), they do mark an important role for the default mode network in the psychopathology of schizophrenia (Whitfield-Gabrieli et al., 2009).

How can graph analysis help in the understanding of schizophrenia? Disruptions of functional connectivity across the brain network could lead to aberrant information integration across the brain network (Liu et al., 2008). Functional disconnectivity has been linked to altered connectivity of specific functional connections and/or functional networks (Bluhm et al., 2007; Zhou et al., 2007b; Whitfield-Gabrieli et al., 2009), but could also be related to a more global disruption functional organization of the brain network. Indeed, schizophrenic patients have been suggested to show a less overall efficient organization of the functional brain network (Micheloyannis et al., 2006; Liu et al., 2008). These studies indicate an important role for graph analysis in the examination of brain network alterations in schizophrenia. Especially, examining the brain network in high spatial detail could provide new insights in which brain regions have a differentiating role in the overall network organization in schizophrenic patients in comparison to healthy controls. For example, with the help of the applied voxel-wise graph analysis techniques we might be able to test the hypothesis whether in schizophrenic patients particular brain regions have an altered functional access to information across the brain network. In summary, examining the functional brain network of patients within a graph theoretical approach may help us to examine and better understand a possible disintegration of information in schizophrenia and, hopefully, at some point this will aid to a better treatment of this disease.

other neurodegenerative brain diseases

Although our main focus is on schizophrenia, it is evident that resting-state fMRI and graph analysis techniques can also play an important role in the understanding of other functional brain connectivity diseases, including other psychiatric diseases like bipolar disorder, but also diseases like multiple sclerosis (Lowe et al., 2008), Alzheimer's disease (Greicius et al., 2004; Rombouts et al., 2005; Stam et al., 2007; Buckner et al., 2008; Buckner et al., 2009) and amyotrophic lateral sclerosis. This is of special interest as these brain diseases are known to have destructive effect on white matter (Xie et al., 2005; Andrews-Hanna et al., 2007; Zhang et al., 2007; Lowe et al., 2008).

brain development, the rise and fall of the brain network

Besides examining brain connectivity diseases, it is evident that graph analysis techniques also form a valuable tool in understanding the

development of the brain during aging. It is well known that in young children and during adolescence, as well as during older aging, both gray matter and white matter structures in the brain change, a process that is suggested to be highly influenced by genetic factors (Shaw et al., 2008; Peper et al., 2009; Peper et al. 2007). These structural changes of the brain network mark an important role for possible functional network changes during brain development and aging. Cortical gray matter changes within young children and adolescents are likely to mark the maturation of the cortical nodes of the network and the white matter changes mark the development of the structural axonal connections between these regions. These structural pruning processes indicate the possible changes of specific functional networks during aging. Indeed, recent studies have shown developing default mode network connectivity in younger children over time (Fair et al., 2008) and a decrease in default mode connectivity during older aging (Damoiseaux et al., 2007), with even anti-correlated effects in old age (Andrews-Hanna et al., 2007). These studies clearly demonstrate that functional connectivity is a dynamic process during aging. However, although recent studies have given us new insights about the development of individual cortical regions and individual white matter structures during aging and specific functional connectivity changes, less is known about a possible change of overall network topology during brain development and aging. A recent resting-state/memory task EEG study has shown that brain development in young children and adolescence is related to a changing network topology, showing a developmental decrease in local clustering, as well as a shorter characteristic path normalized path length indicating a shift towards a more global organized network organization (Micheloyannis et al., 2009). Interestingly, recent resting-state fMRI studies have reported that the organization of functional networks may shift from a more local anatomical emphasis in children to a more global orientation in adults (Fair et al., 2009) and evolving community structure in aging (Meunier et al., 2009). Interpreted in the view of our observed negative association between IQ and path length, these findings may suggest that brain development is related to an increase in efficient global integration and supports the idea that the functional brain networks show an optimization towards a high level of information integration and information processing speed.

Interestingly, functional brain network organization has been suggested to be influenced by genetic factors (Smit et al., 2008) as are white matter and gray matter organization (Chiang et al. 2009, Hulshoff Pol et al. 2006, Peper et al., 2009). This marks the importance of examining genetic influences of network topology during aging. More specifically, they may provide new insight in the neuronal network re-organization underlying the

believed increasing network efficiency of brain networks during brain development. We think that resting-state fMRI analysis may play an important role in this, especially a voxel-wise approach. It allows for testing the hypothesis of developing integration patterns between multiple brain regions and the potential increasing role of specific brain regions in the overall brain network during brain development. A voxel-wise approach may provide new information about how cognitive development is related to changes in of overall network topology during brain development. Especially, we believe that a voxel approach potentially allows for the examination of how functional synchronization patterns develop during aging and how these processes are influenced by underlying genetic factors. In short, we believe that novel graph analysis techniques may play a crucial role in examining the rise and fall of functional brain networks during brain development and aging.

final words

The main aim of this thesis was to probe the complex organization of the functional brain network at a high spatial resolution using voxel-wise resting-state fMRI and novel graph analysis techniques. We aimed to show that combining new voxel-wise graph techniques with resting-state functional neuroimaging data can provide important new information about the intrinsic organization of the brain network. Our studies clearly mark that our brain is a highly integrative, complex but efficiently organized network of functionally and structurally interconnected regions.

references

Achard S, Bullmore E (2007) Efficiency and cost of economical brain functional networks. PLoS Comput Biol 3:e17.

Achard S, Salvador R, Whitcher B, Suckling J, Bullmore E (2006) A resilient, low-frequency, small-world human brain functional network with highly connected association cortical hubs. J Neurosci 26:63-72.

Albert R, Jeong H, Barabasi AL (2000) Error and attack tolerance of complex networks. Nature 406:378-382.

Andreasen NC, Paradiso S, O'Leary DS (1998) "Cognitive dysmetria" as an integrative theory of schizophrenia: a dysfunction in cortical-subcortical-cerebellar circuitry? Schizophr Bull 24:203-218.

Andrews-Hanna JR, Snyder AZ, Vincent JL, Lustig C, Head D, Raichle ME, Buckner RL (2007) Disruption of large-scale brain systems in advanced aging. Neuron 56:924-935.

Barabasi AL, Bonabeau E (2003) Scale-free networks. Sci Am 288:60-69.

Bassett DS, Bullmore E, Verchinski BA, Mattay VS, Weinberger DR, Meyer-Lindenberg A (2008) Hierarchical organization of human cortical networks in health and schizophrenia. J Neurosci 28:9239-9248.

Beckmann CF, DeLuca M, Devlin JT, Smith SM (2005) Investigations into resting-state connectivity using independent component analysis. Philos Trans R Soc Lond B Biol Sci 360:1001-1013.

Birn RM, Diamond JB, Smith MA, Bandettini PA (2006) Separating respiratory-variation-related fluctuations from neuronal-activity-related fluctuations in fMRI. Neuroimage 31:1536-1548.

Birn RM, Smith MA, Jones TB, Bandettini PA (2008) The respiration response function: the temporal dynamics of fMRI signal fluctuations related to changes in respiration. Neuroimage 40:644-654.

Biswal B, Yetkin FZ, Haughton VM, Hyde JS (1995) Functional connectivity in the motor cortex of resting human brain using echo-planar MRI. Magn Reson Med 34:537-541.

Bluhm RL, Miller J, Lanius RA, Osuch EA, Boksman K, Neufeld R, Theberge J, Schaefer B, Williamson P (2007) Spontaneous Low-Frequency Fluctuations in the BOLD Signal in Schizophrenic Patients: Anomalies in the Default Network. Schizophr Bull 33:1004-1012.

Broyd SJ, Demanuele C, Debener S, Helps SK, James CJ, Sonuga-Barke EJ (2008) Default-mode brain dysfunction in mental disorders: A systematic review. Neurosci Biobehav Rev.

Buckner RL, Andrews-Hanna JR, Schacter DL (2008) The brain's default network: anatomy, function, and relevance to disease. Ann N Y Acad Sci 1124:1-38.

Buckner RL, Sepulcre J, Talukdar T, Krienen FM, Liu H, Hedden T, Andrews-Hanna JR, Sperling RA, Johnson KA (2009) Cortical hubs revealed by intrinsic functional connectivity: mapping, assessment of stability, and relation to Alzheimer's disease. J Neurosci 29:1860-1873.

Bullmore E, Sporns O (2009) Complex brain networks: graph theoretical analysis of structural and functional systems. Nat Rev Neurosci 10:186-198.

Buzsaki G, Draguhn A (2004) Neuronal oscillations in cortical networks. Science 304:1926-1929.

Calhoun VD, Adali T, Pearlson GD, Pekar JJ (2001) A method for making group inferences from functional MRI data using independent component analysis. Hum Brain Mapp 14:140-151.

Callaway DS, Newman ME, Strogatz SH, Watts DJ (2000) Network robustness and fragility: percolation on random graphs. Phys Rev Lett 85:5468-5471.

Chang C, Cunningham JP, Glover GH (2009) Influence of heart rate on the BOLD signal: the cardiac response function. Neuroimage 44:857-869.

Chen BL, Hall DH, Chklovskii DB (2006) Wiring optimization can relate neuronal structure and function. Proc Natl Acad Sci U S A 103:4723-4728.

Chen ZJ, He Y, Rosa-Neto P, Germann J, Evans AC (2008) Revealing modular architecture of human brain structural networks by using cortical thickness from MRI. Cereb Cortex 18:2374-2381.

Chiang MC, Barysheva M, Shattuck DW, Lee AD, Madsen SK, Avedissian C, Klunder AD, Toga AW, McMahon KL, de Zubicaray GI, Wright MJ, Srivastava A, Balov N, Thompson PM (2009) Genetics of Brain Fiber Architecture and Intellectual Performance. J Neurosci 29:2212-2224.

Chklovskii DB (2004) Synaptic connectivity and neuronal morphology: two sides of the same coin. Neuron 43:609-617.

Chklovskii DB, Schikorski T, Stevens CF (2002) Wiring optimization in cortical circuits. Neuron 34:341-347.

Choi YY, Shamosh NA, Cho SH, DeYoung CG, Lee MJ, Lee JM, Kim SI, Cho ZH, Kim K, Gray JR, Lee KH (2008) Multiple bases of human intelligence revealed by cortical thickness and neural activation. J Neurosci 28:10323-10329.

Cordes D, Haughton VM, Arfanakis K, Wendt GJ, Turski PA, Moritz CH, Quigley MA, Meyerand ME (2000) Mapping functionally related regions of brain with functional connectivity MR imaging. AJNR Am J Neuroradiol 21:1636-1644.

Cordes D, Haughton VM, Arfanakis K, Carew JD, Turski PA, Moritz CH, Quigley MA, myelination rand ME (2001) Frequencies contributing to functional connectivity in the cerebral cortex in "resting-state" data. AJNR Am J Neuroradiol 22:1326-1333.

Damoiseaux JS, Rombouts SA, Barkhof F, Scheltens P, Stam CJ, Smith SM, Beckmann CF (2006) Consistent resting-state networks across healthy subjects. Proc Natl Acad Sci U S A 103:13848-13853.

De Luca M, Beckmann CF, De Stefano N, Matthews PM, Smith SM (2006) fMRI resting state networks define distinct modes of long-distance interactions in the human brain. Neuroimage 29:1359-1367.

Duncan J, Seitz RJ, Kolodny J, Bor D, Herzog H, Ahmed A, Newell FN, Emslie H (2000) A neural basis for general intelligence. Science 289:457-460.

Eguiluz VM, Chialvo DR, Cecchi GA, Baliki M, Apkarian AV (2005) Scale-free brain functional networks. Phys Rev Lett 94:018102.

Fair DA, Cohen AL, Dosenbach NU, Church JA, Miezin FM, Barch DM, Raichle ME, Petersen SE, Schlaggar BL (2008) The maturing architecture of the brain's default network. Proc Natl Acad Sci U S A 105:4028-4032.

Fair DA, Cohen AL, Power JD, Dosenbach NU, Church JA, Miezin FM, Schlaggar BL, Petersen SE (2009) Functional brain networks develop from a "local to distributed" organization. PLoS Comput Biol 5:e1000381.

Ferrarini L, Veer IM, Baerends E, van Tol MJ, Renken RJ, van der Wee NJ, Veltman DJ, Aleman A, Zitman FG, Penninx BW, van Buchem MA, Reiber JH, Rombouts SA, Milles J (2009) Hierarchical functional modularity in the resting-state human brain. Hum Brain Mapp 30:2220-2231.

Fox MD, Raichle ME (2007) Spontaneous fluctuations in brain activity observed with functional magnetic resonance imaging. Nat Rev Neurosci 8:700-711.

Friston KJ (1998) The disconnection hypothesis. Schizophr Res 30:115-125.

Friston KJ, Frith CD (1995) Schizophrenia: a disconnection syndrome? Clin Neurosci 3:89-97.

Goh KI, Oh E, Jeong H, Kahng B, Kim D (2002) Classification of scale-free networks. Proc Natl Acad Sci U S A 99:12583-12588.

Gray JR, Chabris CF, Braver TS (2003) Neural mechanisms of general fluid intelligence. Nat Neurosci 6:316-322.

Greicius MD, Krasnow B, Reiss AL, Menon V (2003) Functional connectivity in the resting brain: a network analysis of the default mode hypothesis. Proc Natl Acad Sci U S A 100:253-258.

Greicius MD, Srivastava G, Reiss AL, Menon V (2004) Default-mode network activity distinguishes Alzheimer's disease from healthy aging: evidence from functional MRI. Proc Natl Acad Sci U S A 101:4637-4642.

Greicius MD, Supekar K, Menon V, Dougherty RF (2008) Resting-State Functional Connectivity Reflects Structural Connectivity in the Default Mode Network. Cereb Cortex.

Grigorov MG (2005) Global properties of biological networks. Drug Discov Today 10:365-372.

Gusnard DA, Raichle ME, Raichle ME (2001) Searching for a baseline: functional imaging and the resting human brain. Nat Rev Neurosci 2:685-694.

Hagmann P, Kurant M, Gigandet X, Thiran P, Wedeen VJ, Meuli R, Thiran JP (2007) Mapping human whole-brain structural networks with diffusion MRI. PLoS ONE 2:e597.

Hagmann P, Cammoun L, Gigandet X, Meuli R, Honey CJ, Wedeen VJ, Sporns O (2008) Mapping the Structural Core of Human Cerebral Cortex. PLoS Biol 6:e159.

Haier RJ, Jung RE, Yeo RA, Head K, Alkire MT (2004) Structural brain variation and general intelligence. Neuroimage 23:425-433.

He Y, Chen ZJ, Evans AC (2007) Small-world anatomical networks in the human brain revealed by cortical thickness from MRI. Cereb Cortex 17:2407-2419.

Honey CJ, Sporns O, Cammoun L, Gigandet X, Thiran JP, Meuli R, Hagmann P (2009) Predicting human resting-state functional connectivity from structural connectivity. Proc Natl Acad Sci U S A 106:2035-2040.

Hulshoff Pol HE, Schnack HG, Posthuma D, Mandl RC, Baare WF, van Oel C, van Haren NE, Collins DL, Evans AC, Amunts K, Burgel U, Zilles K, de Geus E, Boomsma DI, Kahn RS (2006) Genetic contributions to human brain morphology and intelligence. J Neurosci 26:10235-10242.

Hulshoff Pol HE, Schnack HG, Mandl RC, Cahn W, Collins DL, Evans AC, Kahn RS (2004) Focal white matter density changes in schizophrenia: reduced inter-hemispheric connectivity. Neuroimage 21:27-35.

Hulshoff Pol HE, Schnack HG, Mandl RC, van Haren NE, Koning H, Collins DL, Evans AC, Kahn RS (2001) Focal gray matter density changes in schizophrenia. Arch Gen Psychiatry 58:1118-1125.

Kaiser M, Martin R, Andras P, Young MP (2007) Simulation of robustness against lesions of cortical networks. Eur J Neurosci 25:3185-3192.

Kim JJ, Ho Seok J, Park HJ, Soo Lee D, Chul Lee M, Kwon JS (2005) Functional disconnection of the semantic networks in schizophrenia. Neuroreport 16:355-359.

Kim JJ, Kwon JS, Park HJ, Youn T, Kang DH, Kim MS, Lee DS, Lee MC (2003) Functional disconnection between the prefrontal and parietal cortices during working memory processing in schizophrenia: a[15 (O)]H2O PET study. Am J Psychiatry 160:919-923.

Koch MA, Norris DG, Hund-Georgiadis M (2002) An investigation of functional and anatomical connectivity using magnetic resonance imaging. Neuroimage 16:241-250.

Kubicki M, McCarley RW, Shenton ME (2005a) Evidence for white matter abnormalities in schizophrenia. Curr Opin Psychiatry 18:121-134.
Kubicki M, McCarley R, Westin CF, Park HJ, Maier S, Kikinis R, Jolesz FA, Shenton ME (2007) A review of diffusion tensor imaging studies in schizophrenia. J Psychiatr Res 41:15-30.
Kubicki M, Westin CF, Maier SE, Frumin M, Nestor PG, Salisbury DF, Kikinis R, Jolesz FA, McCarley RW, Shenton ME (2002) Uncinate fasciculus findings in schizophrenia: a magnetic resonance diffusion tensor imaging study. Am J Psychiatry 159:813-820.
Kubicki M, Park H, Westin CF, Nestor PG, Mulkern RV, Maier SE, Niznikiewicz M, Connor EE, Levitt JJ, Frumin M, Kikinis R, Jolesz FA, McCarley RW, Shenton ME (2005b) DTI and MTR abnormalities in schizophrenia: analysis of white matter integrity. Neuroimage 26:1109-1118.
Latora V, Marchiori M (2001) Efficient behavior of small-world networks. Phys Rev Lett 87:198701.
Li Y, Liu Y, Li J, Qin W, Li K, Yu C, Jiang T (2009) Brain anatomical network and intelligence. PLoS Comput Biol 5:e1000395.
Liu H, Liu Z, Liang M, Hao Y, Tan L, Kuang F, Yi Y, Xu L, Jiang T (2006) Decreased regional homogeneity in schizophrenia: a resting state functional magnetic resonance imaging study. Neuroreport 17:19-22.
Liu Y, Liang M, Zhou Y, He Y, Hao Y, Song M, Yu C, Liu H, Liu Z, Jiang T (2008) Disrupted small-world networks in schizophrenia. Brain 131:945.
Lowe MJ, Beall EB, Sakaie KE, Koenig KA, Stone L, Marrie RA, Phillips MD (2008) Resting state sensorimotor functional connectivity in multiple sclerosis inversely correlates with transcallosal motor pathway transverse diffusivity. Hum Brain Mapp.
Mandl RC, Schnack HG, Zwiers MP, van der Schaaf A, Kahn RS, Hulshoff Pol HE (2008a) Functional diffusion tensor imaging: measuring task-related fractional anisotropy changes in the human brain along white matter tracts. PLoS ONE 3:e3631.
Mandl RC, Schnack HG, Luigjes J, van den Heuvel MP, Cahn W, Kahn RS, Hulshoff Pol HE (2008b) Tract-based Analysis of Magnetization Transfer Ratio and Diffusion Tensor Imaging of the Frontal and Frontotemporal Connections in Schizophrenia. Schizophr Bull.
Mason MF, Norton MI, Van Horn JD, Wegner DM, Grafton ST, Macrae CN (2007) Wandering minds: the default network and stimulus-independent thought. Science 315:393-395.
Mathias N, Gopal V (2001) Small worlds: how and why. Phys Rev E Stat Nonlin Soft Matter Phys 63:021117.

Meunier D, Achard S, Morcom A, Bullmore E (2009) Age-related changes in modular organization of human brain functional networks. Neuroimage 44:715-723.

Micheloyannis S, Pachou E, Stam CJ, Breakspear M, Bitsios P, Vourkas M, Erimaki S, Zervakis M (2006) Small-world networks and disturbed functional connectivity in schizophrenia. Schizophr Res 87:60-66.

Micheloyannis S, Vourkas M, Tsirka V, Karakonstantaki E, Kanatsouli K, Stam CJ (2009) The influence of ageing on complex brain networks: a graph theoretical analysis. Hum Brain Mapp 30:200-208.

Nestor PG, Kubicki M, Spencer KM, Niznikiewicz M, McCarley RW, Shenton ME (2007) Attentional networks and cingulum bundle in chronic schizophrenia. Schizophr Res 90:308-315.

Nir Y, Mukamel R, Dinstein I, Privman E, Harel M, Fisch L, Gelbard-Sagiv H, Kipervasser S, Andelman F, Neufeld MY, Kramer U, Arieli A, Fried I, Malach R (2008) Interhemispheric correlations of slow spontaneous neuronal fluctuations revealed in human sensory cortex. Nat Neurosci 11:8.

Peper JS, Schnack HG, Brouwer RM, Van Baal GC, Pjetri E, Szekely E, van Leeuwen M, van den Berg SM, Collins DL, Evans AC, Boomsma DI, Kahn RS, Hulshoff Pol HE (2009) Heritability of regional and global brain structure at the onset of puberty: A magnetic resonance imaging study in 9-year-old twin pairs. Hum Brain Mapp.

Peper JS, Brouwer RM, Boomsma DI, Kahn RS, Hulshoff Pol HE (2007) Genetic influences on human brain structure: a review of brain imaging studies in twins. Hum Brain Mapp 28:464-473.

Posthuma D, De Geus EJ, Baare WF, Hulshoff Pol HE, Kahn RS, Boomsma DI (2002) The association between brain volume and intelligence is of genetic origin. Nat Neurosci 5:83-84.

Rombouts SA, Barkhof F, Goekoop R, Stam CJ, Scheltens P (2005) Altered resting state networks in mild cognitive impairment and mild Alzheimer's disease: an fMRI study. Hum Brain Mapp 26:231-239.

Rombouts SA, Damoiseaux JS, Goekoop R, Barkhof F, Scheltens P, Smith SM, Beckmann CF (2009) Model-free group analysis shows altered BOLD FMRI networks in dementia. Hum Brain Mapp 30:256-266.

Salvador R, Suckling J, Schwarzbauer C, Bullmore E (2005a) Undirected graphs of frequency-dependent functional connectivity in whole brain networks. Philos Trans R Soc Lond B Biol Sci 360:937-946.

Salvador R, Suckling J, Coleman MR, Pickard JD, Menon D, Bullmore E (2005b) Neurophysiological architecture of functional magnetic resonance images of human brain. Cereb Cortex 15:1332-1342.

Shaw P, Greenstein D, Lerch J, Clasen L, Lenroot R, Gogtay N, Evans A, Rapoport J, Giedd J (2006) Intellectual ability and cortical development in children and adolescents. Nature 440:676-679.

Shaw P, Kabani NJ, Lerch JP, Eckstrand K, Lenroot R, Gogtay N, Greenstein D, Clasen L, Evans A, Rapoport JL, Giedd JN, Wise SP (2008) Neurodevelopmental trajectories of the human cerebral cortex. J Neurosci 28:3586-3594.

Shmuel A, Leopold DA (2008) Neuronal correlates of spontaneous fluctuations in fMRI signals in monkey visual cortex: Implications for functional connectivity at rest. Hum Brain Mapp.

Shmueli K, van Gelderen P, de Zwart JA, Horovitz SG, Fukunaga M, Jansma JM, Duyn JH (2007) Low-frequency fluctuations in the cardiac rate as a source of variance in the resting-state fMRI BOLD signal. Neuroimage 38:306-320.

Song M, Zhou Y, Li J, Liu Y, Tian L, Yu C, Jiang T (2008) Brain spontaneous functional connectivity and intelligence. Neuroimage 41:1168-1176.

Sporns O, Zwi JD (2004) The small world of the cerebral cortex. Neuroinformatics 2:145-162.

Sporns O, Honey CJ, Kotter R (2007) Identification and classification of hubs in brain networks. PLoS ONE 2:e1049.

Sporns O, Chialvo DR, Kaiser M, Hilgetag CC (2004) Organization, development and function of complex brain networks. Trends Cogn Sci 8:418-425.

Stam CJ (2004) Functional connectivity patterns of human magnetoencephalographic recordings: a 'small-world' network? Neurosci Lett 355:25-28.

Stam CJ, Reijneveld JC (2007) Graph theoretical analysis of complex networks in the brain. Nonlinear Biomed Phys 1:3.

Stam CJ, Breakspear M, van Cappellen van Walsum AM, van Dijk BW (2003) Nonlinear synchronization in EEG and whole-head MEG recordings of healthy subjects. Hum Brain Mapp 19:63-78.

Stam CJ, Jones BF, Nolte G, Breakspear M, Scheltens P (2007) Small-world networks and functional connectivity in Alzheimer's disease. Cereb Cortex 17:92-99.

Smit DJ, Stam CJ, Posthuma D, Boomsma DI, de Geus EJ (2008) Heritability of "small-world" networks in the brain: a graph theoretical analysis of resting-state EEG functional connectivity. Hum Brain Mapp 29:1368-1378.

Sun Z, Wang F, Cui L, Breeze J, Du X, Wang X, Cong Z, Zhang H, Li B, Hong N, Zhang D (2003) Abnormal anterior cingulum in patients with

schizophrenia: a diffusion tensor imaging study. Neuroreport 14:1833-1836.

Thompson PM, Cannon TD, Narr KL, van Erp T, Poutanen VP, Huttunen M, Lonnqvist J, Standertskjold-Nordenstam CG, Kaprio J, Khaledy M, Dail R, Zoumalan CI, Toga AW (2001) Genetic influences on brain structure. Nat Neurosci 4:1253-1258.

Toosy AT, Ciccarelli O, Parker GJ, Wheeler-Kingshott CA, Miller DH, Thompson AJ (2004) Characterizing function-structure relationships in the human visual system with functional MRI and diffusion tensor imaging. Neuroimage 21:1452-1463.

Toroczkai Z, Bassler KE (2004) Network dynamics: jamming is limited in scale-free systems. Nature 428:716.

van Buuren M, Gladwin TE, Zandbelt BB, van den Heuvel M, Ramsey NF, Kahn RS, Vink M (2009) Cardiorespiratory effects on default-mode network activity as measured with fMRI. Hum Brain Mapp.

Van den Heuvel MP, Mandl RC, Hulshoff Pol HE (2008a) Normalized group clustering of resting-state fMRI data. PLoS ONE 3:e2001.

Van den Heuvel MP, Mandl RC, Luigjes J, Hulshoff Pol HE (2008c) Microstructural organization of the cingulum tract and the level of default mode functional connectivity. J Neurosci 28:7.

Van den Heuvel MP, Stam CJ, Boersma M, Hulshoff Pol HE (2008c) Small-world and scale-free organization of voxel based resting-state functional connectivity in the human brain. Neuroimage 43:11.

Van den Heuvel MP, Mandl RCW, Kahn RS, Hulshoff Pol HE (2009) Functionally linked resting-state networks reflect the underlying structural connectivity architecture of the human brain. Human Brain MappingIn Press.

Van den Heuvel MP, Stam CJ, Kahn RS, Hulshoff Pol HE (2009b) Efficiency of functional brain networks and intellectual performance. J Neurosci 29(23):7619-24.

van Haren NE, Hulshoff Pol HE, Schnack HG, Cahn W, Mandl RC, Collins DL, Evans AC, Kahn RS (2007) Focal gray matter changes in schizophrenia across the course of the illness: a 5-year follow-up study. Neuropsychopharmacology 32:2057-2066.

Vincent JL, Kahn I, Snyder AZ, Raichle ME, Buckner RL (2008) Evidence for a Frontoparietal Control System Revealed by Intrinsic Functional Connectivity. J Neurophysiol.

Wang J, Wang L, Zang Y, Yang H, Tang H, Gong Q, Chen Z, Zhu C, He Y (2008) Parcellation-dependent small-world brain functional networks: A resting-state fMRI study. Hum Brain Mapp.

Watts DJ, Strogatz SH (1998) Collective dynamics of 'small-world' networks. Nature 393:440-442.

Whitfield-Gabrieli S, Thermenos HW, Milanovic S, Tsuang MT, Faraone SV, McCarley RW, Shenton ME, Green AI, Nieto-Castanon A, Laviolette P, Wojcik J, Gabrieli JD, Seidman LJ (2009) Hyperactivity and hyperconnectivity of the default network in schizophrenia and in first-degree relatives of persons with schizophrenia. Proc Natl Acad Sci U S A.

Wise RG, Ide K, Poulin MJ, Tracey I (2004) Resting fluctuations in arterial carbon dioxide induce significant low frequency variations in BOLD signal. Neuroimage 21:1652-1664.

Xie S, Xiao JX, Wang YH, Wu HK, Gong GL, Jiang XX (2005) Evaluation of bilateral cingulum with tractography in patients with Alzheimer's disease. Neuroreport 16:1275-1278.

Xiong J, Ma L, Wang B, Narayana S, Duff EP, Egan GF, Fox PT (2008) Long-term motor training induced changes in regional cerebral blood flow in both task and resting states. Neuroimage.

Zhang Y, Schuff N, Jahng GH, Bayne W, Mori S, Schad L, Mueller S, Du AT, Kramer JH, Yaffe K, Chui H, Jagust WJ, Miller BL, Weiner MW (2007) Diffusion tensor imaging of cingulum fibers in mild cognitive impairment and Alzheimer disease. Neurology 68:13-19.

Zhou Y, Liang M, Tian L, Wang K, Hao Y, Liu H, Liu Z, Jiang T (2007a) Functional disintegration in paranoid schizophrenia using resting-state fMRI. Schizophr Res 97:194-205.

Zhou Y, Liang M, Jiang T, Tian L, Liu Y, Liu Z, Liu H, Kuang F (2007b) Functional dysconnectivity of the dorsolateral prefrontal cortex in first-episode schizophrenia using resting-state fMRI. Neurosci Lett 417:297-302.

nederlandse samenvatting

het verbonden brein

Eigenlijk hoeft u maar één boodschap van dit proefschrift te onthouden: ons brein is een netwerk. Maar dan wel één met een erg efficiënte organisatie.

Ons brein bestaat uit allerlei gebieden, elk met hun eigen taak en functie, maar al die gebieden moeten continue met elkaar samenwerken en informatie uitwisselen, en vormen zo één functioneel geïntegreerd netwerk. Ons brein bestaat uit miljarden cellen, neuronen genaamd, die met elkaar verbonden zijn door axonen. De neuronen worden grijze stof genoemd en zijn de 'reken-units' van het brein. De axonen noemen we de witte stof en je zou kunnen zeggen dat de witte stofbanen structurele informatiesnelwegen vormen tussen de verschillende gebieden van ons brein en zo functionele communicatie tussen de verschillende hersengebieden mogelijk maken. Al die grijze en witte stof moet continue miljarden bits aan informatie verwerken en integreren. Zo hebben we speciale hersengebieden die verantwoordelijk zijn voor het verwerken van visuele informatie van onze ogen, speciale gebieden die onze spieren aansturen, maar ook speciale gebieden die een belangrijke rol spelen in cognitieve taken, zoals het tijdelijk onthouden van een telefoonnummer of het uitrekenen van een moeilijke som. Functionele communicatie tussen al deze hersengebieden is cruciaal, gaat altijd door, en stelt ons in staat om snel en flexibel te reageren op situaties die we elke dag tegenkomen. Neem nu autorijden. Continu moet ons brein visuele informatie verwerken van de weg voor ons, deze informatie koppelen aan opgeslagen kennis over de auto's die om ons heen rijden, linken aan kennis over hoe de snelwegen lopen, al deze informatie integreren met onze intentie om te reizen van Utrecht naar Amsterdam om een goede vriend te gaan bezoeken en uiteindelijk de spieren aansturen om de auto te besturen. Maar hoe is ons breinnetwerk georganiseerd dat het in staat is om al deze verschillende vormen van informatie aan elkaar te koppelen?

In de laatste 20 jaar hebben functionele neuroimaging studies ons erg veel geleerd over de specifieke functies van de verschillende gebieden van het brein. Maar hoe de communicatie tussen deze gebieden is georganiseerd is vrijwel onbekend. Dit proefschrift gaat over het onderzoeken van deze organisatie met de kernvragen: (1) Hoe is het breinnetwerk georganiseerd? (2) hoe is functionele communicatie tussen de verschillende hersengebieden gerelateerd aan structurele witte stofverbindingen in het brein? en (3) hoe is het niveau van efficiëntie van ons breinnetwerk gerelateerd aan cognitief gedrag?

het brein bekijken als een netwerk

Waarom is het eigenlijk zo belangrijk om naar ons brein te kijken als een netwerk? Laten we dit bekijken door een parallel te trekken tussen ons brein en Nederland. Als we naar een satellietfoto van Nederland kijken (figuur 1.2, pagina 10) dan zien we duidelijk dat Nederland niet een verzameling is van losse steden, maar dat alle steden met elkaar verbonden zijn door snelwegen. Dit snelwegennet zorgt ervoor dat goederen vervoerd kunnen worden van A naar B en dat mensen kunnen reizen tussen hun woon en werkplek. Deze structurele snelwegen faciliteren functionele communicatie tussen de steden van Nederland. Als we nu Nederland bekijken als een netwerk van structureel en functioneel verbonden steden dan kan dit nieuwe informatie geven over hoe Nederland georganiseerd is. Zo zien we bijvoorbeeld dat een stad niet standaard verbonden is met alle andere steden, maar juist vaak meer verbonden is met maar een paar andere steden die ook weer sterk onderling verbonden zijn. Zo vormt bijvoorbeeld de randstad een sub-netwerk binnen het totale netwerk, omdat deze steden met name sterk onderling verbonden zijn en in mindere mate met de rest van de steden van Nederland. Verder kunt u zich eenvoudig voorstellen dat de organisatie van de structurele en functionele verbindingen tussen de steden van Nederland cruciaal is voor onze economie. Een goede verdeling van de wegen kan zorgen voor minder files en daardoor een efficiëntere communicatie tussen de steden, wat weer zou kunnen resulteren in een sterkere economie. Door Nederland te bekijken als een netwerk, kunnen we onderzoeken hoe en hoe efficiënt de goederentransport tussen de steden georganiseerd is en hoe het niveau van efficiëntie gelinkt is aan onze economie.

Net als Nederland is ons brein een netwerk. Onze hersenen bestaan uit allerlei gebieden, die elk hun eigen karakter en functie hebben, maar toch onderling sterk verbonden zijn, zowel structureel als functioneel. Als we nu

net als Nederland de hersenen bekijken als een netwerk van functioneel en structureel verbonden gebieden, dan kan dit nieuwe inzichten geven over kerneigenschappen van het menselijk brein. Zo kunnen we bekijken hoe functionele communicatie in ons brein is georganiseerd. Zijn er bepaalde gebieden die sterk onderling verbonden zijn en zo een sub-netwerk vormen? Hoe is functionele communicatie tussen de gebieden van ons brein mogelijk? Wordt dit gefaciliteerd door de structurele connecties van ons brein, zijnde de witte stofbanen? En hoe is het niveau van efficiëntie van functionele communicatie in ons brein gerelateerd aan cognitief gedrag? Hebben efficiënter georganiseerde breinnetwerken een hogere 'brein economie'? Samenvattend, kijken naar ons brein als een netwerk van structureel en functioneel verbonden gebieden kan ons nieuwe inzichten geven over hoe het menselijk brein georganiseerd is.

graaftheorie en netwerkorganisatie

Om de organisatie van het breinnetwerk te onderzoeken hebben we een theoretisch raamwerk nodig. 'graaftheorie' biedt uitkomst. Met gebruik van graaftheorie, kunnen we een netwerk beschrijven als een graaf, bestaande uit nodes die onderling met elkaar verbonden zijn door paden die connecties worden genoemd. In figuur n.1a ziet u zo'n voorbeeld van een als graaf weergegeven netwerk. Van de wiskunde klas komt u dit vast bekend voor. We kunnen ons vast nog wel de Euler-graaf herinneren, gedefinieerd door de grondlegger van de graaftheorie Leonhard Euler.

Graventheorie biedt een uitgebreid raamwerk om complexe systemen te bestuderen en om cruciale eigenschappen van de organisatie van een graaf te bestuderen, zoals de clustering-coëfficiënt, padlengte , en graad. De clustering-coëfficiënt geeft het niveau van lokale verbondenheid aan en is gedefinieerd als de ratio tussen het aantal verbindingen tussen de buren van een node en de totaal aantal mogelijke verbindingen (figuur n.1b). De padlengte van een graaf is gedefinieerd als de gemiddelde reisafstand tussen twee punten in de graaf en geeft informatie over de globale verbondenheid (figuur n.1c). De graad van een node is het aantal connecties dat een node heeft en de verdelingsfunctie van de graad beschrijft de kans dat een node in een graaf een bepaald aantal connecties heeft en samen geven ze informatie over de verbondenheid van een graaf (figuur n.1d).

Gezamenlijk geven de clustering-coëfficiënt, padlengte, en graad belangrijke informatie over de organisatie van een netwerk. Zogenaamde small-world netwerken hebben een hoge lokale clustering, reflecterend in een hoge clustering-coëfficiënt, maar nog wel met een gemiddelde korte globale reisafstand aangegeven door een korte gemiddelde padlengte . Watts

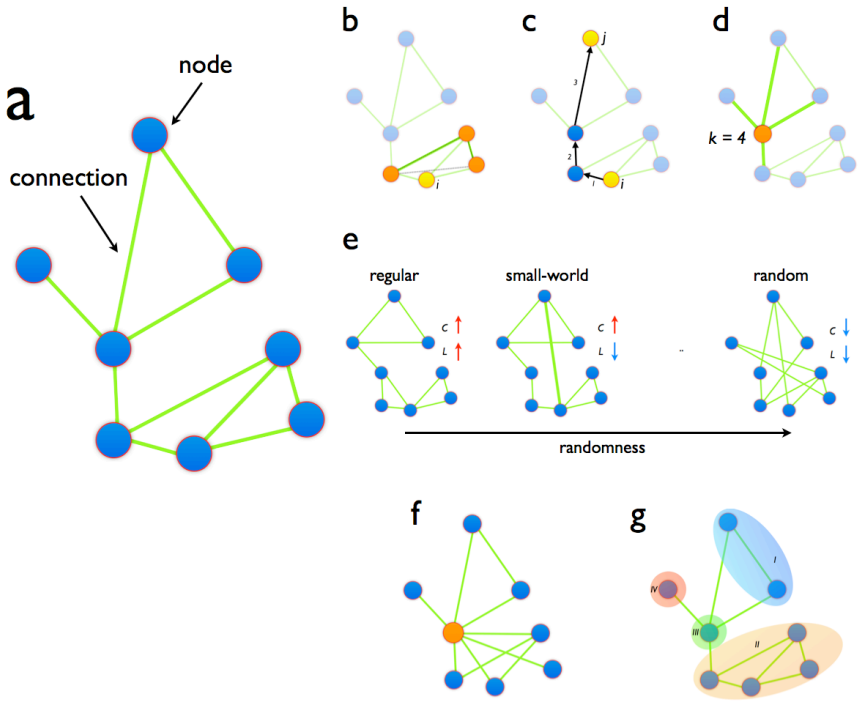

figuur n.1

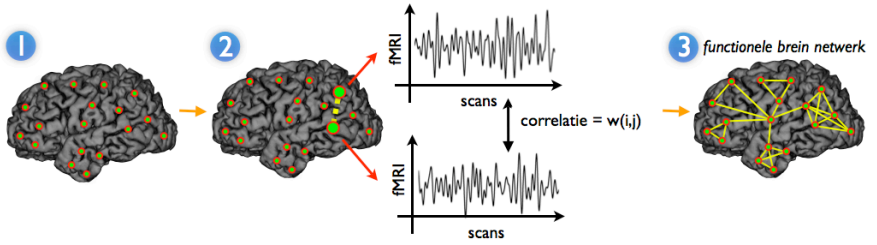

figuur n.2 het functionele breinnetwerk Het functionele breinnetwerk kan worden gerepresenteerd als een graaf met de verschillende hersengebieden als nodes (*1*). Functionele connectiviteit geeft de mate van correlatie tussen de hersenactiviteit van twee anatomisch gescheiden gebieden in het brein weer (2). Door nu voor alle hersengebieden hun mate van connectiviteit te berekenen en een connectie tussen twee gebieden weer te geven indien hun mate van connectiviteit boven een bepaalde drempel uit komt kunnen we een representatie maken functionele connectiviteit in het menselijk brein: het functionele breinnetwerk (*3*).

legenda of figuur n.1

een graaf (*a*) Een graaf is een theoretische beschrijving van een netwerk, bestaande uit een verzameling punten (nodes genaamd) met connecties tussen de nodes, welke een relatie tussen de verschillende punten van het netwerk aangeven. Met behulp van graaftheorie kunnen we de organisatie van een netwerk onderzoeken.

clustering-coëfficiënt, padlengte , graad
(*b*) De clustering-coëfficiënt van een node is de mate waarin de directe buren van de node onderling zelf weer verbonden zijn. De genormaliseerde clustering-coëfficiënt gamma geeft informatie over de mate van lokale clustering. (*c*) De padlengte van een node is de gemiddelde reisafstand tussen deze node en de rest van de de nodes in de graaf, met de reisafstand tussen twee punten gedefinieerd als het aantal verbindingen dat overgestoken moet worden om van een node naar een andere node te reizen. De genormaliseerde padlengte lambda geeft informatie over de mate van globale communicatie-efficiëntie in het netwerk. (*d*) De graad van een node is het aantal verbindingen dat een node heeft.

small-world, scale-free, modulair
(*e*) Een zogenaamd *small-world* netwerk is een netwerk met zowel een hoge clustering-coëfficiënt *gamma*, gezamenlijk met een korte gemiddelde reisafstand *lambda*. Watts en Storgatz lieten zien dat als je de connecties van een volledig gestructureerd netwerk (ook wel een regulier netwerk met een hoge clustering-coëfficiënt *C*, hoge padlengte *L*) één voor één willekeurig verbind en uiteindelijk een random netwerk overhoudt (lage *C*, lage *L*), dat bij een klein aantal herplaatsingen een small-world netwerk ontstaat met zowel een hoge clustering-coëfficiënt *C* en een korte padlengte *L*. De sterk verminderde padlengte (tov een regulier netwerk) komt door het ontstaan van een aantal langeafstandsverbindingen die cruciaal zijn voor snelle globale informatie overdracht. (*f*) In scale-free netwerken hebben de meeste nodes een laag aantal verbindingen, maar zijn er een paar hub-nodes die veel meer verbindingen hebben dan de rest. Scale-free netwerken hebben een graaddistributie met een power-law distributie. (*g*) Een modulair netwerk is gekenmerkt doordat er binnen het netwerk sub-netwerken zijn met nodes die onderling erg sterk verbonden en in mindere mate verbonden zijn met andere nodes uit andere sub-netwerken.

en Strogatz definieerden het begrip small-world netwerken en lieten zien dat in dit type netwerken een paar lange afstand verbindingen een cruciale rol spelen in het hoge niveau van globale communicatie-efficiëntie (Watts and Strogatz, 1998)(figuur n.1e). Daarnaast, hebben zogenaamde scale-free netwerken een graadverdeling waarin gemiddeld gezien de nodes van het netwerk een laag aantal verbindingen hebben, maar met de uitzondering van een klein aantal nodes dat veel meer verbindingen heeft dan de rest (Barabasi and Bonabeau, 2003). Deze nodes worden ook wel hub-nodes genoemd en spelen een cruciale rol in snel en efficiënt informatietransport in een netwerk (figuur n.1f). Verder vertoont een zogenaamde modulair netwerk de formatie van sterk onderling verbonden sub-netwerken in de totale netwerkorganisatie (figuur n.1g). Small-world, scale-free en modulaire

netwerken worden gekenmerkt door een hoge mate van lokale en globale efficiëntie met een hoog niveau van robuustheid en vormen zo een interessant model voor het breinnetwerk.

functionele connectiviteit

In het wegen-netwerk van Nederland hebben we functionele communicatie gedefinieerd als de hoeveelheid goederentransport tussen de steden. Maar hoe bepalen we functionele communicatie in het brein? Conventionele functionele imaging studies, zoals taak-fMRI studies, hebben ons veel geleerd over de specifieke rol van elk breingebied, maar geven geen informatie over functionele communicatie tussen de gebieden. Dit, omdat conventionele fMRI technieken elk breingebied apart bekijken en niet kijken naar verbanden tussen gebieden. In tegenstelling, nieuwere resting-state fMRI analyses kunnen wel informatie geven over functionele connectiviteit tussen hersengebieden. In een resting-state fMRI experiment wordt voor een bepaalde periode de spontane activiteit van het brein gemeten, dit alles tijdens rust. Vervolgens wordt gekeken hoe de activiteitspatronen van de verschillende breingebieden overeenkomen. Functionele connectiviteit tussen twee hersengebieden is gedefinieerd als de mate van correlatie tussen hun hersenactiviteitspatronen en wordt gezien als de mate van intrinsieke functionele communicatie tussen deze gebieden (Aertsen et al., 1989; Friston et al., 1993). Door te kijken naar de correlatie tussen resting-state fMRI-patronen kunnen we functionele connectiviteit in het brein bestuderen. Bovendien, door resting-state metingen te combineren met graaf analyses kunnen we de organisatie van intrinsieke functionele communicatie in het brein in kaart brengen. Door het hersenactiviteitspatroon van een specifiek gebied in het brein te vergelijken met het patroon van elk ander gebied, kunnen we kijken met welke hersengebieden ons gekozen gebied functioneel verbonden is. Als we nu op deze manier stuk voor stuk van alle hersengebieden hun functionele connecties in kaart brengen (figuur n.2), kunnen we een netwerk opbouwen van alle functioneel verbonden gebieden: het functionele breinnetwerk.

Een klein aantal pionierende neuroimaging studies hebben de organisatie van het functionele breinnetwerk onderzocht en hebben laten zien dat ons brein een zeer efficiënte small-world organisatie heeft (Sporns and Zwi, 2004; Stam, 2004; Achard et al., 2006; Achard and Bullmore, 2007). Resting-state fMRI netwerk studies hebben tot nu toe echter het brein in 90 klassieke grijze stof gebieden opgedeeld en gekeken naar functionele communicatie tussen deze 90 gebieden. Vernieuwd aan onze aanpak is dat we het breinnetwerk opdelen in ongeveer 9500 grijze stof, wat een veel

hoger onderscheidend vermogen kan geven. Deze aanpak zou mogelijk meer spatiele details kunnen oppikken en daardoor aanvullende informatie geven over de organisatie van het breinnetwerk.

onze studies

organisatie van het breinnetwerk

In dit proefschrift hebben we gekeken naar de organisatie van het breinnetwerk. Hoe is functionele connectiviteit in ons brein georganiseerd? In **hoofdstuk 2** hebben we een voxel-wise analysemethode gebruikt om functionele hersennetwerken te onderzoeken. In een resting-state fMRI studie hebben we van 28 mensen hun spontane hersenactiviteit gemeten tijdens rust en hebben we tussen elk hersengebied de mate van functionele connectiviteit berekend. De totale grijze stof was opgedeeld in ongeveer 9500 kleine gebieden (voxels genaamd) en er werd gekeken naar functionele connectiviteit tussen deze gebieden, wat voor elke individuele dataset een functioneel hersennetwerk opleverde. We vonden nu dat deze netwerken een veel hogere clustering-coëfficiënt vertoonden dan een random (=willekeurig) georganiseerd netwerk, maar nog steeds met een relatief lage gemiddelde padlengte tussen alle gebieden, wat een zogenaamde *small-world* organisatie van het breinnetwerk aangeeft (Stam, 2004; Achard et al., 2006). Bovendien vonden we dat de graaddistributie een zogenaamde power-law volgde, wat mogelijkerwijs een *scale-free* architectuur aangeeft van functionele communicatie in het breinnetwerk. Dit suggereert het bestaan van een klein aantal, maar zeer belangrijke, hub-gebieden in het brein die een groot aantal connecties hebben, meer dan andere gebieden, en zo een belangrijke rol spelen in efficiënte communicatie en integratie van informatie in het totale netwerk .

Onze studie in **hoofdstuk 2** laat zien dat ons brein een erg efficiënt en robuust georganiseerd netwerk is, met een optimale combinatie van lokale verbondenheid en globale efficiëntie, mogelijkerwijs gefaciliteerd door sterk verbonden hub-gebieden. Samenvattend, onze data suggereert een zeer efficiënte organisatie van hersenactiviteit van het menselijk brein tijdens rust.

resting-state netwerken

Alhoewel het geen directe gevolgtrekking is, geeft de hoge mate van lokale clustering van het breinnetwerk een mogelijke aanwijzing voor de formatie van sub-netwerken in het breinnetwerk. Dit suggereert een mogelijke modulaire organisatie van het brein. Dit houdt in dat bepaalde gebieden in

het brein meer met elkaar verbonden zijn dan met de rest en zo een functionele eenheid (ook wel '*sub-netwerk* '*module*' of '*community*' genoemd) vormen binnen het totale netwerk. Inderdaad, recente studies hebben aangetoond dat tijdens rust bepaalde gebieden sterk gesynchroniseerde hersensignalen laten zien. Dit geeft aan dat tijdens rust ons brein niet stilstaat, maar dat een groot aantal gebieden spontane activiteit vertoont dat sterk correleert tussen gebieden met een zelfde functie (Gusnard et al., 2001; Raichle et al., 2001; Raichle and Snyder, 2007). Gebieden die dit coherente gedrag vertonen tijdens rust vormen een zogenaamd resting-state netwerk. Tot nu toe zijn ongeveer 8 tot 10 van deze sub-netwerken gerapporteerd. Deze netwerken overlappen met name met gebieden die een gezamenlijke taak of functie hebben, bijvoorbeeld gebieden die alle betrokken zijn bij motorisch gedrag of bijvoorbeeld bij het verwerken van visuele informatie van de ogen (Greicius et al., 2003; Beckmann et al., 2005; Damoiseaux et al., 2006). Er zijn een klein aantal methodes voorgesteld om deze netwerken te selecteren. Bij de zogenaamde seed-methode wordt gekeken naar de correlatie van de tijd-series van een vooraf gedefinieerd gebied met de tijd-series van de andere gebieden van het brein (Biswal et al., 1995). Dit is verreweg de meest gebruikte en simpelste methode en heeft het grote voordeel dat de resulterende functionele connectiviteitsmappen een duidelijk beeld van de functionele connecties van een bepaald gebied geven. Deze methode heeft echter de beperking dat maar naar één gebied per keer gekeken kan worden en is daardoor wat we noemen 'model gestuurd', immers er wordt alleen gekeken naar de connecties van één bepaald gebied dat model staat. Om zonder vooraf gedefinieerd model te kijken naar de functionele connecties van het breinnetwerk zijn recentelijk 'model vrije' methodes voorgesteld en gebruikt voor het selecteren van resting-state netwerken, de meeste gebaseerd op Independent Component Analyse (ICA). Echter, het selecteren van functioneel verbonden netwerken op groepsniveau blijft een ingewikkelde taak en vraagt vaak interventie van de gebruiker. ICA methodes worden vaak ervaren als gecompliceerd en de resultaten blijken in de praktijk moeilijker te interpreteren dan functionele correlatiemappen. In **hoofdstuk 3** hebben we een nieuwe aanpak voorgesteld, gebaseerd op graaftheorie en clustering van resting-state fMRI data. Deze *normalized cut group clustering* aanpak maakt gebruik van graafclustering om voxels (i.e kleine grijze stof gebieden van ongeveer 4 mm3 groot) in resting-state netwerken op groepsniveau te selecteren.

De normalized cut group clustering methode combineert clustering op individueel niveau (cluster stap 1) met clusteren op groepsniveau (cluster stap 2). In de clustering op individueel niveau stap wordt van elke individuele resting-state fMRI dataset een functioneel netwerk gemaakt, met

de nodes als de grijze stof voxels en connecties tussen die voxels waarvan hun tijdseries een hoge mate van correlatie vertonen. Vervolgens wordt de resulterende connectiviteits graaf geclusterd, waarin de voxels zo in groepen werden verdeeld waarin binnen één groep (i.e. sub-netwerk) de voxels een hoge mate van functionele connectiviteit vertonen (i.e. een hoog aantal verbindingen) en tussen de groepen een laag niveau van functionele connectiviteit vertonen. Daarna, in de groepsclustering-stap (cluster stap 2), worden de individuele clustermappen zo gecombineerd dat de voxels die consistent over de subjecten samen geclusterd werden, nu ook samen gegroepeerd in één groep restings-state netwerk. Deze model-vrije clustering aanpak resulteert in geclusterde sub-netwerken die een hoge mate van interne functionele connectiviteit hebben en zijn op die manier gemakkelijk te vergelijken met de meer traditionele seed-methode connectiviteits-mappen.

De normalized cut group clustering aanpak resulteerde in het groeperen van het functionele brein in 9 resting-state netwerken, die sterk overlappen met rustnetwerken die eerder gevonden zijn (Beckmann et al., 2005; Damoiseaux et al., 2006). Deze netwerken overlappen met motorische gebieden, visuele gebieden, parietale en frontale gebieden en het zogenaamde default mode netwerk. Interessant is dat allereerst de visuele en motor gebieden als één netwerk werden gegroepeerd. Dit is interessant, omdat dit een hoge mate van functionele connectiviteit tussen primaire motor en primaire visuele gebieden aangeeft. Recente studies lijken deze sterke mate van functionele connectiviteit tussen motor en visuele gebieden te bevestigen door ook de motor en visuele gebieden als één sterk verbonden netwerk te rapporteren (Vincent et al., 2008). Gelijk aan andere groepsstudies, resulteerde sub-clustering van het gecombineerde motor/visueel netwerk in gescheiden sub-netwerken voor motor en visuele gebieden.

Deze onderverdeling van resting-state netwerken leidde tot de vraag of andere netwerken ook niet een onderverdeling hebben. Het is bekend dat de primaire motor cortex, welke verantwoordelijk is voor het aansturen van de spieren van ons lichaam, niet één homogeen gebied is, maar dat het motor netwerk een zogenaamde somatotopische[1] organisatie heeft met specifieke gebieden voor het aansturen van onze handen, specifieke gebieden voor het aansturen van onze benen etc. Maar hoe functionele connectiviteit tussen deze gebieden georganiseerd is en of deze ook een somatotopische organisatie volgt is onbekend. Tot nu toe hebben alle groep resting-state studies de motor gebieden als één resting-state netwerk

[1] 'volgende het lichaam'

gegroepeerd (Beckmann et al., 2005; Damoiseaux et al., 2006)(hoofdstuk 3) en is er weinig bekend over functionele sub-netwerken binnen bekende resting-state netwerken. In hoofstuk 4 hebben we gekeken naar een onderverdeling van het primaire motor resting-state netwerk in meerdere sub-netwerken. Onze data laat zien dat het motor netwerk niet één homogeen netwerk is, maar dat het bestaat uit meerder sub-netwerken, waarvan gebieden die eenzelfde motortaak hebben, bijvoorbeeld linker en rechter handgebied of linker en rechter voetgebied, juist het sterkst intrinsiek functioneel verbonden zijn. Dit geeft aan dat resting-state netwerken mogelijk een sterke onderverdeling hebben in sub-netwerken. Het selecteren van resting-state netwerken in hoofstuk 3 en de mogelijke onderverdeling van deze netwerken in hoofdstuk 4 suggereert dat het functionele breinnetwerk een modulair karakter heeft.

structurele witte stofverbindingen in resting-state netwerken

Maar hoe is al die functionele communicatie tussen hersengebieden die anatomisch uit elkaar liggen mogelijk? De meeste van de resting-state netwerken bestaan uit gebieden die verdeeld zijn over het hele brein. Hoe is functionele connectiviteit tussen deze anatomisch gescheiden gebieden mogelijk? Hiervoor verwacht je het bestaan van structurele connecties tussen die gebieden om de functionele communicatie te faciliteren. Immers, in het Nederland-netwerk is voor goederentransport tussen twee steden het bestaan van een structurele snelweg tussen stad A en B nodig. Hoe is dat in het brein geregeld? Een recente studie laat zien dat de gebieden van het default mode netwerk structureel verbonden zijn door witte stofbanen (Greicius et al. 2009). Echter, of resting-state netwerken in het algemeen verbonden zijn was onduidelijk. In **hoofdstuk 5** hebben we resting-state fMRI opnames gecombineerd met structurele *diffusion tensor imaging* (DTI) data. DTI is een techniek om de witte stofbanen van het brein te reconstrueren, door het diffusieprofiel van water moleculen te meten. Door middel van DTI kunnen we de structurele informatie snelwegen van het brein in kaart brengen. In onze gecombineerde DTI/resting-state fMRI studie hebben we gekeken of de gebieden die functioneel verbonden zijn ook structureel verbonden zijn door middel van witte stofbanen. Inderdaad, onze studie laat zien dat vrijwel alle resting-state netwerken een structurele kern hebben met witte stofbanen tussen alle functioneel verbonden resting-state netwerkgebieden. Onze studie geeft een directe link aan tussen de functionele en structurele verbindingen in onze hersenen en laat zien dat functionele resting-state netwerken sterk overlappen met structurele structuren in de hersenen.

Speciale interesse gaat uit naar het zogenaamde *default mode netwerk*. In de laatste paar jaar is het aantal neurowetenschappelijke studies naar dit specifieke netwerk sterk toegenomen. Interessant is dat het default mode netwerk tijdens rust meer activiteit vertoont dan tijdens het uitvoeren van cognitieve taken, wat een basis activiteit (vandaar de naam default state) van het brein suggereert. Dit default mode netwerk bestaat uit een aantal frontale en, parietale gebieden die een sterke mate van functionele connectiviteit laten zien tijdens rust. Dit netwerk is van speciale interesse voor neurowetenschappers omdat activiteit en synchroniciteit van dit netwerk in verband wordt gebracht met cognitieve hersenprocessen zoals het integreren van aandacht en emotieprocessen en mogelijker wijs betrokken is bij zelfperceptie. Alhoewel er steeds meer bekend wordt over de functionele verbindingen van dit netwerk, is er nog weinig bekend over de structurele verbindingen van het default mode netwerk en hoe deze structurele verbinden zich verhouden ten opzichte van de mate van functionele synchroniciteit van dit netwerk. Echter, het is eenvoudig voor te stellen dat deze twee vormen van connectiviteit sterk mogelijk met aan elkaar gerelateerd zijn. Immers, een verbreding van de A2 tussen Utrecht en Amsterdam zal de doorstroming van verkeer tussen deze steden ten goede komen en daardoor kan de totale hoeveelheid verkeer tussen deze steden toenemen. Interessant, is dat recente neurowetenschappelijke studies hebben aangetoond dat de gebieden van het default mode netwerk inderdaad verbonden zijn door witte stofbanen (Greicius et al., 2009)(hoofdstuk 5). Maar hoe verhoud zich de 'kwaliteit' van deze witte stofbanen tot de hoeveelheid functionele communicatie tussen deze gebieden? In **hoofdstuk 6** hebben we laten zien dat de mate van organisatie van het cingulum en de mate van functionele communicatie tussen twee sleutelgebieden van het default mode netwerk aan elkaar gerelateerd zijn. Vrijwilligers met een hogere mate van microstructurele organisatie van het cingulum, als aangegeven door de berekende *fractionele anisotropie (*FA) lieten ook een hogere mate van unieke functionele synchronisatie tussen de frontale en parietale gebieden van het default mode netwerk zien. Dit demonstreert een duidelijk verband tussen de structurele en functionele verbindingen van het brein en laat als eerste zien dat de kwaliteit van deze twee vormen van connectiviteit tijdens rust direct aan elkaar gerelateerd zijn. Niet alleen zijn functioneel verbonden gebieden van het belangrijke default mode netwerk structureel verbonden, maar juist hoe sterk deze gebieden structureel verbonden zijn is gelinkt aan de hoeveelheid functionele communicatie tussen deze gebieden. De structurele verbindingen van het brein lijken daardoor een directe invloed te hebben op de basisstaat van functionele communicatie in het brein tijdens rust.

efficiënter georganiseerde breinen zijn slimmer

In **hoofstuk 2** hebben we laten zien dat onze hersenen een functioneel netwerk zijn met een erg efficiënte organisatie. Deze organisatie laat een erg sterke mate van lokale clustering zien, gecombineerd met een aantal cruciale 'lange-afstands' verbindingen en sterk verbonden gebieden die zorgen voor een hoge mate van globale communicatie-efficiëntie. In **hoofdstuk 3** en **4** hebben we ons vervolgens gericht op de sterke mate van lokale clustering en modulariteit van het breinnetwerk en in **hoofdstuk 5** en **6** hebben we bekeken of en hoe deze netwerken gerelateerd zijn aan de structurele witte stofverbindingen van de hersenen. Echter, small-world netwerken worden ook juist gekarakteriseerd door hun relatief hoge mate van efficiënte globale communicatie, wat volgt uit de korte padlengte die deze netwerken hebben. Maar hoe verhoudt deze hoge mate van globale efficiëntie tot menselijk gedrag? De mate van organisatie van een netwerk is direct gelinkt aan de mate van efficiëntie van communicatie in een netwerk. Dit is eenvoudig voorstellen als dat de mate van hoe efficiënt snelwegen aangelegd zijn direct gerelateerd is aan hoe effectief de goederentransport tussen steden kan zijn. Deze eigenschap brengt de vraag naar boven hoe het niveau van efficiëntie van functionele communicatie in ons breinnetwerk gerelateerd is aan ons intellectueel gedrag. Neuroimaging studies hebben laten zien dat intelligentie is gerelateerd is aan specifieke eigenschappen van bepaalde grijze en witte stof structuren in het brein, maar de link tussen de totale netwerkorganisatie van het brein en intelligentieniveau is nog onbekend. In **hoofdstuk 7** hebben we de lokale en globale organisatie van functionele breinnetwerken bekeken en laten we een sterke positieve relatie zien tussen de mate van hoe efficiënt globale communicatie in het breinnetwerk is georganiseerd en de mate van intelligentie. De resultaten lieten zien dat IQ sterk negatief gecorreleerd is met de genormaliseerde padlengte *lambda* ($r<-0.6$, $p<0.001$). Interessant is dat IQ niet gecorreleerd bleek te zijn met de lokale clustering-coëfficiënt *gamma* en ook niet met de totale hoeveelheid connecties *k*. Samen met de sterke correlatie tussen *lambda* en IQ geeft dit aan dat intelligentie sterk gerelateerd is aan hoe efficiënt het brein informatie tussen de verschillende gebieden en sub-netwerken kan integreren en in mindere mate met hoe efficiënt informatie lokaal verwerkt kan worden of met de totale hoeveelheid functionele communicatie. De meest sterke effecten tussen padlengte en IQ werden gevonden in frontale en pariëtale gebieden, gebieden die met name betrokken zijn bij meer ingewikkeldere cognitieve functies. Dit laat zien dat intelligentie waarschijnlijk te maken heeft met hoe snel deze 'hoger orde' gebieden toegang hebben tot informatie van de rest van het brein. Slimmere breinen hebben mogelijk een snellere en daardoor meer efficiëntere toegang tot informatie en kunnen zo efficiënter

informatie integreren tussen de verschillende gebieden van het breinnetwerk. Dit suggereert dat ons functionele breinnetwerk is geoptimaliseerd naar een zo kort mogelijke functionele padlengte en dus een zo efficiënt mogelijke integratie van informatie.

wat kunnen we leren van deze studies?

De belangrijkste conclusie van onze studies is dat ons brein niet een verzameling is van losse gebieden, maar juist dat het een netwerk is. Een erg efficiënt georganiseerd netwerk van sterk intern verbonden sub-netwerken die hoewel ze elk hun eigen functie hebben op hun beurt weer erg efficiënt verbonden zijn met elkaar en zo één robuust functioneel breinnetwerk vormen. Interessant is dat de mate van onderling efficiënte communicatie tussen de verschillende gebieden van ons brein gerelateerd is aan intellectuele performance. Slimmere breinen hebben een efficiënter georganiseerd brein. Verder laten onze studies zien dat intrinsieke functionele communicatie tussen hersengebieden mogelijk gemaakt wordt door witte stofverbindingen tussen de anatomisch gescheiden gebieden. Bovendien is de sterkte van functionele communicatie tussen gebieden gelinkt aan de microstructurele organisatie van deze witte stofbanen. Sterkere structurele verbindingen maken sterkere functionele communicatie mogelijk. Omdat al onze studies gebaseerd zijn op rustmetingen laat dit zien dat tijdens rust ons brein zeker niet stilstaat, maar een grote hoeveelheid spontane activiteit vertoont dat sterk gesynchroniseerd is tussen verschillende gebieden. Dit suggereert dat de verwerking en integratie van informatie tijdens rust gewoon doorgaat en dat witte stofverbindingen hier een belangrijke rol in spelen. Bovendien lijkt de organisatie van deze rust activiteits patronen voorspellend te zijn voor intellectuele performance. Al met al, ons brein is een complex, robuust en efficiënt georganiseerd netwerk van anatomisch gescheiden gebieden die ieder hun eigen taak en functie hebben, maar onderling structureel en functioneel sterk verbonden zijn voor continue informatieverwerking en informatieuitwisseling.

en nu? nieuwe vragen...

Bij het lezen van deze studies komen ongetwijfeld vele nieuwe vragen naar boven. Een paar belangrijke punten, waarvan wij vinden dat ze extra aandacht verdienen, wil ik hier kort bespreken.

functionele versus structurele connectiviteit

In **hoofdstuk 5** en **6** hebben we gekeken naar een verband tussen structurele en functionele connectiviteit in het brein. Functionele connectiviteit werd gemeten als de correlatie tussen de resting-state tijdseries van de verschillende hersengebieden en geeft hiermee zowel directe als indirecte verbindingen aan. Omdat DTI alleen directe verbindingen verbindingen weergeeft, zouden de functionele en structurele data mogelijk gedeeltelijk kunnen overlappen. Interessant is juist dat onze data laat zien dat vrijwel alle gebieden van resting-state netwerken direct structureel met elkaar verbonden zijn, wat suggereert dat de functionele resting-state netwerkverbindingen ook direct zijn; althans de structurele infrastructuur is aanwezig om directe communicatie mogelijk te maken.

Kunnen we met zekerheid zeggen dat deze structurele banen ook daadwerkelijk gebruikt worden? Onze studies laten zien dat anatomisch gescheiden gebieden hun neurale activiteit synchroniseren tijdens rust en dat deze gebieden ook direct structureel verbonden zijn, wat erop lijkt dat deze structurele verbindingen een noodzakelijke voorwaarde vormen voor functionele synchronisatie tijdens rust. Inderdaad, recente studies laten zien dat functionele connectiviteit tijdens rust verminderd is bij patiënten met multiple sclerosis (Lowe et al. 2008), waarvan bekend is dat structurele witte stofverbindingen beschadigd zijn. Verder is ook gevonden dat operatieve doorsnijding van corpus callosumbanen kan leiden tot vrijwel totaal verlies van functionele connectiviteit tijdens rust tussen de linker en rechter hersenhelft (Johnston et al., 2008). Bovendien, onze eigen studie in **hoofdstuk 6** laat zien dat de microstructurele organisatie van de witte stofbanen in het default mode netwerk in verband staan met het niveau van functionele synchronisatie tussen die gebieden. Bij elkaar genomen laten deze studies zien dat structurele witte stofbanen een cruciale rol kunnen spelen in functionele synchronisatie tijdens rust tussen anatomisch gescheiden gebieden in het breinnetwerk. Echter dit blijf ietwat indirect bewijs. Het mooiste zou zijn om de directe informatieoverdracht over de structurele banen te meten en te kijken hoe dit verhoud tot de functionele connectiviteit van de grijze stof gebieden tijdens rust. Echter, tot voor kort was het niet mogelijk om activiteit van witte stofbanen te meten. Recentelijk is echter een nieuwe techniek getoond, die de morphologische veranderingen van witte stof meet die optreden bij signaal overdracht. Deze techniek is passend functionele DTI genoemd (Mandl et al., 2008) en naast het meten van activiteit tijdens het uitvoeren van een taak, stelt deze techniek ons nu mogelijk ook in staat om tijdens rust witte stof activiteit te meten.

graaftheorie

In dit proefschrift hebben we gebruikt gemaakt van graaftheorie om de organisatie van functionele connectiviteit in het menselijk brein te onderzoeken. In tegenstelling tot andere groepen, hebben we een 'voxel aanpak' gebruikt, omdat dit een veel hoger onderscheidend vermogen geeft en we daardoor mogelijk beter in staat zijn om functionele communicatie in kaart te brengen. Onze voxel-aanpak gaf een indicatie voor een mogelijke scale-free organisatie van het breinnetwerk, maar hoewel een voxel-aanpak het breinnetwerk al in een veel hoger aantal nodes verdeelt, blijft de mogelijkheid voor het onderzoeken van zo'n organisatie beperkt. Scale-free eigenschappen worden meestal toegekend aan netwerken met een groot aantal nodes om goed de connectiviteitsverdeling in kaart te kunnen brengen (Barabasi and Bonabeau, 2003), bijvoorbeeld van het internet met zijn meer dan 100 miljoen pagina's (in 2009) en ruim meer dan 500 miljoen documenten (geteld in 2001)(wikipedia). Hoog-resolutie fMRI in combinatie met een voxel representatie van het breinnetwerk zou nieuwe inzichten kunnen geven.

Een voxel-aanpak is met name geschikt voor het in detail bekijken van de rol van de verschillende nodes in het netwerk. Zo hebben we in **hoofdstuk 7** een eerste aanzet laten zien om te kijken naar welke gebieden in het totale netwerk een belangrijke rol spelen in het efficiënt integreren van informatie. Hiervoor hebben we relatief grove maten gebruikt. Recent zijn nieuwe, meer specifieke maten geïntroduceerd en succesvol gebruikt in pionierende neuroimaging netwerk studies, zoals *Assortativiteits* maten, *Centraliteits* maten en directe *Modulariteits* en *Participatie* maten (Sporns et al., 2007; Bullmore and Sporns, 2009). Interessant is dat deze maten met name gespecificeerd zijn voor het in kaart brengen van het gedrag van individuele nodes in het netwerk en om die reden zijn ze juist geschikt om met een voxel-aanpak te combineren. Nieuwe studies zijn gericht op het bekijken van de mogelijkheden om deze maten te gebruiken in de gebruikte voxel-aanpak.

taakactiviteit versus rustactiviteit

In onze studies hebben we het functionele breinnetwerk bekeken als een netwerk of gebieden met een hoge mate van functionele connectiviteit. Dit alles is gemeten tijdens rust, wat natuurlijk een versimpeling is van de werkelijkheid. Ons brein is niet altijd in rust, maar moet vaak een bepaalde taak of meerdere taken uitvoeren. Maar hoe is 'rustactiviteit' verbonden met 'taak activiteit' ? Vroeger werd gedacht dat tijdens rust het brein 'uit' was, maar recente studies laten zien dat dit duidelijk niet het geval is. Tijdens rust

is er veel spontane activiteit dat gesynchroniseerd is tussen verschillende breingebieden. Interessant is dat met name deze functionele connecties worden gevonden tussen gebieden waarvan we weten dat ze vaak samen een gezamenlijke rol vervullen. Zo zijn de gebieden van het motorische netwerk en gebieden van het visuele netwerk sterk functioneel met elkaar verbonden tijdens rust. Mogelijkerwijs is het zo dat deze functionele rustconnecties een intrinsieke staat van het brein aangeven, waarin de functionele connecties onderhouden worden die nodig zijn voor functionele communicatie indien gebieden hun gezamenlijke taak moeten uitvoeren. Bewijs voor een dergelijke rol komt van studies die laten zien dat het niveau van rustactiviteit gerelateerd is aan de uitvoering van een taak (Xiong et al., 2008). Echter, wat het brein tijdens rust precies doet blijft onbekend, maar dat rustactiviteit op zijn minst net zo belangrijk is als taakgerelateerde activiteit wordt steeds duidelijker.

schizofrenie

Alhoewel alle studies in dit proefschrift gaan over de organisatie van functionele connectiviteit in de hersenen van gezonde vrijwilligers, is het belangrijk om te weten dat onze studies er op gericht zijn om nieuwe analyse methodes te ontwikkelen voor het in kaart brengen van mogelijke afwijkende hersenprocessen in hersenziektes. Onze focus is op schizofrenie, een ernstige psychiatrische ziekte die gekenmerkt wordt door psychose, vermindering van emoties en afwijkend cognitief gedrag. Al vroeg is gesuggereerd dat schizofrenie een mogelijke 'connectiviteitsziekte' zou kunnen zijn, met veranderde verbindingen en veranderde informatie overdracht tussen verschillende hersengebieden. Inderdaad, in de laatste paar jaren hebben structurele studies laten zien dat schizofrenie gepaard gaat met progressieve vermindering van grijze en witte stof van bepaalde hersengebieden (Hulshoff Pol et al., 2001; van Haren et al., 2008). Bovendien hebben studies recentelijk aangetoond dat schizofreniepatiënten andere hersenactiviteitspatronen laten zien tijdens rust, met veranderde activiteit en synchronisatie in het default mode netwerk (Bluhm et al., 2007; Garrity et al., 2007; Whitfield-Gabrieli et al., 2009). Interessant is dat met name deze veranderde functionele connectiviteit gevonden wordt voor gebieden die sterk overlappen met de gebieden die ook morfologisch veranderd zijn. Gezamenlijk suggereren deze studies een verstoord rustpatroon in patiënten met schizofrenie. Graafanalyse zou mogelijk een belangrijke rol kunnen spelen in het bestuderen van deze veranderde rustactiviteit. Recente studies hebben een verstoorde functionele breinnetwerkorganisatie laten zien in patiënten met schizofrenie, met een minder efficiënte organisatie in vergelijking tot gezonde vrijwilligers (Micheloyannis et al., 2006; Liu et al.,

2008). De door ons gebruikte voxel gebaseerde netwerk analyse zou in dit onderzoek een belangrijke rol kunnen spelen. Een voxel aanpak, met een hoog spatieel onderscheidend vermogen, kan mogelijk meer subtielere verschillen oppikken in vergelijking met een regionale aanpak en biedt zo de mogelijkheid om verschillen te lokaliseren naar specifieke hersengebieden (hoofdstuk 7). Op deze manier kunnen we mogelijk bekijken of schizofrenie te maken heeft met veranderde informatie integratie tussen verschillende hersengebieden. Deze informatie zou kunnen bijdragen aan een beter begrip van deze ernstige ziekte.

conclusie

Ons brein is een netwerk. Een erg efficiënt netwerk wel te verstaan, bestaande uit allerlei hersengebieden, elk met hun eigen functie en taak, maar sterk onderling structureel en functioneel verbonden. Onze studies laten de mogelijkheid zien van het onderzoeken van de organisatie van het functionele breinnetwerk met behulp voxel-wise resting-state fMRI en graaf analyse en vormen zo een nieuw platform voor het onderzoeken van hersenziektes.

referenties

Achard S, Bullmore E (2007) Efficiency and cost of economical brain functional networks. PLoS Comput Biol 3:e17.

Achard S, Salvador R, Whitcher B, Suckling J, Bullmore E (2006) A resilient, low-frequency, small-world human brain functional network with highly connected association cortical hubs. J Neurosci 26:63-72.

Aertsen AM, Gerstein GL, Habib MK, Palm G (1989) Dynamics of neuronal firing correlation: modulation of "effective connectivity". J Neurophysiol 61:900-917.

Barabasi AL, Bonabeau E (2003) Scale-free networks. Sci Am 288:60-69.

Beckmann CF, DeLuca M, Devlin JT, Smith SM (2005) Investigations into resting-state connectivity using independent component analysis. Philos Trans R Soc Lond B Biol Sci 360:1001-1013.

Biswal B, Yetkin FZ, Haughton VM, Hyde JS (1995) Functional connectivity in the motor cortex of resting human brain using echo-planar MRI. Magn Reson Med 34:537-541.

Bluhm RL, Miller J, Lanius RA, Osuch EA, Boksman K, Neufeld R, Theberge J, Schaefer B, Williamson P (2007) Spontaneous Low-Frequency

Fluctuations in the BOLD Signal in Schizophrenic Patients: Anomalies in the Default Network. Schizophr Bull 33:1004-1012.
Bullmore E, Sporns O (2009) Complex brain networks: graph theoretical analysis of structural and functional systems. Nat Rev Neurosci 10:186-198.
Damoiseaux JS, Rombouts SA, Barkhof F, Scheltens P, Stam CJ, Smith SM, Beckmann CF (2006) Consistent resting-state networks across healthy subjects. Proc Natl Acad Sci U S A 103:13848-13853.
Eguiluz VM, Chialvo DR, Cecchi GA, Baliki M, Apkarian AV (2005) Scale-free brain functional networks. Phys Rev Lett 94:018102.
Friston KJ, Frith CD, Liddle PF, Frackowiak RS (1993) Functional connectivity: the principal-component analysis of large (PET) data sets. J Cereb Blood Flow Metab 13:5-14.
Garrity AG, Pearlson GD, McKiernan K, Lloyd D, Kiehl KA, Calhoun VD (2007) Aberrant "default mode" functional connectivity in schizophrenia. Am J Psychiatry 164:450-457.
Greicius MD, Krasnow B, Reiss AL, Menon V (2003) Functional connectivity in the resting brain: a network analysis of the default mode hypothesis. Proc Natl Acad Sci U S A 100:253-258.
Greicius MD, Supekar K, Menon V, Dougherty RF (2008) Resting-State Functional Connectivity Reflects Structural Connectivity in the Default Mode Network. Cereb Cortex.
Gusnard DA, Raichle ME, Raichle ME (2001) Searching for a baseline: functional imaging and the resting human brain. Nat Rev Neurosci 2:685-694.
Hulshoff Pol HE, Schnack HG, Mandl RC, van Haren NE, Koning H, Collins DL, Evans AC, Kahn RS (2001) Focal gray matter density changes in schizophrenia. Arch Gen Psychiatry 58:1118-1125.
Johnston JM, Vaishnavi SN, Smyth MD, Zhang D, He BJ, Zempel JM, Shimony JS, Snyder AZ, Raichle ME (2008) Loss of resting interhemispheric functional connectivity after complete section of the corpus callosum. J Neurosci 28:6453-6458.
Liu Y, Liang M, Zhou Y, He Y, Hao Y, Song M, Yu C, Liu H, Liu Z, Jiang T (2008) Disrupted small-world networks in schizophrenia. Brain 131:945.
Lowe MJ, Beall EB, Sakaie KE, Koenig KA, Stone L, Marrie RA, Phillips MD (2008) Resting state sensorimotor functional connectivity in multiple sclerosis inversely correlates with transcallosal motor pathway transverse diffusivity. Hum Brain Mapp.
Mandl RC, Schnack HG, Zwiers MP, van der Schaaf A, Kahn RS, Hulshoff Pol HE (2008) Functional diffusion tensor imaging: measuring task-

related fractional anisotropy changes in the human brain along white matter tracts. PLoS ONE 3:e3631.

Micheloyannis S, Pachou E, Stam CJ, Breakspear M, Bitsios P, Vourkas M, Erimaki S, Zervakis M (2006) Small-world networks and disturbed functional connectivity in schizophrenia. Schizophr Res 87:60-66.

Raichle ME, Snyder AZ (2007) A default mode of brain function: A brief history of an evolving idea. Neuroimage 37:1083-1090.

Raichle ME, MacLeod AM, Snyder AZ, Powers WJ, Gusnard DA, Shulman GL (2001) A default mode of brain function. Proc Natl Acad Sci U S A 98:676-682.

Sporns O, Zwi JD (2004) The small world of the cerebral cortex. Neuroinformatics 2:145-162.

Sporns O, Honey CJ, Kotter R (2007) Identification and classification of hubs in brain networks. PLoS ONE 2:e1049.

Stam CJ (2004) Functional connectivity patterns of human magnetoencephalographic recordings: a 'small-world' network? Neurosci Lett 355:25-28.

van Haren NE, Hulshoff Pol HE, Schnack HG, Cahn W, Brans R, Carati I, Rais M, Kahn RS (2008) Progressive brain volume loss in schizophrenia over the course of the illness: evidence of maturational abnormalities in early adulthood. Biol Psychiatry 63:106-113.

Vincent JL, Kahn I, Snyder AZ, Raichle ME, Buckner RL (2008) Evidence for a Frontoparietal Control System Revealed by Intrinsic Functional Connectivity. J Neurophysiol.

Watts DJ, Strogatz SH (1998) Collective dynamics of 'small-world' networks. Nature 393:440-442.

Whitfield-Gabrieli S, Thermenos HW, Milanovic S, Tsuang MT, Faraone SV, McCarley RW, Shenton ME, Green AI, Nieto-Castanon A, Laviolette P, Wojcik J, Gabrieli JD, Seidman LJ (2009) Hyperactivity and hyperconnectivity of the default network in schizophrenia and in first-degree relatives of persons with schizophrenia. Proc Natl Acad Sci U S A.

Xiong J, Ma L, Wang B, Narayana S, Duff EP, Egan GF, Fox PT (2008) Long-term motor training induced changes in regional cerebral blood flow in both task and resting states. Neuroimage.

list of publications

van den Heuvel MP, Hulshoff Pol HE. (2009) Specific somatotopic organization of functional connections of the primary motor network during resting-state Hum Brain Mapp in press.

van den Heuvel MP, Stam CJ, Kahn RS, Hulshoff Pol HE (2009) Efficiency of functional brain networks and intellectual performance J Neurosci 29(23):7619-24.

van den Heuvel MP, Mandl RCW, Kahn RS, Hulshoff Pol HE. (2009) Functionally linked resting-state networks reflect the underlying structural connectivity architecture of the human brain Hum Brain Mapp epub ahead of print.

van den Heuvel MP, Stam CJ, Boersma M, Hulshoff Pol HE. (2008) Small-world and scale-free organization of voxel-based resting-state functional connectivity in the human brain Neuroimage 43(3): 528-39.

van den Heuvel MP, Mandl RCW, Luigjes J, Hulshoff Pol HE. (2008) Microstructural organization of the cingulum tract and the level of default mode functional connectivity J Neurosci 28(43):10844-51.

van den Heuvel MP, Mandl RCW, Hulshoff Pol HE. (2008) Normalized cut group clustering of resting-state FMRI data PLoS ONE 3(4):e2001.

van Buuren M, Gladwin TE, Zandbelt BB, **van den Heuvel MP**, Ramsey NF, Kahn RS, Vink M. (2009) Cardiorespiratory effects on default-mode network activity as measured with fMRI Hum Brain Mapp epub ahead of print.

Mandl RC, Schnack HG, Luigjes J, **van den Heuvel MP**, Cahn W, Kahn RS, Hulshoff Pol HE. (2008) Tract-based analysis of magnetization

transfer ratio and diffusion tensor imaging of the frontal and frontotemporal connections in schizophrenia Schizophr Bull epub ahead of print.

Ramsey NF, **van den Heuvel MP**, Kho KH, Leijten FS. (2006) Towards human BCI applications based on cognitive brain systems: an investigation of neural signals recorded from the dorsolateral prefrontal cortex IEEE Trans Neural Syst Rehabil Eng 14(2):214-7.

Raemaekers M, Vink M, **van den Heuvel MP**, Kahn RS, Ramsey NF. (2006) Effects of aging on BOLD fMRI during prosaccades and antisaccades J Cogn Neurosci 18(4):594-603.

Raemaekers M, Ramsey NF, Vink M, **van den Heuvel MP**, Kahn RS. (2006) Brain activation during antisaccades in unaffected relatives of schizophrenic patients Biol Psychiatry 59(6):530-5.

Raemaekers M, Vink M, **van den Heuvel MP**, Kahn RS, Ramsey NF. (2005) Brain activation related to retrosaccades in saccade experiments Neuroreport 16(10):1043-7.

Vink M, Kahn RS, Raemaekers M, **van den Heuvel MP**, Boersma M, Ramsey NF. (2005) Function of striatum beyond inhibition and execution of motor responses Hum Brain Mapp 25(3):336-44.

curriculum vitae

Martijn Pieter van den Heuvel was born on the 24th of July 1980 in Gouda, The Netherlands. After finishing high school he started his university study Cognitive Artificial Intelligence at the University of Utrecht, The Netherlands (CKI). During his study he focussed on artificial neural networks and brain dynamics. He followed an internship at the University Medical Center Utrecht, examining the neuronal basis of implicit learning in the human brain, using functional Magnetic Resonance Imaging. After receiving his MSc degree in 2004, he continued to work in the field of functional MRI in combination with the signal processing of electrocortical recordings at the department of Psychiatry at the University Medical Center Utrecht. In 2005 he worked in the real-time EEG program and the spatial auditory signal processing program at the Dutch Technical Research Institute (TNO). In 2006 Martijn started his PhD project on resting-state fMRI under the supervision of prof dr Hilleke Hulshoff Pol and prof dr René Kahn at the Department of Psychiatry at the University Medical Center Utrecht. This project was focussed on the development and implementation of resting-state fMRI analysis techniques to examine functional and structural connectivity in the human brain at high field strengths and resulted in this thesis. Since 2009 Martijn is working as a researcher at the department of Psychiatry, Neuroimaging group at the University Medical Center Utrecht, with prof dr Hilleke Hulshoff Pol and prof dr René Kahn.